

**University of Oviedo**

Department of Chemical and Environmental Engineering

**Ageing under extreme pH conditions,  
modification and characterization of  
ultrafiltration and nanofiltration membranes**

**DOCTORAL THESIS**

Program in Process and Environmental Engineering

**BY**

**Faustino Enrique Ant3n Rodr3guez**

**Oviedo**

**September, 2014**







## RESUMEN DEL CONTENIDO DE TESIS DOCTORAL

1.- Título de la Tesis	
Español/Otro Idioma: <b>ENVEJECIMIENTO BAJO CONDICIONES EXTREMAS DE pH, MODIFICACION Y CARACTERIZACION DE MEMBRANAS DE ULTRAFILTRACION Y NANOFILTRACION</b>	Inglés: <b>AGEING UNDER EXTREME pH CONDITIONS, MODIFICATION AND CHARACTERIZATION OF ULTRAFILTRATION AND NANOFILTRATION MEMBRANES</b>
2.- Autor	
Nombre: <b>Pascual Fernando Antón Rodríguez</b>	DNI/Pasaporte/NIE:
<b>INGENIERIA DE PROCESOS Y AMBIENTAL (Mención de calidad MCD2005-00213)</b>	
Órgano responsable: <b>UNIVERSIDAD DE OVIEDO</b>	

### RESUMEN (en español)

El objetivo de este trabajo ha sido el estudio del envejecimiento de membranas de ultrafiltración (UF) y nanofiltración (NF) expuestas a disoluciones ácidas y alcalinas de limpieza. Se ha desarrollado un modelo teórico para interpretar los resultados de la porosimetría de desplazamiento líquido-líquido (LLDP). También se han preparado membranas resistentes al ensuciamiento por co-polimerización de hidrogeles electrolíticos sobre la superficie de membranas de ultrafiltración.

Se incluye una revisión bibliográfica detallada sobre los principales agentes de ensuciamiento, los agentes de limpieza más comunes, las técnicas consolidadas para determinar la eficacia de limpieza, los parámetros que afectan a los tratamientos y los procedimientos de limpieza más adecuados en función del tipo de ensuciamiento.

La primera sección del trabajo experimental se centra en el envejecimiento, bajo condiciones extremas de pH, de membranas de UF (hechas de polietersulfona) y de NF (hechas de poliamida). Se sometieron seis membranas comerciales de UF (de Nadir, Koch y GE Osmonics) y dos membranas de NF (de Dow Filmtec) a disoluciones con distintas concentraciones de ácido nítrico e hidróxido sódico, a distintas temperaturas y periodos de tiempo largos (hasta seis meses) para simular las sucesivas operaciones de limpieza a lo largo de su vida útil. El comportamiento de las membranas se evaluó mediante medidas de permeabilidad y de retención. Se realizaron caracterizaciones fisicoquímicas de las membranas envejecidas y en su estado original. La composición superficial de las membranas se analizó por ATR-FTIR y EDS. La estructura, la morfología y la hidrofiliidad de las membranas se estudiaron mediante caracterizaciones por SEM, AFM y medidas de ángulos de contacto, respectivamente.

En la segunda sección del trabajo experimental se propone un método de interpretación de las medidas mediante LLDP para caracterizar membranas de UF. Se estudiaron cuatro membranas poliméricas de UF con tamaños de corte entre 5 y 300 kDa. El comportamiento de las membranas modelo, definidas por una distribución log-normal del número de poros y una densidad de poros total dada, se ajustó al de las membranas reales durante el análisis por LLDP. La validación del modelo se llevó a cabo comparando las distribuciones de número de poros y de permeabilidad así como otros parámetros típicos (radios medios, permeabilidad asintótica, etc.) obtenidos a partir del modelo con los resultados procedentes del método tradicional desarrollado por Grabar-Nikitine.



Se han desarrollado también nuevas membranas con baja tendencia al ensuciamiento, caracterizadas por una elevada carga y una baja rugosidad, mediante la modificación de membranas de UF por co-polimerización de hidrogeles electrolíticos inducida por radiación ultravioleta. Se investigaron los efectos de la concentración del monómero funcional, la concentración del reticulador, la intensidad de la radiación, y el tiempo de modificación sobre el grado de polimerización, la composición, la estructura, y el comportamiento funcional de la membrana de hidrogel.

### RESUMEN (en Inglés)

The aim of this work has been the study of the ageing of ultrafiltration (UF) and nanofiltration (NF) membranes under long-term exposure to acidic and alkaline cleaning solutions. A theoretical model has been developed for the interpretation of liquid-liquid displacement porosimetry (LLDP) results. In addition, membranes with an improved fouling resistance have been prepared by graft copolymerization of a polyelectrolyte hydrogel on the top of an UF membrane.

A comprehensive literature review, concerning the main foulants, the most common cleaners, the consolidated techniques to determine cleaning effectiveness, the parameters affecting such process and the most suitable cleaning procedures as function of the fouling nature, is also included in this work.

The first section of the experimental work is devoted to the ageing of polyethersulfone UF and polyamide NF membranes under long-term exposures to acidic and alkaline conditions. Six commercial UF membranes from Nadir, Koch and GE Osmonics manufacturers and two NF ones from Dow Filmtec were subjected to different concentration nitric acid and sodium hydroxide solutions at several temperatures for long periods of time (up to six months) to simulate the successive cleaning steps throughout their lifetime. Permeability and rejection were used to evaluate membrane performance. Membranes were also characterized in their pristine state and after ageing by physicochemical techniques. Attenuated total reflection Fourier transform infrared and energy-dispersive X-ray spectroscopy were used to analyze surface membrane composition. Scanning electron microscopy, atomic force microscopy and contact angle measurements allowed characterizing structure, morphology and wettability of membrane surfaces, respectively.

The second section of the experimental work describes a new approach to LLDP to characterize UF membranes. Four polymeric UF membranes with molecular weight cut-offs ranging from 5 to 300 kDa were employed. A model membrane defined by a log-normal pore number distribution and a given pore number density was fitted to the actual membrane during the LLDP analysis. Model validation was carried out comparing the pore number and permeance distributions as well as typical LLDP parameters (mean radius, asymptotic permeance, etc.) obtained from the proposed model with those from the traditional Grabar-Nikitine method.

New NF membranes, characterized by a high charge density and a low roughness, thus, low prone to fouling, have been manufactured using UV-photo initiated copolymerization of strong polyelectrolyte hydrogels on the surface of PES membranes. The effects of the functional monomer concentration, the cross-linker fraction, the irradiation intensity and the modification time on the degree of grafting, composition, structure and membrane performance of the hydrogel membranes were studied.



R. Bernstein, E. Antón, M. Ulbricht, UV-photo graft functionalization of polyethersulfone membrane with strong polyelectrolyte hydrogel and its application for nanofiltration, ACS Applied Materials and Interfaces 4 (2012) 3438-3446. **Impact factor: 5.008**

R. Bernstein, E. Antón, M. Ulbricht, Tuning the nanofiltration performance of thin film strong polyelectrolyte hydrogel composite membranes by photo-grafting conditions, Journal of Membrane Science 427 (2013) 129-138. **Impact factor: 4.093**

E. Antón, J.I. Ignacio, J.R. Álvarez, A. Hernández, S. Luque, Fitting approach to liquid-liquid displacement porosimetry based on the log-normal pore size distribution, Journal of Membrane Science. <http://dx.doi.org/10.1016/j.memsci.2014.07.035>. Accepted (2014). **Impact factor: 4.093**

Además, en el momento de depositar la misma se encuentran en revisión los siguientes artículos, cuyo contenido se ha incluido en la tesis en forma de capítulos:

E. Antón, D. Vázquez, J.R. Álvarez, S. Luque, Ageing of nanofiltration polymeric membranes under the exposure to acidic and alkaline cleaning solutions, Separation and Purification Technology. Submitted (2014).

E. Antón, J.R. Álvarez, L. Palacio, P. Prádanos, A. Hernández, A. Pihlajamäki, S. Luque, Ageing of polyethersulfone ultrafiltration membranes under long-term exposures to alkaline and acidic cleaning solutions. Part I: physicochemical changes, Journal of Membrane Science. Submitted (2014).

E. Antón, J.R. Álvarez, S. Luque, Ageing of polyethersulfone ultrafiltration membranes under long-term exposures to alkaline and acidic cleaning solutions. Part II: membrane performance, Journal of Membrane Science. Submitted (2014).

En Oviedo a 29 de julio de 2014

Director/es de la Tesis Doctoral

Fdo.: Susana Luque Rodríguez

Fdo.: José Ramón Álvarez Sáiz



---

**Fwd: Your Submission, JMS-14-644R2**

---

17 de julio de 2014, 20:42

Forwarded Message:

> A:  
> Desde: "Pierre Aimar" <[aimar@chimie.ups-tlse.fr](mailto:aimar@chimie.ups-tlse.fr)>  
> Asunto: Your Submission, JMS-14-644R2  
> Fecha: 17 Jul 2014 17:18:13 +0100  
> -----  
> Ref.: Ms. No. JMS-14-644R2  
> FITTING APPROACH TO LIQUID-LIQUID DISPLACEMENT POROSIMETRY BASED ON THE LOG-NORMAL PORE SIZE DISTRIBUTION  
> Journal of Membrane Science  
>  
> Dear Prof. Calvo,  
>  
> Thank you for accounting for the latest reviewers remarks. I am pleased to tell you that your work has now been accepted for publication in the Journal of Membrane Science.  
>  
>  
> When your paper is published on ScienceDirect, you want to make sure it gets the attention it deserves. To help you get your message across, Elsevier has developed a new, free service called AudioSlides: brief, webcast-style presentations that are shown (publicly available) next to your published article. This format gives you the opportunity to explain your research in your own words and attract interest. You will receive an invitation email to create an AudioSlides presentation shortly. For more information and examples, please visit <http://www.elsevier.com/audioslides>.  
>  
> Thank you for submitting your work to this journal.  
>  
> Best Regards,  
>  
> Pierre Aimar  
> JMS Editor  
> Journal of Membrane Science  
>





























# INDEX

---

---

<b>Abstract.....</b>	<b>VII</b>
<b>1. Introduction.....</b>	<b>1</b>
<b>1.1. Membrane technology .....</b>	<b>3</b>
<b>1.2. Membrane process applications .....</b>	<b>4</b>
<b>1.3. Membrane fouling and cleaning.....</b>	<b>4</b>
<b>1.4. Membrane ageing.....</b>	<b>6</b>
<b>1.5. Thesis work scope .....</b>	<b>8</b>
<b>2. Objectives.....</b>	<b>11</b>
<b>2.1. General considerations .....</b>	<b>13</b>
<b>2.2. Membrane ageing.....</b>	<b>13</b>
2.2.1. Ageing of PES UF membranes under acidic and alkaline cleaning solutions.....	13
2.2.2. Ageing of NF membranes under acidic and alkaline cleaning solutions .....	14
<b>2.3. Membrane characterization.....</b>	<b>14</b>
2.3.1. Fitting approach to characterize UF membranes through LLDP .....	14
<b>2.4. Membrane modification .....</b>	<b>14</b>
2.4.1. Functionalization of UF membranes with strong polyelectrolyte hydrogels for NF applications and the tuning of their performance .....	14
<b>3. Cleaning of UF membranes: A review.....</b>	<b>17</b>
<b>3.1. Introduction.....</b>	<b>19</b>
<b>3.2. Cleaning systems .....</b>	<b>20</b>
3.2.1. Membranes and modules.....	20
3.2.2. Fouling and foulants.....	21
3.2.3. Cleaning and cleaners .....	24
3.2.4. Evaluation of cleaning effectiveness.....	26

<b>3.3. Influence of main cleaning factors .....</b>	<b>35</b>
3.3.1. Process stream filtration conditions.....	35
3.3.2. Membrane properties.....	35
3.3.3. Filtration modules.....	36
3.3.4. Cleaner concentration.....	36
3.3.5. Cleaning time.....	37
3.3.6. Cleaning temperature.....	38
3.3.7. Cleaning solution pH.....	39
3.3.8. Interfacial energy of the cleaner .....	39
3.3.9. Cleaning water quality.....	39
3.3.10. Cross-flow velocity during the cleaning.....	40
3.3.11. Transmembrane pressure during the cleaning .....	41
3.3.12. BW and FF flow .....	41
3.3.13. Importance of the factors and interactions among them.....	42
<b>3.4. Major difficulties in the studying of membrane cleaning.....</b>	<b>43</b>
3.4.1. Possible unreliability of cleaning evaluation parameters .....	43
3.4.2. Lack of cleaning standardized parameters and models .....	46
<b>3.5. Membrane cleaning systems.....</b>	<b>47</b>
3.5.1. Chemical cleaning of NOM.....	47
3.5.2. Chemical cleaning of microbial species .....	48
3.5.3. Chemical cleaning of fouling from wastewaters .....	48
3.5.4. Chemical cleaning of fouling from dairy streams .....	49
3.5.5. Chemical cleaning of BSA .....	51
3.5.6. Chemical cleaning of fouling from oily wastewater.....	52
3.5.7. Enzymatic cleaning remarks.....	52
3.5.8. Physical cleaning protocols .....	53
3.5.9. Performance of several cycles of fouling/chemical cleaning .....	55
<b>3.6. Conclusions .....</b>	<b>56</b>

<b>4. Materials and methods.....</b>	<b>59</b>
<b>4.1. General considerations .....</b>	<b>61</b>
<b>4.2. Materials .....</b>	<b>61</b>
4.2.1. Membranes .....	61
4.2.2. Chemicals .....	61
<b>4.3. Ageing procedures.....</b>	<b>63</b>
4.3.1. Ageing procedures at small scale .....	63
4.3.2. Ageing procedures using a cross-flow system .....	64
<b>4.4. Characterization techniques .....</b>	<b>64</b>
4.4.1. Membrane permeability .....	65
4.4.2. Membrane rejection capability .....	66
4.4.3. ATR-FTIR.....	68
4.4.4. SEM micrographs and EDS .....	68
4.4.5. AFM .....	69
4.4.6. Contact angle.....	71
4.4.7. LLDP.....	73
4.4.8. HPLC.....	73
4.4.9. Gas chromatography - mass spectrometer (GC-MS).....	74
<b>5. Results and discussion.....</b>	<b>75</b>
<b>5.1. Ageing of PES UF membranes under acidic and alkaline cleaning solutions .....</b>	<b>77</b>
5.1.1. Abstract .....	77
5.1.2. Surface composition of the non-aged membranes .....	77
5.1.3. Effects of ageing on Nadir membranes .....	79
5.1.3.1. Membrane performance throughout the alkaline ageing .....	79
5.1.3.2. Membrane performance throughout the acidic ageing.....	81
5.1.3.3. Effects of the ageing conditions on membrane MWCOs.....	82
5.1.3.4. Effects of the ageing conditions on membrane surface composition..	85

5.1.3.5.	<i>Effects of the ageing conditions on membrane structure .....</i>	86
5.1.3.6.	<i>Effects of the ageing conditions on membrane topography .....</i>	88
5.1.3.7.	<i>Effects of the ageing conditions on membrane hydrophobicity.....</i>	90
5.1.3.8.	<i>Discussion.....</i>	90
5.1.4.	Effects of ageing on Koch and GE Osmonics membranes.....	92
5.1.4.1.	<i>Membrane performance throughout the alkaline ageing.....</i>	92
5.1.4.2.	<i>Membrane performance throughout the acidic ageing.....</i>	92
5.1.4.3.	<i>Effects of the ageing conditions on membrane MWCOs.....</i>	94
5.1.4.4.	<i>Effects of the ageing conditions on membrane surface composition.....</i>	95
5.1.4.5.	<i>Effects of the ageing conditions on membrane structure .....</i>	97
5.1.4.6.	<i>Effects of the ageing conditions on membrane topography .....</i>	98
5.1.4.7.	<i>Effects of the ageing conditions on membrane hydrophobicity.....</i>	100
5.1.4.8.	<i>Discussion.....</i>	103
5.1.5.	Effect of temperature on 5 kDa PES membrane ageing.....	104
<b>5.2.</b>	<b>Ageing of NF membranes under acidic and alkaline cleaning solutions.....</b>	<b>107</b>
5.2.1.	Abstract.....	107
5.2.2.	Ageing of the NF90 membrane .....	107
5.2.3.	Ageing of the NF270 membrane .....	112
5.2.4.	Ageing of the NF270 membrane in cross-flow mode .....	118
<b>5.3.</b>	<b>Fitting approach to characterize UF membranes through LLDP .....</b>	<b>121</b>
<b>5.4.</b>	<b>Functionalization of UF membranes with strong polyelectrolyte hydrogels for NF applications with a low fouling prone.....</b>	<b>147</b>
<b>6.</b>	<b>Conclusions .....</b>	<b>169</b>
<b>6.1.</b>	<b>Membrane ageing .....</b>	<b>171</b>
<b>6.2.</b>	<b>Membrane characterization .....</b>	<b>172</b>
<b>6.3.</b>	<b>Membrane modification.....</b>	<b>172</b>
<b>6.</b>	<b>Conclusiones.....</b>	<b>175</b>

<b>7. References .....</b>	<b>181</b>
<b>8. Appendix .....</b>	<b>201</b>
<b>8.1. Program for the data acquisition and permeability determination in the dead-end filtration system (LabVIEW code) .....</b>	<b>203</b>
<b>8.2. List of publications.....</b>	<b>209</b>
<b>8.3. List of figures.....</b>	<b>211</b>
<b>8.4. List of tables.....</b>	<b>215</b>
<b>8.5. Nomenclature .....</b>	<b>217</b>
8.5.1. Symbols.....	217
8.5.2. Greek symbols.....	219
8.5.3. Abbreviations .....	219





## ABSTRACT

---

The aim of this work has been the study of the ageing of ultrafiltration (UF) and nanofiltration (NF) membranes under long-term exposure to acidic and alkaline cleaning solutions. A theoretical model has been developed for the interpretation of liquid-liquid displacement porosimetry (LLDP) results. In addition, membranes with an improved fouling resistance have been prepared by graft copolymerization of a polyelectrolyte hydrogel on the top of an UF membrane.

A comprehensive literature review, concerning the main foulants, the most common cleaners, the consolidated techniques to determine cleaning effectiveness, the parameters affecting such process and the most suitable cleaning procedures as function of the fouling nature, is also included in this work.

The first section of the experimental work is devoted to the ageing of polyethersulfone UF and polyamide NF membranes under long-term exposures to acidic and alkaline conditions. Six commercial UF membranes from Nadir, Koch and GE Osmonics manufacturers and two NF ones from Dow Filmtec were subjected to different concentration nitric acid and sodium hydroxide solutions at several temperatures for long periods of time (up to six months) to simulate the successive cleaning steps throughout their lifetime. Permeability and rejection were used to evaluate membrane performance. Membranes were also characterized in their pristine state and after ageing by physicochemical techniques. Attenuated total reflection Fourier transform infrared and energy-dispersive X-ray spectroscopy were used to analyze surface membrane composition. Scanning electron microscopy, atomic force microscopy and contact angle measurements allowed characterizing structure, morphology and wettability of membrane surfaces, respectively.

The second section of the experimental work describes a new approach to LLDP to characterize UF membranes. Four polymeric UF membranes with molecular weight cut-offs ranging from 5 to 300 kDa were employed. A model membrane defined by a log-normal pore number distribution and a given pore number density was fitted to the actual membrane during the LLDP analysis. Model validation was carried out comparing the pore number and permeance distributions as well as typical LLDP parameters (mean radius, asymptotic permeance, etc.) obtained from the proposed model with those from the traditional Grabar-Nikitine method.

New NF membranes, characterized by a high charge density and a low roughness, thus, low prone to fouling, have been manufactured using UV-photo initiated co-polymerization of strong polyelectrolyte hydrogels on the surface of PES membranes. The effects of the functional monomer concentration, the cross-linker fraction, the irradiation intensity and the modification time on the degree of grafting, composition, structure and membrane performance of the hydrogel membranes were studied.



## RESUMEN

---

El objetivo de este trabajo ha sido el estudio del envejecimiento de membranas de ultrafiltración (UF) y nanofiltración (NF) expuestas a disoluciones ácidas y alcalinas de limpieza. Se ha desarrollado un modelo teórico para interpretar los resultados de la porosimetría de desplazamiento líquido-líquido (LLDP). También se han preparado membranas resistentes al ensuciamiento por co-polimerización de hidrogeles electrolíticos sobre membranas de UF.

Se incluye una revisión bibliográfica detallada sobre los principales agentes de ensuciamiento, los agentes de limpieza más comunes, las técnicas consolidadas para determinar la eficacia de limpieza, los parámetros que afectan a los tratamientos y los procedimientos de limpieza más adecuados en función del tipo de ensuciamiento.

La primera sección del trabajo experimental se centra en el envejecimiento, bajo condiciones extremas de pH, de membranas de UF (hechas de polietersulfona) y de NF (hechas de poliamida). Se sometieron seis membranas comerciales de UF (de Nadir, Koch y GE Osmonics) y dos membranas de NF (de Dow Filmtec) a disoluciones con distintas concentraciones de ácido nítrico e hidróxido sódico, a distintas temperaturas y periodos de tiempo largos (hasta seis meses) para simular las sucesivas operaciones de limpieza a lo largo de su vida útil. El comportamiento de las membranas se evaluó mediante medidas de permeabilidad y de retención. Se realizaron caracterizaciones fisicoquímicas de las membranas envejecidas y en su estado original. La composición superficial de las membranas se analizó por ATR-FTIR y EDS. La estructura, la morfología y la hidrofiliidad de las membranas se estudiaron mediante caracterizaciones por SEM, AFM y medidas de ángulos de contacto, respectivamente.

En la segunda sección del trabajo experimental se propone un método de interpretación de las medidas mediante LLDP para caracterizar membranas de UF. Se estudiaron cuatro membranas poliméricas de UF con tamaños de corte entre 5 y 300 kDa. El comportamiento de las membranas modelo, definidas por una distribución log-normal del número de poros y una densidad de poros total dada, se ajustó al de las membranas reales durante el análisis por LLDP. La validación del modelo se llevó a cabo comparando las distribuciones de número de poros y de permeabilidad así como otros parámetros típicos (radios medios, permeabilidad asintótica, etc.) obtenidos a partir del modelo con los resultados procedentes del método tradicional desarrollado por Grabar-Nikitine.

Se han desarrollado también nuevas membranas con baja tendencia al ensuciamiento, caracterizadas por una elevada carga y una baja rugosidad, mediante la modificación de membranas de UF por co-polimerización de hidrogeles electrolíticos inducida por radiación ultravioleta. Se investigaron los efectos de la concentración del monómero funcional, la concentración del reticulador, la intensidad de la radiación, y el tiempo de modificación sobre el grado de polimerización, la composición, la estructura, y el comportamiento funcional de la membrana de hidrogel.



# **1. Introduction**

---

---



## 1.1. Membrane technology

In chemical industry, any process, regardless of its nature and complexity, can be divided into individual operations which can be grouped in different categories according to their principles. These groups are known as unit operations in the field of chemical engineering.

Membrane technology covers a great variety of separation processes which are all characterized by the use of a selective barrier (the membrane) to achieve the separation. Membrane processes can be classified according to the driving force that governs the transport: pressure, concentration, partial pressure, electrical potential or temperature. Each of them can be considered as a single unit operation and so, are based on the same basics independently of the nature of the industry in which are encompassed.

Membranes can be classified according to different criteria: chemical nature, internal structure, configuration and transport mechanism. Therefore, there are natural and synthetic membranes which, in turn, can be polymeric (organic) or inorganic. Following the structural criterion, it is possible to differentiate between porous and dense membranes and at the same time they can be defined as symmetric or asymmetric (usually composite membranes). Depending on how membranes are assembled, membranes can be divided into plate-and-frame, tubular, spiral or hollow fiber modules. The mechanism followed by the solutes to pass through the membrane leads to the last classification in which it is possible to identify viscous flow (Darcy's law), migration (Nernst-Planck equations) and diffusion (Fick's law).

Focusing the discussion on pressure driven membrane processes, filtrations can be classified into microfiltration (MF), ultrafiltration (UF), nanofiltration (NF) or reverse osmosis (RO) operations in ascending order of solute rejection capability. Their typical operation conditions and separation capabilities are collected in **Table 1.1**. [1, 2].

**Table 1.1.** Typical operation conditions and targets of pressure driven membrane processes.

Process	Pressure (bar)	Flux (L/hm <sup>2</sup> )	Solute size	Solute target
Microfiltration	0.1 - 5	100 - 1000	0.1 - 10 $\mu\text{m}$	Particles, biological substances...
Ultrafiltration	1 - 10	10 - 200	1 - 1000 kDa	Proteins, colloids, particulate matter...
Nanofiltration	5 - 30	10 - 100	0.1 - 1 kDa	Divalent ions, solvent recovery...
Reverse Osmosis	10 - 100	5 - 100	< 0.1 kDa	Monovalent ions, dissolved solids...



## **1.2. Membrane process applications**

---

Membrane technology has been widely and successfully applied in many industrial applications. For instance, contemporary water problems such as potable water scarcity or waste water treatment can be effectively addressed using the proper set of MF, UF, NF and RO processes [2]. Membrane technology is also applied in other areas such as the food industry. Juice processing, starch recovery, brine cleaning in fish industry and especially, pre-concentration of milk for cheese production and fractionation of cheese whey for protein concentrates in the dairy industry are examples in which filtration processes are also applied [2, 3]. Other application fields of pressure driven membrane processes involve pharmaceutical and biotechnology industries as well as biomedical applications.

Establishment of membrane technology in industrial applications has been feasible due to their advantageous properties. Separation and purification processes require to optimize mass and energy consumptions. In membrane technology, separation is accomplished by consuming pump energy which leads to low energy requirements since heating energy for phase change is avoided. No extra components are added and so, no additional separation operations are needed. Properties of streams and products remain stable. Scaling up is relatively easy. Their high operational flexibility allows meeting product specifications even during the treatment of feeds with high composition variability. The wide range of available membranes makes this technology have a high selectivity. All these properties explain why membrane technology has been widely implemented and why is becoming increasingly important.

However, there are still limitations which will have to be faced in the near future to improve and expand the use of membrane technology at industrial scale. For instance, investment costs associated to membrane manufacturing are still quite high, chemical incompatibility between membranes, seals or glues and feeds make impossible their use in some applications, membrane temperature limitations may cause the same result, etc. Among all limitations, fouling is definitively the most restrictive one and it has to be carefully studied in order to decide whether membrane technology is feasible or not.

## **1.3. Membrane fouling and cleaning**

---

Fouling is a common shortcoming for all membrane processes. It leads to the worsening of membrane performance with time in terms of permeate flux and retention capability while the other operating parameters remain constant. Fouling is generated as consequence of the adsorption of foulants on membrane surface, membrane pore blocking and/or cake formation through a layer by layer deposition [4]. Unlike concentration polarization phenomenon, fouling is irreversible and so, physical and chemical changes in membrane properties are not spontaneously recovered after the filtration. Thus, a subsequent cleaning step has to be conducted to restore membrane performance.

Fouling nature is generally classified into inorganic/scaling, organic, particulate or biological [5]. Parameters affecting fouling rate include membrane properties (material, morphological structure, surface properties...), feed properties (composition, concentration, pH...) and operational conditions (transmembrane pressure (TMP), cross-flow velocity, temperature...) [6]. The effect of fouling on flux decline was comprehensively studied leading to different models which predict the type of fouling (complete pore blocking, internal pore blocking, partial pore blocking and/or cake formation) [4]. At present, as fouling is practically unavoidable, most efforts are put into the reduction of this phenomenon through direct and indirect methods. Some examples of direct ones are pulsed flow, ultrasounds, rotating blades and vibrating systems, whereas indirect methods include feed pre-treatments, optimization of operating conditions and membrane modifications to reduce their fouling propensity [4].

In return to fouling, cleaning is defined as those physical and chemical treatments whose target is to break the cohesive and adhesive bonds that keep foulants attached to membrane pores and surface [5]. Examples of physical cleaning are forward flushing (FF), backwashing (BW) and ultrasounds, whereas chemical cleaning can be conducted with alkalis, acids, surfactants, chelatants, oxidizers, enzymes or disinfectants [5]. Optimization of cleaning protocols is a complex process which has to account for process stream nature, membrane characteristics, hydrodynamics, water quality, type of cleaner, concentration, pH, temperature, time and frequency [5].

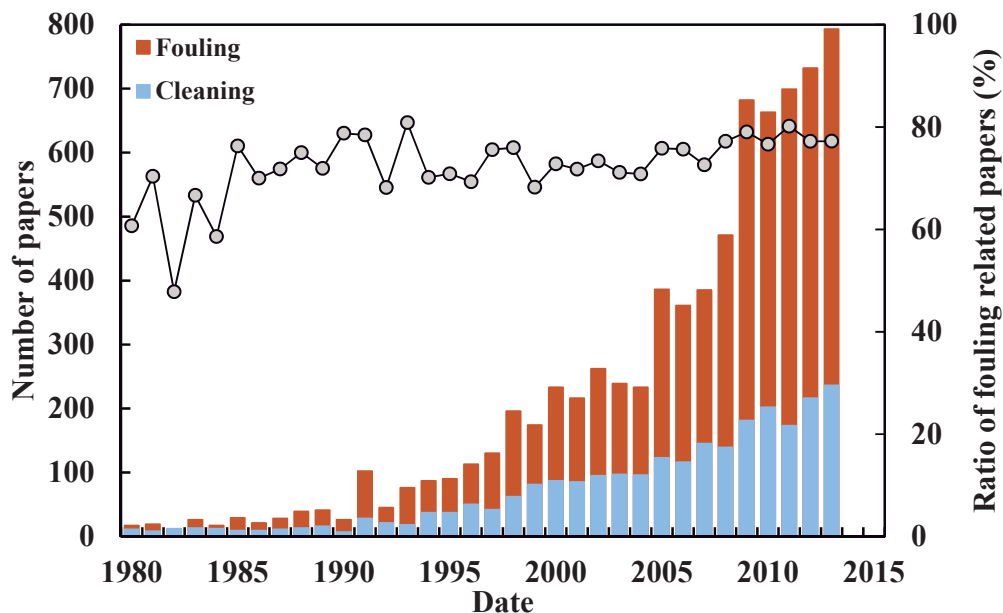


**Fig. 1.1.** Number of publications in the past three decades related to membrane fouling and cleaning in pressure driven processes according to Scopus (July 2014). Search criteria contained the words fouling or cleaning in the title, keywords or abstract.

To date, membrane fouling has been exhaustively studied with the aim of understanding fouling basics. The great deal of works in this area contrasts with the relatively low number of publications related to membrane cleaning (**Fig. 1.1.**). As consequence, cleaning fundamentals are not so well known and so, cleaning protocols are not standardized at present time. In fact, in many researches and even in industrial applications, the aim of membrane cleaning is not yet defined as the recovery of membrane properties but, as the recovery of membrane performance. This definition together with the current trend of following manufacturer's guidelines leads to set cleaning procedures that are conducted under excessive dosages, temperatures and exposure times. In the long term, these hard conditions speed up the worsening of membrane properties (process commonly so called membrane ageing), shortening membrane lifetime [6].

#### **1.4. Membrane ageing**

---

Membrane ageing comes from the chemical and physical membrane degradation caused by the successive filtration (fouling)-cleaning cycles. Membrane lifetime (given by the time from which membrane properties cannot be recovered and so, performance specifications are not met) depends on how fast and severe degradation takes place during each step. Even though both fouling and cleaning contribute to membrane ageing, it is known that cleaning step contribution is usually higher, especially when it is not optimized [6]. The effect of foulants on membrane ageing has been easily assessed in many works using directly process streams but however, ageing due to cleaning has been always studied as a part of fouling-cleaning studies. Therefore, due to the complex interactions among membranes, foulants and cleaners, the contribution of the last ones has not been clearly isolated.

For instance, concerning UF membranes, sodium hypochlorite (NaClO) is the most studied ageing chemical because it is widely used as disinfectant and it has a strong oxidation character which leads to polymeric membrane degradation [7]. Rouaix *et al.* and Regula *et al.* [8, 9] have recently reviewed membrane ageing studies performed with this chemical. However, ageing has been considered less extensively for acidic [10-13] and alkaline [14-16] reagents.

Paugam *et al.* [10, 11] and Diagne *et al.* [12] studied the cleaning with nitric acid (HNO<sub>3</sub>) -alone or combined with other cleaners- of polyethersulfone (PES) membranes fouled with milk resulting in water flux recoveries without fouling removal. This phenomenon was attributed to a decrease in the membrane hydrophobicity caused by the interaction between HNO<sub>3</sub> and proteins.

Zhu and Nystrom [14] observed that the zeta potential of commercial polysulfone ultrafiltration membranes became more negative after a pretreatment with sodium hydroxide (NaOH), and that the pure water flux was slightly higher than that of the virgin membranes. Furthermore, after a cycle of pretreatment/fouling with bovine serum albumin/cleaning, the attenuated total reflection Fourier transform infrared (ATR-FTIR) spectra showed the emergence

of a new peak, indicating that NaOH reacted with the PES active layer. After twenty cycles of fouling with spent sulfite liquor followed by a cleaning step, using a membrane made of PES, Weis *et al.* [15] reported an increase in the contact angle and a progressive decrease in the zeta potential and in the permeate flux cycle upon cycle. Similar decrease in permeability and increase in contact angle was reported by Tian *et al.* [16], after the alkaline cleaning with NaOH of polyvinyl chloride (PVC) membranes fouled with river water. However, when more comprehensive membrane characterization was carried out through atomic and electron microscopies, it was found that foulants were extensively removed and therefore, the reduction in permeability was attributed to an increase in hydrophobicity.

Often, membrane degradation as consequence of the ageing is determined by comparing the permeability and sometimes the molecular weight cut-off (MWCO) of the membrane before and after exposure to the chemical reagent [17-22]. Nevertheless, other membrane surface characterization methods have also been successfully employed to determine the membrane condition before and after the treatment.

Some of these techniques are the scanning electron microscopy (SEM) and the atomic force microscopy (AFM), which provide information of the membrane surface morphology. For instance, Väisänen *et al.* [23] used SEM images to evaluate the state of several UF membranes after being fouled with ground wood mill circulation water and then cleaned with Ultrasil 11, Libranone 960 or NaOH, concluding that foulant deposits were only partially removed after the cleaning.

Another physicochemical technique widely employed is the above mentioned ATR-FTIR spectroscopy, which provides an insight of the chemical functional groups of the membrane surface. For instance, Bégoïn *et al.* [13] found no changes in the ATR-FTIR spectra of PES UF membranes aged with 1.0 M HNO<sub>3</sub> and 0.003 M NaOH. However, their work was exclusively focused on the active layer. Furthermore, this technique was also used to characterize cleaning performance, by relating normalized peaks associated to a given foulant before and after the cleaning [24, 25]. Nevertheless, if the membranes are not resistant to cleaners, the changes in the spectra could be wrongly associated to the foulant.

Another characterization parameter, which has also been considered in cleaning and ageing studies, is the contact angle, whose value can be related to the hydrophobicity of the membrane [21, 22].

Concerning NF membranes, a great effort has been made to understand and optimize cleaning procedures in the last few years. Most of these cleaning studies have been carried out for specific applications, such as surface water treatment [26-28], effluents from membrane bioreactors [29], streams from water recycling applications [30], pulp and paper water [31], etc. However, the impact of cleaning agents on the integrity of the membrane has not been usually considered until

recent years, when an increasing number of studies focused on the effects of cleaning agents on NF membranes have been published.

Nilsson *et al.* [32, 33] studied the effect of the order of acidic and alkaline cleanings, on several membranes including the NF90 and NF200 Membranes were subjected to commercial cleaners at 0.5 wt. % to simulate the alkaline and the acidic cleanings, respectively. NF90 membrane did not show differences in permeability and rejection regardless of the acidic and alkaline cleaning order at any tested feed temperatures. However, NF200 showed a slight increase in permeability and a decrease in potassium chloride (KCl) rejection when the last cleaning step was the alkaline at all feed temperatures. Al-Amoudi *et al.* [34, 35] studied the effects of NaOH, hydrochloric acid (HCl) and some other cleaning agents on several virgin NF membranes by soaking them in the cleaning solutions overnight. By means of permeability, zeta potential and positron annihilation spectroscopic measurements, they found that most of the cleaning agents caused an increase in the pore size of the virgin membranes and thus, in the permeability. In addition, they found that depending on the cleaning agent, changes in zeta potential values were more or less significant. Similar results were found by Simon *et al.* [36], who found an increase in the pore size of the NF270 membrane which led to an increase in permeability and a decrease in rejection when it was soaked in NaOH solutions at pH 11.5 containing ethylenediaminetetraacetic acid (EDTA) and sodium dodecyl sulfate (SDS) at 35°C for 18 h. However, NF90 membrane did not show such increase in pore size which was attributed to its higher active layer thickness. Another study was carried out by the same group [37] with the NF270 membrane employing different temperatures. NF270 membrane permeability increased with temperature while the effects of rejection were variable depending on the solute marker. However, there was not any change in the membrane charge or in its composition according to the ATR-FTIR spectra when subjected to NaOH (pH 11.5). Manttari *et al.* [38] studied the effect of pH on the filtration efficiency of NF membranes relating performance to charge effects due to the presence of carboxylic groups on the membrane active layer. Also Nilsson *et al.* [39] studied the effect of pH combined with salt concentration and temperature on NF membrane performance.

However, as stated previously, most of these studies concerning the ageing of UF and NF membranes have been performed as a part of a wider research topic involving fouling-cleaning cycles. Therefore, it is difficult to establish the actual influence of the cleaning agents on the membranes.

## **1.5. Thesis work scope**

---

The main objective of this Thesis work has been the study of membrane ageing due exclusively to cleaning agents. Previously to develop every point of the research, objectives are

individually defined and a comprehensively review about UF membrane cleaning, easily extendable to NF membranes, is presented.

The aim of the first experimental part, which is the core of the Thesis, was to study the ageing of UF and NF membranes under long-term exposures to acidic and alkaline cleaning solutions. This work was focused on the effects of the different ageing conditions on membrane performance in terms of permeability and rejection capability and on the physicochemical changes of the membranes.

As a result of the experimental work carried out in the first section, a model to interpret liquid-liquid displacement porosimetry (LLDP) results was developed based on a theoretical log-normal distribution for the number of pores, leading to the second part of the Thesis.

Finally, in the same context of membrane fouling, cleaning and ageing research, an additional target was defined concerning one of the above explained indirect methods to reduce membrane fouling. PES UF membranes were covered with highly charged polyelectrolyte hydrogels through the UV-photo initiated graft polymerization technique, leading to NF membranes less prone to fouling.



## **2. Objectives**

---

---





## **2.1. General considerations**

---

The core of this Thesis work was the study of membrane ageing as consequence of cleaning agents. Complementarily to these ageing studies, a theoretical model was developed to process LLDP analysis results. As an additional goal, the feasibility of membrane modification through graft polymerization technique in order to obtain NF membranes with a less fouling prone was studied.

This Thesis involves a comprehensive bibliographic review about UF membrane cleaning which is included in “chapter 3”. The aim of this chapter is to describe the main foulants, most common cleaners, consolidated techniques to determine cleaning effectiveness, the parameters affecting the process and the most suitable cleaning procedure as function of fouling nature. Even though the study was focused on UF membranes, general considerations can be easily extrapolated to NF membranes.

All the materials and procedures which were used in the research of UF and NF membrane ageing are comprehensively described in “chapter 4”. The results of this Thesis and the discussion are gathered in “chapter 5” which in turn, is divided into four sections (UF membrane ageing, NF membrane ageing, modelling of LLDP results and UF membrane functionalization to obtain NF membranes) whose objectives are described in next sections.

## **2.2. Membrane ageing**

---

### **2.2.1. Ageing of PES UF membranes under acidic and alkaline cleaning solutions**

The first section of “chapter 5” involves the ageing of PES UF membranes under long-term exposures to acidic and alkaline conditions. Six commercial membranes from Nadir, Koch and GE Osmonics manufacturers were subjected to HNO<sub>3</sub> and NaOH solutions at different concentrations and temperatures for long periods of time to simulate the successive cleaning steps throughout their lifetime. Permeability and MWCO determinations were conducted to evaluate membrane performance. Membranes were also characterized in their pristine state and after the ageing procedures by means of physicochemical techniques. ATR-FTIR and energy-dispersive X-ray spectroscopy (EDS) were used to analyze surface membrane compositions. SEM, AFM and contact angle measurements allow characterizing structure, morphology and wettability of membrane surfaces, respectively.

The aim of this section is to describe the effects of the different ageing conditions on the permeability and MWCO of the membranes as function of time as well as to determine those physicochemical changes which explain membrane performance.

### **2.2.2. Ageing of NF membranes under acidic and alkaline cleaning solutions**

The second section is focused on the ageing of polymeric NF membranes under the exposure to acidic and alkaline cleaning solutions. The NF90 and NF270 membranes from Dow Filmtec were soaked in HNO<sub>3</sub> and NaOH solutions with different concentrations at 50°C for a long period of time in order to simulate their ageing over successive cleaning cycles. The goal of this part was to determine the effects of the cleaners on membrane properties by means of ATR-FTIR and SEM techniques and correlate their degradation to their performance in terms of permeability and rejection of charged and uncharged molecular markers throughout the ageing.

## **2.3. Membrane characterization**

---

---

### **2.3.1. Fitting approach to characterize UF membranes through LLDP**

The third section describes a new approach to process LLDP results in order to characterize UF membranes. Four polymeric UF membranes with MWCOs ranging from 5 to 300 kDa were employed. The goal of this part was to develop a model membrane (defined by a log-normal pore number distribution and a given pore number density) whose behavior resembles actual membrane performance throughout the LLDP analysis. Model validation was carried out comparing pore number and permeance distribution as well as typical LLDP parameters obtained from the proposed model with those from the traditional Grabar-Nikitine method.

## **2.4. Membrane modification**

---

---

### **2.4.1. Functionalization of UF membranes with strong polyelectrolyte hydrogels for NF applications and the tuning of their performance**

Modification of PES UF membranes for NF applications via UV-initiated graft polymerization of a strong polyelectrolyte hydrogel is studied in the last fourth section in which results are shown as two published papers.

The aim of this work was to develop a low fouling prone NF membrane characterized by a high charge density and a low roughness. Vinyl sulfonic acid (VSA) and N,N'-methylenebisacrylamide (MBAA) were employed in the modification as the functional and the cross-linker monomers, respectively. In the first paper, the effects of VSA concentration, cross-linker fraction, irradiation time and irradiation intensity on the gravimetric and spectrophotometric (based on ATR-FTIR measurements) degree of polymerization were evaluated. Modified membranes under different conditions were characterized by X-ray photoelectron spectroscopy (XPS), AFM and ion exchange capacity measurements. Besides, membrane performance as function of cross-linker fraction was assessed in terms of permeability and rejection of charged and

uncharged molecular markers. Membrane performance stability was also evaluated under increasing salt concentrations and under extreme pHs.

The goal of the second paper of this section was to improve the performance of the polyelectrolyte hydrogel composite membranes modifying VSA concentration, cross-linker fraction, irradiation time and dose and MWCO of the UF support membranes. Permeability and rejection measurements of single and mixed salt solutions as well as uncharged solutes were used to characterize modified membranes. A scale up of the modification process was also conducted, including performance tests. Last, zeta potential measurements, ATR-FTIR and SEM techniques were used for a more comprehensive characterization.



### **3. Cleaning of UF membranes: A review**



### 3.1. Introduction

---

Although there are many examples of membranes and membrane separation processes in the nature and most of them are critical to the existence of life, development of synthetic membranes and their application at industrial scale is relatively recent. Nonetheless, thanks to its advantageous features, this short period of time was not a problem in the development of applications in various important sectors as water desalination, waste water treatment, food industry (processing of dairy, milk, fruit juices, wine and beverages), biotechnology and pharmaceutical industries, etc. [2].

The entry of membrane applications in these industrial sectors has been possible due to their great properties: high performance, simplicity, operational flexibility, high selectivity, low energy requirements, stability in long-term operations, easy size-up, process control, etc. These properties have led to the development of a wide variety of specific processes as molecular separations, fractionation, clarification, purification, etc. but not all of them related only to separation processes, as could be emulsification and crystallization operations.

However, membrane processes also present some drawbacks which restrict their use. From an operational point of view, concentration polarization and fouling are the major limitations to deal with. Both phenomena lead to a lower permeate flux during the feed filtration ( $J_F$ ) with respect to the initial flux with the pure solvent working at constant operating conditions.

Concentration polarization is the result of a balance among the convective transport of solutes to the membrane carried by the solvent flux, solute accumulation at the membrane due to its rejection and back-diffusion of solute into the bulk phase driven by the established concentration gradient [40]. This phenomenon is inevitable but reversible. Therefore, pure solvent permeate flux is spontaneously restored at the end of the filtration.

On the other hand, fouling is caused by the solutes which get adsorbed on membrane surface, blocked into membrane pores and/or formed a cake through a layer by layer deposition [4]. This phenomenon reduces the pure solvent water flux after the filtration and eventually makes necessary to clean the membrane to restore its original properties.

It has to be pointed out that UF processes can be also performed keeping  $J_F$  constant, and in that case concentration polarization and fouling makes the TMP increase with time from its initial value at time zero ( $TMP_0$ ) which is equivalent to the value when filtering the pure solvent with the pristine membrane ( $TMP_{w0}$ ).

Fouling has been widely studied. However, the general approach has not been focused on the development of cleaning strategies, as probes the fact that there is considerably less papers dedicated to membrane cleaning than to fouling [41]. According to Liu *et al.* [42], the inadequate



address of the issue is due to the still poor understanding of fouling basics (despite the high research effort), the common employment of cleaning protocol recommended by membrane manufacturers and the fact that some cleaners are patents whose exact composition is unknown making difficult the compression and/or modification of their cleaning abilities.

As previously stated, UF is the most employed pressure-driven membrane separation process at industrial level nowadays [43]. It is usually used to retain species such as particles, bacteria, viruses, colloidal matter, macromolecules and heavy metal complexes that are present in liquid streams [44]. Separation mechanism is based on sieving effects and particles are separated according to their dimensions [2]. UF membranes have nominal pore sizes (NPS) between 1 and 10 nm, which correspond to MWCOs from 0.3 to 500 kDa [45]. Therefore, inorganic salts and small organic molecules freely pass through the pores. Occasionally, membranes with NPS from 20 to 40 nm are also considered UF membranes [46-50].

Previous reports gathering information about membrane cleaning were found [5, 40, 41, 51, 52], including one from Regula *et al.* [53] which specifically addresses UF membrane fouling, cleaning and ageing. Nonetheless, the objective of this study was to develop a comprehensive literature review focused specifically on the cleaning protocol studies carried out over the last years, tackling the issue from different perspectives.

This chapter gather all physical and chemical cleaning procedures described in the literature for polymeric UF membranes.

Firstly, all the information related to typical foulants and cleaners are gathered as well as the main parameters defined in the literature to evaluate cleaning effectiveness in an attempt to unify their nomenclature. Selection of the most suitable cleaning procedure as well as its effectiveness depend on many factors such as foulant and fouling conditions, membrane material, cleaner concentration and/or pH, cleaning time and temperature, and the interactions among them. All of them are carefully analyzed throughout this comprehensive review in order to give guidelines to approach cleaning procedures successfully. Shortcomings and difficulties in the study of cleaning protocols are also pointed out. Finally, since fouling nature is the major factor to take into account when deciding the cleaning strategy, the main and most effective cleaning protocols applied to UF membranes as function of foulants are presented in a systematic study.

## **3.2. Cleaning systems**

---

---

### **3.2.1. Membranes and modules**

Researches on membrane processes are generally carried out using flat, tubular, spiral, hollow-fibers membranes. Filtrations are operated in either cross-flow (CF) or dead-end (DE) mode. Main UF membrane materials are polysulfone (PS<sub>u</sub>) and PES, combined occasionally with

polyvinylpyrrolidone (PVP) or dichlorodiphenyl sulfone-phenolphthalein (DCP). Other typical materials are regenerated cellulose (RC), cellulose acetate (CA), cellulose ester (CE), fluoropolymer (FP), polyamide (PA), polyacrylonitrile (PAN), polyvinylidene fluoride (PVDF), PVC and cellulose derivatives.

### 3.2.2. Fouling and foulants

**Table 2.1** summarizes applied cleaning procedures, cleaning evaluation techniques and membrane materials as function of the filtered stream which caused the fouling. In its construction, 126 papers [10-12, 15, 16, 19, 23-25, 46-50, 54-165] were found to be related to polymeric UF membrane cleaning or with interesting remarks on the matter.

**Table 3.1.** Summary of all the publications focused on the cleaning of polymeric UF membranes as function of the feed stream.

Filtered stream	Cleaning treatment	Evaluation	Membrane material	Reference
Surface water with NOM or solutions with model components	FF, BW, air assisted BW and ultrasounds with FF and BW Alkaline, acidic, surfactant, chelating, oxidizer and enzymatic agents, together with formulated cleaners	J measurements	PS <sub>u</sub>	[16, 54-74]
		TMP measurements	PES	
		SP	PES-PVP	
		Contact angles	CA	
		FTIR	PVC	
		SEM		
		AFM		
		Turbidity		
		Rejection		
		pH		
Seawater	BW and air assisted BW	J measurements	PS <sub>u</sub>	[47-50, 75]
		TMP measurements	PAN	
			PVDF	
Water with colloids	FF, BW and air assisted BW	TMP measurements	PS <sub>u</sub>	[76-79]
		Turbidity	PES	
		Suspended matter	CE	
			Cellulosic	
Surface water with high microbiological content or solutions with model components of EPS	FF and BW Alkaline, acidic, chelating, oxidizer and disinfectant agents, together with formulated cleaners	J measurements	CA	[80-90]
		Rejection	PS <sub>u</sub>	
		FTIR	PAN	
		SEM	PVC	
		EDX	PVDF	
		AFM		

Filtered stream	Cleaning treatment	Evaluation	Membrane material	Reference
Effluents of wastewater treatment plants	FF, BW	J measurements	PES	[46, 91-94]
	Alkaline, acidic, oxidizer and enzymatic agents, together with formulated cleaners	TMP measurements SEM	CA	
Milk and skim milk	Ultrasounds, FF Alkaline, acidic, surfactant, chelating, oxidizer and enzymatic agents, together with formulated cleaners	J measurements	PS <sub>u</sub>	[10-12, 25, 95-104]
		SP	PES	
		Contact angles	CA	
		FTIR		
		SEM		
Whey	Ultrasounds Alkaline, acidic, surfactant, enzymatic and disinfectant agents, together with formulated cleaners	J measurements	PS <sub>u</sub>	[105-115]
		SEM	PES	
		MALDI-MS		
		Lowry method		
		Electrophoresis		
Whey protein	Alkaline, acidic, surfactant, enzymatic agents, together with formulated cleaners	J measurements	PS <sub>u</sub>	[23, 116-120]
		Lowry method	PES	
		Electrophoresis	RC	
			PA	
BSA alone or mixed with beta-lactoglobulin (bLG)	Ultrasounds Alkaline, acidic, surfactant, chelating, oxidizer and enzymatic agents, together with formulated cleaners	J measurements	PS <sub>u</sub>	[19, 24, 111, 116, 121-131]
		SP and ZP	PES	
		Contact angles	PVDF	
		FTIR	PS <sub>u</sub> -PVDF	
		SEM		
		MALDI-MS		
		Lowry method (modified)		
		Electrophoresis		
		Membrane staining		
		Fluorescent microscopy		
Proteinaceous feed	Alkaline, acidic, oxidizer and formulated agents	J measurements SEM	PS <sub>u</sub>	[132, 133]
Abattoir effluents	Surfactant and enzymatic agents	J measurements Contact angle Protein content Lipid content	PS <sub>u</sub>	[134-136]
Peptone	Ultrasounds	J measurements	PS <sub>u</sub> PAN	[137, 138]

Filtered stream	Cleaning treatment	Evaluation	Membrane material	Reference
Paper mill related wastewater	BW, ultrasounds Alkaline, acidic, surfactant and enzymatic agents, together with formulated cleaners	J measurements	PS <sub>u</sub>	[15, 23, 139-145]
		TMP measurements	PES	
		Rejection	RC	
		ZP	CA	
		Contact angles	FP	
		FTIR		
		SEM		
		EDX		
		AFM		
		Ultrasounds		
Black tea or model components	Alkaline agent	J measurements	PS <sub>u</sub>	[146-148]
		ZP	RC	
		Contact angles	FP	
		FTIR		
		SEM		
Wastewater from banknote printing works	Alkaline, acidic and chelating agents, together with formulated cleaner	J measurements	PS <sub>u</sub> -DCP	[149, 150]
		SEM-EDX		
Emulsions of oil in water or related	Ultrasounds Alkaline, acidic, surfactant, chelating and oxidizer agents, together with formulated cleaners	J measurements	PS <sub>u</sub>	[151-155]
		XPS	PAN	
		SEM	PVDF	
		EDX		
Fermentation broths	FF, BW, ultrasounds Alkaline, acidic, surfactant and oxidizer agents, together with formulated cleaners	J measurements	PS <sub>u</sub>	[156-158]
		SEM	PES	
		EDX	PVDF	
		Fluorescence spectroscopy		
Others	FF, BW, ultrasounds Alkaline, acidic, surfactant, chelating, oxidizer and enzymatic agents, together with formulated cleaners	J measurements	PS <sub>u</sub>	[159-165]
		FTIR	PES	
		SEM	PA PVDF	

Most studied areas are those concerning surface water, milk, whey and bovine serum albumin (BSA). Therefore, main foulants involved in UF processes are natural organic matter (NOM) and proteins.

NOM is a complex mixture of macromolecular components, such as polysaccharides and humic substances [66], neutral or negatively charged at the pH of the river and canal waters [62]. It is known that heavy metals and pesticides make it more stable and denser [58], and that the presence of Ca<sup>2+</sup> facilitate its adsorption on polymeric UF membranes [62]. Researchers do not

agree about the role of the hydrophobic and hydrophilic fractions in this adsorption. Nonetheless, it is likely due to the differences in composition of NOM from different sources and hence the different interactions with membranes [65]. NOM is usually accompanied by microorganisms and colloidal particles in surface water. First ones are able to form biofilms or releasing extracellular polymeric substances (EPS), which modify the membrane performance. The second ones are accumulated on the polymeric surface and can get inside [5].

Proteins are very difficult to remove because of their labile and dynamic nature which depends on the pH, temperature and interactions with other agents [5]. According to D'Souza and Mawson [40], the key phenomena in UF membrane fouling by dairy solutions is linked to protein adsorption, protein deposition layer by layer and deposition of fats and minerals. Lactose and lipids are generally considered to have a lesser importance in membrane fouling and they are more prone to foul membrane surface than the pores. Moreover, fouling associated to minerals takes place in a higher degree when filtering whey than milk due to the stabilizing influence of the casein micelles [95]. In this regard, Rabiller-Baudry *et al.* [25] found that, after filtering diluted skim milk, proteins, minerals (salts) and lactose were adsorbed on their PES membrane, but after a water rinsing only proteins remained.

### 3.2.3. Cleaning and cleaners

Cleaning can be physical or chemical [5]. Physical methods employ mechanical forces to dislodge and remove foulants from the membrane surface, such as FF, BW, ultrasounds and BW combined with air or ultrasounds. They are often adopted in UF for drinking water treatments. The basics of these physical techniques are described below.

- **FF**: It is performed by passing wash water, or permeate as feed, instead of the real feed stream in CF filtration mode, but usually with a higher flow and without permeation. This operation allows removing loosely bounded foulants from the membrane surface.
- **BW**: It consists in passing wash water (usually, the permeate itself) for a few seconds from the permeate side to the feed side at given time intervals with the aim of removing the foulants present on membrane surface and inside the pores. Two important modifications of this technique are the air assisted BW, that uses air in the feed side for increasing the shear stress at the membrane surface [48, 64, 76, 79, 86] and the reverse-pressure BW, consisting in consecutive FF and very short reverse-pressure pulsations (spikes of up to -80 kPa, which level off after a few seconds to -40 kPa), responsible of reversing permeate direction through the membrane wall [58]. In this introduction, it has not been considered the process known as “backpulsing” [166, 167] because, despite its similarities with BW, it is more a fouling prevention method in which flow reversal occurs for fractions of second every few seconds, rather than a cleaning procedure.

- **Ultrasounds:** When ultrasounds are irradiated to the membrane through a liquid medium, acoustic streaming (steady current caused by the absorption of the waves), cavitation (formation, growth and sudden collapse of micro bubbles) and turbulence take place. If these phenomena overcome the interactions between the foulant and the membrane, the foulant will be removed from the polymeric surface [103, 110, 131]. Ultrasounds can be combined with FF and BW [72, 141] or with chemical cleaners [103, 109, 110, 131, 153, 158, 160, 163].

On the other hand, chemical cleaning fundamentally involves heterogeneous reactions between the foulant layer and the cleaner. Cleaners are classified according to their nature into alkaline, acidic, surfactant, chelating, oxidant, enzymatic or disinfectant. Besides the non-formulated cleaning solutions, there are also “commercial formulated cleaners”, containing a mixture of several of these reagents, e.g. P3 Ultrasil 10 (alkali + surfactant + chelant), Ultrasil 75 (acid composition), P3 Ultrasil 53 (enzymatic mixture), Terg-A-zyme (TAZ, constituted by enzymes and surfactants) or oxonia active (oxidant + acids). The main chemical agents are listed below.

- **Alkaline or caustic reagents:** NaOH and potassium hydroxide (KOH) promote the hydrolysis of proteins and polysaccharides, the saponification of fats and lipids and the peptization of colloidal particles [5]. Alkaline cleaners increase the pH and so, the negative charge of protein deposits which disrupts foulant packaging [11]. They also dissolve weakly acidic organic matter and expands NOM molecules making the mass transfer processes easier [41].
- **Acidic reagents:** Mineral acids, such as HCl, HNO<sub>3</sub> and sulfuric acid (H<sub>2</sub>SO<sub>4</sub>), are commonly used for dissolving inorganic salts or oxide films. Phosphoric acid (H<sub>3</sub>PO<sub>4</sub>), oxalic acid and citric acid are less aggressive, but also have good chelating abilities [41]. Acidic cleaners are sometimes employed after the alkaline cleaning to dissolve formed precipitates [5], and it is reported that they are able to hydrolyze some organic molecules, such as polysaccharides and proteins [42].
- **Surfactants or wetting agents:** They decrease surface tension (promoting the contact between the cleaning solution and the foulant layer), stabilize foams, adsorb on foulants and transported them away from the surfaces, form micelles or emulsify fat, oil, and proteins in water [5, 115, 130, 168]. They can be classified into anionic, cationic, non-ionic and amphoteric according to whether they are ionized in solution or not and the charge that they have when it happens [40]. For instance, Tween 20, Triton X100 and Triton X114 are non-ionic, dodecyltrimethylammonium bromide (DTAB), tetradecyltrimethylammonium bromide (TTAB) and cetyltrimethylammonium bromide (CTAB) are cationic, and SDS

(also called sodium lauryl sulphate, SLS) and surfactin (a biosurfactant) are anionic [115, 130]. The recommended ones are usually the anionic or non-ionic ones.

- **Chelatants or sequestrants:** They form soluble complexes with cations such as  $\text{Ca}^{2+}$ ,  $\text{Mg}^{2+}$  and heavy metals, removing them from foulant deposits [5, 165]. The best known chelatants are polyphosphates and the EDTA. For the latter, it is reported that its efficiency increases with the pH [103] because in acidic solutions only two of the four carboxylic groups are deprotonated, while at pH 11 almost all the carboxylic groups are deprotonated and available for complexation with cations.
- **Oxidizer reagents:** The oxidation of organic polymers generates more oxygen-containing functional groups which reduce the adhesion of the fouling material to the membrane [42]. NaClO (basic) is the most widely employed, followed by hydrogen peroxide ( $\text{H}_2\text{O}_2$ , acid), being the oxidation mechanism different for both of them [104].
- **Enzymes:** Proteases, lipases, cellulases and amylases split specific bonds in proteins, lipids, cellulose and starch, respectively, breaking the foulants into smaller species which are more easily removed. Enzymes are biodegradable and operate in mild conditions, but on the other hand, they work in relative narrow ranges of temperature and pH, are expensive, act slowly and residual enzyme activity can affect the industrial process [40].
- **Disinfectants and sanitizers:** They are employed at the end of the cleaning cycle, and are intended to destroy the deleterious microorganisms on the membrane surface or into its pores. NaClO and  $\text{H}_2\text{O}_2$  supposedly clean and sanitize, but they could be not effective. In that case, other substances have to be employed, i.e. sodium dichlorisocyanurate, chlorine dioxide ( $\text{ClO}_2$ ) [106], sodium metabisulfite [80, 114], formaldehyde [80], peroxyacetic acid, electrolyzed water or ozonated water [112].

#### 3.2.4. Evaluation of cleaning effectiveness

Cleaning evaluation techniques are as important as cleaning procedures themselves since they allow studying the effectiveness of the treatment and determining the optimum conditions. All the common methods used to determine cleaning goodness are based on either permeate flux measurements or membrane surface characterization. Both types are carefully detailed in the two following sections.

##### 3.2.4.1. Techniques based on permeate flux measurements

Measurements of permeate flux (J) or TMP allow to obtain several cleaning evaluation parameters. All of them are based on the comparison of membrane properties in its pristine, fouled and cleaned state.

As aforementioned, filtration experiments can be performed at either constant TMP or at constant  $J_F$ , leading to different parameters to evaluate cleaning effectiveness. The first kind of procedures are more common at lab-scale in just one fouling/cleaning cycle, whereas the second ones, are usually studied at pilot-plant scale operating in multiple cycles. In addition, there are less published papers concerning several cycles of fouling/chemical cleaning than those dealing with fouling/physical cleaning.

**Fig. 3.1** shows a conventional fouling/chemical cleaning cycle at constant TMP. In a first place, the pure water flux of the pristine membrane ( $J_{w0}$ ) is determined by filtrating deionized, distilled or ultrapure water. Then, the working solution is filtered and the  $J_F$  decreases with time until reaching the steady state value [119]. Once the filtration is stopped, the membrane is rinsed with water to remove the concentration polarization layer and the loosely-bound foulants, obtaining a flux denoted by  $J_{WF}$ . Then, the chemical cleaning reagent acts for a determined period and a new rinsing with water is carried out for measuring the water flux after cleaning ( $J_{WC}$ ). Chemical cleaning is not always implemented under pressure, but when it is applied, the permeate in this stage ( $J_C$ ) can increase until a plateau is reached or go through a maximum.

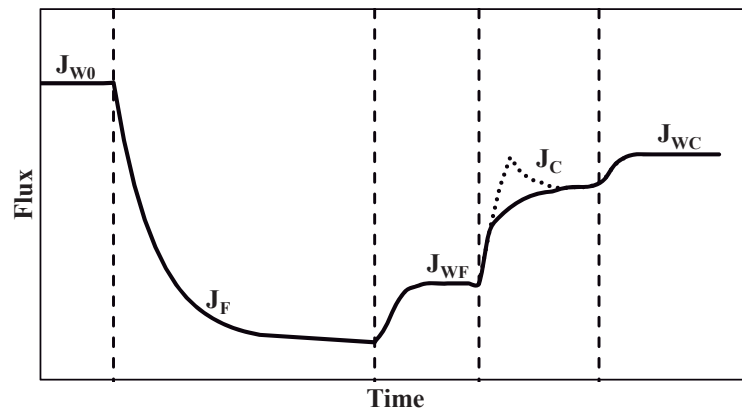


**Fig. 3.1.** Typical UF fouling/chemical cleaning cycle at constant TMP.

In the case of applying physical cleaning instead of chemical reagents,  $J_{WF}$ ,  $J_C$  and  $J_{WC}$  can merge together into a unique permeate flux (when dealing with ultrasounds or with FF and BW not preceded by water rinsing). Therefore, this unique permeate flux value obtained after the physical cleaning is compared to  $J_{w0}$  [55, 96, 103, 137, 138, 153, 160, 161].

The main parameters that can be determined from these fluxes (following the terminology of Astudillo *et al.* [169] as much as possible) are:

- *Water flux recovery*, which is, by far, the most widely employed [11, 19, 23-25, 56, 59, 68-70, 72, 84, 91, 104, 109, 111, 115-118, 120-123, 125, 127, 130, 134, 140, 141, 145, 146, 148, 154, 156, 158, 159, 162-164] is defined according to Eq. (3.1). Nevertheless,



sometimes, the ratio is not calculated and both  $J_{WC}$  and  $J_{W0}$  are shown visually [90, 105, 124, 149, 157, 165].

$$\text{Water flux recovery} = \frac{J_{WC}}{J_{W0}} \quad (3.1)$$

- *Water flux decline* [124, 142]:

$$\text{Water flux decline} = 1 - \left( \frac{J_{WC}}{J_{W0}} \right) \quad (3.2)$$

- *Water flux recovery ratio* [68, 97, 102, 129]:

$$\text{Water flux recovery ratio} = \frac{J_{WC} - J_{WF}}{J_{W0} - J_{WF}} \quad (3.3)$$

- *Water flux improvement* [109, 136]:

$$\text{Water flux improvement} = \frac{J_{WC} - J_{WF}}{J_{WF}} \quad (3.4)$$

- In some researches, when  $J_{W0}$  is not available or not measured, then the ratio between  $J_{WC}$  and  $J_{WF}$  is the cleaning criterion [57, 87-89, 151], or simply, the highest value of  $J_{WC}$  [144, 152].
- When several cycles of fouling/cleaning are conducted, comparing the time-evolution of  $J_F$  from one cycle to another can also serve for evaluation purposes [24, 47, 55, 56, 58, 81, 93, 121, 149, 152, 157]. In such way, Weis *et al.* [15] used the steady state value of  $J_F$  in each cycle [139]. Another example was found in the optimization of the BW duration and frequency, where Massé *et al.* [75] employed the “*net steady state permeate flux*”, corresponding to the permeate flux from which the BW flux had been removed.
- In other cases, the rinsing after chemical cleaning is not done, and  $J_C$  is directly compared to  $J_{W0}$  [56, 95, 96, 119, 135, 150]. For instance, Razavi *et al.* [132] defined a new parameter, Eq. (3.5), based on the  $J_C$  which could be called “*flux restoration*”, by analogy with the parameter of Zheng *et al.* [94]. The main shortcoming of employing  $J_C$  instead of  $J_{WC}$  is that the results may be quite different [99, 101, 125].

$$\text{Flux restoration} = \frac{J_C - J_F}{J_{W0} - J_F} \quad (3.5)$$

The alternative working mode consists in keeping the  $J_F$  constant by increasing the TMP with time. A typical evolution of the TMP throughout this operation mode is displayed in **Fig. 3.2**. In this case, physical cleaning by means of FF or BW cycles are carried out in order to keep TMP

as low as possible. It can be observed that TMP increases with time over the filtration operation due to the fouling. Then, the BW or FF procedure is applied in order to recover  $TMP_0$ , but only a part of the total fouling (removable fouling) vanishes. In this way, TMP increases over the cycles until the point in which the accumulated irreducible fouling makes mandatory to apply a chemical cleaning [54, 60].

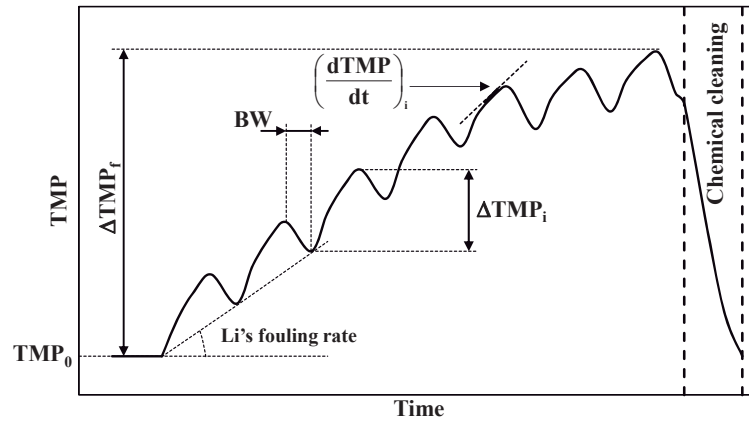


**Fig. 3.2.** Typical UF fouling/physical and chemical cleaning cycles at constant  $J_F$ .

When working at constant  $J_F$ , the following parameters to determine cleaning effectiveness can be defined.

- *Evolution of TMP with time.* The TMP throughout the filtration can be compared to the initial value [54, 58, 60, 61, 66, 71, 76, 78, 94, 143]. For instance, Ye *et al.* [48] employed the total TMP increase between the beginning and the end of the experiment ( $\Delta TMP = TMP^{final} - TMP_0$ ), Oriol *et al.* [50] used a relative increase ( $\Delta TMP/TMP_0$ ) and Guigui *et al.* [77] measured the TMP at the beginning and at the end of each filtration cycle.
- The *removable fouling* in each cycle was determined by Ye *et al.* [48] following the Eq. (3.6). Where  $TMP_i^{initial}$  and  $TMP_i^{final}$  are the initial and final TMP values of the filtration cycle  $i$ , respectively and  $TMP_{i+1}^{initial}$  is the initial TMP value of the filtration cycle  $i+1$ .

$$Removable\ fouling = \frac{TMP_i^{final} - TMP_{i+1}^{initial}}{TMP_i^{final} - TMP_i^{initial}} \quad (3.6)$$

- The *global fouling rate* was defined as the slope of the line that connects the initial TMP of each filtration cycle divided by  $TMP_0$  (**Fig. 3.2**). Li *et al.* [67] assumed that this slope was constant, a supposition which did not turned out to be always true.
- The *volumetric fouling rate* was defined by Abrahamse *et al.* [62] based on the representation of the quotient  $TMP_0/TMP$  as function of the permeate volume collected in

a certain time. The rate was taken as the initial slope of the line that connects the values of the  $TMP_0/TMP$  ratio at the beginning of each filtration cycle.

- The *fouling rate* in each filtration cycle  $i$  [48, 64] is defined by Eq. (3.7) (**Fig. 3.2**). This parameter is linked to the accumulation of material during the filtration cycle and the cake properties. As pointed out by Ye *et al.* [48], in each filtration cycle, the TMP profile as function of time have two stages: a short quick TMP increase followed by another stage of linear increase. These authors calculated the *fouling rate* with data of the second stage, and obtained an average value with the slopes of the last filtration cycles of their experiments. However, Bessiere *et al.* [64] did not average these values and did not indicate in which stage the calculations were done. In a similar way, Resosudarmo *et al.* [49] calculated a *relative fouling rate* taking the *fouling rate* of the first cycle as reference in order to measure the change in the *fouling rate* throughout all the process.

$$Fouling\ rate = \left( \frac{dTMP}{dt} \right)_i \quad (3.7)$$

It has to be pointed out that not all the fouling can be detected with TMP measurements. For instance, Heijman *et al.* [78] carried out 60 cycles of DE filtration/purging/BW/FF (nearly 18 h) employing capillary PES membranes, and observed that at high FF velocities, TMP was always restored to the original level (indicating effective solid removal from the membrane surface by the previous BW). However, the FF pressure increased during the first six cycles and then remained constant, which indicated that not all the fouling had been removed. This type of fouling was identified to be caused by the blocking of capillaries in the potting of the module.

Last but not least, there are also some other parameters to determine cleaning effectiveness, regardless of whether the operation is carried out at constant TMP or constant  $J_F$ , and they are all based on the Darcy's Law [43] showed in Eq. (3.8).

$$J = \frac{TMP}{\mu r_{tot}} = L_p \cdot TMP \quad (3.8)$$

Where  $\mu$  is the permeate viscosity,  $r_{tot}$  is the total resistance and  $L_p$  the permeability. The total resistance and so, the permeability, varies according to the fouling or cleaning state of the membrane [169]. When obtained from  $J_{wo}$  or  $TMP_0$ , the permeability is denoted by  $L_{pwo}$  and the total resistance is  $r_m$ , which is the intrinsic membrane resistance. If fluxes or pressures correspond to the filtration stage, permeability is  $L_{pF}$  and the total resistance will be equal to the sum of  $r_m$ ,  $r_{if}$  and  $r_{rf}$  (where  $r_{if}$  and  $r_{rf}$  are the resistances caused by irremovable and removable fouling, respectively, being the resistance due to the concentration polarization included in the last term). After the first rinsing,  $r_{rf}$  vanishes and the permeability becomes  $L_{pWF}$ . When the post-cleaning rinsing is performed, the permeability is  $L_{pWC}$  and  $r_{if}$  is reduced to a residual resistance ( $r_{res}$ ). Thus,

the total resistance after the cleaning ( $r_{WC}$ ) is given by the sum of  $r_m$  and  $r_{res}$ . Cleaning yield can be evaluated through these parameters too.

- The *permeability recovery* [23, 46, 79, 86, 98, 99, 133, 155, 165], which at constant TMP is equal to the *water flux recovery*, is shown in Eq. (3.9).

$$\text{Permeability recovery} = \frac{Lp_{WC}}{Lp_{W0}} \quad (3.9)$$

- The *normalized permeability* is defined by the ratio between  $Lp_F$  and  $Lp_{W0}$ . This parameter, at the beginning of each cycle  $i$ , has been used to follow the cleaning yield throughout multiple fouling/cleaning cycles [46, 64]. At constant  $J_F$ , *normalized permeability* is the same as  $TMP_0/TMP_i^{initial}$  [92]. The *successive normalized permeability* is given by the ratio between the permeability at the beginning of the cycle  $i$  and that at the beginning of the cycle  $i-1$  [79].

$$\text{Normalized permeability} = \frac{Lp_F}{Lp_{W0}} \quad (3.10)$$

- *Water permeability recovery ratio* [155], which is similar to *water flux recovery ratio* at constant TMP:

$$\text{Water permeability recovery ratio} = \frac{Lp_{WC} - Lp_{WF}}{Lp_{W0} - Lp_{WF}} \quad (3.11)$$

- *Permeability restoration* [94], which is similar to *flux restoration* at constant TMP, is given by Eq. (3.12):

$$\text{Permeability restoration} = \frac{Lp_{WC} - Lp_F}{Lp_{W0} - Lp_F} \quad (3.12)$$

- Comparison of the permeability time-evolution from one cycle to another [46, 65, 86].
- *Resistance removal* [97, 102, 108, 115, 116, 120, 121, 154]:

$$\text{Resistance removal} = \frac{r_{if} + r_{rf} - r_{WC}}{r_{if} + r_{rf}} \quad (3.13)$$

- *Cleaning efficiency* [16, 85, 110, 111, 113, 120, 126, 131, 137]:

$$\text{Cleaning efficiency} = \frac{r_{if} - r_{res}}{r_{if}} = \frac{r_{if} + r_m - r_{WC}}{r_{if}} \quad (3.14)$$

- Sometimes, resistances are evaluated alone, as the  $r_{tot}$  at the end of each cycle [63, 103], the  $r_{res}$  [100, 101, 122] or  $r_{if}$  and  $r_{rf}$  [145, 159].

Finally, it is important to stand out that there are no consensus for the names of these parameters in the literature. For instance, Guo *et al.* [65] designated the “*permeability recovery*” as “*water flux recovery*” when working at constant TMP (although numerically, in this case they were the same), te Poele and van der Graaf [46] called “*clean water flux*” to actual permeability values, Kazemimogham and Mohammadi [102], Mohammadi *et al.* [97] and Salahi *et al.* [154] used the “*water flux recovery ratio*” under the name of “*water flux recovery*”, Razavi *et al.* [132] called the “*water flux recovery*” to their new parameter defined by themselves and Chen *et al.* [111], Wu and Bird [148] and Lujan-Facundo *et al.* [131] nominated the “*cleaning efficiency*” as “*resistance removal*”, “*fouling resistance recovery*” and “*flux recovery*”, respectively.

#### 3.2.4.2. Techniques based on surface characterizations

The other way employed to determine cleaning goodness is based on physicochemical techniques for membrane surface characterization. At this point, it is important to stand out that these techniques are destructive and so, they are not feasible at industrial scale. Nonetheless, they provide a great variety of information, making them appealing for the understanding of cleaning basics.

- Streaming potential (SP) is determined by measuring the electrical potential difference created when a hydrostatic pressure gradient induces a relative motion between a charged fluid (an electrolyte) and the charged membrane (through its pores or along its surface). Membrane charge comes from the ionization of particular functional groups existed on the surface and therefore, it depends on the pH [42]. By measuring the SP at different pressure gradients, the zeta potential (ZP) can be determined for a given pH [170]. As these potentials change with fouling and cleaning, the closeness of the zeta potential of a cleaned membrane to that of the pristine membrane can be considered an evaluation of the cleaning yield, as long as no modification had taken place on the membrane surface due to the cleaner [146].
- The contact angle is the angle at which the water interface meets the membrane surface. It depends on the interface/surface tensions of the liquid and the solid surrounded by a gas/vapor (usually air). When the liquid is water, contact angle is a measurement of the membrane hydrophilicity (low contact angle) or hydrophobicity (high contact angle). This parameter changes with the presence of foulants and/or cleaners on membrane surface [12, 21, 43, 171]. Nonetheless, membranes made of the same base material but from different manufacturers can have different contact angles due to small changes in their formulation modifying significantly their hydrophobicity [42].
- XPS is a surface-sensitive technique based on measurements of the number and kinetic energy of the electrons generated by an X-ray excitation of the sample. It measures the

elemental composition (except H) and provides chemical binding information of the surface top region (1-5 nm) [21]. As an example, it was employed by Lindau and Jonsson [151] to monitor the cleaning.

- The ATR-FTIR measures the absorption of IR radiation by the sample. Depending on the wavenumber, the absorption of IR radiation makes specific bonds vibrate in such a way that peaks on spectra are characteristic of specific bonds and functional groups which in turn, are associated to the membrane surface itself or to the foulants [142]. When comparing spectra of fouled and cleaned membranes, the intensity of peaks corresponding to membrane material decrease and new peaks (due to the foulant deposits) appear. In an ideal process, ATR-FTIR analysis of virgin membranes should be the same as the cleaned ones [23]. Although, ATR-FTIR is usually applied for qualitative analysis, it is also possible to use it as a quantitative technique in some specific cases using the ratio between the height of one peak associated to the foulant and one to the membrane material [10, 12, 98-101, 104, 127]. This technique can also detect if there are modifications on the membrane surface due to the cleaner [15, 146]. Main shortcomings are that it is a destructive technique [99, 100] and cannot reveal the fouling if it happens inside the pores [65].
- SEM provides a detailed visual indication of the state of the membrane surface before and after cleaning by exciting the sample with a high-energy beam of electrons and then, detecting commonly the secondary electrons emitted. Occasionally, SEM is connected to an EDS system to conduct an elemental analysis of the substances present on the membrane [25, 87, 144, 149, 150]. The method also has the disadvantage of only monitoring the polymeric surface [158], but if membrane is transversally cut, the in-pore fouling can be observed too [16].
- AFM is a scanning probe microscopy through which is possible to obtain micrograph images of the membrane surface. Changes in roughness during fouling/cleaning cycles due to the accumulation or removal of the foulants can be monitored through AFM. Usually, the root mean square roughness is calculated [68, 145], making the comparison less subjective.
- Membrane rejection is not actually related to either surface characterizations or permeability measurements, but it is included in this section. Rejection is defined as one minus the ratio between the concentration of a solute in the permeate and the concentration of the same compound in the retentate. If membrane cleaning is good, the rejection in following filtration stages should be very close to that in the first one. Nevertheless, only Maartens *et al.* [70] and Jones *et al.* [145] commented the variation of this parameter after the cleaning. Other authors who measured it, only make brief statements on its performance [56, 65, 81, 127, 128].

More techniques to determine the goodness of cleaning procedures are also shown below. However, at present, they have few and specific applications.

- Matrix assisted laser desorption ionization - mass spectrometry (MALDI-MS) is sensitive to very low protein concentrations, but it only reveals the composition of the fouling cake top layer. Therefore, it is not suitable if the protein distribution in the cake is uneven [126].
- Opposite to MALDI-MS, the Lowry method (modified or not) and the gel electrophoresis, allow obtaining the overall amount of each protein in the deposit [111, 120, 126]. In both cases, the foulant deposit is extracted from the membrane by solubilization, being analyzed spectrophotometrically or separated through a polyacrylamide gel, respectively.
- Lipid and protein contents can also be analyzed after extracting the foulant deposit from the membrane with appropriate solvents. The amount of lipids is obtained gravimetrically, and the amount of protein, spectrophotometrically [136, 172].
- Ultrasounds can be used as a real-time non-invasive technique to determine the organic fouling deposition and removal by relating the signal to the thickness of the layer [141].
- Membrane staining with Amido Black as dye can be used for protein detection [125].
- Turbidimetry and suspended matter concentration analysis can be linked to the particle removal from the membrane during BW or air assisted BW [55, 76, 77, 79]. Zondervan *et al.* [60, 61] used turbidity measurements to estimate the chemical cleaning goodness of the reagent in fouled membranes with surface water filtration.
- Microbiological tests, based on colony forming units and microbial populations, can be used to evaluate how good the sanitization of the chemical cleaners was.
- Fluorescent microscopy allows observing the amount of fluorescent proteins that are on or inside the membrane. However, it barely has any practical application, since it is necessary to modify the protein to make it fluorescent. Fluorescent microscopy was employed with the only aim of seeing the distribution of the foulants [129].
- Fluorescence excitation - emission matrix spectroscopy has a wider application field than fluorescent microscopy. Wang *et al.* [158] used it to detect microbial metabolites and humic acid-like compounds present on the surfaces of PVDF UF membranes that had filtered fermentation broths. However, Peiris *et al.* [73, 74, 173] managed to relate this information with the major foulant groups present in surface water, i.e. humic substances, protein-like matter, inorganic components and colloids/particles.

### 3.3. Influence of main cleaning factors

#### 3.3.1. Process stream filtration conditions

In the end, the proper cleaning procedure depends on the previous fouling stage. It is interesting to stand out that the behavior of a foulant mixture is not the additive sum of the individual contributions from each foulant [65]. For instance, high feed concentrations usually difficult the cleaning [137, 157]; pH modifies the net charge of the proteins and dramatically influence the performance of the consequent cleaner [116, 121]; the *cleaning efficiency* depends on the fouling time [126]; the higher the  $J_F$  values (when TMP is allowed varying) are, the lower the BW effectiveness is [48, 54]; working at low constant TMP commonly facilitates the following chemical cleaning [12, 121], although there are exceptions [68]; different results are obtained for a fixed duration and frequency of BW if different types of fouling mitigation techniques are utilized during the filtration [174]; and the presence of  $Ca^{2+}$  can also either improve [81] or make worse [62] the physical cleaning by BW.

#### 3.3.2. Membrane properties

Both fouling and cleaning depend on membrane properties such as NPS (related to MWCO), material (linked to surface tension and so, hydrophobicity) and roughness.

For two CA membranes fouled with a humic acid solution and cleaned with NaOH, the one with the higher MWCO and NPS (75 kDa and 10 nm, respectively) is easier cleaned than that with lower MWCO and NPS (2 kDa and 2 nm), due to the fact that the pore blocking takes place at the pore entrance for the more permeable membrane [59]. PES membranes with higher MWCO exhibited a steeper flux decline during the UF of a similar solution, but better cleanability. Moreover, for a cleaning consisting in BW followed by NaOH, the impact of the physical method on the *water flux recovery* increased with MWCO, and the contribution of the chemical reagent became lower [69]. However, in the case of PES membranes fouled with humic acid and cleaned by ultrasounds, it was found that those of 10 kDa showed higher *water flux recoveries* than those of 100 kDa [72]. The researchers attributed the phenomenon to the fact that ultrasounds were more effective removing particles on the surface than in the pores.

For FP and RC membranes with the same MWCO, Evans *et al.* [146] found that the fouling due to black tea in the RC membranes (more hydrophilic than the FP ones) was not very severe, and that the *water flux recoveries* after NaOH treatment were close to 100 %, whereas in the FP membranes, the amount of fouling was considerable and *water flux recoveries* higher than 150 %.

Weis *et al.* [15] conducted chemical cleaning on PES, PS<sub>u</sub> and RC membranes after filtering spent sulphite liquor. They found that for membranes with similar hydrophobicity but different roughnesses (PS<sub>u</sub> and PES), flux decline over multiple fouling/cleaning cycles was more significant



for the rougher membrane (PS<sub>u</sub>). However, when membrane hydrophilicity was not comparable, the RC membrane (rougher and more hydrophilic) was less prone to adsorb the foulants than the smoother but more hydrophobic PES one.

### 3.3.3. Filtration modules

Cleaning is sensitive to the geometry of the modules and the hydrodynamic conditions [19, 25]. Rabiller-Baudry *et al.* [99-101] cleaned chemically PES membranes fouled with skim milk in a stirred system and in a plate-and-frame module under the same experimental conditions and found that the obtained results were different. When dealing with ultrasounds for treating membranes that had filtered whey or skim milk, Maskooki *et al.* [103] and Muthukumaran *et al.* [109, 113] reported that the module type and the supporting base affected the ultrasonic power that reaches the membrane. For air assisted BW and membranes fouled with bentonite suspensions, Serra *et al.* [76] found that the optimum air flow determined on bench-scale was very different from that on full-scale, and attributed it to channeling and wall effects which are present in small modules but not in pilot plant nor in full-scale setups.

### 3.3.4. Cleaner concentration

In general, cleaning goodness increases with concentration until a plateau is reached or it increases reaching a maximum and then, decreases.

It can be cited, for the first case, the NaClO cleaning of milk-fouled PS<sub>u</sub> membranes [97], the action of SDS or *Thermus* Rt4.1A proteinase on membranes used in whey processing [107], EDTA treatment of PAN membranes fouled with oily wastewater [154], the performance of the mixture EDTA + NaOH + turkey red oil when applied to PS<sub>u</sub> membranes that had filtered wastewater from banknote printing works [150], the cleaning with SDS or EDTA of PA membranes employed for juice clarification [165] and the removal of whey from home-made PES UF membranes by means of H<sub>2</sub>O<sub>2</sub>, guanidinium hydrochloride, SDS, CTAB, DTAB, TTAB, Triton X100 or Triton X114 [115].

Examples of systems having a cleaning effectiveness maximum are the cleaning with the  $\alpha$ -chymotrypsin enzyme ( $\alpha$ -CT) of PS<sub>u</sub> membranes fouled with BSA [116], the treatment with HCl, NaOH and SDS of PES membranes fouled with whey [111], the cleaning with proteinase type M of PES membranes fouled with BSA or BSA + bLG [126] and the treatment with H<sub>2</sub>SO<sub>4</sub>, HCl, HNO<sub>3</sub>, KOH and NaOH of PES membranes fouled with whey [108, 115].

In some cases, the scarce experimental points reported makes impossible to discern if the cleaning effectiveness tends to a plateau or goes through a maximum [84, 156].

Anyway, optimum concentration depends on the system, and can vary very much for the same cleaner. For instance, optimum NaOH concentration is 0.8 wt. % when cleaning milk-fouled

PS<sub>u</sub> membranes [97] and 0.075 wt. % if the foulant is whey and the membrane material is RC, PES or PA [23].

Moreover, the same system can present maximum or plateau according to the temperature and/or pH. For PS<sub>u</sub> membranes fouled with BSA and cleaned with the enzymatic detergent TAZ, Muñoz-Aguado *et al.* [116] saw that the *water flux recovery* and *cleaning efficiency* continuously increased with the cleaner concentration when the cleaning was performed at 20°C, but they went through a maximum if that temperature was risen to 40°C. Muthukumaran *et al.* [110] observed that the *cleaning efficiency* of PS<sub>u</sub> membranes fouled with whey increased with SDS molarity and reached a plateau when the pH of the surfactant was 6.5 but it went through a maximum at pH 12.

The existence of an optimum concentration was explained in several ways: the more chemical amount, the higher foulant removal, but also the higher degree of swelling of the fouling deposits. This last fact facilitates the pore blocking by the foulants and causes the reduction of  $J_c$  [119]; too high concentrations break down the foulants into small pieces so fast that they do not have time enough to get the bulk solution and they enter into the pores causing a more severe in-pore fouling [96]; excessive chemical concentrations may produce solidification or gelation of deposits [5]; high amounts of reagent act as a foulant itself, which was confirmed by MALDI-MS and gel electrophoresis measurements in the case of protein-fouled PES membranes cleaned with proteinase type M [126].

On the contrary, it has been also reported that the higher the amount of NaOH (from 0.2 to 0.5 wt. %), H<sub>2</sub>O<sub>2</sub> (0.3 - 1 wt. %), protease A (0.0005 - 0.1 wt. %) or HNO<sub>3</sub> (0.01 - 1.0 wt. %) are, the lower the cleaning goodness gets [97, 111, 119, 156]. Nevertheless, this could be due to the fact that the optimum cleaner concentration was lower than the chosen range and so, it was not detected.

### 3.3.5. Cleaning time

Fouling removal usually increases with cleaning time until a plateau is reached and no further improvement is seen under both physical [103, 109, 113] and chemical [97, 107, 116, 120, 132, 134, 154, 155] cleanings. Another observed trends includes a maximum before tending to the plateau [95, 96, 107, 119] and a maximum without reaching any plateau. Examples for the last case were reported by Petrus *et al.* [126] during the removal of BSA + bLG in PES membranes using proteinase type M and by Saha and Balakrishnan [164] after the treatment with NaClO of fouled UF membranes due to sugarcane juice. Nevertheless, in both cases only three experimental points were displayed and so, trends may be biased.

Given explanations for the existence of an optimum time are similar to those mentioned for the concentration effect: higher exposure times to the chemical allow further swelling [119], a more breakage of foulants [96] or facilitates the fouling action of the cleaner [126].

Time dependence can be very sensitive to other variables in cleaning processes. For example, in CA membranes fouled with skim milk and cleaned with a mixture of an alkaline protease and Ultrasil, the flux recovery changed from the simple plateau pattern at low amounts of enzyme to the maximum-before-the-plateau pattern at higher concentrations [95].

Other anomalies were also seen in the time dependence of  $J_{wc}$ . Vaisanem *et al.* [23] reported a maximum after treating membranes of RC, PES and PA with Libranone 960 and Lindau and Jonsson [151] observed that  $J_{wc}$  decreased continually until a constant value after treating oily-fouled  $PS_u$  membranes with commercial acidic cleaners. In the first case, the maximum was explained by the adsorption and subsequent desorption of the non-ionic surfactants that comprise the Libranone 960. In the second case, the effect was due to the compaction of the fouling cake over the rinsing which was caused by the dissolution of the inorganic compounds during cleaning which in turn, made the cake more porous.

Efficiency of specific physical cleaning process, such as BW, is not only a function of the cleaning duration, but also of its frequency (defined as the filtration time between two successive BW in multiple fouling/cleaning cycles). In this cases, BW frequency becomes even more important than the BW duration [92, 94, 143]. At constant frequency, cleaning goodness usually increases with duration until a plateau is reached [48, 84]. Nevertheless, Kennedy *et al.* [55] saw that this increase was lower from 0.5 to 1 min than from 1 to 2 min. On the other hand, if  $J_F$  is increased, a higher BW frequency is necessary to keep membrane performance [54].

The frequency of the chemical cleaning has been studied by Kim *et al.* [121] with  $PS_u$  membranes fouled with BSA and treated with HCl. They compared three combinations as function of the permeate volume: I) cleaning after every 200 mL of permeate (200 mL UF/clean/200 mL UF/clean/200 mL UF/clean); II) 300 mL UF/clean/300 mL UF/clean; and III) 600 mL UF/clean.  $J_F$  followed the order  $III < I \leq II$  which indicated that too low or excessive cleaning frequencies resulted in lower productivity.

Occasionally, a prolonged cleaning can lead to the damage of the membrane or the reduction of the separation efficiency in following filtration cycles [127, 128].

### 3.3.6. Cleaning temperature

There are not many papers dealing with the effects of temperature in cleaning procedures, and most of them only try a few number of temperatures. In general, higher temperatures increase cleaning yield, but they can also increase the membrane damage or cause changes in foulant structure making it harder to remove [5, 41].

The level of improvement due to a temperature rise is specific of each system. When  $PS_u$  membranes fouled with wastewater from banknote printing works are cleaned with a mixture of EDTA + NaOH + turkey red oil between 20 and 60°C, a S-shape curve emerged [150]. When FF

with hot water is performed on skim milk fouled PS<sub>u</sub> membranes from 25 to 65°C, a maximum is observed at 55°C [96]. In the range 25-50°C, the removal of oily wastes from a PAN membrane with SDS + EDTA increased with temperature until reaching a plateau at 45°C [154]. A same trend looks to take place for the cleaning of a PS<sub>u</sub> membrane fouled with milk and treated with SDS + EDTA + NaOH between 17 and 63°C. In this case, both *water flux recovery ratio* and *resistance removal* took the highest 100 % value at 63°C but experiments did not continue, not being possible to assure that the plateau was reached [102].

### 3.3.7. Cleaning solution pH

The pH effect is linked to the foulant type and cleaner concentration. There is not a direct relation between pH and *water flux recoveries* [156] and two cleaners at the same pH (acidic or alkaline) can give different results [104]. The maximum efficiency observed by Muthukumaran *et al.* [110] when varying the water pH under ultrasounds was a consequence of reaching the optimum concentration of NaOH which was used to adjust the basicity. In the same way as for the concentration dependence, cleaning yield as function of the pH usually increases initially and later it reaches a plateau as reported by Kazemimoghadam and Mohammadi [102] for SDS + EDTA + NaOH between 9.2 and 12.7, and by Salahi *et al.* [154] for SDS + EDTA from 8 to 11.

### 3.3.8. Interfacial energy of the cleaner

Rabiller-Baudry *et al.* [100, 101] treated skim milk fouled PES membranes with several cleaners at pH 11.5 and 12, and suggested that the cleaning yield in a given system (expressed as amount of residual protein ( $r_{if}$ ) or *permeability recovery*) increases as the cleaner interfacial energy decreases. This parameter involves the nature, characteristics and concentration of the cleaning solution. Platt and Nystrom [125] also saw that the lower the surface tension is, the better the cleaning of BSA-fouled PS<sub>u</sub> membranes, but they pointed out that pH has to be taken into account as well, because at the same interfacial energy, the *water flux recovery* was better under alkaline conditions. Unfortunately, to the best of our knowledge no more research on this topic has been done.

### 3.3.9. Cleaning water quality

The water quality of the rinsing steps and the cleaning solutions plays an important role which was studied by several authors. Muñoz-Aguado *et al.* [116] investigated the effect of the water rinsing pH and temperature on the BSA removal from PS<sub>u</sub> membranes. The cleaning was carried out through a two-step procedure, consisting in  $\alpha$ -CT (pH 7.5) followed by CTAB (pH 4.1) with 15 min of MilliQ water rinsing after each step. This water was tested in four conditions: 1) At neutral pH and ambient temperature; 2) At ambient temperature and the same pH as the  $\alpha$ -CT or CTAB solutions; 3) At neutral pH and 40°C; 4) At 40°C and the same pH as the  $\alpha$ -CT or CTAB

solutions. The best *water flux recoveries* and cleaning effectiveness were obtained at neutral pH and 40°C (3), followed by the two no neutral pHs (2 and 4). The first condition (1) gave worst results than no rinsing.

The presence of several salts in the rinsing water and in the CTAB cleaning solution in PS<sub>u</sub> membranes fouled with whey was studied by Tran-Ha *et al.* [117, 118]. NaNO<sub>3</sub>, NaCl, CaNO<sub>3</sub>, CaCl<sub>2</sub>, MgCl<sub>2</sub> and FeCl<sub>3</sub> were employed. At low concentrations, only the addition of NaNO<sub>3</sub> improved the *water flux recovery* given by CTAB in MilliQ water. However, the *water flux recovery* dependence with salt concentration was more complex at higher values: for example, with FeCl<sub>3</sub> it initially decreased, went through a minimum, then increased, reached a maximum and decreased beyond that. With CaNO<sub>3</sub>, the pattern was just the opposite: increase, maximum, drop, minimum and increase again. In presence of NaNO<sub>3</sub> and NaCl, *water flux recovery* increased monotonously. At high concentrations, all the sodium and calcium salts (and probably MgCl<sub>2</sub>) improved the cleaning goodness of the CTAB. If the ionic strength was set, these concentration dependences varied, being a function of the salt employed for fixing it as well.

Zheng *et al.* [94] cleaned PES membranes fouled with a tertiary effluent. When soaking and backwashing them using demineralized water, tap water and permeate, they found that the *permeability restoration* decreased following that order. They attributed these results to the low amount of Ca<sup>2+</sup> in demineralized water, which reduces the charge-screening effect and leads to an increase in the repulsion force between the negatively charged membrane and organic compounds. The presence of cations in the BW water was also analyzed by other authors for the removal of NOM. Abrahamse *et al.* [62] compared permeate (which contained Mg<sup>2+</sup> and Ca<sup>2+</sup>), permeate treated by ion exchange (containing mainly Na<sup>+</sup>) and MilliQ water (very low ionic strength), and pointed out that the *volumetric fouling rate* decreased in the order permeate > permeate treated by ion exchange > MilliQ water (on other words, the lower the ionic concentration is, the lower the irremovable fouling is obtained). They supposed that the NOM matter in both permeates influences the BW goodness too, but Li *et al.* [66] probed that it was not true. Demineralized water and permeate treated by dialysis (without cations, only with NOM) gave almost the same results. Therefore, they stated that only cations influenced the fouling removal through BW. Moreover, Ca<sup>2+</sup> has a stronger impact than Na<sup>+</sup> at the same concentration due to its divalent charge [67].

### 3.3.10. Cross-flow velocity during the cleaning

The influence of either the cross-flow velocity (CFV) or the agitation speed is linked to the mass transfer phenomena between the bulk and the interface of the membrane. This factor becomes important when the rate limiting step is the mass transfer and not the reaction kinetics [51].

For the cleaning of PS<sub>u</sub> membranes with NaOH without applying pressure in a stirred cell, Madaeni and Sharifnia [108] stated that the removal of whey deposits increased linearly with the

stirring rate from 200 to 800 rpm. However, Kim *et al.* [121] found little effect in the range from 200 to 600 rpm for HCl treatment of BSA residues.

When the cleaning was carried out under CF, the velocity dependence is not simple either. Salahi *et al.* [154] observed that an increase of velocity from 0.75 to 1.25 m/s led to an increase in the cleaning yield of oil-fouled PAN membranes with a SDS + EDTA mixture but an increase from 1.25 to 1.5 m/s did not enhance the obtained results. However, the opposite trend was reported by Zhang *et al.* [150] in PS<sub>u</sub> membranes that had filtered wastewater from banknote printing works. When applying a mixture of NaOH + Na<sub>2</sub>EDTA + turkey red oil at 0.1 MPa for 30 min, the results at 0.8, 1.1 and 1.5 m/s were very close, and only the value at 1.8 m/s was considerably higher. Moreover, the cleaning with NaOH of PES membranes fouled with NOM is better at 0.172 m/s than at 0.086 m/s, but if the cleaner is NaCl, there was not any influence of CFV [56]. Muthukamaran *et al.* [110] neither appreciated the effect of the CFV variation under the laminar regime (from 0.2 to 0.33 m/s) when employing ultrasounds combined with SDS on whey-fouled PS<sub>u</sub> membranes at 55 kPa.

### 3.3.11. Transmembrane pressure during the cleaning

Concerning the TMP influence on the cleaning effectiveness, Kim *et al.* [121] and Muthukumaran *et al.* [110] found opposite trends. The first one reported that the increase of TMP from 0 kPa (no permeation) to 100 kPa slightly improved the *cleaning efficiency*, while the second one showed that the resistance recovery ratio decreased a 30 % from 50 to 350 kPa. As the last possibility, Nystrom and Zhu [123] do not observed any TMP effect between 10 and 90 kPa for PS<sub>u</sub> and PVDF membranes fouled with BSA and cleaned with Ultrasil 10 in a stirred cell.

### 3.3.12. BW and FF flow

Considering physical cleaning procedures exclusively, working at constant TMP, Kennedy *et al.* [55] saw that flux recovery initially increased with the BW pressure (linked to the BW flow) and remained constant beyond certain value. This plateau can explain why the cleaning improvement was almost negligible in the work of Xu *et al.* [47], after increasing the BW flow from 45 L/m<sup>2</sup>h to 157 L/m<sup>2</sup>h. At constant J<sub>F</sub>, Ye *et al.* [48] found a minimum for  $\Delta$ TMP and *fouling rate* between 36.5 and 146 L/m<sup>2</sup>h when filtering seawater and Remize *et al.* [79] pointed out that the particle removal after the filtration of a clay suspension increased with BW pressure from 1.2 to 2 bar, but that the permeability measurements were unsuitable to detect this risen.

Ye *et al.* [48] also studied the air assisted BW, and reported that *fouling rate* went through a minimum with the bubbling flow rate as consequence of the bubble shape. However, Serra *et al.* [76], dealing with bentonite suspension in a bench-scale, saw the same minimum and attributed it to the experimental setup size, since in pilot and full-scale modules, this minimum vanished and the cleaning goodness reached a plateau when the air flow increased.

At constant TMP, flux recoveries obtained through FF also followed the same trend that BW. It was proposed that at laminar regime, cleaning effectiveness depends on the velocity and once the turbulent flow is established, a further increase in velocity do not cause any significant improvement [55].

### 3.3.13. Importance of the factors and interactions among them

It has been pointed out previously that the cleaning effectiveness as function of concentration can go through a maximum or reach a plateau depending on the temperature or the pH. Similar trends can be also seen as cleaning time increases as indicated. These different behaviors are due to the interactions among the several factors involved in cleaning procedures, which usually are not taken into account when searching the best conditions for a cleaning protocol. Most of the researchers found these interactions varying one factor at a time [48, 102, 108, 116, 150, 154], a procedure that, in many cases, neither allows to know the relative importance of each one in the fouling removal.

Busca *et al.* [152] developed an experimental plan based on Plackett-Burman matrix to evaluate the importance of several factors on the chemical cleaning of PVDF membranes fouled during CF filtration of a metalworking fluid. These factors were surfactant concentration, volume of cleaner, temperature, time, recirculation velocity and presence/absence of pressure. The importance, in decreasing order, turned out to be: temperature > velocity > time  $\approx$  pressure > concentration > volume. Surprisingly, the effect of recirculation velocity was negative (the increase in velocity decreased the flux recovery), and the authors attributed it qualitatively to an interaction between velocity and pressure, which resulted in membrane fouling because of the surfactant.

A similar study was carried out by Chen *et al.* [91], for both chemical and physical cleaning of PES membranes fouled with a secondary effluent. Not only did they identify the key factors and their interactions through a statistical factorial design, but also optimized the value of each one, obtaining better cleaning goodness than that reached with the procedure recommended by the supplier. For chemical cleaning with TriClean 212F at pH 11-12, the five analyzed factors were: recirculation duration of cleaner (1), its concentration (2), temperature (3), static soak or not (4) and the employment of BW or FF after the chemical cleaning (5). Significant factors were (2), (3), (5) and interaction (2&3). Their importance followed the order (3) > (5)  $\geq$  (2) > (2&3). The concentration and temperature of the cleaning solution should be set at a high level and the chemical cleaning should be followed by BW. The interaction (2&3) showed that concentration changes have a large effect on *water flux recovery* when cleaning is done at low temperature. However, when cleaning is done at high temperature, the effect of concentration becomes smaller. This implies that if chemical cleaning is performed at elevated temperature, cleaning effectiveness can be high even at low concentration. On the other hand, for the physical cleaning, not only the pure *water flux recovery* was analyzed, but also the wash water usage. The six factors tested in this

part were: production interval between physical cleanings (filtration duration) (1), duration of FF (2), duration of BW (3), FF pressure (4), water quality (permeate from reverse osmosis or tap water) (5) and sequence of FF and BW (BW followed by FF or FF followed by BW) (6).

For pure *water flux recovery*, (1), (3), (4) and (1&3) were the most significant factors, and their importance order was  $(1) > (3) > (4) \geq (1\&3)$ . Filtration periods should be short, BW duration long and FF pressure low. The (1&3) interaction implies that the longer the production interval between cleanings, the longer the backwash duration was required (in accordance with the statements of section “3.3.5. Cleaning time”). The wash water usage was dependent on (1), (2), (3), (1&2) and (1&3). Nevertheless, the statistical factorial design is not perfect. It stated that (6) was not significant, but further researches from other authors proved that BW followed by FF was better than the opposite combination [84, 86].

On the other hand, cleaning factors can affect differently depending on the chosen parameter to define cleaning goodness. For instance, Ye *et al.* [48] showed that the importance of the factors BW frequency, BW flow and BW duration were different for the three specific cleaning effectiveness parameters defined in their work. When using the *evolution of the TMP with time*, their importance decreased in the order frequency > duration > flow. When using the *fouling rate* (Eq. (3.7)), the order was frequency > interaction between flow and duration. And when using the *removable fouling* (Eq. (3.6)), the interaction between frequency and flow is the most important factor, followed by the frequency.

### **3.4. Major difficulties in the studying of membrane cleaning**

---

#### **3.4.1. Possible unreliability of cleaning evaluation parameters**

Cleaning goodness given by parameters derived from pure water flux measurements are not always in accordance with the results obtained by other more precise methods based on chemical or physical surface analysis, such as FTIR or Lowry [10, 104, 120, 126]. For instance, Paugam *et al.* [104] observed for PES membranes fouled with skim milk, that the *water flux recovery* of the several cleaners increased following the trend oxonia active < PVP-iodine < water rinsing < oxonia < sodium perborate < NaOH < NaClO, whereas when the residual protein deposits were analyzed, the cleaners gave higher removal following a different order: PVP-iodine < water rinsing < oxonia < oxonia active < sodium perborate < NaOH < NaClO as depicted in **Fig. 3.3**.



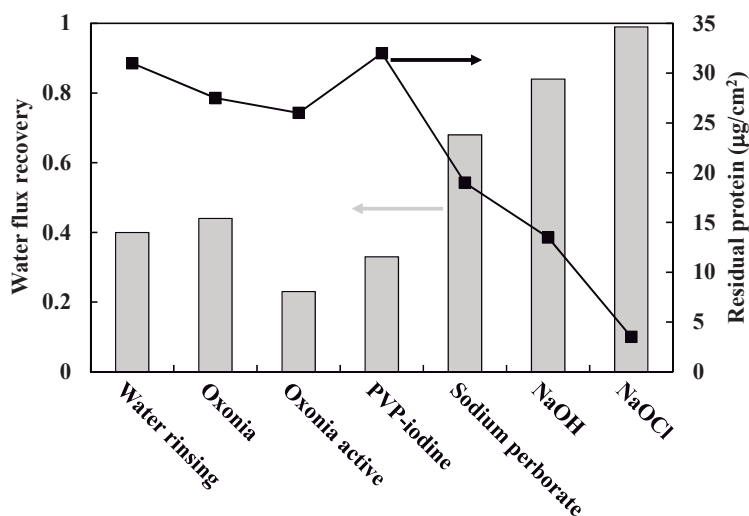


**Fig. 3.3.** Water flux recovery and residual quantity of protein, measured by ATR-FTIR, on a flat PES membrane fouled with skim milk after the rinsing and treatment with various oxidants. Taken from Paugam *et al.* [104].

In this regard, Petrus *et al.* [126] reported that for PES membranes fouled with an equimolar mixture of BSA and bLG and then, cleaned with proteinase type M, the *cleaning efficiency* calculated with resistances was different from that estimated with the amounts of extracted protein (**Fig. 3.4**). Even though cleaning effectiveness trends were identical, when goodness was determined through the Lowry method, it was always higher than that using the *cleaning efficiency* parameter.

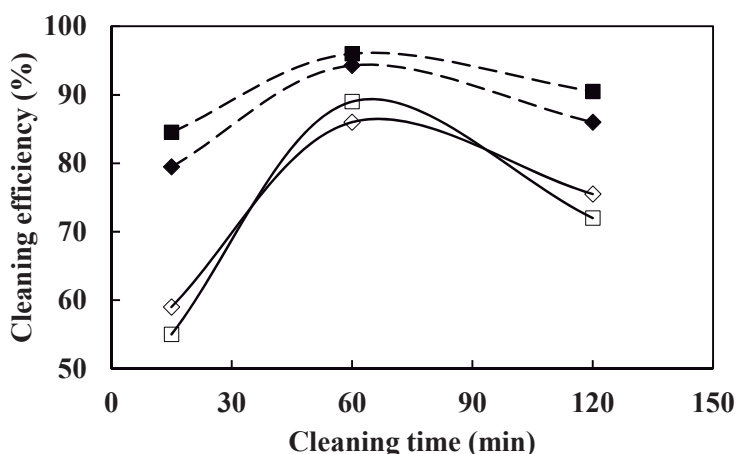


**Fig. 3.4.** Cleaning efficiency of proteinase M as a function of cleaning time for membranes fouled after filtrating a protein mixture for 2 h (◆, ◇) and 5 h (■, □). Closed symbols are those evaluated with Eq. (3.15) and open symbols correspond to the results from the Lowry analysis. Lines are only guides for the eye. Adapted from Petrus *et al.* [126].

This inconsistency is likely due to modifications of the membrane surface and/or the fouling layer caused by the cleaning reagent. These changes can increase or decrease the water flux that permeates through the membrane without affecting the foulant deposits. The best example of these interactions occurs when an unfouled membrane is treated with a surfactant-based cleaner, and  $J_{w0}$  and so,  $r_m$  values change [101, 123, 168]. Surfactant adsorption can also modify the values of SP as well as contact angle [175], and can be responsible of *permeability recoveries* higher than 100 %, since the membrane surface becomes more hydrophilic [98]. After studying the BSA removal from PS<sub>u</sub> membranes with EDTA + NaOH + surfactant, Platt and Nystrom [125] suggested that surfactant adsorption only begins after removing a enough amount of protein. Therefore, *water flux recovery* over 100 % would be a sign of good cleanliness. This hypothesis was confirm through their experiments with the formulated reagents F80 Filter HE and F83 Filter E. In addition, the results from Maartens *et al.* [134] with Lipase A + Triton X100, those from Vaisanen *et al.* [23] with Libranone 960 and the work of Delaunay *et al.* [98] with Ultraclean II also pointed out that there were less residual foulants when *permeability recoveries* were above 100 % than below, but there was never a total removal.

However, when the involved cleaner is not surfactant-based, the goodness of the cleaning cannot be assured basing on high permeate fluxes. For instance, when using HNO<sub>3</sub> to remove skim milk, the interactions between the cleaner and the foulant (not between cleaner and membrane) cause the hydrophilicity risen without any milk removal [10-12, 104]. The treatment of a virgin PES membrane with this acid does not lead to a flux change (which probes no adsorption on the membrane), but the higher the amount of protein on the membrane, the higher the *water flux recovery* when the acidic cleaning is applied.

NaClO increases the hydrophilicity of PES and PVDF membranes [127, 128, 176], and high cleaning times and/or doses make the membrane more prone to BSA adsorption in the next fouling stage when several cycles of fouling/cleaning are performed [24, 127]. Moreover, hypochlorite can provoke degradation of PES and PS<sub>u</sub> membranes [7, 8, 21, 177, 178], leading to different values of cleaning effectiveness if it is not taken into account.

In the previous situations, the cleaning goodness given through flux-based parameters is overestimated compared to that from surface or chemical analysis which analyze the foulant removal itself. Nevertheless, there are opposite situations. For instance, Platt and Nystrom [125] themselves placed the formulated agent F89 Filter HH (consisting in organic acids), which gave a *water flux recovery* lower than 50 %, but on the other hand, all protein content of membrane surface was removed and no remains of proteins were found by the Amido Black test. They did not try to explain the phenomenon, but it could be due to the fact that acid solutions cause a negatively charged membrane to become more hydrophobic [144].

In this regard, it has been proved that NaOH decreases the hydrophilicity of some PVC membranes, which leads to negative cleaning effectiveness based on flux measurements despite of a considerable fouling removal [16]. However, without employing additional techniques such as SEM, AFM or ATR-FTIR is not possible to know if the low cleaning yields are due to surface modifications or to a bad performance of the cleaner. In fact, NaOH can interact with the foulants instead of with the membrane, modifying their structure and making more difficult their removal, which leads to low *cleaning efficiencies* too [85].

Finally, although the interactions between chemical cleaner, foulant and/or membrane are the most reported cases of unreliable results, physical cleaning methods are neither apart from inconsistencies. Remize *et al.* [79] applied conventional BW and air assisted BW on PS<sub>u</sub> membranes while filtering clay suspensions, and evaluated both *permeability recovery* and percentage of removed matter (**Table 3.2**). If only permeability measurements were taken into account, it seemed that the two BW procedures enabled the overall removal of the particulate foulants, and that there was no pressure dependence on the cleaning goodness. Nevertheless, when the removed matter is considered, the use of air considerably improves the BW effect and the cleaning goodness increase with the applied pressure, but effectiveness is always lower than 100 %. After a considerable number of filtration/cleaning cycles, the accumulated matter causes a sudden drop of the *successive normalized permeability* in the process with customary BW, which is not seen using the air assisted BW.

**Table 3.2.** Removal of suspended matter for different BW procedures [79].

Procedure	BW pressure (bar)	Permeability recovery (%)	Removed matter (%)
Customary BW	1.2	99	25
	1.6	100	39
	2.0	97	44
Air-assisted BW	1.2	103	88
	1.6	100	72
	2.0	100	100

#### 3.4.2. Lack of cleaning standardized parameters and models

The possible combinations of membrane materials, feed compositions, system geometries, cleaner characteristics and other system conditions are enormous [40]. As long as dimensionless quantities or theoretical equations that can represent this diversity in a univocal way are not defined, the comparison between the results of the several researchers becomes very difficult and so, all the analysis on cleaning polymeric UF membranes turns out to be qualitative.

Concerning theoretical modeling of cleaning procedures, Zondervan *et al.* [61] found that only three simple models had been proposed for the chemical cleaning until the year 2007, including that one developed by themselves [60]. In the year 2008, Petrus *et al.* [126] modified one of these reported equations to describe the enzymatic cleaning of PES membranes fouled with proteins.

For the physical cleaning techniques, no mathematical modeling was carried out until 2012, when Peiris *et al.* [73, 74] began to use the fluorescence spectroscopy to evaluate the major foulants in natural water and described their accumulation over the filtration and their removal through BW procedures by a set of non-linear differential equations. These researchers were able to optimize the frequency of BW for a five-cycle filtration of surface water, but their model required a high amount of experimental data to fit a wide number of parameters.

### **3.5. Membrane cleaning systems**

---

Throughout this section, the main chemical cleaning protocols are described as function of the foulant since its nature is the major factor when deciding the proper cleaning strategy. Physical cleaning protocols are gathered in another subsection since the influence of the foulant type is lower.

#### **3.5.1. Chemical cleaning of NOM**

In general, after the filtration of surface water, NaClO is the best chemical reagent for cleaning the membrane, NaOH is good and acidic cleaners are the worst. Beyond that, the efficiency of cleaners depends on the specific interaction between the membrane and the particular NOM characteristics. A clear example is given by Lee *et al.* [56] who used PES membranes fouled with hydrophobic and hydrophilic NOM. *Water flux recoveries* after applying NaOH to remove the hydrophobic matter was of 64.8 %, but it decreased to 18.9 % when removing hydrophilic organics. The same authors suggested the use of NaCl to increase the ionic strength of the solution in order to obtain *water flux recoveries* between 43 and 55 % for the hydrophilic matter. However, Kimura *et al.* [57] reported that the results using this salt were the same as employing just MilliQ water for PS<sub>u</sub> membranes.

Sometimes, citric acid acts better than HCl due to its chelant properties [57], but in other cases it is the opposite [61]. Moreover, as aforementioned in “section 3.4.1”, some cleaners such as NaOH can interact with the membrane, modifying its hydrophobicity and leading to erroneous conclusions from the flux measurements [16].

From the work of Zondervan *et al.* [61], it is drawn that formulated cleaners are not necessarily better than simple chemicals on PES membranes. The same happens with enzymes. When filtering a humic acid solution instead of surface water, Yu *et al.* [68] found that  $\alpha$ -amylase,

lipase, cellulose and protease were unable to clean the PS<sub>u</sub> membrane, until the surfactant Triton X100 was added, and even using the surfactant, NaOH was still better than the best of those mixtures enzyme + surfactant.

A two-step chemical cleaning sequence was studied by some of these authors too, and in general, results were better or equal than those employing only one of the reagents. Kimura *et al.* [57] pointed out that a procedure consisting in 24 h of NaOH followed by 24 h of NaClO gave the same  $J_{WC}$  to  $J_{WF}$  ratio than a single step of 24 h with NaClO, but the result improved considerably if oxalic or HCl were used instead of NaOH.

Additive and synergic effects were observed by Yu *et al.* [68] with the sequences NaOH/enzyme, citric acid/enzyme and  $\alpha$ -amylase/lipase (all the enzymes mixed with 0.1 % of Triton X100), being the synergy very pronounced for the caustic case when the fouling was performed at 135 kPa. In the work of Tiang *et al.* [16] with PVC membranes, the sequence NaOH/ethanol was better than the single cleaning with ethanol, but the synergy was not evaluable due to the fact that the negative *cleaning efficiency* caused by NaOH alone is not related with a fouling increase, but with membrane modifications.

### 3.5.2. Chemical cleaning of microbial species

It was found that the most effective cleaners at room temperature for fouled membranes with microbial species are commercial formulated ones [82, 83, 87, 90] and the NaClO or the NaHClO [82, 84, 85, 87, 88]. Although at high temperatures (around 40°C) the cleaning yield of the NaClO decreases, being lower than that of the NaOH [82, 87, 88]. The cleaning effectiveness for the NaOH was high for the fouled PS<sub>u</sub> membrane of Liang *et al.* [84], but however, moderate for the PS<sub>u</sub> and PVDF membranes of Sun *et al.* [90] and very low for the PVC membrane of Zhang *et al.* [85] and the PS<sub>u</sub> membrane of Arnal *et al.* [82], which is another probe that cleaning goodness of a reagent also depends on the specific surface materials.

Concerning acidic cleaners, moderate goodness of the citric acid and the HCl was seen by Liang *et al.* [84] and Zhang *et al.* [85], while Arnal *et al.* [82] reported that the citric acid was unable to remove the biofilm formed in his membrane.

Liang *et al.* [84] also pointed out that several mixtures of NaOH and NaClO gave higher cleaning effectiveness than applying them independently, but the effect was far from being additive.

### 3.5.3. Chemical cleaning of fouling from wastewaters

Zheng *et al.* [94] compared the *permeability restoration* after applying H<sub>2</sub>SO<sub>4</sub>, permeate, tap water, H<sub>2</sub>O<sub>2</sub>, demineralized water, NaClO, NaOH and the mixture NaOH + NaClO to clean a 100 kDa PES membrane that had filtered a tertiary effluent at constant  $J_F$ . The *permeability*

*restoration* took the values 15, 18, 24, 24, 45, 61, 65 and 91 % respectively, probing the good ability of the alkaline reagents (the hydroxide and oxidizer) to remove the foulants. These authors also added the NaOH, NaClO and H<sub>2</sub>O<sub>2</sub> cleaners to the permeate stream used for BW after each filtration cycle. Once defined an upper TMP limit, the presence of NaClO allowed operating longer hours than using the permeate alone, followed in decreasing order by H<sub>2</sub>O<sub>2</sub> and NaOH. The change of the effectiveness order of the cleaners when applying the chemical cleaning straight forward or using the reagents during the BW is due to the fact that BW modifies the cake structure after its application (“section 3.5.8”).

Te Poele and van der Graaf [46] used the formulated alkaline cleaner Divos 110 alone and mixed with a protease, finding that the presence of the enzyme was important only if the effluent of the wastewater treatment plant contained a considerably amount of proteins. If a coagulant was added to the wastewater, the formation of metal salts needed additional acidic treatments to restore the initial permeability.

#### 3.5.4. Chemical cleaning of fouling from dairy streams

For PES membranes fouled with skim milk, Delaunay *et al.* [98] and Rabiller-Baudry *et al.* [25, 99-101] found that the formulated cleaner Ultraclean II (a complex mixture of anionic and non-ionic surfactants) was better than Ultrasil 10, and both were more efficient than NaOH. Concerning surfactants, the last authors indicated that Tween 20 was similar to the NaOH, but that SDS was intermediate between Ultrasil 10 and NaOH [99-101]. This superior performance of the SDS over the NaOH was also seen by Kazemimoghadam and Mohammadi [102] using not-skim milk as foulant and the same concentrations for both cleaners. After filtering a sweet whey powder solution, Chen *et al.* [111] obtained that the maximum cleaning goodness of SDS (concentrations between 0.1 and 2 wt. %) was also higher than that of NaOH (concentrations between 0.01 and 1 M), but opposite to Mohammadi *et al.* [97], who reported that the maximum effectiveness of SDS was lower than that of the NaOH when cleaning the fouling generated by filtrating normal milk.

NaClO or chlorinated alkaline reagents give *water flux recoveries*, *water flux recovery ratios* or *resistance removals* higher than those obtained with NaOH or SDS individually [11, 97, 102, 104], although if both NaOH and SDS are mixed, the result can overcome that of the alkaline oxidizer [102]. When compared with Ultrasil 10 on a spiral membrane fouled with skim milk, the goodness of NaClO depends on the ratio between the solution volume and the membrane surface area [104]. At 3.8 L/m<sup>2</sup>, the *water flux recovery* of NaClO is 82 % and at 7.7 L/m<sup>2</sup> is 99 %, being 92 % that obtained with the formulated agent regardless of the employed ratio.

Acidic oxidizers [104], mineral acids and EDTA [11, 102] give poor *water flux recoveries*, and sometimes, negative *resistance removals* [97], which can be associated to the modification of the foulant layer structure (making it more difficultly to be removed) or with an increase in the hydrophobicity of the membrane. After filtering whey, Madaeni and Sharifnia [108] showed that

at 0.1 N, *water flux recoveries* of NaOH, HCl and H<sub>2</sub>SO<sub>4</sub> reached their maxima, being all of them higher than 80 % (around 93 % for the H<sub>2</sub>SO<sub>4</sub>). At higher concentration (1 N), NaOH gave worse *water flux recoveries* (65 %), as well as HCl and H<sub>2</sub>SO<sub>4</sub>, which had a higher drop in their effectiveness, reaching only 40 and 18 %, respectively.

Sometimes, these reagents are sequentially applied. For instance, Madaeni and Sharifnia found that 0.5 % of NaOH followed by 0.5 % of HCl did not improve the *resistance removal* of the NaOH alone (91 %), but if the sequence was changed to acid followed by alkali, the *resistance removal* was enhanced (94 %). Similar results were obtained when the sequence was alkali/acid/alkali or acid/alkali/acid. For the first sequence, the *resistance removals* were 90 %, 91 % and 91 %, while for the second sequence they were 85 %, 95 % and 94 %. However, it has to be pointed out that in this work, HCl concentration was close to the optimum, which caused an unusual high fouling removal due to the acidic cleaner. Vaisanen *et al.* [23] saw that 0.075 wt. % NaOH followed by 0.3 wt. % HNO<sub>3</sub> decreased the *water flux recovery* obtained with NaOH alone in RC, PES and PA membranes fouled with reconstituted whey protein. When dealing with skim milk and PES membranes, Paugam *et al.* [10, 11] observed that the addition of NaOH after a previous HNO<sub>3</sub> treatment gave a *water flux recovery* similar to that of employing the hydroxide alone, but if the first step consisted in the alkali and the second in the acid, the *water flux recovery* increased. Nevertheless, it was due to interactions between the foulant and the acid, because ATR-FTIR did not confirm further protein removal. Additionally, two-step procedures with the same cleaner, either NaOH twice or NaOH + NaClO twice were also applied and it was found that they were better than the single step procedure [11]. In another paper, Paugam *et al.* [104] also studied the sequence NaClO/Ultrasil 10, finding that the *water flux recovery* was the same as that obtained by applying NaClO alone with the ratio 3.8 L/m<sup>2</sup> (80 %), but lower than that obtained using Ultrasil 10 alone (92 %). However, when the formulated cleaner was applied after other reagents such as NaOH, acid or surfactant, cleaning goodness improved which could be a probe that the NaClO do not only degrades proteins, but also changes the structure of the fouling layer, making it more difficult to be removed.

Feed pH may considerably affect water flux and *resistance removal* on some cleaning systems. Muñoz-Aguado *et al.* [116] filtered a reconstituted whey protein solution at pH 5 and 7 through a PS<sub>u</sub> membrane and cleaned it with 0.75 % TAZ, 0.2 % CTAB and the sequential addition of 0.01 %  $\alpha$ -CT and 0.1 - 0.2 % CTAB (with and without hot water rinsing between the steps), finding that, in general, the cleaning goodness was lower at pH 5 (mean isoelectric point of whey proteins) than at pH 7. TAZ performed better than the surfactant and the enzyme/surfactant sequence except when compared with the combination  $\alpha$ -CT/rinsing/CTAB (0.2 %) fouled at pH 5, being this last sequence the only case in which the cleaner yield was higher at pH 5 than at pH 7.

With regard to the sanitization, in literature dealing with cheese whey [105, 106, 112, 114] it was found that the reduction of the microorganism population was not always reliable with the ordinary cleaning processes and suggested the use of electrolyzed water or chlorinated disinfectants for further sanitization.

### 3.5.5. Chemical cleaning of BSA

Kim *et al.* [121] employed 0.1 wt. % HCl, NaOH, SDS and CTAB solutions to clean 30 kDa PS<sub>u</sub> membranes after filtering a BSA solution at pH 5 and 7. The *resistance removals* with the acid, the alkali and the SDS were lower for the membrane fouled at pH 7 than at pH 5, likely due to the net protein charge (zero at 5 and negative at pH > 5). At pH 5, both NaOH and HCl were equally good, giving *resistance removals* around 85 %. CTAB and SDS were not so efficient, giving values of 60 and 40 %, respectively. However, when fouling was conducted at pH 7, CTAB was the most effective, with a cleaning effectiveness slightly higher than that at pH 5.

Using 20 kDa PES membranes fouled at pH 7.4, Kuzmenko *et al.* [24] tested individually NaOH (100 – 3000 ppm), NaClO (100 – 5000 ppm of free Cl<sub>2</sub>) and H<sub>2</sub>O<sub>2</sub> (100 – 3000 ppm) for 30 min. *Water flux recoveries* followed the order NaClO > NaOH > rinsing with distilled water > no cleaning > H<sub>2</sub>O<sub>2</sub>. Concentration was only important in the case of the NaClO solution, because the higher the amount of free chlorine, the higher the *water flux recovery* (more than 100 % in some cases). The improvement due to NaOH when compared with the water rinsing was very low (only of 5 %), in accordance to the cleaning effectiveness of Kim *et al.* [121] at pH 7. The work of Zhu and Nystrom [124] was also in agreement with the pH dependence pointed out by Kim *et al.* [121]. They fouled hydrophobic PS<sub>u</sub> membranes at pH 5, finding that 0.5 wt. % NaOH performed slightly better than NaClO, with *water flux recoveries* around 95 %, while citric acid and oxalic acid gave results of 89 % (lower than those of the hydroxide and hypochlorite, but high in absolute terms). The pH of the cleaning solutions did not influence very much the results, because NH<sub>4</sub>OH was also tested and a *water flux recovery* was 82 %.

Platt and Nystrom [125] fouled PS<sub>u</sub> membranes with BSA solutions at pH 5 too, but found that the 0.055 % NaOH solution was not very effective, giving a *water flux recovery* of 44.5 %. Only the 0.5 % of the commercial acidic cleaner F91 Filter VH and 0.06 % of the anionic surfactant Mersolat W40 gave lower protein removals. However, if the same concentrations of NaOH and Mersolat were mixed together with 0.023 % of EDTA, the *water flux recovery* reached the 100 %, and the Amido Black test gave the same intensity that the commercial alkaline agent F83 Filter E, which its *water flux recovery* was 242.5 %. The authors explained that the change in pH due to the NaOH, increases the electrostatic repulsion between the proteins, disrupting the foulant packing, but it is needed that the contact between the protein and the hydroxide had to be improved by decreasing the surface tension by adding the surfactant. In addition, this surfactant is also adsorbed to the protein increasing its charge and solubility.



CTAB is not the only cleaner which its cleaning effectiveness increases when the fouling pH rises from 5 to 7. Muñoz-Aguado *et al.* [116] observed that 0.4 % TAZ and the sequence 0.01 %  $\alpha$ -CT/0.1 % CTAB (without hot water rinsing between the steps) performed better when the fouling had been carried out at the highest pH, using a similar membrane to that of Kim *et al.* [121]. Nevertheless, other modifications of the  $\alpha$ -CT/CTAB sequence (varying surfactant concentrations or frequency of the hot water rinsing) were more effective at the lowest pH.

### 3.5.6. Chemical cleaning of fouling from oily wastewater

Results vary widely from one author to another. PAN membranes from the studies of Salahi *et al.* [154] were considerably well cleaned by a mixture of SDS + EDTA at pH 10, while the *water flux recovery ratios* of inorganic acids, such as H<sub>2</sub>SO<sub>4</sub>, HCl, HNO<sub>3</sub> and peroxomonophosphoric acid (H<sub>3</sub>PO<sub>5</sub>), were negative. On the other hand, the fouling of the PS<sub>u</sub> membranes of Lindau and Jonsson [151] was better removed with Ultrasil 75 (a mixture of HNO<sub>3</sub> and phosphoric acid) than with Ultrasil 11 (Na<sub>4</sub>EDTA + NaOH + anionic and non-ionic surfactants). Nevertheless, when a two-step cleaning was performed, the J<sub>wc</sub> obtained was higher with the sequence Ultrasil 11/Ultrasil 70 (acidic) than with Ultrasil 70/Ultrasil 11.

### 3.5.7. Enzymatic cleaning remarks

Maartens *et al.* [134] noted that for the cleaning of a PS<sub>u</sub> membrane fouled with an abattoir effluent, a mixture of the commercial agents Alkazyme and Zymex (both with proteolytic activity) gave protein and lipid content reductions of 95.9 and 57.4 %, respectively. The protein removal was considerably higher than that obtained with SDS, Triton X100, lipase A and protease A, but the lipid removal was comparable to that of the protease A and SDS.

The commercial TAZ was also more effective than NaOH or HCl removing the extracts of soy flour [132] and more suitable than CTAB for membranes fouled at pH 5 and 7 with reconstituted whey protein and BSA [116].

However, enzymes (or formulated cleaners containing them) do not necessarily perform better than other reagents in all the systems. For example, Coolbear *et al.* [107] achieved a higher water flux at 70°C with NaOH + EDTA than with the *Thermus* T351 proteinase after the cleaning of membranes which had processed whey.

Chen *et al.* [111] observed that surfactin-fouled PES membranes treated with NaOH at pH 13 were more cleaned than those treated with TAZ. Although, if the pH of NaOH was lowered to 11, the TAZ gave better results.

Lipnizki *et al.* [133] compared three methods with two or three steps (enzymatic/caustic, caustic/acid/caustic and caustic/enzymatic/caustic) obtaining the same 100 % *permeability*

*recovery* in spiral membranes fouled with proteins. Nonetheless, the two-step method was economically and environmentally better.

The higher effectiveness of surfactants over enzymatic cleaners in some cases was pointed out by the work of Mendoza-Roca *et al.* [162], who found that 40 kDa membranes fouled with unhairing wastewater from a tannery were more effectively cleaned by SDS than by Riberzim MPX, Defat 50 or a binary mixture of both with Na<sub>4</sub>EDTA. Chen *et al.* [111] reported that in PS<sub>u</sub> and PES membranes fouled with BSA + bLG and whey, respectively, the *water flux recoveries* at the optimum concentration followed the decreasing order SDS > Protease or TAZ > NaOH > HCl. Maartens *et al.* [140] also saw that Triton X100 and SDS + NaOH gave better cleaning than cellulase, zumyzyme and peroxidase for treating PES membranes fouled with pulp and paper effluent. Nevertheless, if that membrane was coated with Pluronic F108 previously to the filtration, cellulase and zumyzyme were better than the mixture SDS + NaOH. This is another probe that the membrane characteristics dramatically conditioned the cleaning yield.

The addition of surfactant to the enzymes enhances their cleaning abilities [68, 107, 134, 140]. The aforementioned Maartens *et al.* [140] reported that the mixture of Lipase A + Triton X100 gave results very close to the mixture of Alkazyme and Zymex. The sequential combination of  $\alpha$ -CT and CTAB also worked better than the individual reagents [116].

### 3.5.8. Physical cleaning protocols

The main objective of BW is to reduce the frequency of chemical cleaning, because the use of chemical reagents is typically cumbersome. It requires the shutdown of the membrane unit for several hours and may affect the membrane lifetime [54]. However, BW consumes permeate and increases downtime periods for its application, both of which reduce the overall plant capacity. Thus, an optimization of BW duration, frequency and flow (or pressure) has to be done in order to obtain the maximum net permeate volume [47, 55] or net steady state  $J_F$  [75].

In this regard, van de Ven *et al.* [63] also proposed to carry out the BW only at the final part of a hollow-fiber module (partial BW) working in DE filtration mode, because foulants are not equally distribute over the length of the module. However, there is not “a priori”, a way to know if the foulants are more concentrated at the end of the module or along it.

Sometimes, chemicals are added to the permeate in order to avoid biofouling or to improve the BW efficiency [86]. This addition also allows lowering the BW frequency, the velocity and the BW duration [54], and can modify the conclusions if synthetic solutions are filtered instead of real process streams [76].

According to Ye *et al.* [48], BW removes not only the reversible foulants, but also modifies the structure of the deposits making *fouling rate* change from cycle to cycle. This is in agreement with the findings of Zheng *et al.* [94], who reported that, when filtering tertiary effluents, the

activity of the  $H_2O_2$  when used it with the BW water was higher than when used it as mere a chemical cleaner after several UF/BW cycles. Later on, Resosudarmo *et al.* [49] confirmed this structure change by the analysis of the fouling layers through mass measurements, inductively coupled plasma optical emission spectroscopy (ICP-OES) and liquid chromatography organic carbon detector (LC-OCD).

FF is rarely employed alone, but usually combined with BW, because it is only able to remove the fouling on the membrane surface and not that inside the pores. FF velocity and duration can be adjusted to improve *water flux recovery* getting almost a complete removal of the turbidity, but if BW is applied right after, the turbidity increases again because of the mentioned pore-related foulants [55].

Two or three-steps procedures, consisting in BW followed by FF, FF followed by BW or BW followed by FF and then BW again improve the flux recovery of BW or FF alone [55, 84]. The best strategy is applying FF after BW, because FF flush out debris resulting from BW and break up the fouling layer weakened (but not totally removed) by the BW. In the opposite sequence, FF does not seem so good removing the fouling layer without weakening it previously with BW [91].

The right combination of FF, BW an air bubbling can greatly reduce the permeability drop and the energy consumption when compared to the air assisted BW, which in turn, is better than customary BW [50, 64, 77]. However, sometimes, the increase in  $J_F$  does not compensate the energy consumption due to the air [75].

Additional techniques have been developed in order to improve traditional physical cleaning methods. For instance, pressure pulsing, which consists in closing the permeate valve at given time intervals, was used to reduced BW frequency. Kennedy *et al.* [55] probed that the use of pressure pulses every 5 min for 5 s in combination with conventional BW allowed reducing the BW frequency. In addition, Jacobs *et al.* [58] showed that combinations of reverse-pressure BW, FF and reverse-pressure pulsations were able to clean part of the hydraulically irreversible fouling left by conventional BW and could operate for long time without chemical cleaning.

Concerning the application of ultrasounds for membrane cleaning, Muthukumaran *et al.* [110] successfully applied them for the treatment of  $PS_u$  membranes fouled with whey. The cleaning effectiveness as function of the water pH (adjusted with NaOH and a mixture of 1:1 nitric/orthophosphoric acid), the SDS concentration, the TMP, the CFV or the temperature was similar and qualitatively independent of the use or not of ultrasounds. Nevertheless, in all the cases, there was an enhancement in cleaning goodness due to the ultrasonic irradiation at 50 kHz and 300 W. Other researchers has also pointed out this improvement in the action of EDTA [103], NaOH [131], citric acid [153], NaClO [158] and even of FF [141] when using ultrasounds.

When varying the ultrasonic frequency between 28 and 100 kHz, Kobayashi *et al.* [138] found that the lowest frequency gave the best removal of peptone residues on PS<sub>u</sub> membranes, in agreement with the works of Cai *et al.* [161], Ng *et al.* [72], Lujan-Facundo *et al.* [131] and Maskooki *et al.* [103] who fouled PES membranes with dextrans, humic acid, BSA and skim milk, respectively. However, Maskooki *et al.* [103] also tested a mixed wave (in which the system was set to switch between 28, 45 and 100 kHz frequencies every 1 min at constant power), and results were better than those at a constant frequency of 28 kHz.

On the other hand, fixing the frequency at 20 kHz, the *water flux recovery* increased with the ultrasonic power (varied from 30 to 180 W) for the cleaning of PES membranes fouled with a Radix astragalus extract, but it seems to tend to a plateau [160]. Moreover, this improvement caused by ultrasonic power was much greater than those induced by a temperature rise or a frequency decrease [160]. Nonetheless, high ultrasonic powers and/or high sonication times may lead to membrane damage [153].

### 3.5.9. Performance of several cycles of fouling/chemical cleaning

Two cycles of filtration/cleaning were carried out by Tran-Ha *et al.* [118] and by Muñoz Aguado *et al.* [116] on PS<sub>u</sub> membranes. The first researchers employed CTAB to remove remains of reconstituted whey protein and the second ones used TAZ and the sequence  $\alpha$ -CT/CTAB to clean BSA or reconstituted whey protein. They found that the drop of  $J_{wc}$  after the first fouling/cleaning cycle (with respect to the permeate flux before the fouling) was greater than that after the second cycle. In addition, Kim *et al.* considered three cycles of BSA filtration/HCl cleaning [121] and four cycles of BSA filtration/NaOH cleaning [122], and there was again a greater water flux drop after the  $i$  cycle than that after the  $i+1$  cycle, being the most steep drop that after the first usage of the membrane too. Therefore, these authors assumed that the initial flux decline was due to the solute-membrane interactions, which were stronger than the protein-protein interactions, predominant in the subsequent cycles.

Norazman *et al.* [120] pointed out the same features on the membrane water flux deterioration than Kim *et al.* [121, 122] after fouling four times a PES membrane with whey protein isolate and cleaning it four times with a sequence of NaOH/HCl. However, they attributed the lower water flux drops of the consecutive cycles to the fact that the spots for irremovable fouling were already saturated during the first cycle.

On the other hand, Jones *et al.* [145] found no such clear trend in the  $J_{wc}$  reduction through a four-cycle experiment consisting in filtrating a spent sulphite liquor through a FP membrane and then a cleaning step with NaOH. Moreover, the four cycles of filtration and cleaning performed by Saha and Balakrishnan [164] on a PES UF membrane remarked the difficulty of making generalizations. In their work,  $J_{wc}$  increased from cycle to cycle if the feed was sugarcane juice,

but decreased if only the polysaccharide fraction of the juice was filtered. The chemical cleaner was a mixture of NaOH and NaClO for both feeds.

The comparison between several cleaners is also cycle-dependent. For example, when lignosulphonates were filtered for five times using a PES membrane and the membrane was cleaned after each filtration, the ratio between the steady state  $J_F$  during the filtration and the permeate flux at the beginning of the cycle remained constant when using Ultrasil 11 (75 %) from the second to the last cycle. However, it decreased from 90 % in the second cycle to 75 % in the fifth cycle when using  $HNO_3$  [139]. On the other hand, when filtering spent sulphite liquor through PES and  $PS_u$  membranes and cleaning them with Ultrasil 11 or NaOH, the changes of the steady state permeate flux ( $J_F$ ) were slight from the first to the second cycle, and until the sixth cycle these permeate flux reductions were similar for both cleaners. However, from the eighth to the fifteenth cycle, Ultrasil 11 gave lower reduction than the NaOH [142]. Weis *et al.* [15] also employed Ultrasil 11 and NaOH to clean PES and RC membranes fouled with spent sulphite liquor. As for the PES membranes, NaOH and Ultrasil 11 gave steady state product fluxes ( $J_F$ ) very similar after several cycles but the pure water fluxes ( $J_{WC}$ ) decreased from cycle to cycle with the NaOH until reaching a constant value after the seventh cycle. With the Ultrasil 11 the  $J_{WC}$  increased from cycle to cycle, being higher than the pure water flux of the pristine membrane ( $J_{W0}$ ) after the 7<sup>th</sup> cycle. FTIR showed that Ultrasil 11 covered the PES surface with a surfactant layer after each cleaning, which decreased the foulant deposition in the following filtration. Concerning the RC membranes and the NaOH cleaner, both the  $J_{WC}$  and the steady state permeate flux ( $J_F$ ) decreased with the cycle number and reached a plateau after the seventh cycle. With Ultrasil 11, the trends and the final value of the pure water flux  $J_{WC}$  were the same, but  $J_F$  went through a minimum before tending to the plateau. Therefore, for the first cycles, NaOH was better than Ultrasil 11 as long as the  $J_F$  was considered instead of the  $J_{WC}$ .

### 3.6. Conclusions

---

In this section, physical and chemical cleaning of polymeric UF membranes has been reviewed. The first one includes FF, BW (alone, pulsated or combined with air) and ultrasounds. These physical procedures have been applied successfully, not only as cleaning steps themselves, but also as a way to reduce the frequency of chemical cleaning procedures which are more aggressive for the membranes. The chemical cleaning is constituted by alkalis, acids, surfactants, chelatants, oxidizers, enzymes, disinfectants and formulated cleaners. But, there is not an absolute scale to define which one is the best in terms of cleaning effectiveness. In fact, cleaning goodness of the reagents depends on many factors, which have been carefully described such as foulant and fouling conditions, membrane material, geometry and size of the system, cleaner concentration and pH, cleaning time and temperature and the interactions among them. Thus, due to the complexity

of the systems, some opposite trends in the results from many authors who studied similar cases were found.

Throughout this review, all the parameters defined to evaluate cleaning effectiveness have been gathered and unified in terms of nomenclature in order to serve as reference and to make easier result comparison. These parameters can be divided into two groups depending on the measured properties: functional properties which include flux measurements, TMP values, permeabilities or resistances and surface properties which involve physicochemical analyses of the membranes.

Although, parameters based on flux measurements and TMP are the most employed ones, their results are not always reliable due to interactions of the cleaning agent with the membrane or with the foulant which can mislead the results. In these cases, more sophisticated techniques such as SEM, AFM or FTIR are specially required. However, these techniques are not available in plants operating at full-scale, mainly, because they are destructive.

At present time, due to the high number of factors which affects the cleaning goodness, there is not a standardized procedure, valid for all the cases, to develop cleaning protocols. So far, the best way found to face the problem is the trial-and-error method going from lab to full scale. Nevertheless, it seems that the nature of the foulant is the major aspect to take into account when deciding the cleaning strategy which involves cleaners and conditions.

In order to show general trends, it was observed that NOM was more efficiently removed from membranes by formulated cleaners, NaClO and NaOH. When it comes to microbial species, NaClO gave good cleaning effectiveness, citric acid showed a moderate performance and NaOH alone was not efficient, but mixed with NaClO performed very well. Concerning fouling from wastewaters, the mixture NaOH + NaClO gave the best cleaning yield followed by themselves alone. Moving on to dairy residues, formulated cleaners, such as Ultraclean II and Ultrasil 10, were the most efficient above the NaOH and the NaClO in some cases, nevertheless surfactants, such as SDS, can play an important role in the removal mechanisms increasing efficiencies. With regard to the BSA, the NaClO was again the most effective followed by NaOH, but it was found a strong influence of the feed pH during the filtration. In the case of several cycles of fouling/cleaning formulated cleaners such as Ultrasil 11 turned out to be more efficient in the long run.

Finally, extensive theoretical work is needed not only for cleaning understanding, but also for fouling comprehension, as cleaning depends on the previous filtration stage. In this regard, the development of mathematical models which would provide parameters to compare the data from several researches, would be very valuable for the cleaning progress.



## **4. Materials and methods**

---

---





## 4.1. General considerations

---

This chapter is devoted to show the materials, procedures and techniques employed during the experimental part of this Thesis. First of all, the chemicals used for both the ageing and the analysis procedures are gathered in “section 4.2”. Then, the ageing procedures are commented in “section 4.3”. Finally, the characterization techniques, including functional and physicochemical analyses are described in “section 4.4”.

## 4.2. Materials

---

### 4.2.1. Membranes

Six commercial polymeric UF membranes made of PES on a nonwoven support from different manufacturers and two polyamide thin-film composite NF membranes were selected for the ageing studies. Four UF membranes made of PES and PS<sub>u</sub> were used in the development of the model to analyze LLDP results. Membrane details are gathered in **Table 4.1**.

### 4.2.2. Chemicals

Alkaline ageing solutions were prepared with NaOH pellets (Panreac - reagent grade) and the acidic ones from a 65% HNO<sub>3</sub> solution (Sigma-Aldrich – puriss. grade). Sodium chloride (NaCl, Merck Millipore - analysis grade) solutions were also used for some tests.

Membrane rejection performance for NF membranes was determined using a single salt solution of sodium sulfate (Na<sub>2</sub>SO<sub>4</sub>, Fluka - puriss grade) and a mixture of uncharged solutes: glucose and sucrose (both from Panreac - puriss grade).

All the previous solutions as well as the one used to determine the permeability of the membranes were prepared with dionized (DI) water (>0.8 MΩ·cm).

MWCO determination for UF membranes was made by filtrating a mixture of polyethylene glycols (PEG) with ten different nominal molecular weights (MW): 1.5, 2.05, 3.0, 4.6, 6.0, 8.0, 10, 12, 20 and 35 kDa (from Fluka and Sigma-Aldrich). The mobile phase used for the subsequent size exclusion chromatography (HPSEC) analysis (and for diluting the PEG standards) was prepared with sodium azide (NaN<sub>3</sub>) (Sigma-Aldrich - Reagent Plus) in ultrapure water (>18 MΩ·cm).

Ultrapure water was also employed to analyze membrane hydrophobicity throughout contact angle measurements. Contributions to the total solid surface energy were determined using formamide (Fluka Microselect, >99.0% purity) and methylene iodide (Fluka purum, >98% purity, stored over copper filings) as wetting liquids.

Dimethyl sulfoxide (DMSO) (Panreac - ACS reagent) and 37 % hydrochloric acid (Panreac - ACS reagent) were used in the determination of terephthalic acid through gas chromatography.

**Table 4.1.** Details of the membranes used in the ageing studies and the development of the LLDP model. Data reported by manufacturers.

Membrane	Manufacturer	Material	Type	MWCO (kDa)	pH range (Long-Term)	pH range (Short-Term)	Maximum temperature	Permeability (L/hm <sup>2</sup> bar)	This work*
NF90	Dow Filmtec	PA	NF	N/A	2 – 11	1 – 12	45°C	9	7 ± 1
NF270	Dow Filmtec	PA	NF	N/A	2 – 11	1 – 12	45°C	11	13 ± 1
UH004	Microdyn Nadir	PES	UF	4	0 – 14	0 – 14	95°C	> 20	13 ± 1
UP005	Microdyn Nadir	PES	UF	5	0 – 14	0 – 14	95°C	> 30	15 ± 2
HFK-328	Koch Membrane Systems	PES	UF	5	2 – 10	1.8 – 11	55°C	24 - 53	50 ± 4
PT	GE Osmonics	PES	UF	5	2 – 10	1 – 11.5	50°C	44	27 ± 3
UP010	Microdyn Nadir	PES	UF	10	0 – 14	0 – 14	95°C	> 150	144 ± 17
UP020	Microdyn Nadir	PES	UF	20	0 – 14	0 – 14	95°C	> 200	220 ± 25
M030	Merck Millipore	PS <sub>u</sub>	UF	30	N/A	N/A	N/A	N/A	N/A
M300	Merck Millipore	PS <sub>u</sub>	UF	300	N/A	N/A	N/A	N/A	N/A

\*Experimentally determined in this work (intervals as standard deviations).

### 4.3. Ageing procedures

Two different size scales were used to study membrane ageing. For the small one, which was employed for both UF and NF membranes, circular flat-sheet membrane coupons of 13.4 cm<sup>2</sup> were used and ageing was conducted in soaking mode. For the larger one, which was only used for one NF membrane, the effective surface area of the rectangular flat-sheet membranes was 140 cm<sup>2</sup> and the ageing was carried out in cross-flow.

#### 4.3.1. Ageing procedures at small scale

Membranes were first thoroughly rinsed with DI water and characterized as described in “section 4.4”. Ageing solutions were prepared with HNO<sub>3</sub> and NaOH in three different concentrations (0.01, 0.1 and 1.0 M), obtaining extreme pH values (acidic ones: 0, 1, 2 and alkaline ones: 12, 13, 14) which are close and sometimes beyond the ranges recommended by the manufacturers (**Table 4.1**). These solutions were titrated and renewed throughout the experiments in order to ensure that concentrations were kept constant.

Ageing of UF membranes lasted for 150 days which would be equivalent to 10 years of use assuming that membranes are subjected to 1 h cleaning per day whereas NF membranes were aged for 100 days (which would be equivalent to a lifetime of more than 6 years under the previous assumptions) or until the Na<sub>2</sub>SO<sub>4</sub> rejection became lower than 60 %, which was taken as an indication of membrane failure and used as a criteria for ending the ageing experiment.

The procedure consisted in soaking the membranes in the ageing solutions (using polyethylene flasks) and placing them in a thermostated chamber (Heidolph Unimax 2010, Schwabach Germany) under an orbital agitation of 150 rpm.

Ageing was followed through the characterization of the membranes at given exposure times, which varied from hours to days depending on the ageing rate. Previously to each membrane performance characterization (described in “section 4.4”), membranes were thoroughly rinsed and DI water was filtered to remove the ageing solutions (indicated by a neutral pH).

Four membrane coupons were used under each tested condition. For the NF membranes, all the samples were used for the permeability and rejection characterization, whereas for the UF ones, three of them were exclusively employed to follow the evolution of membrane permeability throughout the ageing and the fourth one was also used to determine the MWCO after the permeability measurement. The permeability of this sample was usually slightly lower than that of the other three membranes, meaning that the PEG filtration step caused some fouling. Nevertheless, this difference was always below 10 % (20 % for the UP010 and UP020 membranes, with higher permeabilities) and was kept approximately constant over the ageing.

At the end of the treatments, the four aged membranes and another set of four new coupons were used to characterize the performance (permeability and MWCO determinations) and the physicochemical properties of the membranes after the ageing and in its original state, respectively. Membrane surface analysis required sample drying at 50°C for 24 h.

Ageing studies were conducted at 25, 35 and 50°C. At 50°C, all membranes were subjected to both NaOH and HNO<sub>3</sub> at the three different concentrations (0.01, 0.1 and 1.0 M) whereas the influence of temperature was only studied for some UF membranes using exclusively 1.0 M NaOH for a period of 60 days.

Finally, an additional set of membranes were soaked in DI water under the same experimental conditions in order to serve as reference.

#### **4.3.2. Ageing procedures using a cross-flow system**

The ageing studies at larger scale were carried out in a cross-flow filtration system SEPA CF II from GE Osmonics (California, USA). A thermostated bath was connected to a heating coil to control the solution temperature and two spacers of 0.15 and 0.02 mm were placed on the retentate and permeate sides, respectively.

This configuration was only used to study the ageing of one NF membrane with the 0.1 M NaOH solution at 50°C. The ageing was carried out as a regular cleaning step, pumping the NaOH solution through the membrane module at 50 L/h, at which the cross-flow velocity was 0.3 m/s, and with no pressure gradient. Two different configurations were tested in which the permeate valve was kept either open or close.

After each ageing step, the system was thoroughly rinsed with tap and DI water. Then, membrane characterization was conducted at 25°C.

### **4.4. Characterization techniques**

---

The characterization techniques employed in this work can be classified into three groups according to their final goal. The first one involves those procedures directed to determine membrane performance in terms of permeability and rejection capabilities (expressed as MWCO or solute rejection). The second one involves those techniques whose aim is the membrane physicochemical characterization (i.e., ATR-FTIR, SEM-EDS, AFM, contact angle measurements and LLDP). The last group involves complementary techniques such as chromatographic and conductivity analyses which are used indirectly for the membrane characterization.

Concerning the functional characterization throughout the ageing, at small scale, the measurements were carried out using stirred dead-end cells (Millipore - Model 8050) with an available volume of 65 mL. Cells were pressurized using nitrogen (Air Liquide, 99.8 % purity) and

the stirring rate was fixed at 400 rpm for all the experiments. TMP was set at 0.5 and 2.0 bar for the MWCO determinations and the permeability measurements of the UF membranes, respectively, and at 5 bar for the permeability and rejection analyses of the NF membranes. At larger scale, membrane characterization was carried out in the cross-flow unit. Feed flow was set at 50 L/h (cross-flow velocity 0.3 m/s) and the TMP was regulated by the retentate valve in order to obtain a permeate flux equal to the initial obtained in the dead-end filtration cell. The TMP which met this condition was 3.6 bar.

#### 4.4.1. Membrane permeability

Measurements were carried out by filtering DI water until constant permeate rate was reached (taking from 2 to 5 min in the dead-end cell and around 15 min for the cross-flow system). Permeate weight, temperature and TMP were measured with time using a scale, a temperature sensor and a pressure transducer, respectively. Data acquisition and processing was performed automatically for the dead-end filtration system by means of a self-made LabVIEW (National Instruments) software program which is explained in detail in the “section 8.1”, whereas in the cross-flow system all the measurements and calculations were done manually.

Firstly, membrane permeability was determined using Eq. (4.1) where the collected permeate weight is divided by the solution density at the filtration temperature (T), the time, the effective membrane filtration area and the applied TMP.

$$Lp^T = \frac{(\text{Weight [g]})/(\text{Density [g/L]})_T}{(\text{Time [h]})(\text{Membrane Surface Area [m}^2\text{]})(\text{TMP [bar]})} \quad (4.1)$$

Although membrane characterization was carried out at controlled room temperature of  $25 \pm 4^\circ\text{C}$ , small temperature fluctuations were taken into account by considering its effect on the viscosity of the solution according to Eq. (4.2) [179]. Therefore, membrane permeability was always referenced to  $25^\circ\text{C}$ .

$$Lp^{25^\circ\text{C}} = \frac{Lp^T \mu^T}{\mu^{25^\circ\text{C}}} \quad (4.2)$$

The use of small membrane coupons leads to a high variability in membrane performance. Thus, a relative permeability (generally denoted as  $Lp/Lp_0$ ) was used to follow the ageing. The relative permeability of one  $i$  coupon at certain point of the ageing was obtained by dividing the measured permeability of that coupon at a given ageing time  $t$  ( $Lp_{i,t}^{25^\circ\text{C}}$ ) by the initial permeability in the pristine state of the coupon ( $Lp_{i,0}^{25^\circ\text{C}}$ ).

Finally, actual permeability magnitudes, used during the discussion, were determined multiplying the relative values by the averaged initial permeability which in turn, was calculated from the 28 membrane coupons needed to cover all the studied conditions.

The use of the relative permeability allows correcting the variability of the coupons and therefore, comparison between ageing conditions becomes clearer.

#### 4.4.2. Membrane rejection capability

Membrane rejection is defined by the amount of solute removed from the feed. However, the common procedures for the evaluation of the rejection performance strongly depends on the membrane type due to the different solute size ranges that membranes are able to separate. Therefore, this section is divided to account for the methodology employed for the UF membranes (MWCO determination) and for the NF ones (single solute rejection measurements).

##### 4.4.2.1. MWCO determination for the UF membranes

Separation performance of UF membranes was characterized by the rejection of molecular markers. A solution containing a mixture of PEGs (at an individual concentration of 0.05 wt. %) dissolved in 0.05 M NaN<sub>3</sub> solution, in order to avoid bacterial proliferation in the analysis step, was used. The filtration experiments were carried out at 0.5 bar and permeate samples were taken after collecting approximately 2 mL of permeate to ensure constant feed concentration. Feed and permeate samples were analyzed by HPSEC (explained in “section 4.4.8”) and MWCO was defined as the solute molecular weight for which the membrane rejection was 90 % [180].

The presence of concentration polarization adds an extra resistance to that of the membrane, which leads to an apparent membrane rejection lower than the real one [181, 182]. In order to minimize this effect, experiments were carried out at the highest possible stirring rate and using PEG concentrations in the feed which were the lowest allowed for accurate HPSEC determination (based on permeate samples from the highest rejecting membranes, UH004 and UP005).

However, the high permeability of UP010 and UP020 membranes as well as the increase in permeability that other ones experience throughout the ageing treatments leads to situations in which concentration polarization may affect the results. In order to take this into account, intrinsic membrane rejections (and not observed ones) were used to determine the MWCO of the membranes.

The observed membrane rejection for the PEG molecular weight fraction  $j$  ( $R_{\text{obs},j}$ ) relates the permeate concentration of the fraction  $j$  ( $c_{p,j}$ ) to its concentration in the bulk solution ( $c_{B,j}$ ) as shown in Eq. (4.3).

$$R_{\text{obs},j} = 1 - \frac{c_{p,j}}{c_{B,j}} = 1 - \frac{RI_{p,j}}{RI_{B,j}} \quad (4.3)$$

On the other hand, the intrinsic membrane rejection ( $R_{m,j}$ ), independent of the formation of a polarization layer, relates the permeate concentration to the concentration at the membrane wall ( $c_{m,j}$ ), Eq. (4.4).

$$R_{m,j} = 1 - \frac{c_{p,j}}{c_{m,j}} \quad (4.4)$$

Concentration polarization phenomenon can be mathematically described by the film model [2] which relates the permeate flux ( $J$ ) to the permeate, bulk and wall PEG concentrations by means of the mass transfer coefficient of the  $j$  fraction ( $k_j$ ). Moreover, taking into account the observed and the intrinsic rejections, both parameters can be related using the well-known Eq. (4.5) [183].

$$\ln\left(\frac{1-R_{obs,j}}{R_{obs,j}}\right) = \ln\left(\frac{1-R_{m,j}}{R_{m,j}}\right) + \frac{J}{k_j} \quad (4.5)$$

The mass transfer coefficient (in m/s) for the PEG molecular weight fraction  $j$  in a stirred batch cell is given by the Eq. (4.6) [183-185], where  $D_j$  is the bulk diffusivity of the PEG molecular weight fraction  $j$ ,  $r$  is the stirred cell radius (0.02 m),  $\mu$  is the bulk viscosity ( $8.93 \cdot 10^{-4}$  Pa·s at 25°C),  $\rho$  is the bulk density ( $997 \text{ kg/m}^3$  at 25°C) and  $\omega$  is the stirring rate (42 rad/s).

$$k_j = 0.0443 \left(\frac{D_j}{r}\right) \left(\frac{\mu}{\rho D_j}\right)^{0.33} \left(\frac{\rho \omega r^2}{\mu}\right)^{0.8} \quad (4.6)$$

Diffusivity (in  $\text{m}^2/\text{s}$ ) of the PEG molecular weight fraction  $j$  is given by Eq. (4.7) [183, 184, 186], where  $MW_j$  (in kg/kmol or Da) is the PEG molecular weight of the  $j$  fraction.

$$D_j = 2.74 \cdot 10^{-9} MW_j^{-1/3} \quad (4.7)$$

The observed membrane rejection for each PEG molecular weight fraction  $j$  was calculated using the refractive index (RI) signals of the permeate ( $RI_{p,j}$ ) and the bulk ( $RI_{b,j}$ ) as concentrations (RI signals are proportional to concentrations) as previously indicated in Eq. (4.3).

Finally, the intrinsic membrane rejection for each PEG molecular weight fraction  $j$  was calculated according to Eq. (4.5) and the actual MWCO of the membrane determined as the molecular weight of the fraction  $j$  which had an intrinsic rejection of 90 %.

MWCO confidence intervals were calculated for the membranes in their original state and after the ageing. Assuming a normal distribution of the determined MWCO values, confidence intervals are defined as the product of the Student's  $t$ -distribution with  $n-1$  degrees of freedom and  $1-\alpha/2$  confidence level ( $t_{n-1, 1-\alpha/2}$ ) and the ratio between the standard deviation ( $S$ ) and the square root of the number of samples ( $n$ ) as shown in Eq. (4.8).



$$\text{MWCO} = \langle \text{MWCO} \rangle \pm t_{n-1, 1-\alpha/2} \frac{S}{\sqrt{n}} \quad (4.8)$$

#### 4.4.2.2. Rejection capability of NF membranes

Separation performance of NF membranes was analyzed with charged and uncharged molecular markers. For the first case, a single salt solution of Na<sub>2</sub>SO<sub>4</sub> (0.01 M) was used. For the second one, a mixture of glucose and sucrose (with different MW) at an individual concentration of 0.01 M was used.

Working in dead-end mode, permeate samples were taken after collecting approximately 2 mL of permeate so, constant concentration is considered. In cross-flow mode, filtrations were conducted in total recirculation mode and permeate and feed samples were taken after 15 min once the steady state was reached.

In all cases and for both charged and uncharged solutes, the observed membrane rejection was determined through the Eq. (4.3).

The salt solution samples were analyzed with a conductivity meter SevenMulti from Mettler-Toledo (Ohio, USA) at 25 ± 4°C, whereas the uncharged solutes solutions were analyzed with a high performance liquid chromatograph (HPLC) which is described in “section 4.4.8”.

#### 4.4.3. ATR-FTIR

Functional group composition of both active and support layers of the membranes were analyzed by FTIR-ATR. Spectra were recorded, at room temperature, on a Thermo Nicolet Nexus Spectrometer (Massachusetts, USA) coupled to an attenuated total reflection accessory which contains the optics to direct the infrared radiation to the zinc selenide (ZnSe) crystal with an incident angle of 45° and 12 internal reflections. Each FTIR-ATR spectrum consists of one hundred merged scans with a nominal resolution of 2 cm<sup>-1</sup> in the region from 650 to 4000 cm<sup>-1</sup>. All spectra were corrected by smooth and base-line automatic correction commands of the device software (OMNIC) and then normalized between 0 and 1.

#### 4.4.4. SEM micrographs and EDS

Morphology of membrane surfaces was studied by a JEOL-6610LV scanning electron microscope (Tokyo, Japan) which used a Wolfram filament as electron gun and allowed working voltages from 0.3 to 30 kV. The microscope was equipped with an X-Max 50 silicon drift detector (SDD) to characterize the elemental composition of the surface, based on the EDS spectroscopy. Previously to the SEM-EDS characterization, membranes were coated with gold to make them electrically conductive.

#### 4.4.5. AFM

Topography of the active and support layers of the UF membranes was also studied through AFM. Images were acquired in the tapping mode at room temperature, with a Nanoscope IIIA microscope from Digital Instruments of the Veeco Metrology Group (Plainview, New York, USA). The tapping tip (Olympus™ OTESPA7) was made of an etched silicon probe with an aluminum coating. It had a length of 14  $\mu\text{m}$  with a high aspect ratio and a 7 nm radius at the end of the tip to minimize the convolution of the tip shape by the membrane surface. The oscillating frequency of the tip was set at 320 kHz and the spring constant was 42 N/m. The scanned areas were carried out over 5  $\mu\text{m}$  x 5  $\mu\text{m}$ , 3  $\mu\text{m}$  x 3  $\mu\text{m}$  and 0.8  $\mu\text{m}$  x 0.8  $\mu\text{m}$  sample sections.

Images were acquired by the Nanoscope software, and they were processed to obtain the final 3D representations [187]. The surface roughness was analyzed through the so-called root mean square (RMS) roughness ( $R_q$ ), the Wenzel's coefficient ( $r_w$ ) and the power spectral density (PSD) fractal dimension ( $d_{fr}$ ).

- The RMS roughness is the average of the difference (in absolute value) between the height at each  $i$  point ( $z_i$ ) and the mean height ( $z_m$ ) for the  $P$  points that define the sample and it is given by Eq. (4.9).

$$R_q = \sqrt{\frac{1}{P} \sum_{i=0}^P (z_i - z_m)^2} \quad (4.9)$$

- The Wenzel's coefficient corresponds to the roughness ratio or the ratio of the true area of the solid surface to its nominal or projected area ( $r_w > 1$ ). This coefficient will play a relevant role, as it will be explained below, in the correct accounting of the influence of roughness on wettability.
- The fractal dimension of the image surfaces is based on the PSD. This magnitude is used to take into account how strongly the roughness depends on the scale at which it is measured.

Among these parameters the PSD fractal dimension ( $d_{fr}$ ) well deserves a detailed explanation. An adequate measure on the surface self-similarity [188] makes use of a Fourier transform whose PSD takes into account the two dimensional roughness spectra of the surface [189]. This spectrum can be evaluated as follow [190, 191].

$$\gamma(p, q) = \gamma(p \Delta\sigma_x, q \Delta\sigma_y) = \left(\frac{2\pi}{L}\right)^2 |z(p \Delta\sigma_x, q \Delta\sigma_y)|^2 \quad (4.10)$$

Where

$$\Delta\sigma_x = \Delta\sigma_y = \frac{\pi}{N \Delta x} = \frac{\pi}{N \Delta y} = \frac{\pi}{L} \quad (4.11)$$

Where  $L$  is the length of each side of the scanned square,  $N$  is the number of points along each side of the square,  $\Delta x$  and  $\Delta y$  are the distance between neighbor points along each direction on the scanned area and  $\hat{z}$  is the discrete bi-dimensional Fourier transform of the height which is obtained as follow.

$$\hat{z}(p, q) = \frac{1}{4 \pi^2} \left( \frac{L}{N} \right)^2 \sum_{m,n=0}^{\infty} z \left( m \frac{L}{N}, n \frac{L}{N} \right) \exp \left[ -j \frac{2 \pi}{N} (m p + n q) \right] \quad (4.12)$$

Where  $j = \sqrt{-1}$ . Therefore, Eq. (4.10) can be rewritten.

$$\gamma(\vec{\sigma}) = \gamma(p, q) = \frac{L^2}{4 \pi^2 N^4} \left| \sum_{m,n=0}^{\infty} z \left( m \frac{L}{N}, n \frac{L}{N} \right) \exp \left[ -j \frac{2 \pi}{N} (m p + n q) \right] \right|^2 \quad (4.13)$$

The bi-dimensional spectrum  $\gamma(\vec{\sigma})$ , or even better, its average on the polar angle  $\gamma(\sigma)$ , where  $\sigma = |\vec{\sigma}|$  can be represented and allows calculating the RMS roughness through Eq. (4.14).

$$R_q = \int_{\vec{\sigma}} \gamma(\vec{\sigma}) d\vec{\sigma} = 2\pi \int_{\sigma} \gamma(\sigma) d\sigma \quad (4.14)$$

The spatial pulsation  $\sigma$  has to be included in the interval:

$$\sigma \in \left[ \frac{\pi}{L}, N \frac{\pi}{L} \right] \quad (4.15)$$

This methodology provides valuable information not only on the height deviation of the roughness profile, but also on its lateral distribution [192].

In a logarithmic scale, this spectrum has a linear behavior in very large ranges, according to Eq. (4.16).

$$\gamma = \frac{\beta}{\sigma^\alpha} \quad (4.16)$$

Where  $\beta$  is a constant and  $\alpha$  the spectrum slope. This power law is typical of fractal behavior of roughness (self-affine behavior). In this situation the corresponding fractal dimension can be evaluated as a function of the spectrum slope [190, 191] using Eq. (4.17).

$$d_{fr} = \frac{(8 - \alpha)}{2} \quad (4.17)$$

#### 4.4.6. Contact angle

Both active and support layer contact angles were determined at room temperature using the sessile drop technique in a FTA200 dynamic contact angle analyzer of First Ten Ångströms (Portsmouth, Virginia, USA). The shown contact angles are the average from 6 to 10 droplets. For the active layer, a droplet of 8  $\mu\text{L}$  was deposited onto its surface and it was observed that contact angle initially decreased with time and reached a plateau beyond 10 s. Therefore, the angle at this time was considered the right value of contact angle. For the support layer, a droplet with the same volume was used, but contact angle was taken as the measured angle at zero time (i.e. at the very moment in which the droplet was left onto the surface), because the support presented a high adsorption, and the droplet quickly disappeared. In addition, due to the high roughness of support layers and their adsorptive character, contact angles of these surfaces do not claim to be actual values, but they offer a valid insight in a comparative analysis.

The Wenzel model [193] describes the homogeneous wetting regime on a rough surface assuming that the wetting liquid reaches from peaks to valleys on the surface of the wetted surface. This leads to an apparent contact angle ( $\theta_{app}$ ), experimentally obtained, which is related to the actual or Young contact angle ( $\theta_Y$ ) which would be measured if the surface was perfectly smooth and flat. The correlation between both contact angles on a rough surface is given by Eq. (4.18) [194, 195].

$$\cos(\theta_{app}) = r_w \cos(\theta_Y) \quad (4.18)$$

The  $r_w$  is the above mentioned Wenzel's coefficient. This equation shows, as it is well-known, that when the surface is hydrophobic ( $\theta_Y > 90^\circ$ ), roughness increases hydrophobicity (hinders wettability) because it increases the contact angle. It is also clear that, when the surface is hydrophilic ( $\theta_Y < 90^\circ$ ), roughness increases hydrophilicity (improves wettability) as the contact angle decreases.

In some cases, the evaluation of contact angle was used in order to perform a deeper analysis, involving the calculations of solid surface energies based on the Lewis acid-base theory. According to Van Oss *et al.* [196] total surface energies ( $\gamma^{TOT}$ ) are the result of the Lifshitz-Van der Waals ( $\gamma^{LW}$ ) and polar acid-base ( $\gamma^{AB}$ ) contributions. The latter is the result of the geometric

mean of the electron acceptor ( $\gamma^+$ ) and the electron donor ( $\gamma^-$ ) character, Eq. (4.19), in which  $i$  can be either solid or liquid.

$$\gamma_i^{\text{TOT}} = \gamma_i^{\text{LW}} + \gamma_i^{\text{AB}} = \gamma_i^{\text{LW}} + 2\sqrt{\gamma_i^+ \gamma_i^-} \quad (4.19)$$

The work of adhesion ( $W_a$ ) is the energy that is necessary to apply in order to separate two interfaces, which in the case of a solid-liquid interface is given by Eq. (4.20).

$$W_a = \gamma_S^{\text{TOT}} + \gamma_L^{\text{TOT}} - \gamma_{\text{SL}}^{\text{TOT}} \quad (4.20)$$

Where  $\gamma_S^{\text{TOT}}$  and  $\gamma_L^{\text{TOT}}$  are the total surface tensions of the solid and the liquid, respectively, and  $\gamma_{\text{SL}}$  is the interfacial tension between the solid and the liquid. Applying the Young-Dupré equation, the work of adhesion between the solid and the liquid can be calculated as function of the  $\gamma_L^{\text{TOT}}$  and the liquid contact angle ( $\theta_Y$ ) following Eq. (4.21).

$$W_a = \gamma_L^{\text{TOT}} [1 + \cos(\theta_Y)] \quad (4.21)$$

The work of adhesion can also be expressed considering the three explained components of the solid surface energy [196, 197], which leads to the Eq. (4.22).

$$W_a = 2 \left( \sqrt{\gamma_S^{\text{LW}} \gamma_L^{\text{LW}}} + \sqrt{\gamma_S^+ \gamma_L^-} + \sqrt{\gamma_S^- \gamma_L^+} \right) \quad (4.22)$$

Finally, combining equations (4.21) and (4.22), Eq. (4.23) is obtained, which allows determining the three contributions of the total solid surface energy of the membrane ( $\gamma_S^{\text{LW}}$ ,  $\gamma_S^+$  and  $\gamma_S^-$ ) by knowing  $\gamma_L^{\text{LW}}$ ,  $\gamma_L^+$  and  $\gamma_L^-$  of three different liquids (subscript  $j$ ) and the obtained young contact angle with each one.

$$\gamma_{L_j}^{\text{TOT}} [1 + \cos(\theta_Y)] = 2 \left( \sqrt{\gamma_S^{\text{LW}} \gamma_{L_j}^{\text{LW}}} + \sqrt{\gamma_S^+ \gamma_{L_j}^-} + \sqrt{\gamma_S^- \gamma_{L_j}^+} \right) \quad j=1-3 \quad (4.23)$$

It has been reported [198] that formamide, methylene iodide and water give good results when it comes to evaluate the total solid surface energies of the membranes as well as their contributions. Lifshitz-Van der Waals, electron acceptor and electron donor contributions together with the total solid surface energies of these liquids are compiled in **Table 4.2**.

**Table 4.2.** Lifshitz-Van der Waals, electron acceptor and electron donor contributions as well as the total liquid surface energies of the probe liquids [198].

Liquid	$\gamma_L^{\text{LW}}$	$\gamma_L^+$	$\gamma_L^-$	$\gamma_L^{\text{TOT}}$
Water	21.8	25.5	25.5	72.8
Formamide	39.0	2.3	39.6	58.1
Methylene iodide	50.8	0.0	0.0	50.8

#### 4.4.7. LLDP

This technique was not employed to follow the ageing of the UF membranes. Nonetheless, it was extensively studied with the aim of developing a model to conduct LLDP characterizations with a lower amount of data and so, to shorten analysis times.

Pore number distributions of UF membranes as function of the pore size can be obtained from LLDP analysis. Moreover, permeance distribution, asymptotic permeance, mean radius (based on pore number or permeance distributions) and MWCO estimation can be obtain in turn from the pore number distribution. Although this model is comprehensively explained in “section 5.3”, the experimental procedure is briefly described here.

The HFK-328, UP020, M030 and M300 membranes were used in this study (**Table 4.1**). The membranes in their pristine state were cut in disk pieces with an effective diameter for the analysis of 36 mm, as defined by the holder size. Membranes were conditioned by washing and soaking them in Milli-Q water for at least 48 h. Then, previously to the characterization, membranes were soaked in the wetting liquid for 12 h. Just before the analysis, the soaking was carried out under vacuum (created by a water jet pump) for 45 min to ensure the complete wetting of the sample.

The displacing liquid was pumped by a precise syringe pump ISCO-250D which allows a very accurate and stable flux without the need of any dampening system. The operation mode consisted in fixing a determined flow and then, waiting for the pressure to stabilize. Increasing the flow stepwise, the experimental pairs of data of flow as function of pressure were obtained until the asymptotic permeance was reached. At this point, the displacing liquid emptied the wetting liquid which was contained inside all the pores.

#### 4.4.8. HPLC

PEG and monosaccharide solutions were analyzed by HPLC for the MWCO determination of UF membranes and the rejection performance of NF ones, respectively. For both solutions, the analysis was conducted with an Agilent 1100 series apparatus equipped with a RI detector (temperature set at 35°C).

PEG concentration as function of the MW was obtained using a Superose 12 (10/300 GL) size exclusion column (GE Healthcare). A volume of 100  $\mu$ L of sample was injected, using  $\text{NaN}_3$  (0.05 M) as mobile phase (0.5 mL/min). A calibration curve with ten PEGs injected one at a time was used to relate the exclusion time with the MW. When this type of columns are used, HPLC technique is usually referred as HPSEC.

Content of glucose and sucrose solutions was quantified with an Aminex HPX87-C column (Bio-Rad Laboratories, Inc.). A volume of 50  $\mu$ L of sample was injected, using ultrapure water as mobile phase (0.5 mL/min).

#### **4.4.9. Gas chromatography - mass spectrometer (GC-MS)**

The degradation of the nonwoven membrane support of some UF membranes was verified using GC-MS. Gas chromatographic analyses were carry out in a HP 6890 series chromatograph coupled to a HP 5973 mass selective detector, both from Hewlett Packard (California, USA). The column was an HP-5MS (30 m length x 250  $\mu\text{m}$  i.d. x 0.25  $\mu\text{m}$   $d_f$ ), the injection and the detector temperatures were 250°C in both cases and the oven temperature was programmed from 45°C to 180°C at 15°C/min, then the rate was set at 5°C/min up to 210°C and finally, 30°C/min until the last temperature of 300°C (kept for two additional minutes).

## **5. Results and discussion**

---

---





## **5.1. Ageing of PES UF membranes under acidic and alkaline cleaning solutions**

---

### **5.1.1. Abstract**

Six commercial ultrafiltration membranes made of polyethersulfone (UH004, UP005, UP010 and UP020 from Microdyn Nadir, HFK-328 from Koch Membrane Systems and PT from GE Osmonics) were subjected to acidic and alkaline ageing using nitric acid (HNO<sub>3</sub>) and sodium hydroxide (NaOH) solutions, respectively. Concentrations of 0.01, 0.1 and 1.0 M were tested for both reagents at 50°C for long periods of time.

The ageing effects were measured through the changes on membrane permeability and molecular weight cut-offs (MWCOs). In addition, ATR-FTIR, SEM-EDS, AFM and contact angle measurements were employed to characterize membranes in their pristine state and after the ageing.

It was found that changes in membrane performance took place mainly in the first 10 days of exposure due to either membrane conditioning or ageing. In addition, it was found that Nadir support layer material was different from that of Koch and GE Osmonics membranes and resulted in significant differences.

When subjected to 1.0 M NaOH and HNO<sub>3</sub> ageing solutions, low MWCO Nadir membranes showed a decreased in permeability and MWCO due to an apparent pore size reduction caused by the osmotic stress at high ionic concentrations. This effect was not significant for the rest of the membranes. Apart from this behavior, all Nadir membranes showed a good stability in all tested conditions which was in accordance with the lack of significant physicochemical changes found for these membranes.

Koch and GE Osmonics were also resistant to the acidic ageing in terms of performance and physicochemical membrane properties. However, under strong alkaline conditions, support layer of these membranes are degraded which leads to the worsening of the performance. This effect is more severe for the GE Osmonics membrane due to its lower active layer thickness.

The influence of temperature on the ageing of UP005, HFK-328 and PT membranes was also studied under the strongest alkaline condition. Its effect on UP005 membrane ageing was negligible whereas for the HFK-328 and PT ones, higher temperatures led to a higher degree of degradation.

### **5.1.2. Surface composition of the non-aged membranes**

The ATR-FTIR spectra of active and support layers of the six tested membranes are displayed in **Fig. 5.1**. The spectra of all the active layers are very similar as expected since they are made of the same material (**Fig. 5.1a**). The main absorption bands of PES can be seen at 1660 (C=C stretching vibration), 1576 (aromatic systems), 1484 (C-S), 1322 (-SO<sub>2</sub>- asymmetric stretching

vibration), 1298 and 1239 (C-O-C stretching vibrations), 1149 (O-H deformation and C-O stretching vibration interaction), and 1104  $\text{cm}^{-1}$  (C-O stretching vibration) [176, 199, 200].

In the case of the support layers, the spectra of the Nadir membranes (**Fig. 5.1b**) are different from those of the Koch and GE Osmonics (**Fig. 5.1c**), indicating that they are made of different material. For this reason, different wavenumber scales are used to avoid the overlapping of the plots and to emphasize the characteristic peaks of each material. According to manufacturer, the support layer material of Nadir membranes is a mixture of polyethylene (PE) and polypropylene (PP), which matches with the absorption bands at 2912, 2845, 1469, 718 ( $\text{CH}_2$  asymmetrical and symmetrical stretching vibration and  $\text{CH}_2$  bending and rocking deformation, respectively) and 1373  $\text{cm}^{-1}$  ( $\text{CH}_3$  symmetric deformation) [201, 202]. On the other hand, Koch and GE Osmonics membranes exhibit absorption bands at 1710 (Carbonyl C=O stretching), 1232 (C(O)-O stretching of ester group) and 1086  $\text{cm}^{-1}$  (Methylene group stretching), which are typical of polyethylene terephthalate (PET) [203, 204]. **Fig. 5.1c** also shows absorption bands below 1050  $\text{cm}^{-1}$ , but they do not reveal the presence of other materials different from PET since they may be due to mechanical or thermal changes suffered by this polymer during the membrane manufacturing [203]. The composition of this layer has been revealing since to the best of our knowledge, it has not been reported elsewhere.

Chemical surface composition was also studied through SEM-EDS to determine elementary composition (**Table 5.1**). The theoretical atomic content of a PES polymer (deduced from the chemical formula of the monomer) matches with the active layer characterization of all membranes. A slight increase in the carbon and sulfur content and a decrease in oxygen can be noticed as MWCO increases, which may be due to the presence of hydrophilic additives. Furthermore, the ratio between carbon and oxygen content of HFK-328 and PT support layers is similar to that of a PET polymer, which confirms the ATR-FTIR results. Finally, only carbon was found in the SEM-EDS determinations of the Nadir support layers (almost 100 % in all cases, not included in the table) as expected since they are made of a mixture of PE and PP.

**Table 5.1.** SEM-EDX analysis of active and support layers of GE Osmonics, Koch and Nadir membranes.

Membrane	Active layer (PES)			Support layer (PET)	
	C (%)	O (%)	S (%)	C (%)	O (%)
<i>Theoretical</i>	75	18.8	6.2	71.4	28.6
PT	76.0 ± 1.1	18.4 ± 1.0	5.6 ± 0.2	69.1 ± 0.8	30.9 ± 0.8
HFK-328	76.1 ± 1.9	18.3 ± 2.0	5.6 ± 1.1	70.3 ± 0.9	29.7 ± 0.9
UP005	75.4 ± 0.4	20.3 ± 0.4	4.3 ± 0.1	-	-
UP010	75.8 ± 0.6	19.1 ± 0.7	5.1 ± 0.1	-	-
UP020	76.4 ± 1.3	17.7 ± 1.2	5.9 ± 0.2	-	-

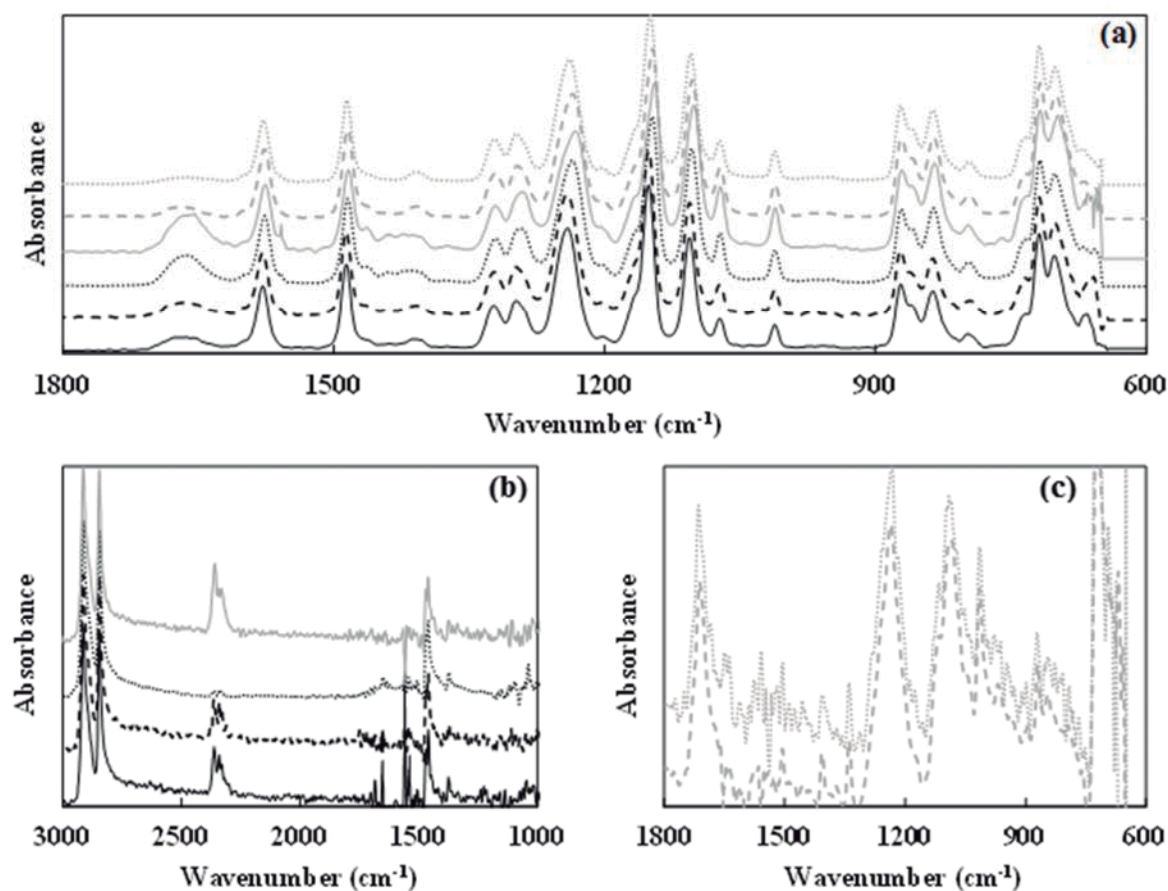


**Fig. 5.1.** ATR-FTIR spectra of the active (a) and the support (b, c) layers of UP020 (black solid line), UP010 (black broken line), UP005 (black dotted line), UH004 (gray solid line), HFK-328 (gray broken line) and PT (gray dotted line). Spectra of the HFK-238 and PT support layers were represented separately from those of the Nadir ones for the sake of clarity.

Results will be divided into two sections according to the support layer material, since -as it will be seen later- it plays an important role. Firstly, the effects of the ageing solutions on the Nadir membranes will be shown and later, the ageing effects on the Koch and GE Osmonics membranes will be discussed.

### 5.1.3. Effects of ageing on Nadir membranes

#### 5.1.3.1. Membrane performance throughout the alkaline ageing

Most of the performance results are presented in graphs in which smoothed lines are added to serve as eye guides (without modelling intention), and error bars (calculated from the standard

deviations of the four measurements linked to the set of membranes at each condition) are added to indicate the dispersion of the measurements from the average.

Permeability changes, as a function of the exposure time, for the Nadir membranes aged with NaOH at 50°C are shown in **Fig. 5.2**. The use of relative permeabilities in these plots makes the initial value one for all the membranes regardless of the actual initial permeability, facilitating the comparisons between them. However, the actual magnitudes go from 13 to 220 L/hm<sup>2</sup>bar following the order UH004, UP005, UP010 and UP020 due to the increase in the pore size of the membranes which, expressed as MWCO, goes from 4 to 20 kDa according to the manufacturer (**Table 4.1**).

An interesting fact is the conditioning time needed by these membranes. There is an increase (of around 50 %) in the relative permeability when exposed to just DI water (**Fig. 5.2**). The time needed to reach 90 % of the final value of relative permeability can last up to 30 days depending on the membrane. This behavior under DI water also takes place under the alkaline (**Fig. 5.2**) and acidic conditions (**Fig. 5.3**) as it will be pointed out later on.

The effects of alkaline ageing on the Nadir UH004 and UP005 membranes are shown in **Fig. 5.2a** and **Fig. 5.2b**. When these membranes are treated with 0.01 and 0.1 M NaOH solutions, there is an increase in the relative permeability which follows the same pattern seen for the membranes soaked in DI water, but with discrepancies around 13 and 8 % for the UH004 and UP005, respectively. However, when these membranes are soaked in the 1.0 M NaOH solution there is not such increase in the permeability. This issue will be addressed later on in “section 5.1.3.8”.

The relative permeability of UP010 and UP020 membranes throughout the ageing in any alkaline condition (including the 1.0 M NaOH solution) follows the same trend as that shown by the membranes in the reference solution (**Figs. 5.2c** and **Fig. 5.2d**).

Assuming that variations between the aged and the reference membranes around 10 % are likely due to experimental discrepancies, one can consider that only the UH004 and UP005 membranes exposed to 1.0 M NaOH solution changes their performance throughout the ageing.

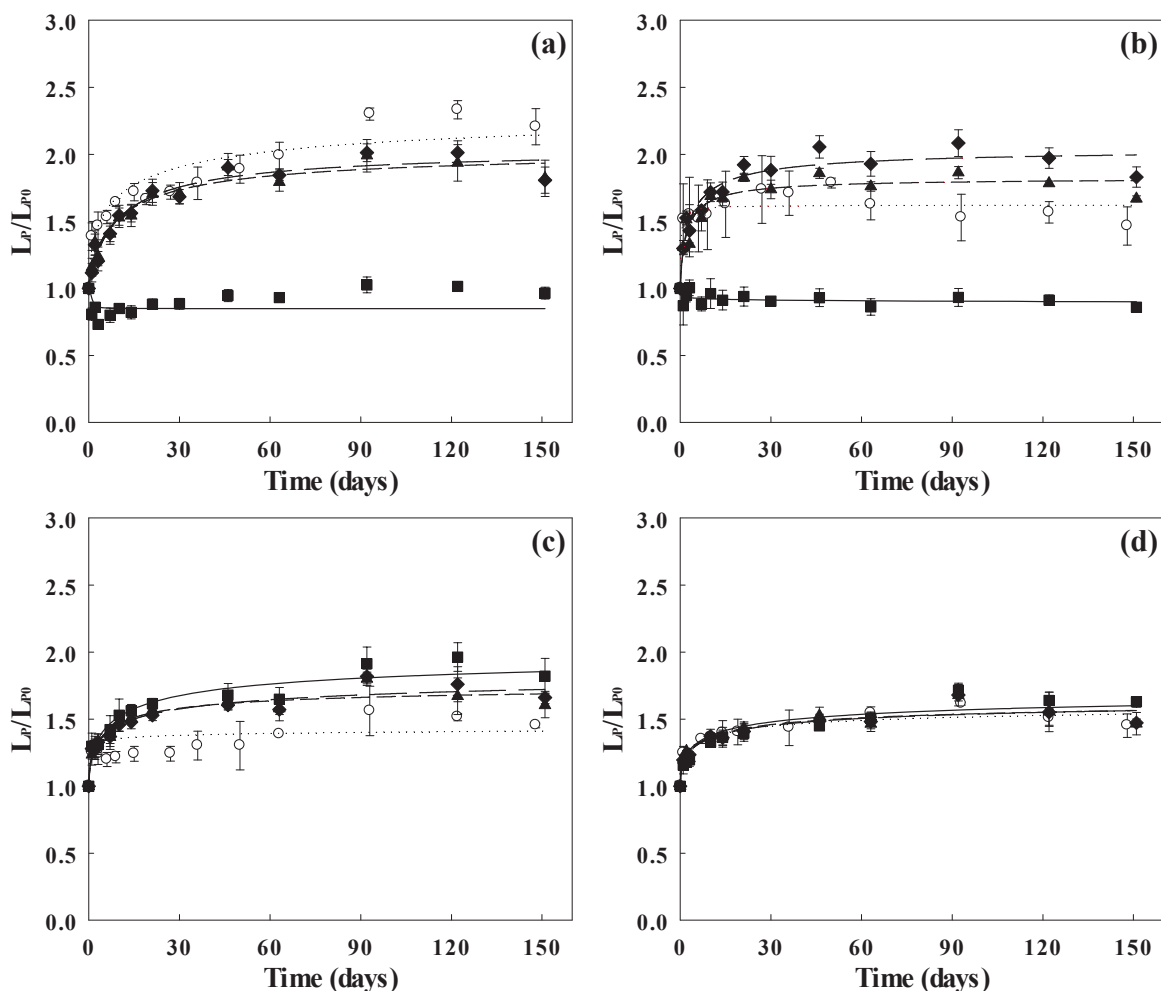


**Fig. 5.2.** Relative permeability of UH004 (a), UP005 (b), UP010 (c) and UP020 (d) membranes aged at 50°C with NaOH solutions of 0.01 M (▲; short-dash line), 0.1 M (◆; long-dash line) and 1.0 M (■; solid line) and soaked in DI water (○; dotted line).

#### 5.1.3.2. Membrane performance throughout the acidic ageing

A second set of the membranes were aged in  $\text{HNO}_3$  at 50°C for 150 days (**Fig. 5.3**). When both the UH004 and UP005 membranes (**Fig. 5.3a** and **Fig. 5.3b**) are exposed to 0.01 and 0.1 M  $\text{HNO}_3$  solutions, the relative permeability increases in a similar way to that of the membrane soaked in DI water, but reaches a plateau at lower values (approximately 13 and 6 %, respectively). Using the membranes subjected to DI water as reference, it can be concluded that the effects of the  $\text{HNO}_3$  at 0.01 and 0.1 M concentration are minor. However, when the  $\text{HNO}_3$  concentration is 1.0 M, the relative permeability of the UH004 and UP005 membranes does not increase as much. This behavior, which is comparable to the ageing of these membranes in 1.0 M NaOH solution was studied in further detail in “section 5.1.3.8”.

On the other hand, both the UP010 and UP020 membranes have a high resistance to any of the tested  $\text{HNO}_3$  concentrations, being the changes in their relative permeabilities (Fig. 5.3c and Fig. 5.3d) lower than 12 % with respect to the reference value.

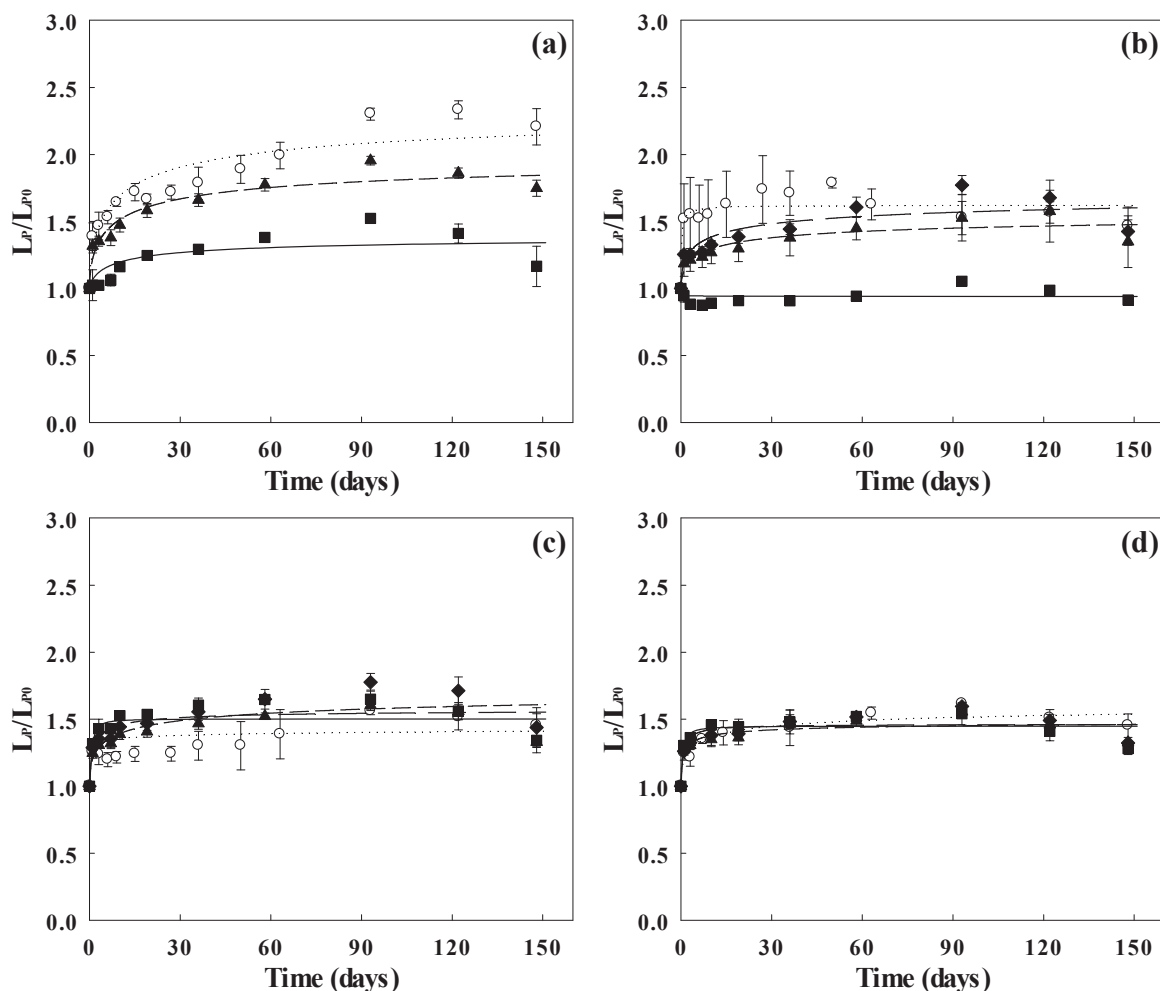


**Fig. 5.3.** Relative permeability of UH004 (a), UP005 (b), UP010 (c) and UP020 (d) membranes aged at 50°C with  $\text{HNO}_3$  solutions of 0.01 M (▲; short-dash line), 0.1 M (◆; long-dash line) and 1.0 M (■; solid line) and soaked in DI water (○; dotted line).

#### 5.1.3.3. Effects of the ageing conditions on membrane MWCOs

In addition to permeability, MWCO determinations were carried out to evaluate the membrane separation performance at the end of the ageing treatments as well as in pristine conditions. The results (Table 5.2) show the averages with a confidence level of 90 % following Eq. (4.8).

All the MWCOs given by manufacturers are higher than those experimentally determined for the pristine membranes. This MWCO underestimation takes place when the measurements are carried out through a single filtration of a mixture of PEG as previously reported [181, 182]. Nevertheless, for the sake of the comparative study carried out in this work, those differences are not considered relevant.

The effect of the concentration polarization is significant for the UP010 and UP020 membranes due to their high permeability. Thus, if the concentration polarization had not been taken into account, the apparent MWCO of these two membranes would have been 5.9 and 12.3 kDa, instead of the actual values, 4.6 and 7.9 kDa, respectively. For the UH004 and UP005 membranes, considering the concentration polarization, a bias around 0.1 kDa is corrected.

UH004 and UP005 membranes in their pristine state and after the treatment in DI water (50°C) do not exhibit any change in their MWCO, indicating that even though there is a conditioning of the membrane in terms of permeability, their separation capabilities are almost the same since the very first filtration. On the other hand, UP010 and UP020 membranes show an increase in the MWCO which goes in accordance to the permeability rise observed throughout the conditioning.

The UH004 and UP005 membranes subjected to low concentrations of either HNO<sub>3</sub> or NaOH do not exhibit strong variations on their MWCO with respect to the reference condition (around 2.2 and 2.0 kDa, respectively) at the end of the ageing (**Table 5.2**), as it was observed in the permeability measurements. However, at high concentration (1.0 M) of both chemicals, MWCOs decrease to 1.8 and 1.6 kDa, respectively, in agreement with the permeability drop pointed out in the previous sections (**Fig. 5.2a**, **Fig. 5.2b**, **Fig. 5.3a** and **Fig. 5.3b**).

The Nadir membranes with higher permeabilities (UP010 and UP020) show a higher dispersion in the MWCO results. Nonetheless, considering the confidence intervals, no significant differences can be considered between the reference values and those of the aged membranes (**Table 5.2**) at any of the tested conditions. Fact that goes in accordance to the permeability characterization (**Fig. 5.2c**, **Fig. 5.2d**, **Fig. 5.3c** and **Fig. 5.3d**).

The effects of the ageing procedures on membrane rejection performance, which were explained on the basis of MWCO values, are also shown in **Fig. 5.4** as whole rejection curves. In addition to the above mentioned trends, it can be pointed out from **Fig. 5.4** that changes in MWCOs are due to the shifting of the curves. For instance, the reported decrease in MWCO of UP005 membrane after the ageing in 1.0 M HNO<sub>3</sub> or in NaOH leads to the narrowing of all membrane pores in such a way that each PEG fraction has a higher rejection than that of the membrane soaked in DI water. This representation also shows that the ageing affects all pore size range and so, MWCO values can be used as representative indicators of the global membrane rejection capabilities.



**Table 5.2.** Determined MWCO of the membranes at the end of the different ageing procedures.

T	Ageing conditions	Membranes							
		UH004	UP005	HFK-328	PT	UP010	UP020		
-	Manufacturer	4	5	5	5	10	20		
	Pristine membrane	2.2 ± 0.1	2.0 ± 0.1	2.6 ± 0.1	1.9 ± 0.1	4.6 ± 0.6	7.9 ± 1.1		
	DI water	2.2 ± 0.1	2.0 ± 0.1	3.4 ± 0.2	2.5 ± 0.4	6.3 ± 0.3	10.0 ± 1.4		
50°C	HNO <sub>3</sub> (0.01 M)	2.2 ± 0.1	1.9 ± 0.1	3.6 ± 0.1	2.8 ± 0.1	6.2 ± 0.4	10.0 ± 1.5		
	HNO <sub>3</sub> (0.1 M)	2.0 ± 0.1	1.9 ± 0.2	3.8 ± 0.1	2.8 ± 0.1	6.1 ± 0.4	9.7 ± 3.0		
	HNO <sub>3</sub> (1.0 M)	1.8 ± 0.1	1.6 ± 0.1	3.6 ± 0.2	2.7 ± 0.3	5.5 ± 0.7	8.7 ± 2.9		
	NaOH (0.01 M)	2.3 ± 0.1	2.0 ± 0.1	3.2 ± 0.1	2.9 ± 0.2	6.9 ± 1.0	9.2 ± 1.6		
35°C	NaOH (0.1 M)	2.2 ± 0.1	1.9 ± 0.1	3.1 ± 0.1	3.7 ± 1.0	6.8 ± 0.3	9.3 ± 0.7		
	NaOH (1.0 M)	1.8 ± 0.1	1.6 ± 0.2	3.5 ± 0.2	5.0 ± 0.8	7.7 ± 0.9	10.2 ± 1.7		
	DI water	-	2.0 ± 0.1	3.1 ± 0.3	2.4 ± 0.3	-	-		
25°C	NaOH (1.0 M)	-	1.6 ± 0.1	3.5 ± 0.5	2.7 ± 0.3	-	-		
	DI water	-	2.0 ± 0.1	3.3 ± 0.7	2.3 ± 0.2	-	-		
	NaOH (1.0 M)	-	1.6 ± 0.1	3.0 ± 0.6	2.3 ± 0.1	-	-		

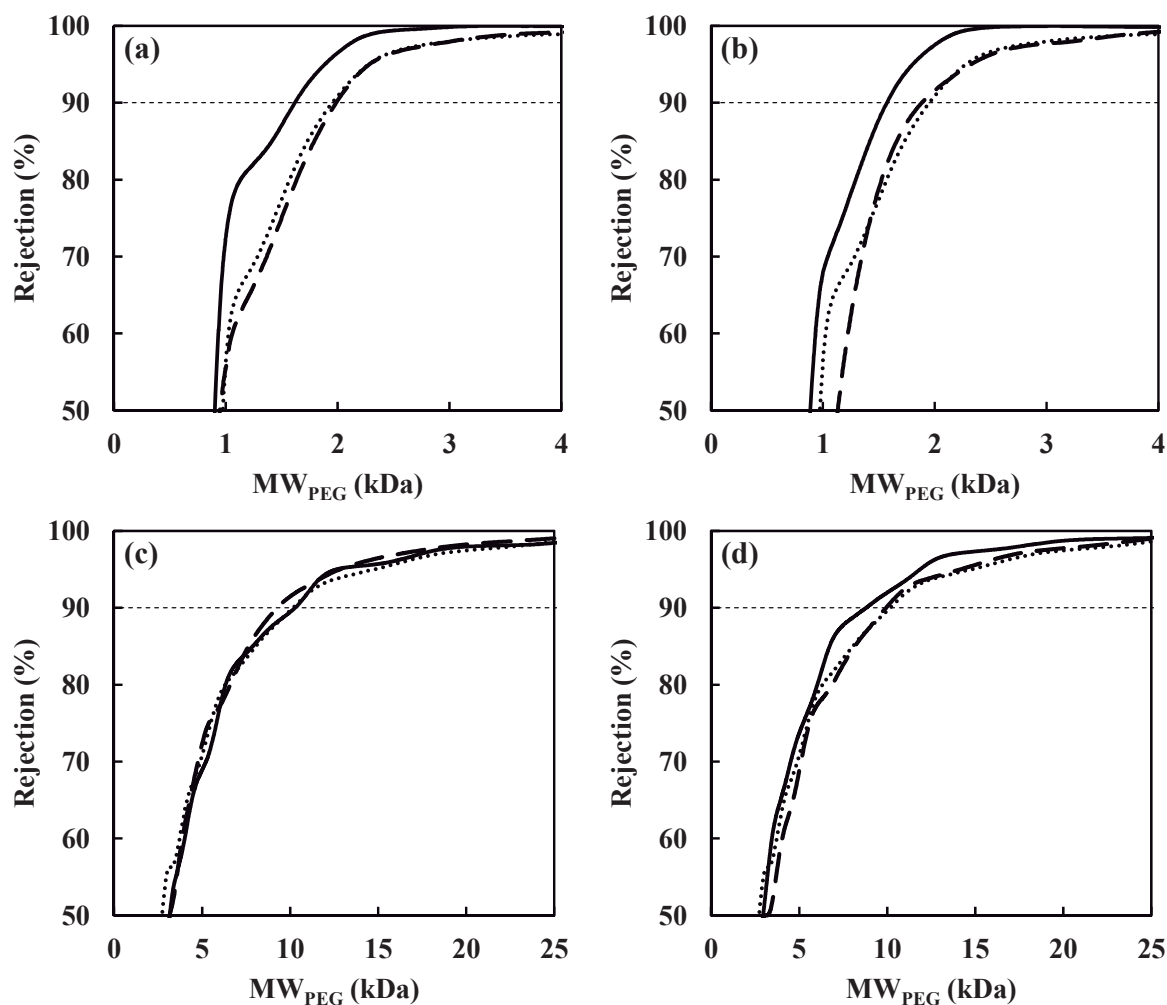


**Fig. 5.4.** Intrinsic rejection curves as function of the PEG fraction MW for the UP005 (a, b) and UP020 (c, d) aged at 50°C with NaOH (a, c) and HNO<sub>3</sub> (b, d) solutions of 0.01 M (broken line) and 1.0 M (solid line) and soaked in DI water (dotted line).

#### 5.1.3.4. Effects of the ageing conditions on membrane surface composition

**Fig. 5.5** displays the ATR-FTIR spectra of Nadir membranes at the end of the treatments with DI water and with HNO<sub>3</sub> and NaOH solutions, respectively. The comparison among these spectra and with those of the pristine membranes (**Fig. 5.1a** and **Fig. 5.1b**) does not reveal any significant change in the functional group composition of either the active or the support layers as consequence of the ageing conditions. Nonetheless, concerning the support layer spectra, there is a double peak at 2350 cm<sup>-1</sup>, typical from O=C=O asymmetric stretching, which is attributed to the presence of carbonate contamination trapped on the PE/PP support layer. This is in agreement with the apparent lower absorbance intensity of the samples subjected to the acidic conditions in which CO<sub>2</sub> is less soluble.

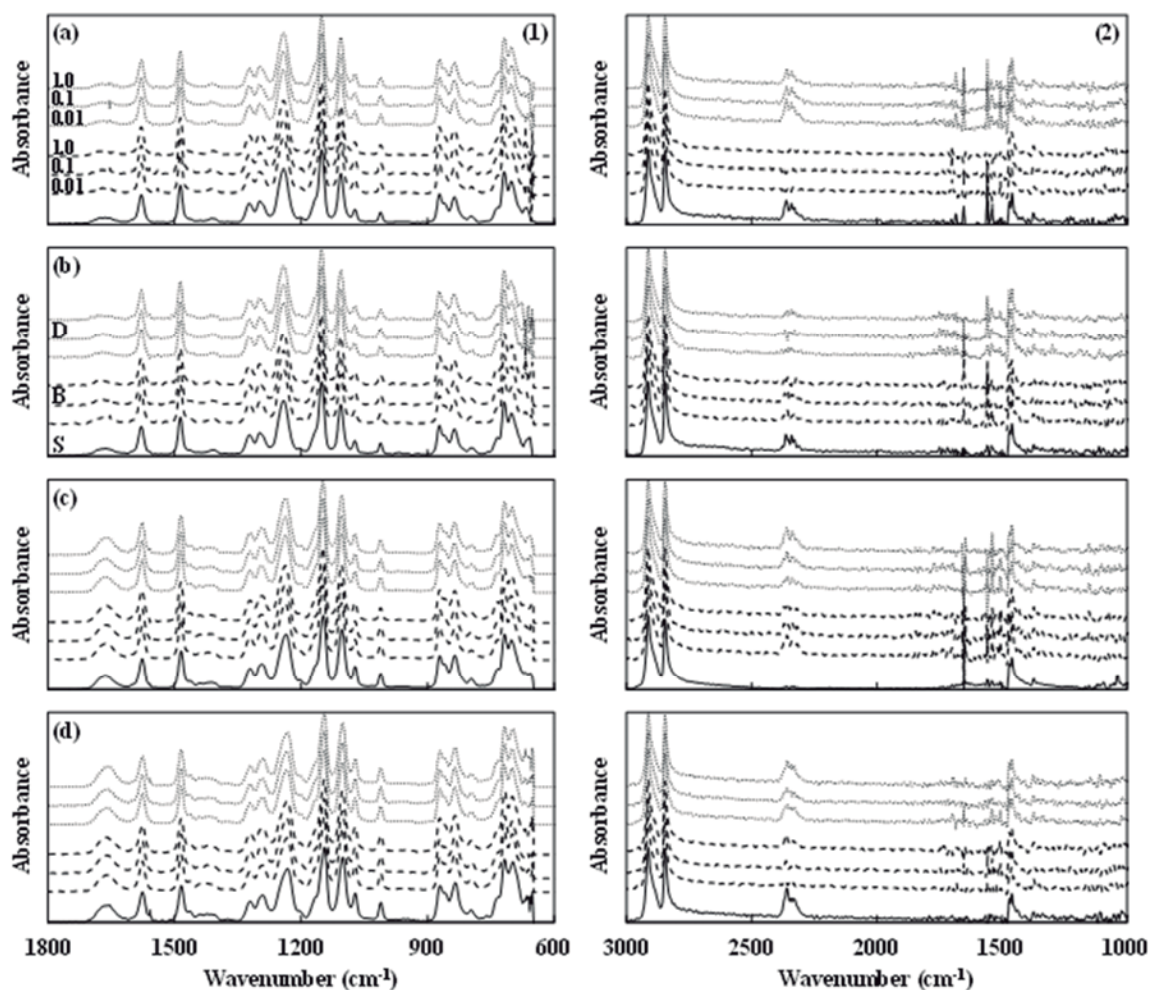


**Fig. 5.5.** ATR-FTIR spectra of the active (1) and support (2) layers of UP020 (a), UP010 (b), UP005 (c) and UH004 (d) membranes after the soaking in DI water (solid line, S) and after the ageing with 0.01, 0.1 and 1.0 M HNO<sub>3</sub> solutions (broken line, B) and with 0.01, 0.1 and 1.0 M NaOH solutions (dotted line, D) at 50°C.

#### 5.1.3.5. Effects of the ageing conditions on membrane structure

SEM images of the support layer of Nadir membranes, but for the UH004 one, are shown in **Fig. 5.6**, whereas active layer images are not included because the pore size is too small to be observed and only a smooth surface is obtained. Support layers of these membranes are made of a nonwoven fabric and even though they all come from the same manufacturer, the threads in UP020 look thicker than those in UP010 and UP005. Nonetheless, the use of different grades of nonwoven materials is a normal practice carried out by manufacturers which would explain the slight differences.

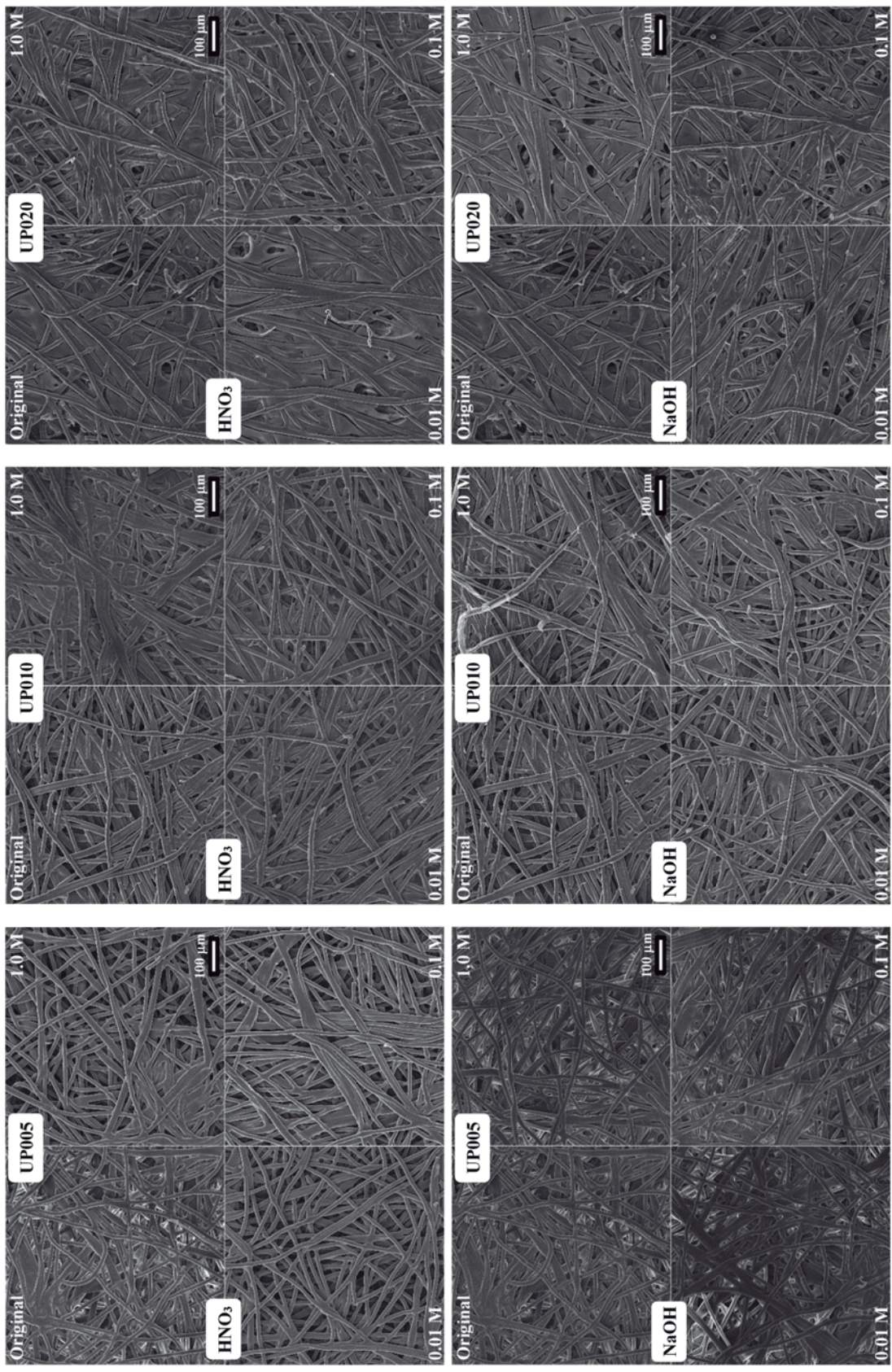


**Fig. 5.6.** SEM micrographs of the support layers of UP005, UP010 and UP020 Nadir membranes in their original conditions and after the ageing with 0.01, 0.1 and 1.0 M HNO<sub>3</sub> and NaOH solutions.

Comparing the membranes before and after the different ageing treatments, neither the  $\text{HNO}_3$  nor the  $\text{NaOH}$  ageing solutions are able to induce visible morphologic changes in any of the three membranes.

#### 5.1.3.6. Effects of the ageing conditions on membrane topography

Resolution of AFM images allows studying the morphology of the active layer surfaces, unlike the SEM technique. Among the four Nadir membranes, only the UP005 one is analyzed in detail here because it has the same MWCO as the Koch and GE Osmonics membranes and thus, it is especially appropriate for comparison. The AFM pictures of the UP005 membrane in its pristine condition and after the ageing with 0.01 and 1.0 M  $\text{HNO}_3$  and  $\text{NaOH}$  solutions are shown in **Fig. 5.7**. The representation of the PSD versus the spatial pulsation (**Fig. 5.8a**) allows the determination of the fractal dimensions of the membrane. In addition, RMS roughness,  $R_q$ , and the own fractal dimension,  $d_{fr}$ , for the above mentioned conditions are shown in **Fig. 5.8b**.

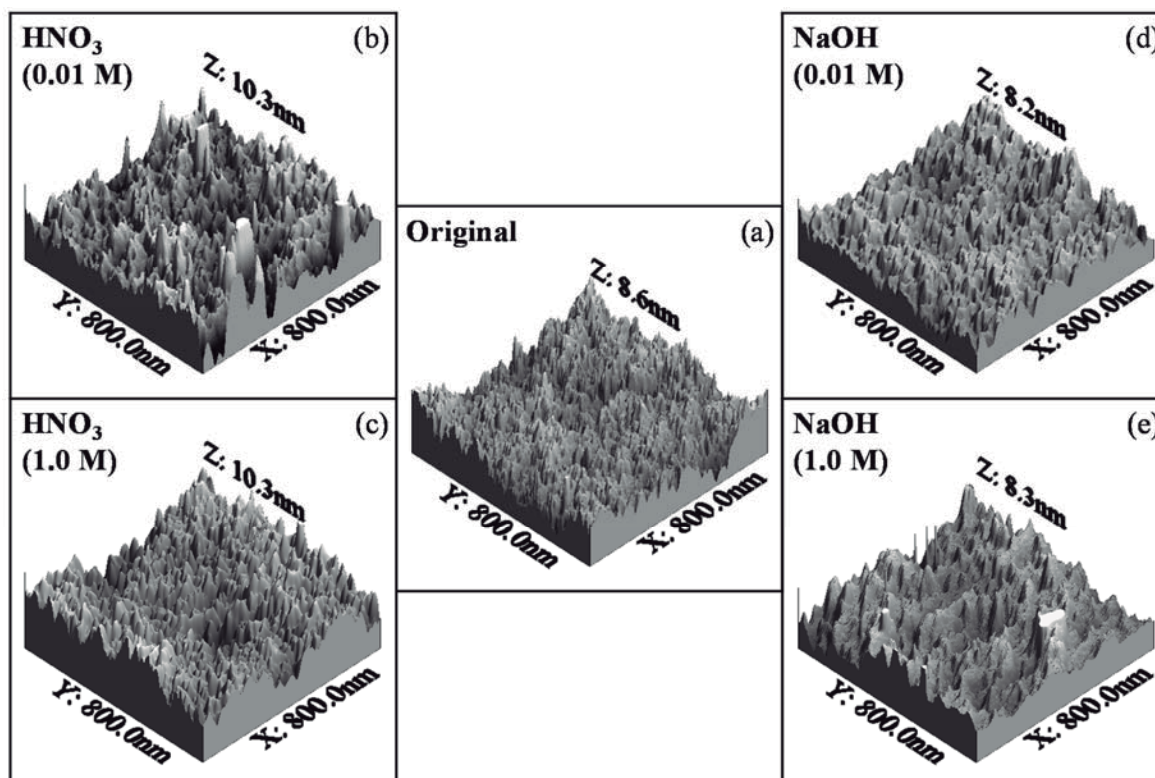


**Fig. 5.7.** AFM images of the UP005 membrane active layer in its original condition (a) and after the ageing with 0.01 and 1.0 M  $\text{HNO}_3$  and  $\text{NaOH}$  solutions (b, c, d and d). All the AFM images have the same z-axis scale and the Z values are the maximum height of each image.

The UP005 active layer in its original condition has an RMS roughness of 1.17 nm and a quite homogeneous pore distribution according to the AMF image in **Fig. 5.7a**. After the ageing with 0.01 M  $\text{HNO}_3$  (**Fig. 5.7b**) there is an increase in roughness up to 1.42 nm but the surface looks

similar to the one in the original condition. When the concentration is increased to 1.0 M (Fig. 5.7c) the active layer surface exhibit only slightly higher roughness (1.43 nm). The ageing with 0.01 M NaOH (Fig. 5.7d) leads to a lower roughness than that of the untreated membrane (1.01 nm), but the surface still looks similar to the pristine condition. The highest concentrations of 1.0 M (Fig. 5.7e) leads to an increase in the roughness (1.44 nm), again similar to those under the acidic conditions, and is reflected in a more heterogeneous surface. In general, both acidic and alkaline ageing treatments lead to a slight increase in membrane roughness around 20 % higher.

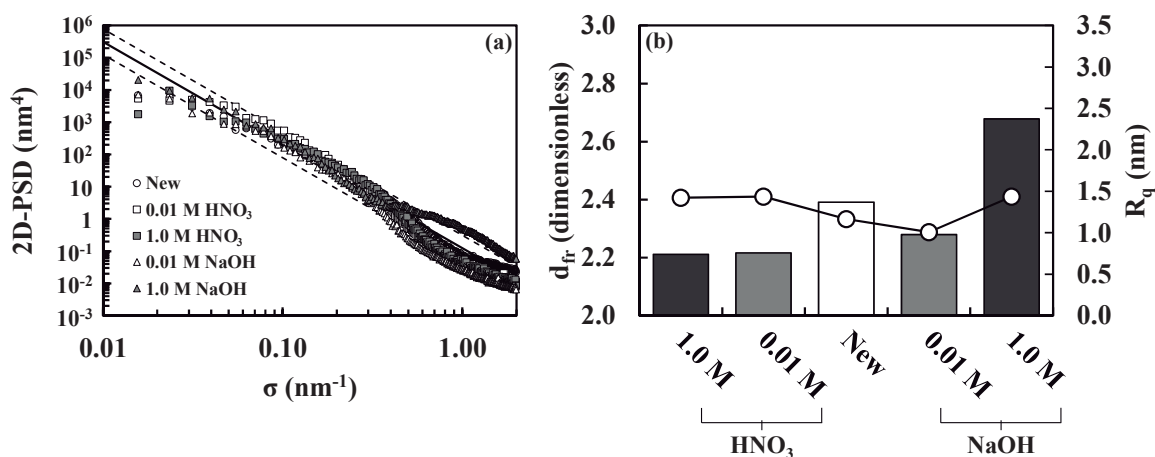


**Fig. 5.8.** Two dimensional power spectral density (a) and PSD fractal dimension (bars) and R<sub>q</sub> roughness (b) for the 0.8 x .08  $\mu$ m scanned areas of the UP005 membrane after the ageing in HNO<sub>3</sub> and NaOH solutions at different concentrations.

However, roughness depends on the scale of investigation, given by the size of the scanned areas, revealing a fractal character. Therefore, the fractal dimension, which is independent of the scale of examination, has been used in order to give the idea of how accessible pores entrances are. The untreated UP005 membrane has a  $d_{fr}$  of 2.39 which decreases after the ageing in HNO<sub>3</sub> to 2.21 (0.01 M) and 2.22 (1.0 M). When aged with NaOH,  $d_{fr}$  goes to 2.28 (0.01 M) and 2.68 (1.0 M). Considering the original membrane as reference, it can be observed that changes are around 10 % in all cases meaning that even though slight variations in roughness are observed after ageing treatments, the accessibility of the membranes for solvent and solutes is still similar, not suggesting changes in performance.

The fractal dimension gives an idea of how similar is the surface to a volume. In other words, when the fractal dimension is two the interface can be seen as (has the topography of) a surface more or less smooth while when the fractal dimension approaches three the interface is topographically a volume. In this way a perfect flat interface with no pores at all would have a  $d_{fr}$  of two, whereas a value of three and a high roughness would correspond to an easily penetrable surface consisting in a connected network of voids. In addition, fractal dimension does not depend on the scanned area size of the surface.

### 5.1.3.7. Effects of the ageing conditions on membrane hydrophobicity

The effects of acidic and alkaline ageing in the hydrophobicity of the active layer of the UH004, UP005, UP010 and UP020 membranes are shown in **Table 5.3**. The contact angle of the pristine membranes before the ageing is around 57° regardless of their initial MWCO which is similar to the values found by other authors for PES membranes [23, 205, 206]. Although it seems that contact angle decreases after the different treatments, considering the confidence intervals, no significant changes in the hydrophilicity of the membranes can be determined. Contact angle highly depends on surface composition and to a less extent on the surface roughness, which was taken into consideration through the Wenzel's coefficient. Therefore, since no significant changes in these properties were found, it is reasonable that contact angle values remained similar within the experimental error.

It is also remarkable, that the UH004, which is supposed to be more hydrophilic according to its manufacturer, has contact angles quite similar to those of the other Nadir membranes.

**Table 5.3.** Contact angle measurements (using ultrapure water) of the active layers of the UP005, UP010, UP020, HFK-328 and PT membranes after the ageing in different conditions at 50°C. Intervals expressed as standard deviations.

Ageing conditions	Membranes				
	UP005	UP010	UP020	HFK-328	PT
Pristine membrane	57 ± 5	58 ± 1	55 ± 5	60 ± 5	57 ± 2
DI water	52 ± 5	53 ± 4	54 ± 2	60 ± 1	57 ± 3
HNO <sub>3</sub> (0.01 M)	46 ± 2	50 ± 1	52 ± 2	53 ± 2	47 ± 6
HNO <sub>3</sub> (0.1 M)	48 ± 2	47 ± 1	49 ± 2	57 ± 3	51 ± 2
HNO <sub>3</sub> (1.0 M)	53 ± 3	50 ± 2	50 ± 1	57 ± 2	54 ± 2
NaOH (0.01 M)	51 ± 5	48 ± 3	52 ± 2	48 ± 3	46 ± 3
NaOH (0.1 M)	62 ± 3	55 ± 3	52 ± 1	50 ± 2	44 ± 1
NaOH (1.0 M)	54 ± 2	52 ± 2	55 ± 5	46 ± 3	42 ± 2

### 5.1.3.8. Discussion

The results from the physicochemical characterizations for the Nadir membranes can be summarized as follows. No changes in either the functional group composition of the active (PES) or the support layer (a mixture of PE/PP) are found under any acidic or alkaline condition and in agreement, membrane active layer hydrophilicity is kept almost constant. Support layer structure remains stable after all ageing conditions. Active layer topography was only studied for the UP005 membrane which shows a slight increase after both ageing conditions. However,

considering the fractal dimension which accounts for the size scale used for the measurement, no differences are found in the accessibility to the pores entrance.

Therefore, since no significant changes in either the hydrophilicity or the functional composition of the membranes were found, the increase in permeability of Nadir membranes in the first days of exposure to DI water or mild acidic and alkaline conditions is likely due to the conditioning and swelling of the membranes which are shipped dry.

Concerning the dissimilar performance of UH004 and UP005 membranes under 1.0 M NaOH and HNO<sub>3</sub> solutions, none of the mentioned physicochemical characterization techniques was able to bring in any significant insight. Therefore, two additional sets of experiments were performed. UH004 and UP005 membranes were subjected to a 1.0 M NaCl solution and the permeability results were identical to those obtained with the concentrated alkali or acid aged membranes. Therefore, the effect is not really associated with ageing, but to an osmotic stress related to the high ion concentration in solution which it has been shown affects polymer conformation and in our case restricts convective water transport. This would go in accordance with the rejection curves shown in **Fig. 5.4** for the UP005 membrane in which the rejection of all PEG fractions increase after the ageing in these strong conditions which in turn, has to be due to a smaller effective pore size.

A final test was conducted to determine whether the effect was permanent. Permeability changes of a new set of UP005 coupons were monitored when treated in 1.0 M NaOH for 20 days and then placed in DI water for different times. The longer the membrane was soaked in DI water the higher was its permeability. After three days the permeability had increased 1.35 times (about 75 % of the increase seen when soaked only in DI water). Therefore, this effect is reversible, as it could be expected from one associated with the osmotic environment.

However, it has to be pointed out that the osmotic stress seen with the lower MWCO membranes is not observed with the 10 and 20 kDa membranes, probably because of their more open porous structure which makes this phenomenon not be relevant.

In summary, the results from this work show that all Nadir membranes are very stable in terms of permeability and rejection performance (with respect to the reference DI water solution) under acidic and alkaline ageing conditions up to 0.1 M concentration in agreement with the physicochemical characterization. Under 1.0 M NaOH and HNO<sub>3</sub> solutions, the high ionic concentration leads to the explained decrease in membrane permeability and the increase in rejection for low MWCO membranes (UH004 and UP005) whereas UP010 and UP020 membranes keeps having the same steady performance as that at lower concentrations. Nevertheless, membrane performance seems more stable as the initial MWCO increases which may be due to the additives or specific manufacturing processes used to get tighter membranes (**Fig. 5.2** and **Fig. 5.3**).



### 5.1.4. Effects of ageing on Koch and GE Osmonics membranes

#### 5.1.4.1. Membrane performance throughout the alkaline ageing

HFK-328 and PT membranes have the same active layer material (PES) and nominal MWCO (4-5 kDa) as the UH004 and UP005 membranes. However, there are significant differences in their initial permeabilities, which go from 13 to 50 L/hm<sup>2</sup>bar, following the order UH004, UP005, PT and HFK-328 (**Table 4.1**).

PT membrane shows the same increase in relative permeability when soaked in DI water as that of Nadir membranes. This is also due to the wetting of the membrane which is initially dry unlike the HFK-328 membrane which is dispatched in glycerin, not showing such increase in permeability (**Fig. 5.9**).

When the HFK-328 membrane (**Fig. 5.9a**) is subjected to the 0.01, 0.1 and 1.0 M NaOH solutions, the relative permeability of the aged membranes increases with the alkali concentration, being the actual permeabilities 7, 12 and 29 % higher than that of the membrane soaked in the reference solution, respectively.

The PT membrane (**Fig. 5.9b**) is the most severely affected by the caustic exposure. For this membrane, the higher the NaOH concentration is, the higher the relative permeability gets with ageing, reaching values approximately twofold the reference value for the 1.0 M solution. In all cases, permeability changes, resulting from the exposure of membranes to the ageing solutions, take place in the very first days of the treatment, reaching a plateau later.

Membrane performance variations shown in this work are exclusively the result of the effects of the NaOH cleaning agent on the membrane. This information, not always available, can be useful when addressing membrane performance throughout several cleaning cycles as well as other phenomena as indicated by previous published studies.

#### 5.1.4.2. Membrane performance throughout the acidic ageing

Both HFK-328 and PT membranes (**Fig. 5.10a** and **Fig. 5.10b**, respectively) exhibit high stability in HNO<sub>3</sub> at all the employed concentrations. The differences in permeability between the aged and the reference membranes is lower than 5 % being the actual permeabilities at the end of the treatments around 50 and 35 L/hm<sup>2</sup>bar, respectively.

The results about the effects of HNO<sub>3</sub> on Nadir, Koch and GE Osmonics membranes can serve as reference to help in the interpretation of other studies. For instance, Paugam *et al.* [11] found that the cleaning of a PES UF membrane with HNO<sub>3</sub> (pH = 1.6) lead to an increase in the water flux, but it did not removed any amount of the residual protein deposit on the membrane surface. Since no changes in permeability were found under acidic pHs, the flux enhancement observed by Paugam *et al.* has to be due to the interaction of the acid with the residual proteins on

the membrane (and not with the membrane), as they correctly hypothesized. Paugam *et al.* [10] confirmed that the increase in membrane water flux was due to the adsorption of the acid on the proteins leading to decrease in membrane hydrophobicity which increased membrane permeability. In a similar way, Weis and Bird [139] observed a more pronounced relative flux decline cycle upon cycle when cleaning a PES UF membrane (fouled with lignosulphonate products) with 0.01 M HNO<sub>3</sub> solution at 50°C. Such phenomenon was not due to the membrane ageing, in accordance to the results of this work as above explained, but to a change of the lignosulphonate fouling charge during the acid cleaning which led to high fouling rates in the following cycles.

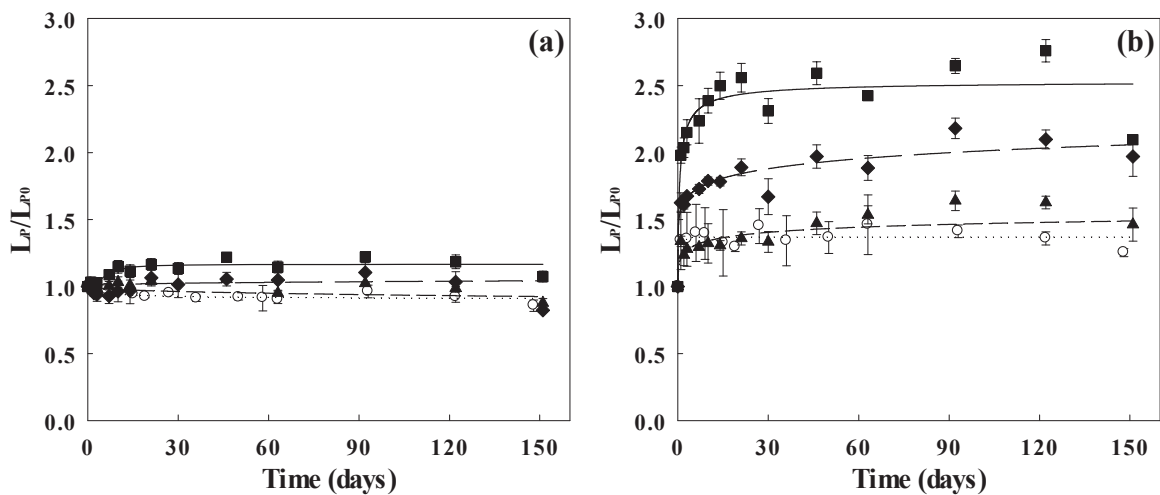


**Fig. 5.9.** Relative permeability of HFK-328 (a) and PT (b) membranes aged at 50°C with NaOH solutions of 0.01 M ( $\blacktriangle$ ; short-dash line), 0.1 M ( $\blacklozenge$ ; long-dash line) and 1.0 M ( $\blacksquare$ ; solid line) and soaked in DI water ( $\circ$ ; dotted line).

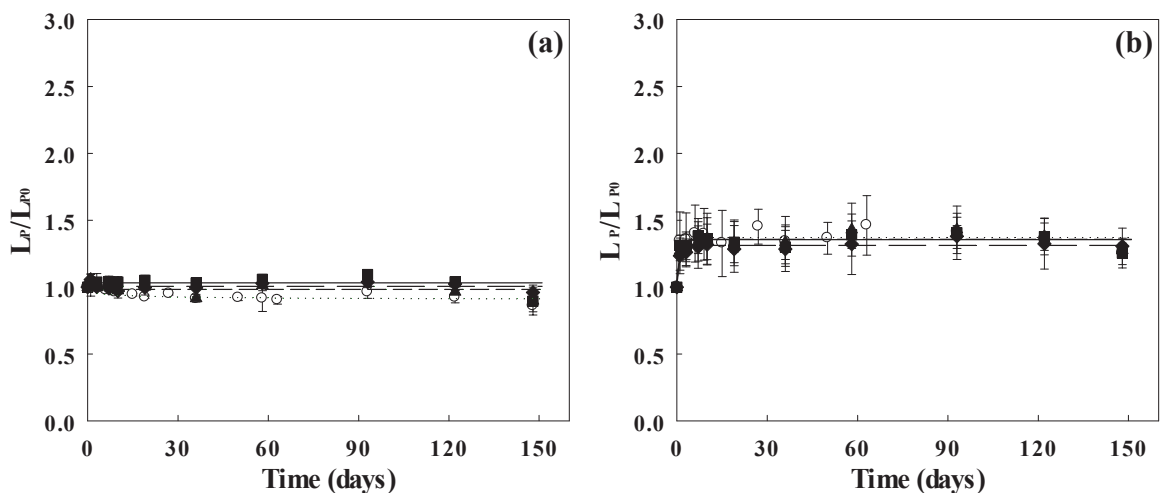


**Fig. 5.10.** Relative permeability of HFK-328 (a) and PT (b) membranes aged at 50°C with HNO<sub>3</sub> solutions of 0.01 M ( $\blacktriangle$ ; short-dash line), 0.1 M ( $\blacklozenge$ ; long-dash line) and 1.0 M ( $\blacksquare$ ; solid line) and soaked in DI water ( $\circ$ ; dotted line).

#### 5.1.4.3. *Effects of the ageing conditions on membrane MWCOs*

The HFK-328 and PT membranes have an increase in their MWCO after the treatment in DI water but due to different phenomena (**Table 5.2**). HFK-328 membrane did not show an increase in permeability, so the lower MWCO in its pristine state may be due to the glycerin solution which is not completely removed by the water, previously to the first filtration. On the other hand, the increase in the MWCO of the PT membrane goes in accordance to the permeability rise observed throughout the membrane conditioning.

After the acidic ageing, both HFK-328 and PT membranes show MWCOs similar to those of reference (3.4 and 2.5 kDa, respectively) regardless of the employed concentration (**Table 5.2**), which is in agreement with the permeability results.

After the alkaline ageing, the MWCOs of the HFK-328 membrane show an upward trend with the NaOH concentration (3.2, 3.1 and 3.5 kDa, respectively), but in the range of the reference value. This trend is steeper for the PT membrane for which, the higher the NaOH concentration is, the higher the MWCO gets. The MWCOs of the aged membranes are 50 % (for the 0.1 M) and 100 % (for the 1.0 M) higher than that of reference, which matches with the permeability increase observed during the alkaline ageing.

It has to be pointed out that the use of the intrinsic PEG rejection in the MWCO determination allows taking into account the different degree of the concentration polarization between the pristine and the alkaline aged PT membranes with higher permeabilities.

The rejection curves for these membranes are shown in **Fig. 5.11**. The mentioned trends keep being valid, but it can be observed that the alkaline ageing of the PT membrane at 1.0 M NaOH leads to a lower rejection of all PEG fractions but especially those with higher MW which means a broadening of the pore distribution towards the larger pores.

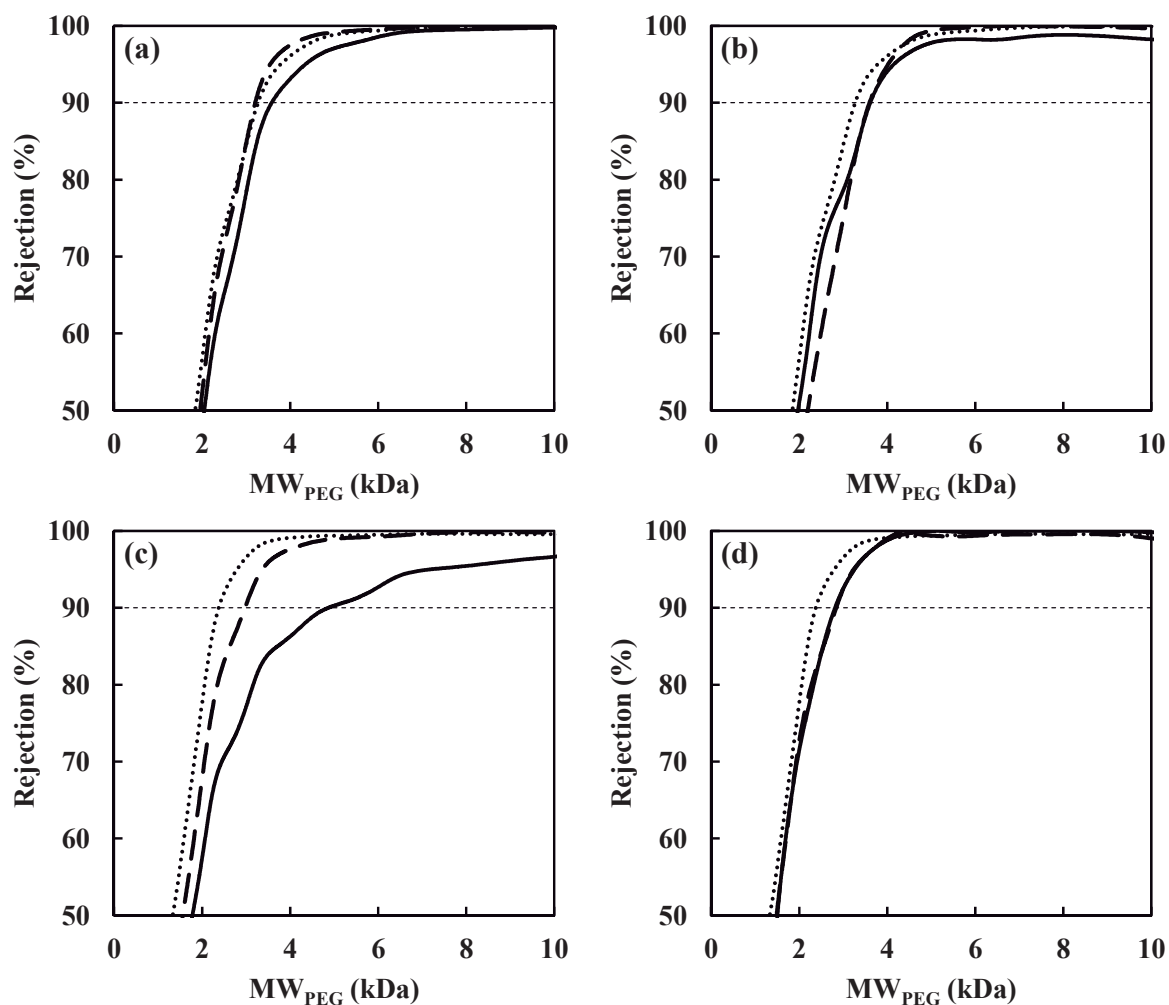


**Fig. 5.11.** Intrinsic rejection curves as function of the PEG fraction MW for the HFK-328 (a, b) and PT (c, d) aged at 50°C with NaOH (a, c) and HNO<sub>3</sub> (b, d) solutions of 0.01 M (broken line) and 1.0 M (solid line) and soaked in DI water (dotted line).

#### 5.1.4.4. Effects of the ageing conditions on membrane surface composition

Active layers of HFK-328 and PT membranes are also resistant to HNO<sub>3</sub> and NaOH solutions at all tested concentrations, showing no changes in their functional group composition (**Fig. 5.12**). However, the support layers exhibit different behavior depending on the ageing chemical. The spectra of the support layers for acidic ageing remained unchanged; which means that the functional group composition of the original and aged support layers is the same (**Fig. 5.12**).

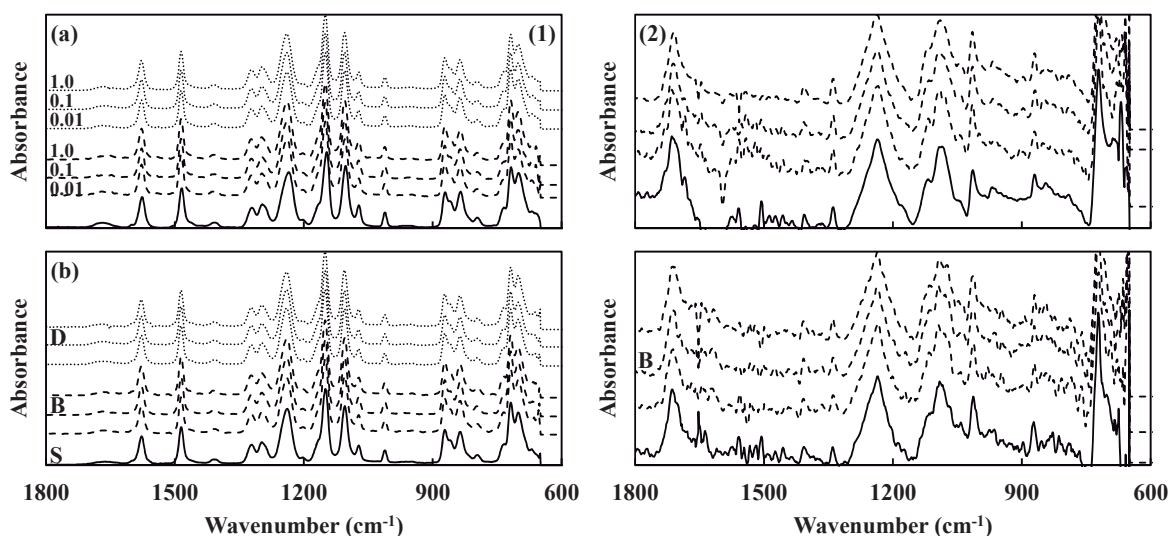
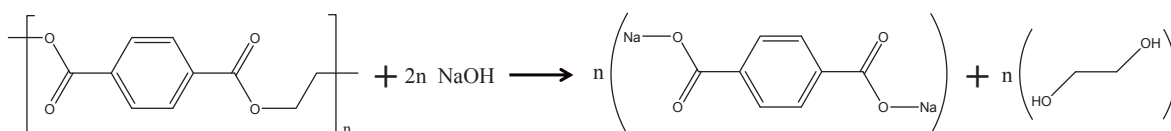


**Fig. 5.12.** ATR-FTIR spectra of the active (1) and support (2) layers of HFK-328 (a) and PT (b) membranes at their original conditions (solid line, S) and after aged with 0.01, 0.1 and 1.0 M HNO<sub>3</sub> solutions (broken line, B) and with 0.01, 0.1 and 1.0 M NaOH solutions (dotted line, D) at 50°C.

Changes in the functional group composition of the support layers of both membranes (**Fig. 5.13**) appear with alkaline ageing and are a function of the NaOH concentration. No changes were observed for the ATR-FTIR spectra of both membranes when ageing was performed with the 0.01 M NaOH solution (pH 12). Nevertheless, when concentration is increased to 0.1 or 1.0 M (pH 13 and 14, respectively), absorption bands at 1710, 1400, 1336, 1232 and 1086 cm<sup>-1</sup> disappear, whereas new bands at 1576, 1484, 1322, 1298, 1149 cm<sup>-1</sup> appear. These spectra are the same as the ones of the active layers (in grey). Therefore, it can be concluded that the support layers are being degraded.

PET is known to break down into its monomers via a hydrolysis reaction when it is treated with NaOH [207], generating ethylene glycol and sodium terephthalate according to the reaction shown below.



In order to verify this hypothesis, a specific experimental procedure to identify the monomer was applied. Two samples of 5 mL from the 1.0 M NaOH solutions at the end of the ageing of the HFK-328 and PT membranes were taken and treated individually. Each sample was acidified with 5 mL of 37 % wt. HCl to transform sodium terephthalate into terephthalic acid. This acid, which is

not soluble in water, forms a white precipitate. After evaporating the water at 50°C to dry the precipitate, 10 mL of DMSO were added and heated at 70°C under stirring (100 rpm) in order to dissolve the precipitate. An aliquot of the DMSO solution was analyzed using GC-MS indicating the presence of terephthalic acid. Therefore, the initial hypothesis was confirmed for the two membranes.

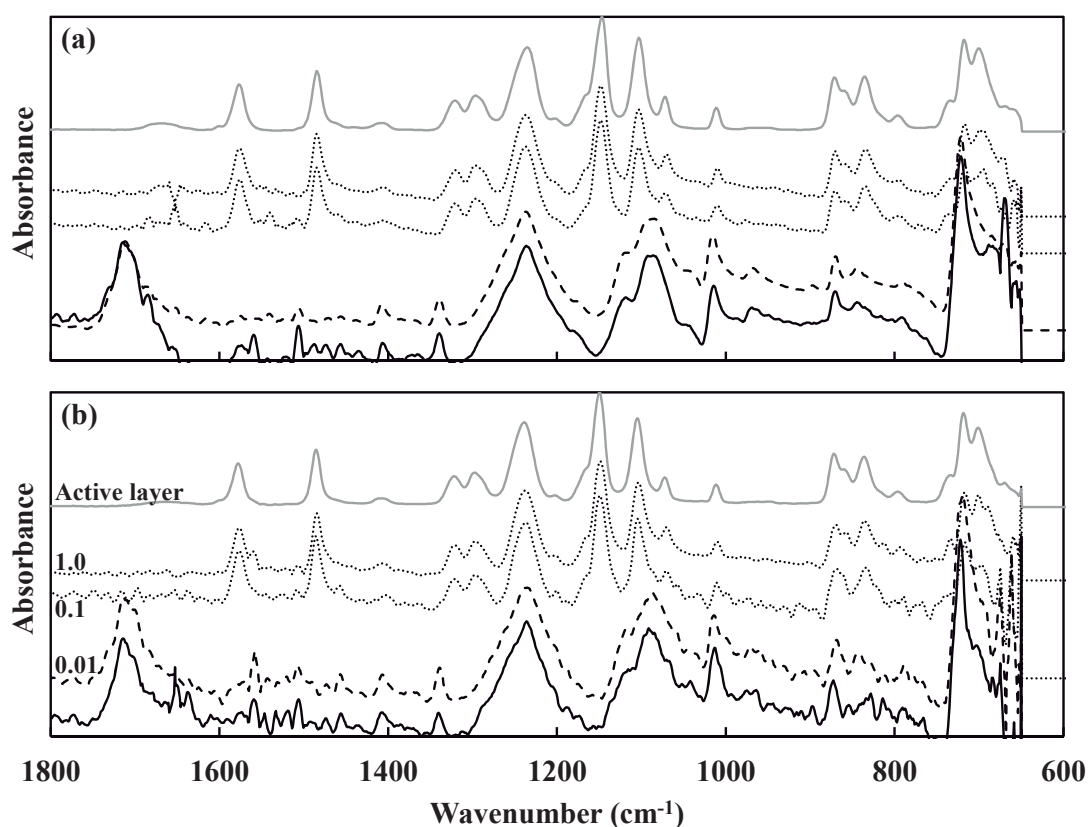


**Fig. 5.13.** ATR-FTIR spectra of HFK-328 (a) and PT (b) support layers at their original conditions (black solid lines) and after the ageing with 0.01 (black broken lines), 0.1 (black dotted lines) and 1.0 M (black dotted lines) at 50°C. The grey solid line that appears at the top of each graph is the spectrum of the active layer, taken from **Fig. 5.1** and displayed here for the sake of comparison.

#### 5.1.4.5. Effects of the ageing conditions on membrane structure

The hypothesis of support layer degradation under certain conditions is also corroborated by the SEM images (**Fig. 5.14**). HFK-328 and PT membrane support layers are resistant to the acidic action, showing no changes in their structural properties, as it can be seen in the SEM micrographs after the ageing with 0.01, 0.1 and 1.0 M HNO<sub>3</sub> solutions. On the other hand, after NaOH ageing procedures, the HFK-328 support layer is not affected at 0.01 M, but there is a

complete degradation at 0.1 and 1.0 M, being possible to observe the footprint that the support layer fibers left in the active layer (**Fig. 5.14**).

Similar results were found for the PT membrane after the alkaline ageing. Nevertheless, its support layer seems to be less resistant than that of the HFK-328, since there is some degradation even at the lowest concentration (0.01 M) and then, degradation increases with concentration. Moreover, the support layer of the PT membrane is not removed as completely as in the case of the HFK-328, since there are some remains of what it could be glue in the backside of the active layer.

The bottom row of **Fig 5.14** displays the cross-section SEM images of the HFK-328 and PT membranes (new and subjected to either 1.0 M HNO<sub>3</sub> or NaOH solution). The degradation of support layers under alkaline conditions is easily noticeable when comparing the original micrograph with that after the soaking in the 1.0 M NaOH solutions. Additionally, the thickness of the active layers was measured from these micrographs, being the HFK-328 one thicker (70 μm) than that of the PT (45 μm).

#### *5.1.4.6. Effects of the ageing conditions on membrane topography*

AFM analysis was carried out to study the physical changes in the active and support layers of the HFK-328 and PT membranes (**Fig. 5.15**). Prior to ageing, the active layer of both membranes exhibits a homogeneous surface with a RMS roughness of 1.50 and 1.45 nm, respectively. After the ageing with HNO<sub>3</sub> or NaOH the active layer roughnesses of all the membranes are slightly higher and in all cases a maximum is observed at 0.1 M concentration. Although the differences are significant, this situation is likely due to experimental discrepancies since measurements are highly dependable on the analyzed sample area. In addition, the evolution of roughness depends on the kinetics of the membrane material modification that would start by localized defects or sensible sites that would act as nucleation points and would be generalized afterwards. The location of these damage nucleation sites would lead to high roughness that afterwards when the corresponding valleys collapse would lead to flatter landscapes and thus to lower roughness. On the other hand, the HFK-328 membrane (**Fig. 5.16a**) shows a higher roughness than that of the PT one (**Fig. 5.16b**) and both membranes have a slightly higher roughness than that of the UP005 one.

The fractal dimensions of the original HFK-328 and PT membranes are 2.20 and 2.54, respectively. After the ageing in HNO<sub>3</sub>, there is a significant increase in the fractal dimension of HFK-328 membrane, especially at 0.01 and 0.1 M concentration. The increase in both, roughness and fractal dimension of this membrane is linked to a more open and accessible pore structure as observed in **Fig. 5.15**. However, for the PT membrane changes in these properties are negligible.

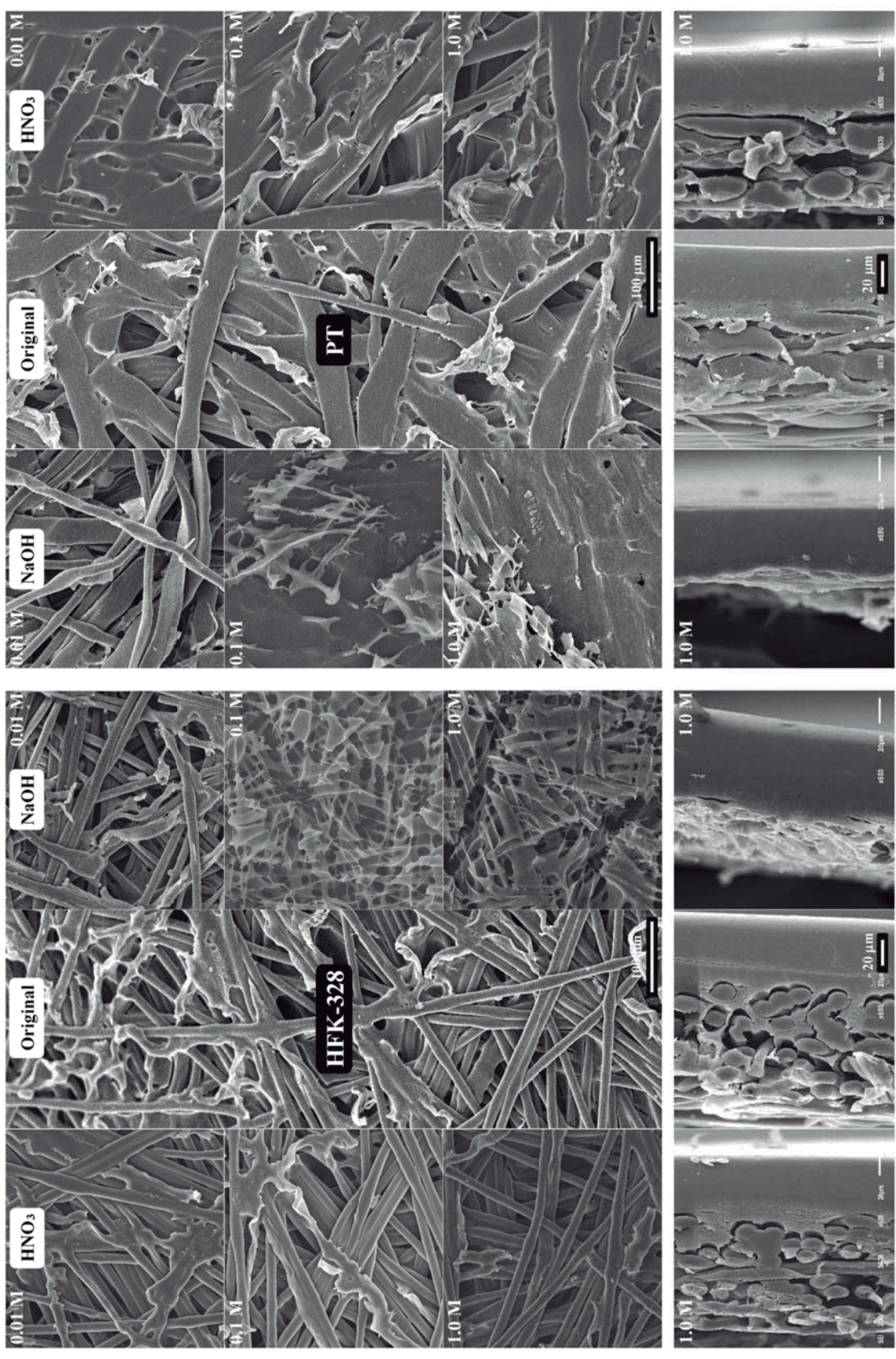


**Fig. 5.14.** SEM micrographs of support layer and membrane cross-section of HFK-328 and PT membranes in their original conditions and after the ageing with 0.01, 0.1 and 1.0 M HNO<sub>3</sub> and NaOH solutions at 50°C.



After the NaOH ageing, the fractal dimensions are lower than the original one for the PT membrane (down to 2.26) and higher for HFK-328 one (up to 2.40). Nonetheless, all changes are around 10 % with respect to the original membrane, so they can be considered not to be significant.

Note that in both cases roughness and fractal dimensions are higher than those for the tested Nadir membrane, which facilitates a higher permeability for these membranes.

Active layer roughness is directly linked to the fouling trend of the membranes as it was already reported [142, 208-210]. The observed steep increase in the roughness and fractal dimension of the HFK-328 membrane aged with HNO<sub>3</sub> would cause high fouling rates. However, the PT membranes after the acidic ageing has a gentle increase in roughness and lower fractal dimensions (compared to those of HFK-328 membranes) which would lead to a less effective fouling. In any case, the roughness-fractal dimension couple can be useful to address membrane performance through several fouling-cleaning cycles, apart from the hydrophilicity.

AFM images of the support layers of HFK-328 and PT membranes are shown in **Fig. 5.15b**. The topography of the membranes aged with 1.0 M NaOH corresponds to the back side of the active layer since the support was almost totally degraded. Nonetheless, the roughness is higher than that of the active layer due to the footprints of the support. After the ageing with the acidic solution, both support layers become significantly smoother.

#### *5.1.4.7. Effects of the ageing conditions on membrane hydrophobicity*

Both active and support layer hydrophobicity were studied due to the changes found in HFK-328 and PT membranes. For the active layer, the contact angles in the original state (**Table 5.3**) are similar to those of Nadir ones as they are made of the same material as confirmed in the ATR-FTIR analysis. However, the active layers of these membranes show an increase in hydrophilicity after the NaOH ageing, with contact angles decreasing with concentration down to 46 and 42° for the HFK-328 and the PT membranes, respectively. The ageing with HNO<sub>3</sub> does not change significantly the hydrophilicity of the pristine membranes.

Support layers are more hydrophobic (**Table 5.4**). Nevertheless, after the alkaline ageing the contact angles decrease, being this reduction more dependent on the NaOH concentration for the HFK-328 than for the PT. At 1.0 M, contact angle values are very close to those of the active layer aged in the same conditions (**Table 5.3** and **Table 5.4**) due to the support layer degradation. The observed fluctuations may be due to the remains of the support layer on the backside of the HFK-328 active layer.

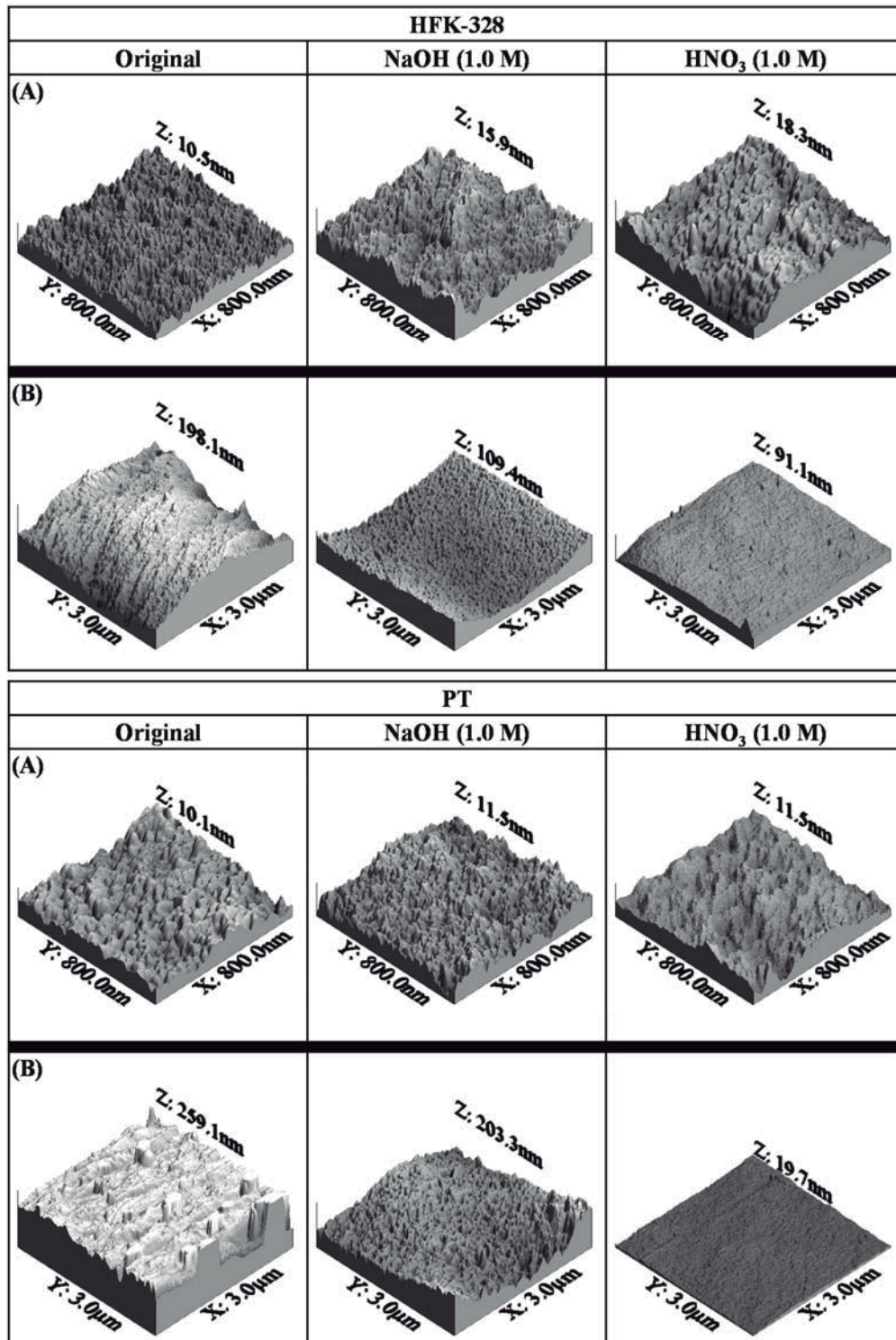
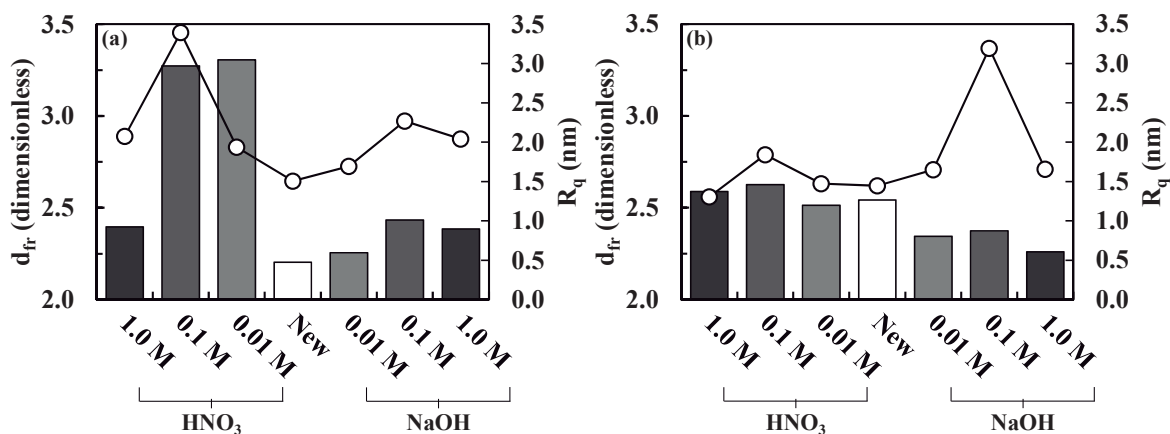


Fig. 5.15. AFM images of the active (A) and the support (B) layers of the HFK-328 and PT membranes in their original conditions and after the ageing with 1.0 M NaOH or HNO<sub>3</sub> solutions. All the AFM images has the same z-axis scale and the Z values are the maximum height of each image.



**Fig. 5.16.** PSD fractal dimension (bars) and RMS roughness for the  $0.8 \times 0.8 \mu\text{m}$  scanned areas of the HFK-328 (a) and PT (b) membranes after the ageing in  $\text{HNO}_3$  and  $\text{NaOH}$  solutions at different concentrations.

**Table 5.4.** Contact angle measurements (using ultrapure water) of the support layers of the HFK-328 and PT membranes after the ageing in 0.01, 0.1 and 1.0 M  $\text{NaOH}$  solutions at  $50^\circ\text{C}$ . Intervals expressed as standard deviations.

Ageing conditions	Membranes	
	HFK-328	PT
Pristine membrane	$92 \pm 6$	$81 \pm 1$
DI water	$95 \pm 2$	$91 \pm 3$
$\text{NaOH}$ (0.01 M)	$69 \pm 1$	$53 \pm 6$
$\text{NaOH}$ (0.1 M)	$67 \pm 3$	$61 \pm 2$
$\text{NaOH}$ (1.0 M)	$49 \pm 3$	$50 \pm 1$

The contributions of Lifshitz-Van der Waals and acid-base interactions to the solid surface energy of the active layers were studied (**Table 5.5**) to account for the variations in the active layer hydrophobicity after the alkaline ageing. Total solid surface energy and the dispersive force contribution are almost constant for the PT membranes in all the tested conditions, but slightly decrease for the HFK-328 ones with the alkaline ageing concentration. Additionally, **Table 5.5** reveals that both membranes have a predominantly electron donor character (Lewis base), as well as that this character increases with  $\text{NaOH}$  concentration. Since no changes in ATR-FTIR spectra were not found, this effect can be explained by the fact that the existing functional groups of these membranes become more negatively charged when they are subjected to alkaline conditions.

**Table 5.5.** Total solid surface energies (mJ/m<sup>2</sup>) and their dispersive and polar components of HFK-328 and PT active layers after the ageing in 0.01, 0.1, 1.0 M NaOH solutions at 50°C.

Ageing conditions	HFK-328				PT			
	$\gamma^{\text{TOT}}$	$\gamma^{\text{LW}}$	$\gamma^+$	$\gamma^-$	$\gamma^{\text{TOT}}$	$\gamma^{\text{LW}}$	$\gamma^+$	$\gamma^-$
Pristine membrane	52.9	46.2	0.854	13.2	48.1	43.9	0.22	20.3
DI water	51.7	46.3	0.501	14.5	49.4	44.0	0.38	19.1
NaOH (0.01 M)	48.0	45.1	0.067	30.7	49.0	45.5	0.10	31.7
NaOH (0.1 M)	45.7	43.8	0.030	30.6	48.4	45.4	0.07	34.6
NaOH (1.0 M)	44.6	43.9	0.004	36.0	48.7	44.8	0.11	36.3

#### 5.1.4.8. Discussion

As for the Koch and GE Osmonics membranes, no changes in the functional group composition of the active and the support layers were found and neither in the structure of the support layers under any acidic ageing condition. Active layer hydrophilicity also remained unchanged for both membranes. However, HFK-328 active layer roughness increased with respect to the new membrane as well as the fractal dimension, leading to a more open surface structure. PT membrane did not showed such changes in roughness and fractal dimension parameters and therefore it would be less prone to fouling than the HFK-328 one after a hypothetical acidic cleaning step with HNO<sub>3</sub>. This lack of significant physicochemical changes at the end of the acidic ageing treatments goes in accordance with the permeability and MWCO results which are similar to those of the reference membranes.

After the ageing under alkaline conditions, although the functional group composition was kept constant, there was an increase in the hydrophilicity of the active layers of both membranes which came together with an increase in their electron donor capacity, attributed to an increase in the negative charge of the existing functional groups of the membranes. Facts that facilitate the increase in the permeability and the MWCO for the HFK-328 (only under the 1.0 M NaOH solution) and the PT membranes. The roughness of the active layers of both membranes also rose. However, considering the fractal dimension, which evaluates the pore entrance accessibility independent of the scale of examination, no significant changes can be considered.

The most remarkable ageing effect was linked to the stability of the backing layer of HFK-328 and PT membranes under certain alkaline conditions. Thus, after the ageing treatments at 0.1 and 1.0 M NaOH concentrations, the support layer was severely affected. By means of ATR-FTIR, contact angle and SEM, it was confirmed that the nonwoven made of PET was degraded via hydrolysis reaction leading to a considerable loss of this layer in the case of the PT membrane and to a complete removal of the Koch one. The last technique also allows

determining the active layer thickness of the HFK-328 and PT membranes. Therefore, the support layer degradation is believed to be the main reason that leads to the mentioned increase in permeability and MWCO of the Koch and GE Osmonics membranes as consequence of the alkaline ageing. The lack of the support layer makes the active layer less stable mechanically in such a way that the stretching of the pores is eased by the absence of the nonwoven, leading to the increase in the permeability and the MWCO. In addition, due to the fact that PT active layer is thinner than the HFK-328 one, the effects on the performance are less severe for the latter, being only significant under the ageing at 1.0 M NaOH concentration as mentioned.

### 5.1.5. Effect of temperature on 5 kDa PES membrane ageing

Permeability and MWCO changes of the 5 kDa PES membranes were followed soaking samples in 1.0 M NaOH solutions at 25°C, 35°C and 50°C respectively. Since constant permeability was reached after the fiftieth day at 50°C, these studies were conducted only for two months, sufficient time to reach comparable steady conditions.

For the UP005 membrane, as seen in **Fig. 5.17** and in **Table 5.2**, the ageing is completely independent of temperature. At the three temperatures, membrane relative permeability is the same, reaching a final permeability of around 13.5 L/hm<sup>2</sup>bar. Furthermore, MWCOs are in agreement with permeability results, following the same downwards trend with cut-off decreasing from 2.0 kDa to 1.6 kDa for the three temperatures.

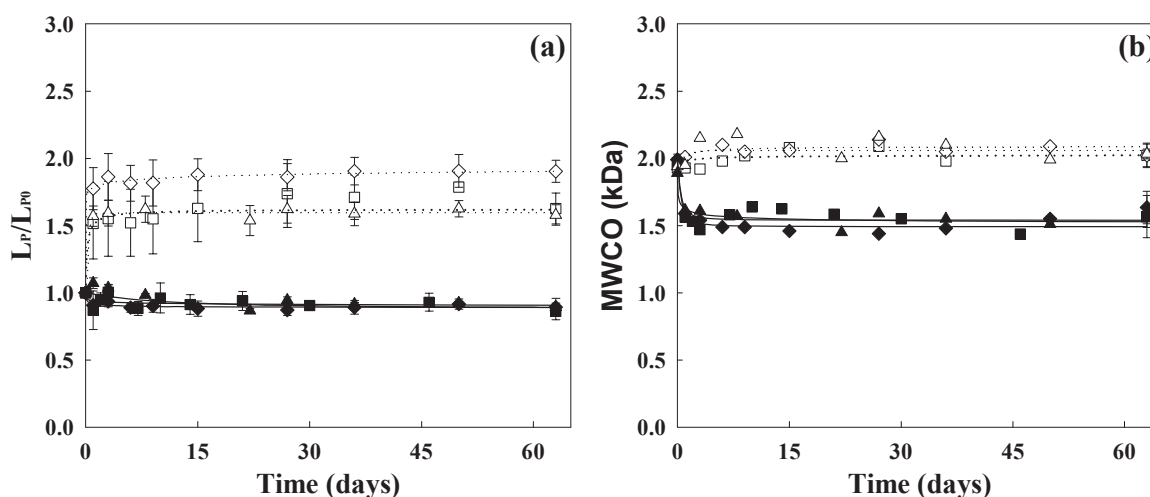


**Fig. 5.17.** Relative permeability (a) and MWCO (b) changes of UP005 membrane soaked in DI water (open symbols and dotted lines) and aged with 1.0 M NaOH solution (closed symbols and solid lines) at 25°C ( $\Delta$ ,  $\blacktriangle$ ), 35°C ( $\diamond$ ,  $\blacklozenge$ ) and 50°C ( $\square$ ,  $\blacksquare$ ).

Even though HFK-328 support layer is degraded at the three temperatures when 1.0 M NaOH solutions are used, performance of HFK-328 membrane is quite stable in terms of permeability (**Fig. 5.18a**), except for the ageing at 50°C in which permeability increases by 29 %.

In terms of rejection performance, the MWCO of the HFK-328 membrane fluctuate from 3.0 to 3.5 kDa.

For the PT membrane, the higher the temperature is, the higher increase in permeability at the end of the ageing treatments is obtained (**Fig. 5.18b**), being the permeability 25, 43 and 71 % higher than the reference value as the temperature increases. Note that after 150 days the increase was 100 % for the ageing at 50°C (**Fig. 5.9b**). In the same way, MWCOs of PT membranes also increase during the ageing as a function of the temperature going from 2.3 to 5 kDa. The influence of the temperature on the ageing of this membrane is due to the support layer degradation and the thickness of its active layer. Therefore, the higher the temperature is, the more severe the degradation of the support layer is, affecting also the active layer.

In summary, the effect of the temperature over three membranes made of PES is different depending on the support layer material. The ageing of UP005 membrane (mixture of PE/PP as nonwoven material) was independent of the temperature, whereas HFK-328 and PT membranes (PET as nonwoven material) showed an influence of this parameter at different levels which in turn, depended on the thickness of the active layer as explained in “section 5.1.4.8”.

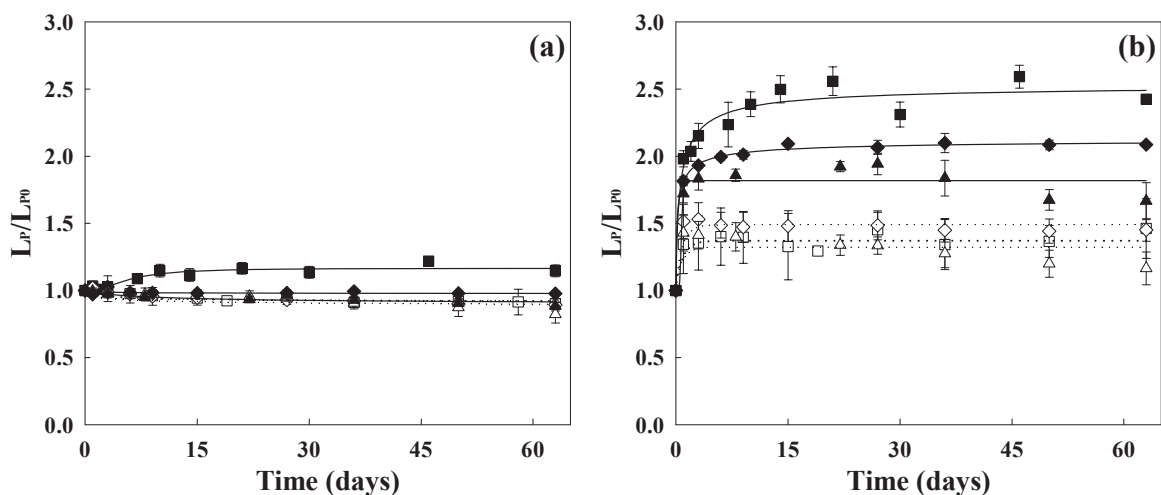


**Fig. 5.18.** Relative permeability of HFK-328 (a) and PT (b) membranes soaked in DI water (open symbols and dotted lines) and aged with 1.0 M NaOH solution (closed symbols and solid lines) at 25°C ( $\triangle$ ,  $\blacktriangle$ ), 35°C ( $\diamond$ ,  $\blacklozenge$ ) and 50°C ( $\square$ ,  $\blacksquare$ ).

Temperature is an important parameter when setting membrane cleaning procedures. In general, the higher the temperature, the higher the cleaning effectiveness [41, 122]. Indeed, this factor was found to be significant by Chen *et al.* [91] through a statistical factorial design of experiments in which a PES UF membrane fouled with a secondary effluent from a local sewage treatment works was cleaned with 0.125 or 0.25 M NaOH solutions resulting in a higher cleaning efficiency when the temperature increased from 25 to 50°C. However, the results from this work

show that high temperatures can result in an increase in the permeability for some specific membranes which can lead to wrong conclusions if the effect of the cleaning agent itself on the membrane is not studied independently.

## **5.2. Ageing of NF membranes under acidic and alkaline cleaning solutions**

---

### **5.2.1. Abstract**

Two commercial NF polymeric membranes (NF90 and NF270 from Dow Filmtec) were subjected to acidic and alkaline ageing using HNO<sub>3</sub> and NaOH, respectively. Concentrations of 0.01, 0.1 and 1.0 M were tested for both cleaners at 50°C. Membrane ageing was conducted either by soaking the membranes in the cleaning solutions or in cross-flow mode. Membrane degradation was followed by permeability and rejection measurements using charged (Na<sub>2</sub>SO<sub>4</sub>) and uncharged (glucose and sucrose) molecular markers. In addition, the active layer surface composition and structure of the aged membranes were analyzed by ATR-FTIR spectroscopy and SEM. Both membranes were more resistant to the acidic than to the alkaline cleaner, and under the same conditions, NF90 was more resistant than NF270. Differences between both ageing modes were found, being the membrane degradation less pronounced in cross-flow mode. Changes in membrane performance were correlated through the FTIR absorbance decrease in the amide I and II bands of NF270 and NF90, respectively. Some degradation of the backing layer of both membranes also took place under certain ageing conditions, especially for 1.0 M NaOH solutions.

### **5.2.2. Ageing of the NF90 membrane**

Changes in permeability and rejection of NF90 membrane as function of the exposure time to HNO<sub>3</sub> and NaOH at 50°C are shown in **Fig. 5.19**. In all the figures error bars are calculated from the standard deviation of the four membrane sample measurements associated to each condition and they are added to show the dispersion. NF90 membrane performance is stable in DI water. These permeability and rejection results are used as reference to determine the ageing under the different acidic and alkaline conditions.

NF90 membrane shows a high stability when it is soaked in 0.01 and 0.1 M HNO<sub>3</sub> solutions. Permeability remains constant around 6.6 L/hm<sup>2</sup>bar as well as Na<sub>2</sub>SO<sub>4</sub>, glucose and sucrose rejections which are around 95 %. Only at the end of the ageing treatment at 0.1 M, the membrane rejection of uncharged solutes starts to decrease. When HNO<sub>3</sub> concentration is increased up to 1.0 M, membrane stability lasts less than 15 days (which would be equivalent to around 1 year of plant operation under the assumptions mentioned in “section 4.3.1”), especially in terms of uncharged solute rejection which shows a sharp decrease after the tenth day.

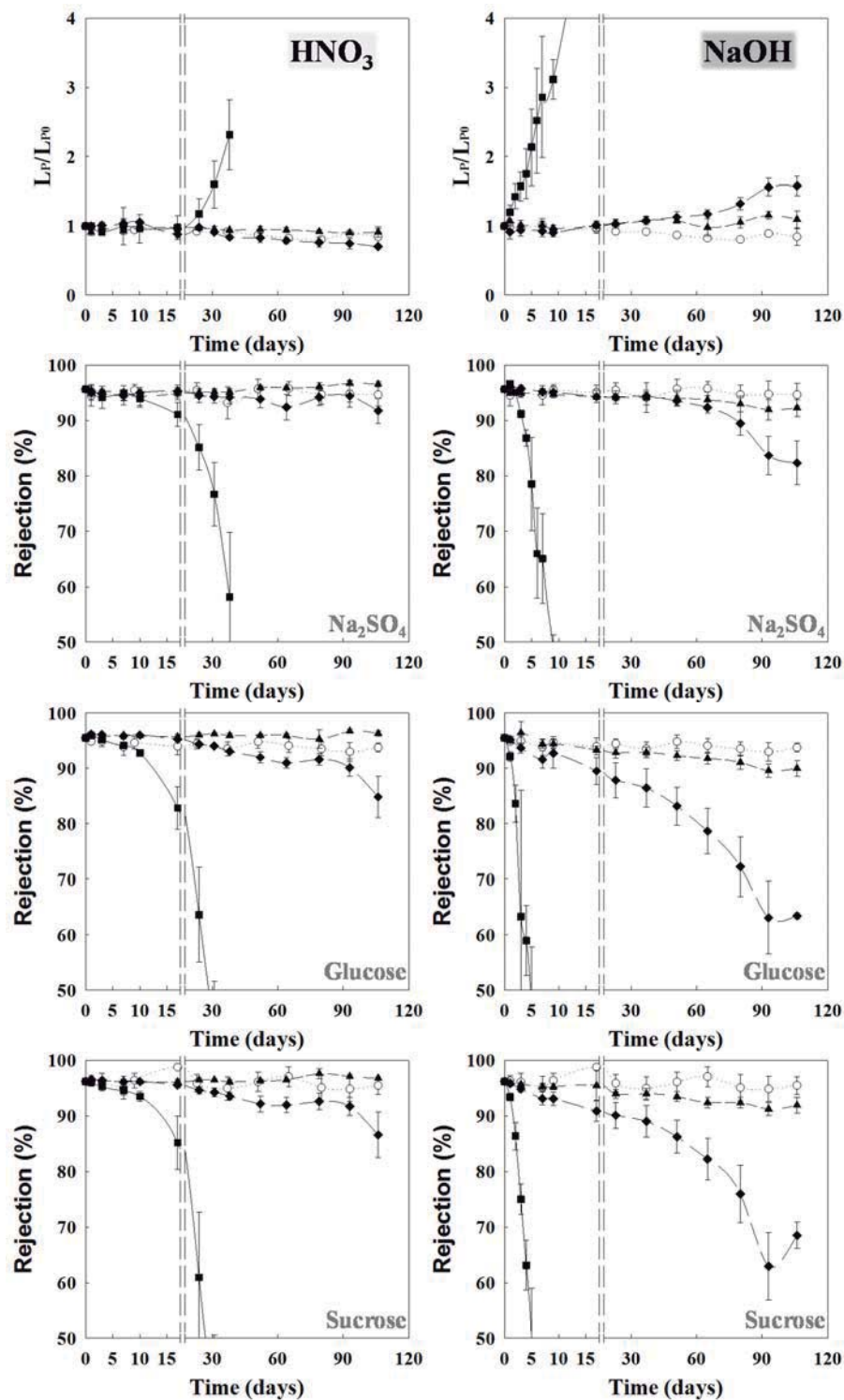
On the other hand, the alkaline treatment has a higher impact on NF90 membrane. The ageing at 1.0 M leads to a quick increase in permeability while Na<sub>2</sub>SO<sub>4</sub> and uncharged solute rejections drop below 85 % after the fifth (equivalent to 4 months) and the third (2.5 months) day, respectively. For 0.1 M NaOH, both NF90 membrane permeability and Na<sub>2</sub>SO<sub>4</sub> rejection remains constant for the first 60 days (4 years), showing the effects of the ageing after that point. However,



in this condition, the glucose and sucrose rejection started to decrease at the beginning of the treatment, being lower than 85 % after the fiftieth day (3.3 years). Therefore, one can conclude that the NF90 membrane is quite stable in terms of permeability and rejection performance under the 0.01 M NaOH treatment. This behavior has been already described by Mänttari *et al.* [32]. The increase in pH increases the permeability and makes the non-charged solutes have a lower rejection. Nonetheless, the authors checked the rejection of NaCl instead of Na<sub>2</sub>SO<sub>4</sub>. Nilsson *et al.* [33] did not find any changes in NF membranes, most likely because they used a very low alkaline detergent concentration equivalent to 0.05 M NaOH and it is clear in **Fig. 5.19** that membranes are not affected until at least 60 days of exposure under this condition.

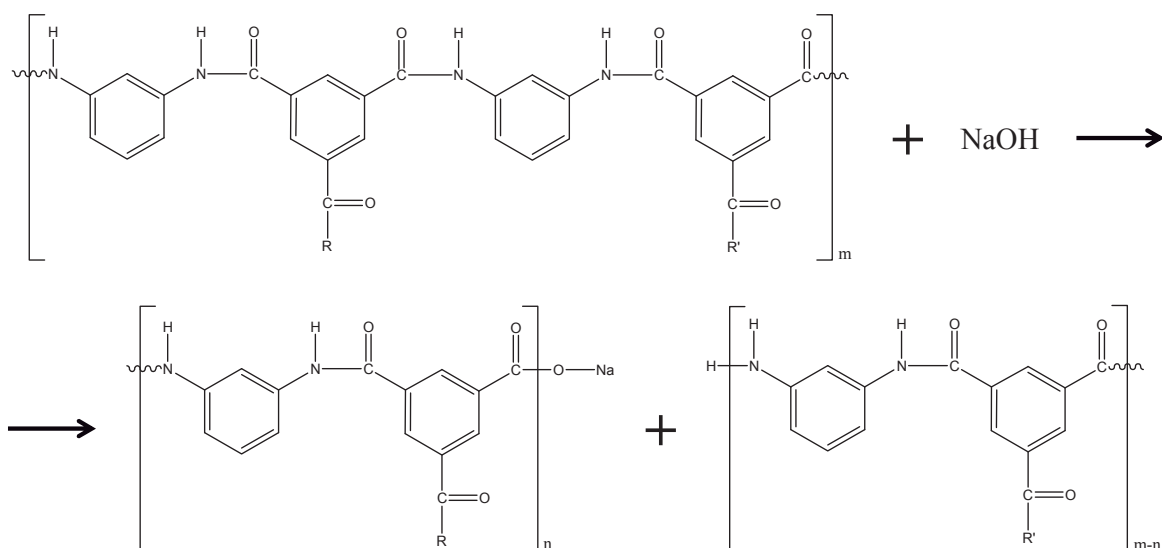
The chemical changes behind the NF90 membrane performance due to the action of the NaOH and HNO<sub>3</sub> cleaning solutions are explained in detail later on.

The NF90 membrane consists of three layers: a fully aromatic polyamide (PA) active layer (made of 1,3-benzenediamine and trimesoyl chloride) which coats a polysulfone (PS<sub>u</sub>) support layer reinforced by a non-woven backing layer made of polyester [211-213]. Due to the relative high penetration of the IR beam into the membrane, the NF90 ATR-FTIR spectrum shows peaks associated to both PS<sub>u</sub> and PA layers. These peaks were already described in detail by Tang *et al.* [212]. At first sight, ATR-FTIR spectra of NF90 membrane (**Fig. 5.21**) do not show any significant change after either the acidic or the alkaline ageing at any concentration because most of the peaks are from the PS<sub>u</sub> layer which is stable in these conditions. In order to separate the effect of both layers, the height ratio,  $I_{1540}/I_{1240}$ , between one of the PA peaks (the amide II band) at 1540 cm<sup>-1</sup> (associated to the N-H in plane bending and N-C stretching vibration of CO-NH groups) and one of the PS<sub>u</sub> peaks at 1240 cm<sup>-1</sup> (associated to the C-O-C asymmetric stretching vibration of aryl-O-aryl groups), which remains invariant, was determined (**Table 5.6**). For those conditions in which no performance changes were observed, the  $I_{1540}/I_{1240}$  ratio remains similar to that of the pristine and reference membranes. However, the value of this height ratio decreases with increasing concentrations of either HNO<sub>3</sub> or NaOH, indicating that there is a decrease in the number of CO-NH bonds on the NF90 active layer surface and, therefore, indicating a degradation of the PA active layer.



**Fig. 5.19.** Permeability and  $\text{Na}_2\text{SO}_4$ , glucose and sucrose rejection behavior of the NF90 membrane aged at  $50^\circ\text{C}$  in  $\text{HNO}_3$  (left column) and  $\text{NaOH}$  (right column) solutions of 0.01 M ( $\blacktriangle$ ; short-dash line), 0.1 M ( $\blacklozenge$ ; long-dash line) and 1.0 M ( $\blacksquare$ ; solid line) and soaked in DI water ( $\circ$ ; dotted line).

The degradation of this polymer, evaluated through the  $I_{1540}/I_{1240}$  ratio, is due to the hydrolysis of the amide bonds (CO–NH). Under alkaline conditions, the hydroxide ion from the NaOH performs a nucleophilic attack to the carbonyl carbon of the amide bond boosting the hydrolysis reaction [214]. On the other hand, at low pHs, the acid ( $\text{HNO}_3$ ) acts as a catalyzer performing a protonation of the carbonyl oxygen atom which boosts the subsequent nucleophilic attack of a water molecule leading to the hydrolysis of the amide bond [214, 215]. The global hydrolysis reaction which takes place on the N90 active layer is shown in **Fig. 5.20** for just one nucleophilic attack under the alkaline conditions. Where the R and R' groups can be either a hydroxide ion or another chain of monomers. The products of the acidic hydrolysis (not shown) would be the same but instead of getting the salt, the reaction leads to a carboxyl acid at the end of the chain.

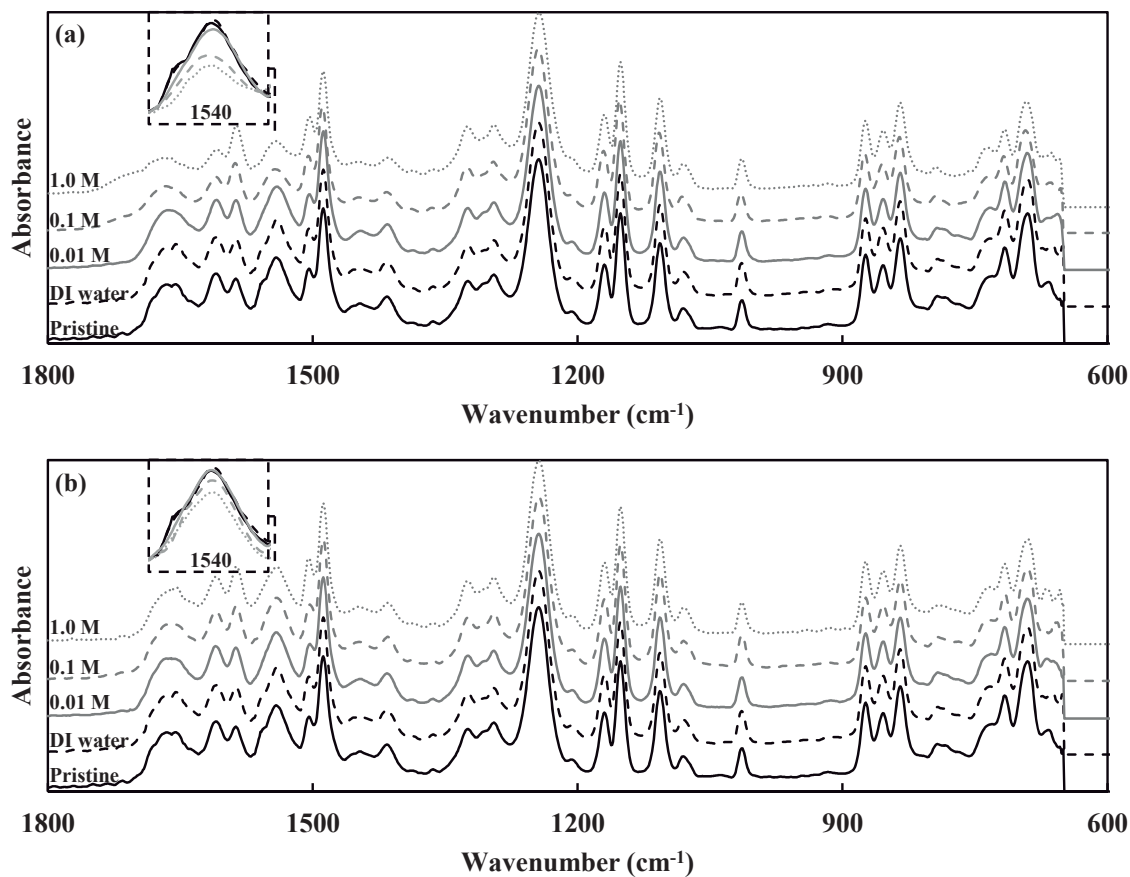


**Fig. 5.20.** Example of one amide bond hydrolysis reaction of the NF90 PA active layer under alkaline conditions.

As a result, the hydrolysis of the amide bonds leads to a less cross-linked active layer and so, to a more open structure. As consequence, there is an increase in permeability and a decrease in the rejection capabilities of the NF 90 membrane throughout certain ageing conditions (shown in **Fig. 5.19**). In addition and according to the work of Duan *et al.* [214] the amide degradation rate constant is slightly higher under alkaline conditions which would explain the faster worsening of the NF90 membrane performance when aged in NaOH with respect to  $\text{HNO}_3$ .

**Table 5.6.** Infrared peak ratios for the NF90 and NF270 membranes after being subjected to different ageing conditions.

Ageing conditions	NF90	NF270
	$I_{1540}/I_{1240}$	$I_{1630}/I_{1240}$
Pristine membrane	0.371	0.103
DI water	0.382	0.100
HNO <sub>3</sub> (0.01 M)	0.345	0.105
HNO <sub>3</sub> (0.1 M)	0.245	0.061
HNO <sub>3</sub> (1.0 M)	0.205	0.036
NaOH (0.01 M)	0.366	0.085
NaOH (0.1 M)	0.328	0.055
NaOH (1.0 M)	0.270	0.025

**Fig. 5.21.** ATR-FTIR spectra of the active layer of the NF90 membrane in its pristine state, soaked in DI water and aged in HNO<sub>3</sub> (a) and NaOH (b) ageing solutions at different concentrations.

SEM analyses were also carried out after the ageing treatments to determine their effects on the NF90 membrane structure (**Fig. 5.22**). SEM images of the NF90 active layer were also taken, but no significant changes were found between the pristine and the aged membranes. Thus, micrographs of the active layer are not shown here. The mechanical resistance of the NF90 membrane is given by the polyester backing layer which is shown in the SEM images of the back side and cross-section of the membrane (**Fig. 5.22**). After the soaking in DI water and the ageing in all the HNO<sub>3</sub> solutions, no changes in the polyester non-woven layer are shown. However, at the end of the alkaline ageing, the higher the concentration is employed, the more significant fiber degradation is found. In fact, at the highest employed NaOH concentration, the non-woven structure is completely removed. The degradation of the backing layer is not believed to be the cause of changes in membrane behavior, since it is well-known that performance of NF membranes is given by the active layer. In agreement with this hypothesis, no degradation of this layer is observed after the ageing in 1.0 M HNO<sub>3</sub> but there is actually a worsening of the NF90 performance. Nevertheless the backing layer removal weakens the membrane structure and thus, the likelihood of a membrane mechanical failure increases.

### 5.2.3. Ageing of the NF270 membrane

Similar ageing studies were carried out for the other Dow Filmtec membrane (NF270) which is a more opened NF membrane [36]. The NF270 membrane has a higher permeability, 13.2 L/hm<sup>2</sup>bar, but under the tested conditions, its Na<sub>2</sub>SO<sub>4</sub> (97.1 %) and sucrose (98.2 %) rejections are similar, and even higher than those of the NF90 membrane (95.7 and 96.2 %, respectively). Only glucose rejection of NF270 membrane (89.8 %) is significantly lower than that of the NF90 membrane (95.5 %).

Performance of NF270 membrane after the acidic and alkaline ageing is shown in Fig. 5. Although, permeability and rejection of the NF270 membrane soaked in DI water has some scattering with time, these values are taken as reference to determine ageing effects of the HNO<sub>3</sub> and NaOH on membrane performance.

**Fig. 5.19** and **Fig. 5.23**, show that NF270 membrane is less stable than the NF90 in both acidic and alkaline conditions. Thus, time scale axis in **Fig. 5.23** was shortened to 60 days in order to show the main changes. There is also an expanded scale showing the first 40 h of ageing.

When the NF270 membrane is aged in a 1.0 M HNO<sub>3</sub> solution, its performance worsens in less than 2 days (equivalent to about 48 days of plant use). When decreasing the concentration to 0.1 M, the permeability starts to increase slowly at the beginning in the same way that glucose rejection decreases. However, the Na<sub>2</sub>SO<sub>4</sub> and sucrose (with a higher MW) rejection values remain stable up to the twentieth day (equivalent to 1.3 years). Only when the ageing takes place at pH 2 (0.01 M HNO<sub>3</sub>), the membrane performance remains constant in terms of permeability and rejection capabilities longer than 120 days (which would correspond to 8 years of industrial use).

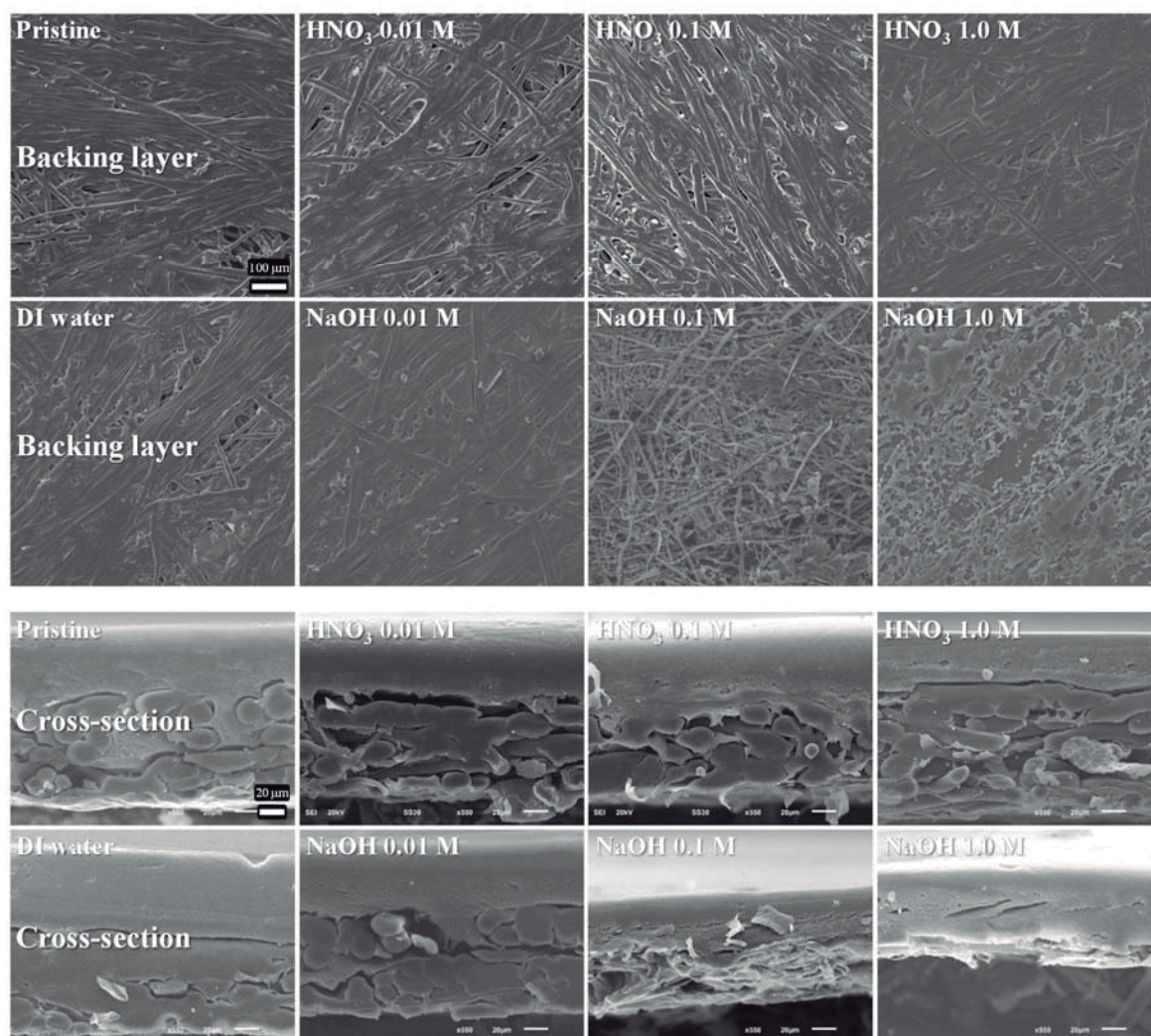


**Fig. 5.22.** SEM micrographs of the backing layer and the cross-section of the NF90 membrane in its pristine state, soaked in DI water and aged in HNO<sub>3</sub> and NaOH ageing solutions at different concentrations.

The alkaline ageing had a higher impact on membrane performance. Stability of NF270 membrane aged with 0.1 and 1.0 M NaOH solutions lasts less than 30 h and 1 h, respectively, as it is shown in **Fig. 5.23**. Moreover, when the ageing is conducted with 0.01 or 0.1 M NaOH concentrations, there is a first jump up in the permeability after the first treatment day and later on, the increase in the permeability takes place gradually. Similar behavior is found for glucose rejection. Mänttari *et al.* [38] also found a behavior similar at pH higher than 8. The effect was less pronounced than the one found in this work, because the solutions tested were adjusted by adding NaOH until the desired pH was reached (the resulting concentration was close to 0.01 M NaOH). At this pH **Fig. 5.23** shows that membrane takes longer to show the increase in permeability and the decrease in rejection. This rejection drop is not so steep for the sucrose, which may be due to

the fact that the membrane degradation takes place progressively in such a way that the small pores are getting bigger along the ageing, making the effects more visible for lower MW molecules (similar to the 0.1 M HNO<sub>3</sub> ageing). Nonetheless, NF270 performance in terms of Na<sub>2</sub>SO<sub>4</sub> rejection is similar to that of the sucrose since the increase in the pore size of the membrane is likely compensated by the electrostatic rejection.

NF270 membrane is also composed of three layers which are made of polyester (the lower layer), PS<sub>u</sub> (the middle support) and PA (the active layer) [211]. More specifically, the active layer is made of a poly(piperazinamide) based semi-aromatic PA [212]. The ATR-FTIR spectrum of the NF270 pristine membrane (**Fig. 5.25**) is similar to that of the NF90 one, especially in the wavenumber range from 600 to 1500 cm<sup>-1</sup>, in which the bands are associated to the PS<sub>u</sub> support layer. However, since the active layer of both membranes is slightly different the peaks from 1500 to 1800 cm<sup>-1</sup> differ from each other. The NF270 membrane only has one peak associated to the PA material which is the amide I band at 1630 cm<sup>-1</sup> (linked to the C=O stretching which is the dominant contributor, the C–N stretching, and the C–C–N deformation vibration in a secondary amide group) [212]. As it happened with the NF90, since most of the peaks of the spectra come from the PS<sub>u</sub> material, there are not significant changes in the spectra of the aged membranes under acidic and alkaline conditions at any concentration. However, considering the amide I band, it is possible to calculate an ATR-FTIR height ratio,  $I_{1630}/I_{1240}$ , between that peak at 1630 cm<sup>-1</sup> and the peak at 1240 cm<sup>-1</sup> associated to the PS<sub>u</sub> (invariant during the ageing treatments) which gives information about the state of the PA active layer.

Comparing the values of this  $I_{1630}/I_{1240}$  ratio at the end of the different ageing treatments (**Table 5.6**), as the cleaning agent concentration increases, the  $I_{1630}/I_{1240}$  ratio decreases and thus, a higher degradation takes place with both HNO<sub>3</sub> and NaOH.

This degradation, as explained for the NF90 membrane, is due to the hydrolysis of the amide bonds, which leads to a more open structure (lower cross-linked active layer) and so, to a higher permeability and a lower rejection capability (**Fig. 5.23**). The global reaction of one nucleophilic attack to the poly(piperazinamide) active layer under acidic conditions is shown in **Fig. 5.24**. Where R and R' groups can be again either a hydroxide ion or a chain of monomers. In this case, the products under the alkaline condition would have the carboxyl group as a salt.

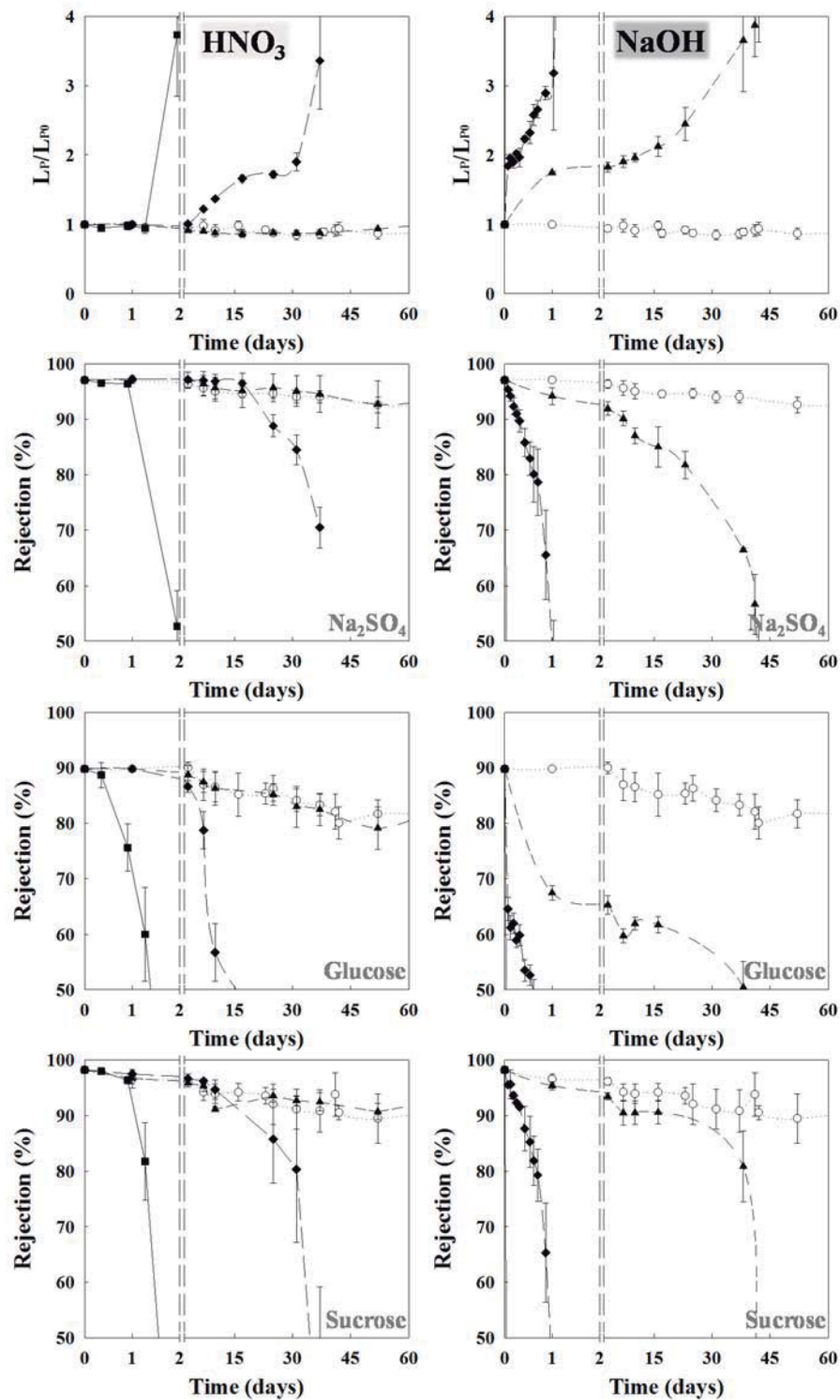
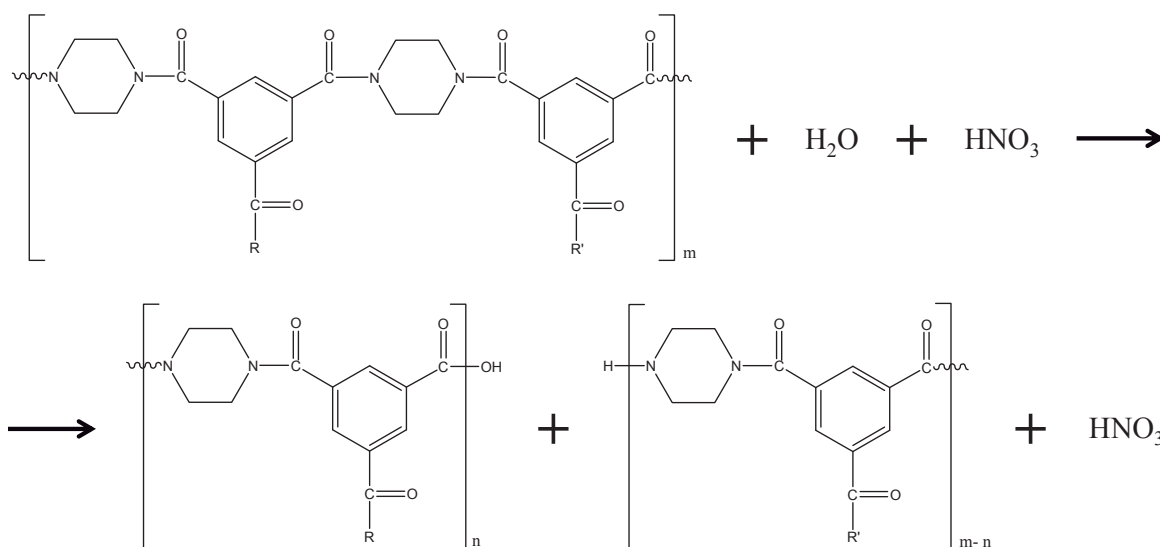


Fig. 5.23. Permeability and  $\text{Na}_2\text{SO}_4$ , glucose and sucrose rejection behavior of the NF270 membrane aged at  $50^\circ\text{C}$  in  $\text{HNO}_3$  (left column) and  $\text{NaOH}$  (right column) solutions of 0.01 M ( $\blacktriangle$ ; short-dash line), 0.1 M ( $\blacklozenge$ ; long-dash line) and 1.0 M ( $\blacksquare$ ; solid line) and soaked in DI water ( $\circ$ ; dotted line).





**Fig. 5.24.** Example of one amide bond hydrolysis reaction of the NF270 poly(piperazinamide) active layer under acidic conditions.

**Table 5.6** also shows that for the NF270 membrane, the PA active layer degradation, at a given concentration, is more severe (lower  $I_{1630}/I_{1240}$  ratio) after the alkaline ageing than after the acidic one. This is in agreement with the membrane performance at the end of the different ageing conditions and with the higher hydrolysis rate constants at alkaline pHs found in the work of Duan *et al.* [214].

Last, it was found that the ageing of the NF270 membrane in terms of performance was more severe than the NF90 one under any same acidic or alkaline condition (**Fig. 5.19** and **Fig. 5.23**). The hydrolysis of the amide bonds at low or high pHs involves a nucleophilic attack from a water molecule or from a hydroxide ion (as above explained), respectively, to the carbonyl carbon atom of the amide bond. This attack is boosted by the higher amount of electron density that the carbon substituents are able to withdraw (which makes the atom more electrophilic) and by the lower size of this groups which makes it easier for the nucleophilic to attack [214]. Since in both membranes, the carbonyl carbon atoms have the same double bond to an oxygen and single bonds to a phenolic group and to a nitrogen atom, the hydrolysis rate is likely to be similar for both membranes under the same conditions (discrepancies would come from the different groups at which the nitrogen atoms are bonded). Therefore, the faster worsening of NF270 membrane performance may be due to its lower active layer thickness ( $21 \pm 5$  nm) with respect to the NF90 one ( $218 \pm 40$  nm) which makes the cross-linking degree reduction more critic for the first membrane [36].

Changes in the absorbance of the amide I band found in this work were not reported by Simon et al. [37]. Nonetheless, in their study, NF270 membrane was subjected to NaOH solution at pH 11.5 for only 18 h, which may explain the lack of changes at that early stage.

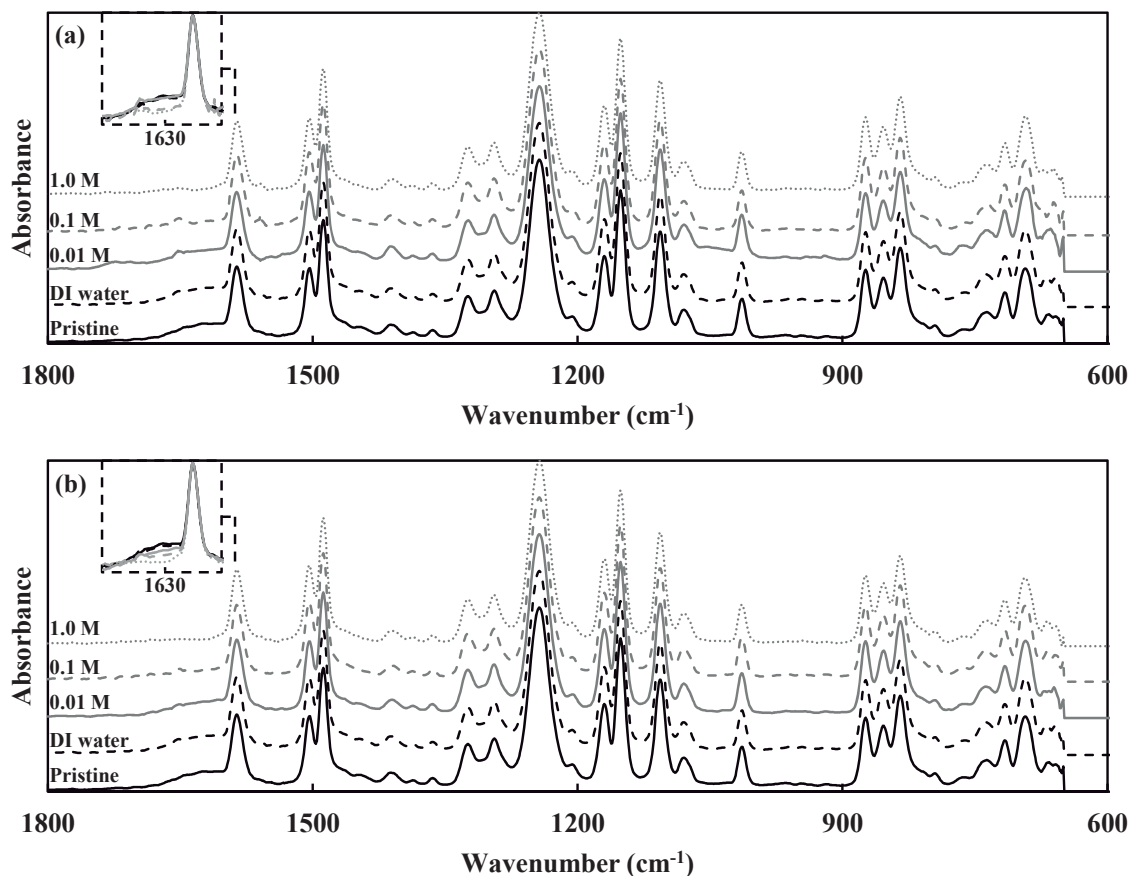


**Fig. 5.25.** ATR-FTIR spectra of the active layer of the NF270 membrane in its pristine state, soaked in DI water and aged in HNO<sub>3</sub> (a) and NaOH (b) ageing solutions at different concentrations.

SEM micrographs of the back side and cross-section of the NF270 membrane are shown in **Fig. 5.26**. It can be observed that the soaking in DI water, as expected, does not have any effect on the membranes. In the same way, the acidic ageing does not affect the membrane structure at any concentration. However at the end of the alkaline ageing at 1.0 M concentration, it is clear that the glue was removed and only the non-woven support remains, making the membrane weaker. At 0.01 and 0.1 M NaOH concentrations, no changes in the membrane structure are found.

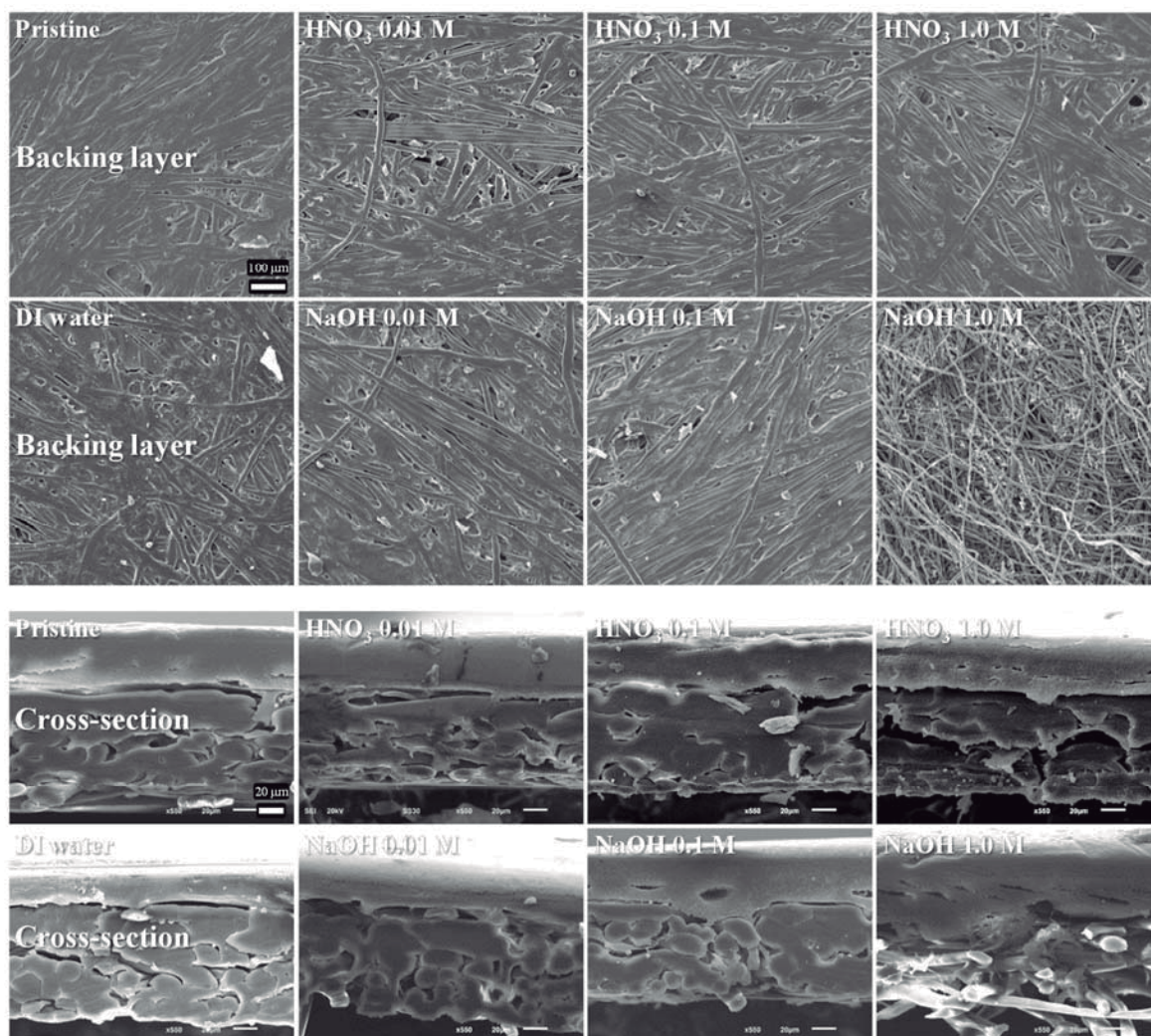


**Fig. 5.26.** SEM micrographs of the backing layer and the cross-section of the NF270 membrane in its pristine state, soaked in DI water and aged in  $\text{HNO}_3$  and  $\text{NaOH}$  ageing solutions at different concentrations.

#### 5.2.4. Ageing of the NF270 membrane in cross-flow mode

The NF270 membrane was also aged in a cross-flow system, simulating real cleaning conditions using the 0.1 M  $\text{NaOH}$  solution at  $50^\circ\text{C}$ . The ageing was conducted in two different configurations: one with the permeate valve open and another with it closed. Changes in permeability (**Fig. 5.27**) are shown as permeate flux changes, since filtration conditions were established in order to have the same initial permeate flux as in the dead-end filtration.

Regardless of the ageing mode, there is a jump up in permeability after the first exposure to the alkaline solution and it is more pronounced when the ageing is conducted with the small coupons (soaking mode). After this initial jump the permeability keeps increasing gradually. In

cross-flow mode (open or closed permeate valve), after the first permeability jump, it remains constant for almost 20 h and then, increases, first gradually, but later exponentially. This exponential growth is not reached for the soaking mode, but one could say the last point would indicate such trend. Again, this behavior is in agreement with the experiments carried out by Mänttari *et al.* [38] showing the increase of permeate flux at high pH and also the decrease in rejection, not so sharp as in the soaking mode.

In terms of separation performance, the ageing of the NF270 membrane in the soaking mode follows the same trend as the permeability, showing a continuous decrease in the  $\text{Na}_2\text{SO}_4$  rejection. However, in cross-flow mode there is an initial decrease in the salt rejection from 99 to 97 % and then, the NF270 membrane behavior is very stable until the 20 h. Beyond this time, membrane rejection drops sharply, being more significant for the configuration with the permeate valve open.

The differences between the membrane performance over the ageing in soaking and cross-flow modes are likely due to the fact that in soaking mode, the membranes are subjected to the whole NaOH solution from the active layer and backside, whereas in cross-flow mode, the membrane is only in direct contact with the ageing solution through the active layer. This is better seen when the permeate valve is closed, which minimizes the passage of ageing solution through the membrane.

Although the ageing mode affects the ageing itself in terms of membrane performance, the tests in soaking mode can be still useful to predict membrane behavior during the ageing in the worst scenario. Thus, the extrapolations from dead-end to cross-flow modes, which are closer to the actual conditions in industry, will lead to conservative predictions of membrane lifetime.

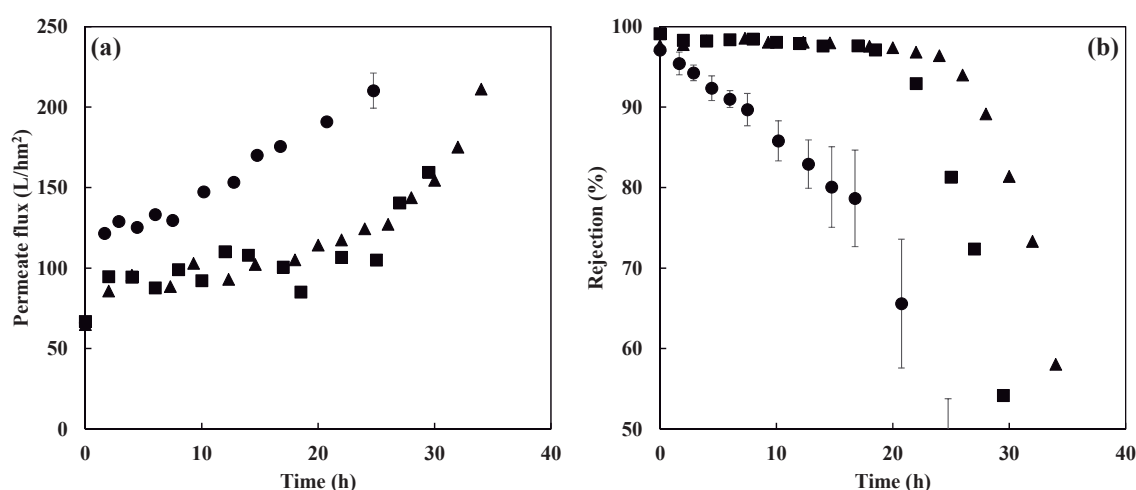


**Fig. 5.27.** Permeate flux (a) and  $\text{Na}_2\text{SO}_4$  rejection (b) of the NF270 membrane throughout the ageing in 0.1 M NaOH at 50°C in soaking mode (●) and in cross-flow mode with the permeate valve open (■) and close (▲).



### **5.3. Fitting approach to characterize UF membranes through LLDP**

---

This chapter is devoted to the development of a new fitting approach to characterize UF membranes through LLDP. This technique is based on the Young-Laplace equation which relates the surface tension of a fluid in a capillary with the radius of such capillary.

In order to conduct the analysis, a displacing liquid is forced to enter inside the sample pores which were previously filled with an immiscible liquid (wetting liquid). The needed pressure to empty a pore depends on its radius. Therefore, as the applied pressure increases, new smaller pores are opened (the wetting liquid inside them is dragged) and higher flows are obtained. LLDP measures the pressure needed to achieve given flows, leading to pairs of data (pressure *vs.* flow) which are the raw data for the calculations.

Traditional methods, such as the employed Grabar-Nikitine one, are able to obtain the pore number distribution through complex calculations in which the contribution of each pore size to the total flow at a given pressure is determined for each pair of data. These methods require a differentiation of the fundamental equations which makes them very sensitive to the experimental values.

The approach presented in this work is to create a theoretical model membrane (defined by a log-normal pore number distribution and a total pore number density) whose performance resembles the actual membrane during the LLDP analysis. For this purpose, three parameters must to be fitted: the geometric mean radius, the geometric standard deviation and the total pore number density.

Validation of the model has been conducted using typical LLDP parameters such as pore number and permeance distributions, asymptotic permeance, mean radius (based on both distributions) and MWCO estimations by comparing the model results to the traditional methods. In addition, the feasibility of the model to obtain reliable results using a less number of raw data has been tested.

The results of this work are presented by means of the accepted publication whose reference and status are shown below.

- **Reference:** E. Antón, J.I. Ignacio, J.R. Álvarez, A. Hernández, S. Luque, Fitting approach to liquid-liquid displacement porosimetry based on the log-normal pore size distribution, *J. Membr. Sci.* Accepted (2014).
- **Status:** Accepted.



**FITTING APPROACH TO LIQUID-LIQUID DISPLACEMENT  
POROSIMETRY BASED ON THE LOG-NORMAL  
PORE SIZE DISTRIBUTION**

*Enrique Antón<sup>a,b</sup>, José Ignacio Calvo<sup>b,†</sup>, José R. Álvarez<sup>a</sup>, Antonio Hernández<sup>b</sup> and  
Susana Luque<sup>a</sup>*

<sup>a</sup> Department of Chemical and Environmental Engineering, University of Oviedo,  
33071 Oviedo, Spain.

<sup>b</sup> Surfaces and Porous Materials Group (SMAP), UA-UVA-CSIC, University of  
Valladolid, 47071 Valladolid, Spain.

<sup>†</sup>Corresponding author: Telephone: +34 979 10 83 73. Fax: +34 979 10 81 01.

E-mail: jicalvo@termo.uva.es



**Keywords**

Membrane characterization

Ultrafiltration (UF) membranes

Liquid-liquid displacement porosimetry (LLDP)

Log-normal pore size distribution

Permeance distribution

**Abstract**

Liquid-liquid displacement porosimetry (LLDP) has been used to characterize several UF membranes in a wide range of molecular weight cut-offs (MWCO). A new method to convert porosimetric data into pore size distributions and related information has been developed based on assuming log-normal pore size distributions. The results of this are in good agreement with those from the customary data conversion algorithm (as derived by Grabar and Nikitine). The proposed method can also be used when a reduced number of experimental data points is available, leading to a significant reduction of data acquisition time needed to complete a reliable analysis.

## 1. Introduction

For most of the membrane separations, especially those based on the application of a pressure gradient across the membrane (namely microfiltration (MF), ultrafiltration (UF) and nanofiltration (NF)) sieving is the main separation mechanism and therefore, the relative size of the membrane pores/interstices and the molecules to be retained, is the key factor to control separation.

A proper knowledge of the porous structure of a membrane (usually consisting of a section which controls separation or active layer, supported on a more open porous substructure or support) is very important to assess its separation capabilities.

This kind of knowledge is the target of multiple characterization methods that can be grouped under the term porosimetries. These methods are based on very different physical principles but all of them try to obtain information about the pore size distribution (PSD), from which important separation parameters such as mean, maximum and minimum pore sizes, porosity or pore density can be calculated. Methods based on the bubble point test have been gaining recognition due to their unique capabilities. For example, these methods test the membrane in wet state, very close to the real operation conditions. In addition, the information given refers only to active layer pores (even when the support is not detached from the whole membrane).

There are two methods based on the bubble point: the gas-liquid displacement porosimetry (GLDP) and the liquid-liquid displacement porosimetry (LLDP), whose main difference relies on the state of the fluids used for displacing the inner liquid. Both techniques have been indistinctly named as capillary flow porometry, [1], liquid extrusion porometry, [2], or even combined bubble pressure and solvent permeance method, [3, 4], but all of them refer to the same principle, [5].

Both LLDP and GLDP are well-known and very similar in concept and even in operation mode. Nevertheless GLDP has gained general recognition while LLDP is still scarcely used, because it is more difficult to operate and less reproducible. Some of the authors have been working over in the last years to improve LLDP in an effort to show the potential of the method, especially for tight UF and NF membranes where other methods have strong difficulties to get reliable results. One of the features of the LLDP that makes it less attractive than GLDP is the shape of the distributions it provides. Certainly the nice aspect of the GLDP results is a consequence of a continuous measurement procedure. Commercial GLDP apparatuses usually divide the experimental range in 256 data points and determine corresponding data pairs (flux, pressure), resulting in a very smooth Gaussian distribution. The same procedure is not accomplished in LLDP because liquid-liquid equilibrium usually takes longer time (the whole experiment should take some hours) and there is no guarantee of obtaining superior results to GLDP.

Different algorithms are used to process data from GLDP and LLDP experiments. Gas-liquid experiments need to account for different gas flow regimes, namely Knudsen molecular flow along with Hagen-Poiseuille convective transport [6]. Moreover, the dependence of the gas permeance with applied pressure requires a different experimental procedure (wet run followed by dry ones) and different algorithms to convert experimental results into pore size information. The algorithms which could be used for processing data from LLDP experiments have been reviewed by Morison [7], who found that all of them are very sensitive to experimental errors requiring some smoothing to get reasonable distributions. Some authors have performed spline smoothing to get better results from LLDP, [8, 9], based on a polynomial fitting that somehow loses the physical meaning.

The approach in this work is to begin assuming a log-normal PSD and then fit the experimental results to such model function. A similar approach was used by Aimar *et al.* [10] to fit log-normal distributions from retention data, sometimes combined with moment theory to get more insight into theoretical distributions [11, 12]. Most of the membranes found in the market are well described by a log-normal distribution of pore sizes, [13], with a continuous range from many very small pores to few much bigger ones. This should lead to a right skewed distribution which is better described by a log-normal function.

## **2. LLDP theory**

### **2.1. Traditional methods to determine pore number distribution**

The final aim of LLDP characterizations is to determine the PSD of a porous sample, in this case a membrane. This technique is based on the Young-Laplace equation which relates the surface tension of a fluid inside a capillary with the radius of such capillary. The experimental procedure consists in forcing a liquid to enter the pores of a membrane previously filled with another immiscible liquid (wetting liquid).

If a perfect wetting of the membrane by the wetting fluid is assumed, the needed pressure to empty a given cylindrical pore is related to the radius of such pore through the so called Cantor equation (Eq. (1)) [14].

$$\Delta P = \frac{2\gamma}{r} \tag{1}$$

where  $\Delta P$  is the applied pressure and  $\gamma$  the interfacial tension (N/m) between both liquids and  $r$  the equivalent pore radius.

This technique accounts for the narrowest section of the pores, because these pore-throats effectively govern the fluid transport and the retention capabilities of the membrane, no matter how complicated the membrane structure is.

The increase in the applied pressure is linked to an increase in the flow due to the opening of new smaller pores. Therefore, by measuring the equilibrium pressure drop corresponding to each increment of flux, the basic experimental information from LLDP is obtained.

A transport model inside the pores is then required to get the PSD. The Hagen-Poiseuille equation through capillary cylindrical pores is regularly used for convective transport of liquids inside pores. This geometry assumption is not as restrictive as it may look; since many membrane geometries can be simplified to a group of more or less straight cylindrical pores having a radius equal to the narrowest section of the actual pores found in the membrane structure. Therefore, the flux  $J_i$  ( $\text{m}^3/\text{m}^2\text{s}$ ) associated to the pores of radius  $r_i$  (m) of the membrane, when a transmembrane pressure  $\Delta P$  (Pa) is applied, is given by the Hagen-Poiseuille equation (Eq. (2)).

$$J_i = \frac{N_i \pi r_i^4}{8 \eta l} \Delta P \quad (2)$$

where  $N_i$  (pore/ $\text{m}^2$ ) is the pore number density of pores having a radius  $r_i$ ,  $\eta$  (Pa·s) is the viscosity of the displacing liquid and  $l$  (m) is the length of the pores (usually the active layer thickness). This term should include a tortuosity factor for not so regular geometries

However, the experimental flow values obtained are not associated to a single pore size, but to those pores with radii higher or equal to the radius obtained through the Cantor equation (Eq. (1)) for the given applied pressure. Thus, Eq. (2) cannot be directly applied to obtain the number of pores of a given pore size and then, more complex mathematical procedures have to be carried out in order to discriminate the contribution of each pore size to the global flux. Different methods have been developed for that purpose, such as the original method of Erbe [15], based on a graphical evaluation, and the method of Grabar and Nikitine [14], which has been selected for this work, and it will be briefly explained below

The volumetric flux for a given  $\Delta P$  ( $J(\Delta P)$ ) is defined in terms of the number of pores per unit area through Eq. (3).

$$J(\Delta P) = N \int_r^{r_{\max}} F_v(r, \Delta P) f_n(r) dr \quad (3)$$

where  $N$  is the total number of pores per unit area (pore/ $\text{m}^2$ ),  $F_v(r, \Delta P)$  is the volumetric flow ( $\text{m}^3/\text{s}$ ) through a single pore of radius  $r$  at  $\Delta P$  and  $f_n(r)$  is the probability distribution function value for a pore of radius  $r$ .

The pore number distribution ( $n(r)$ ) is defined as the number of pores per unit area and per unit radius, and can be calculated using Eq. (4) which is based on the distribution function  $f_n(r)$ .

$$n(r) = N f_n(r) \quad (4)$$

Therefore, the number of pores per unit area with radii between  $r_A$  and  $r_B$  ( $N_{AB}$ ) is given by Eq. (5). Note that if the limits of integration are 0 and  $\infty$  the result of the integral is the total pore population,  $N$ .

$$N_{AB} = \int_{r_A}^{r_B} n(r) dr = \int_{r_A}^{r_B} N f_n(r) dr \quad (5)$$

Taking into account the Hagen-Poiseuille equation and Eq. (4), it is possible to rewrite Eq. (3) to obtain the volumetric flux, as long as the variables are assumed to be independent of pressure.

$$J(\Delta P) = \frac{\pi \Delta P}{8 \eta l} \int_r^{\infty} r^4 n(r) dr \quad (6)$$

where the limits of integration are the lowest radius which is opened at the applied transmembrane pressure  $\Delta P$  (given by Cantor equation) and the highest radius of the membrane which is denoted as  $\infty$ , because the probability distribution is 0 for  $r > r_{max}$ .

According to Grabar and Nikitine method [14], Eq. (6) has to be differentiated, substitute radius by pressure using the Cantor equation, and then, calculate the number of pores per unit area and per unit radius for a given differential of pressure through Eq. (7).

$$n(r) = \frac{8 \eta l \Delta P^5}{\pi (2 \gamma)^5} \left[ \frac{dJ}{d(\Delta P)} - \frac{J}{\Delta P} \right] \quad (7)$$

The algorithm derived by Grabar and Nikitine is, essentially, a differential algorithm which requires the continuous curve of permeance variation for its derivation. However, experimental procedures only give discrete values of flow and pressure, so Eq. (7) has to be converted in an incremental equation as follows.

$$n(r_{av}) = \frac{8 \eta l \Delta P_{av}^5}{\pi (2 \gamma)^5} \left[ \frac{\Delta J}{\Delta(\Delta P)} - \frac{J_{av}}{\Delta P_{av}} \right] \quad (8)$$

where the subscript "av" indicates the average value of the variables in the given increment and  $\Delta J$  and  $\Delta(\Delta P)$  are the increments between two experimental consecutive data pairs,  $\Delta J = J_i - J_{i-1}$  and  $\Delta(\Delta P) = \Delta P_i - \Delta P_{i-1}$ , where the subscript  $i$  is the  $i$ -th experimental point. The ratio  $\Delta J / \Delta(\Delta P)$  is the permeance increment ( $\Delta L$ ) while the ratio  $J_{av} / \Delta P_{av}$  is the mean permeance ( $L_{av}$ ) in that increment. These ratios represent the slope of the porosimetric curve in the considered point and the slope of the straight line passing from that point and the origin, respectively.

In conclusion, from the experimental flow values as a function of pressure and knowing the membrane area and thickness, Eq. (8) can be used to get the number of pores per unit area and unit

radius ( $n(r)$ ). From this pore number distribution, it is possible to determine several membrane parameters as explained in section 2.3.

## 2.2. New approach to analyze LLDP results

In our approach, the idea is to create a model membrane which produces the actual membrane flux as function of pressure during LLDP analysis by means of the well-known log-normal pore number distribution which will be used together with the total pore number density.

The first step is to define a suitable distribution function ( $f_n(r)$ ) for the model membrane. As mentioned above, among the several probability density functions, it has been reported that log-normal distribution is suitable for the pore number distribution of many membranes [7, 16]. The log-normal distribution is given by Eq. (9).

$$f_n(r) = \frac{1}{\ln(S)r\sqrt{2\pi}} \exp\left[-\frac{1}{2}\left(\frac{\ln(r/R)}{\ln(S)}\right)^2\right] \quad (9)$$

where the parameters  $R$  (m) and  $S$  (dimensionless) are the geometric mean radius or location parameter and the geometric standard deviation or scale parameter, respectively.

Therefore, the pore number distribution of the membrane can be obtained by combining Eqs. (4) and (9).

$$n(r) = \frac{N}{\ln(S)r\sqrt{2\pi}} \exp\left[-\frac{1}{2}\left(\frac{\ln(r/R)}{\ln(S)}\right)^2\right] \quad (10)$$

where  $N$  is the total pore number density (pore/m<sup>2</sup>) which is the third and last parameter of this model.

Using Eq. (6), which gives the flux for a given transmembrane pressure  $\Delta P$ , the membrane surface area ( $A$ ) and the pore number distribution given by Eq. (10), the flow at a given pressure is obtained as follows.

$$J(\Delta P) = \frac{N A \pi \Delta P}{8\sqrt{2\pi} \ln(S) \eta l} \int_r^\infty r^3 \exp\left[-\frac{1}{2}\left(\frac{\ln(r/R)}{\ln(S)}\right)^2\right] dr \quad (11)$$

The limits of integration are again the radius of the smallest pore which is opened at the applied transmembrane pressure  $\Delta P$  and the radius of the biggest one.

The next task is to fit  $N$ ,  $R$  and  $S$  to the LLDP characterization values in order to make this model membrane behaves as closely as possible to the real one.

For that purpose initial values are given to the R, S and N parameters. This step is of great importance in real applications (such as in quality control processes), since the required time for the fitting procedure strongly depends on how close are these values to the final ones. Nevertheless, as the goal of this work is to evaluate the feasibility of the proposed approach, the initial values of R, S and N were  $1.5 \cdot 10^{-9}$  m, 1.5 and  $5 \cdot 10^{15}$  pore/m<sup>2</sup>, respectively, for all the membranes and procedures (estimations based on previous knowledge about such values for typical membranes).

LLDP characterizations give discrete pairs of flow and pressure values. Given the initial values of R, S and N and using the experimental pressure values, in Eq. (11), a first estimate of the flow can be obtained. Usually, calculated flow values are far from the experimental ones and new R, S and N values have to be found. For this, an objective function, Eq. (12), was created using the sum of the squared residuals of the k-th flow data ( $e_k$ ), defined as the square of the difference between the experimental flow ( $J_{k, \text{experimental}}$ ) and the flow provided by the model ( $J_{k, \text{modelled}}$ ).

$$\text{Objective} = \sum_k e_k^2 = \sum_k (J_{k, \text{experimental}} - J_{k, \text{modelled}})^2 \quad (12)$$

The objective function is minimized by the least squares method (using the GRG2 algorithm as implemented in Microsoft Solver). In this way, the fitted parameters R, S and N correspond to a model membrane whose behavior resembles that of the actual membrane.

The goodness of the fitting was evaluated by a pseudo coefficient of determination ( $R^2$ ) based on the flux predictions of the model for the given pressure values. This coefficient is obtained through Eq. (13), where RSS is the residual sum of squares, given by Eq. (12), while TSS is the total sum of squares being  $\langle J \rangle$  the average of the experimental fluxes. Despite this definition coming from linear fittings, it was used here as an estimation of the fit goodness.

$$R^2 = 1 - \frac{\text{RSS}}{\text{TSS}} = 1 - \frac{\sum_k (J_{k, \text{experimental}} - J_{k, \text{modelled}})^2}{\sum_k (J_{k, \text{experimental}} - \langle J \rangle)^2} \quad (13)$$

One of the advantages of this model is that no differentiation of Eq. (3) is needed and thus, errors are minimized. In addition, the discrete experimental information is transformed into a continuous function, allowing more comprehensive analysis of the resulting distributions, which can be compared from the parameters of the resulting log-normal PSD's.

### 2.3. Membrane properties from LLDP analysis

The LLDP results give a pore number distribution as a function of the radius ( $n(r)$ ), from where, it is possible to determine several parameters:

- 1) The own differential pore number distribution given by  $n(r)$ .
- 2) In order to determine the permeance distribution of the membranes, the distribution function  $f_L(r)$  ( $m^{-1}$ ) has to be defined to calculate the permeance  $L_{AB}$  associated to the pores with radius between  $r_A$  and  $r_B$  with respect to the total permeance ( $L_{total}$ ).

$$\frac{L_{AB}}{L_{total}} = \int_{r_A}^{r_B} f_L(r) dr \quad (14)$$

Taking into account that  $L=J/\Delta P$ , Eq. (6) can be rewritten, so the integration from  $r_A$  to  $r_B$  and from 0 to  $\infty$  give  $L_{AB}$  and  $L_{total}$ , respectively. By combining all the equations, the differential distribution function for the permeance can be obtained as shown in Eq. (15).

$$\text{Differential permeance distribution} = f_L(r) = \frac{r^4 f_n(r)}{\int_0^{\infty} r^4 f_n(r) dr} \quad (15)$$

- 3) Finally dividing the integral of the differential distributions from 0 to  $r$  by the same integral from 0 to  $\infty$ , the cumulative distributions for the pore number and permeance are obtained as indicated by Eqs. (16) and (17), respectively.

$$\text{Cumulative pore number distribution} (r) = \frac{\int_0^r n(r) dr}{\int_0^{\infty} n(r) dr} = \frac{\int_0^r n(r) dr}{N} \quad (16)$$

$$\text{Cumulative permeance distribution} (r) = \frac{\int_0^r f_L(r) dr}{\int_0^{\infty} f_L(r) dr} = \int_0^r f_L(r) dr \quad (17)$$

- 4) The asymptotic permeance is the permeance once all the pores have been opened and it was already denoted as  $L_{total}$ .
- 5) The mean radius based on the pore number distribution ( $\langle r \rangle_{number}$ ) gives the mean pore radius of the membrane weighting the radius of each pore by the number of them (Eq. (18)).

$$\langle r \rangle_{number} = \frac{\int_0^{\infty} n(r) r dr}{\int_0^{\infty} n(r) dr} = \frac{\int_0^{\infty} n(r) r dr}{N} \quad (18)$$



- 6) The mean radius based on the permeance distribution ( $\langle r \rangle_{\text{perm}}$ ) gives the mean pore radius of the membrane weighting the radius of each pore class by the permeance related to them (Eq. (19)).

$$\langle r \rangle_{\text{perm}} = \frac{\int_0^{\infty} f_L(r) r \, dr}{\int_0^{\infty} f_L(r) \, dr} = \int_0^{\infty} f_L(r) r \, dr \quad (19)$$

- 7) Membrane molecular weight cut-offs (MWCO) can be successfully estimated by finding the highest radius of 90 % of the smallest pores (cumulative pore number distribution equal to 90 %) and then, matching this radius with that of a dextran molecule having the same effective diameter [17]. The procedure has been explained in detail elsewhere [17, 18].

### 3. Experimental

#### 3.1. Membranes and sample preparation

A variety of commercial flat-sheet membranes with MWCO ranging from 5 to 300 kDa were characterized by LLDP and the explained technique. The properties of these membranes, according to manufacturers, are gathered in Table 1.

In order to applied LLDP analysis, several membrane coupons were cut in flat disk pieces where the effective diameter for the analysis was 36 mm, as defined by the holder size. All the analyses were done to the pristine membranes which were conditioned by washing and soaking them in Milli-Q water for at least 48 h. Then, previously to the characterization, membranes were soaked in the wetting liquid for 12 h. Just before the analysis, the soaking was carried out under vacuum (created by a water jet pump) for 45 min to ensure the complete wetting of the sample.

**Table 1.** Membrane details according to manufacturers.

Membrane	Material	Manufacturer	MWCO (kDa)
HFK-328	Polyethersulfone	Koch	5
UP020	Polyethersulfone	Nadir	20
Minitan M030	Polysulfone	Millipore	30
Minitan M300	Polysulfone	Millipore	300

### 3.2. LLDP porosimeter and analysis procedure

The LLDP porosimeter was set up and tested at the University of Valladolid [19-21]. Both the equipment and the experimental procedure have been comprehensively described elsewhere [19]. Nevertheless, the main features are described below.

The displacing liquid is pumped by the use of a precise syringe pump ISCO-250D which allows a very accurate and stable flux without the need of any dampening system. The operation mode consists in fixing a determined flow and then, waiting for the pressure to stabilize. Increasing the flow stepwise, the experimental pairs of data of flow as function of pressure are obtained. As already explained at each equilibrium pressure the pores of a given size are opened.

Evidently the successive pressure increments (more precisely flow increments) should lead to higher permeance values until the asymptotic permeance ( $L_{total}$ ) is reached. This asymptotic permeance should correspond to that of the actual membrane for the displacing liquid once all the pores have been emptied from the wetting liquid. However, in practice, due to uncertainty of experimental data consecutive data points could lead to values of decreasing permeance. The reasons for such decreasing permeance in some consecutive points could be several, being membrane compaction one of them at moderately high pressures. This phenomenon cannot be avoided with a previous membrane conditioning as usually done in normal operation, since that conditioning could make wetting liquid to flow through the pores leading to biased results. In any case, these values of decreasing permeance would be interpreted as newly wetted pores which is impossible, thus, the data conversion algorithm eliminates these decreasing permeance points.

### 3.3. Wetting and displacing liquids and physical parameters

The employed wetting liquid was the alcoholic phase of a two phase mixture of Milli-Q water and isobutanol of reagent grade (1:1 w/w) while the displacing liquid corresponds to the aqueous phase. The mixture was prepared by mixing proper amounts of water and alcohol into a separator funnel, shaking it vigorously and settling it overnight. The separated alcohol-rich phase was drained off and used as the wetting liquid and the aqueous-rich phase was used as the displacing liquid. The resulting surface tension between both liquids is 1.7 mN/m in our working conditions at 20°C [22] and the viscosity of the displacing liquid is  $8.9 \cdot 10^{-4}$  Pa·s [22].

The last parameter, which is needed to convert flux distributions into absolute pore number distributions, is the pore length ( $l$ ) which is estimated as either the thickness of the active layer in asymmetric membranes or the membrane thickness for symmetric ones. As this value is unknown for the characterized membranes, a pore length of 5  $\mu\text{m}$  was assumed. This assumption only affects the value of  $N$ , but note that the effect of such assumption is the same for both the traditional method and the proposed approach since, in any case, both actually calculate the ratio  $N/l$ . Of course, either technique could be used to evaluate the porosity if the length is known and vice versa.

## **4. Results and discussion**

### **4.1. Physical meaning of the model parameters**

The proposed analyzing strategy for LLDP results consists in fitting the actual results to an ideal membrane which has a log-normal distribution of pores characterized by three parameters (N, R and S). The R and S parameters (from the log-normal distribution) define the position and shape of the pore number distribution. An increase in R leads to a shift to the right of the distribution (higher membrane pores) whereas an increase in S means a broadening of the curve which is more significant for the largest pore sizes. On the other hand, the N parameter (coming from the Hagen-Poiseuille equation), does not affect the shape and features of the pore number distribution, but it is related with the overall flow that passes through the membrane. In other words, the higher R and/or S are, the lower N is needed to achieve a certain permeate flux (flux is proportional to fourth power of radius according to Hagen-Poiseuille).

### **4.2. Fitting the model to the experimental results**

The fitting of R, S and N parameters was carried out for four different membranes with very different MWCOs ranging from 5 to 300 kDa (see Fig. 1). Despite the differences in flow and pressure among membranes, the model fits very well the obtained experimental results with pseudo coefficients of determination higher than 0.999 for all membranes. The obtained geometric standard deviations are very similar for most of the membranes (from 1.3 to 1.5).

The mean radius increases, as expected, as the MWCO of the membranes increases, following the order HFK-328 (1.3 nm - 5 kDa), UP020 (1.8 nm - 20 kDa), M030 (2.6 nm - 30 kDa) and M300 (10.0 nm - 300 kDa). The total pore number density fluctuates around  $5 \cdot 10^{16}$  pore/m<sup>2</sup> for the 5, 20 and 30 kDa membranes, but for M300 which has a high mean radius and thus, a lower total pore number density ( $1.6 \cdot 10^{15}$  pore/m<sup>2</sup>) is needed to achieve the given flows.

Therefore, a model membrane defined by the three N, R and S parameters can successfully fit the experimentally determined flow results of a LLDP analysis for very different membranes.

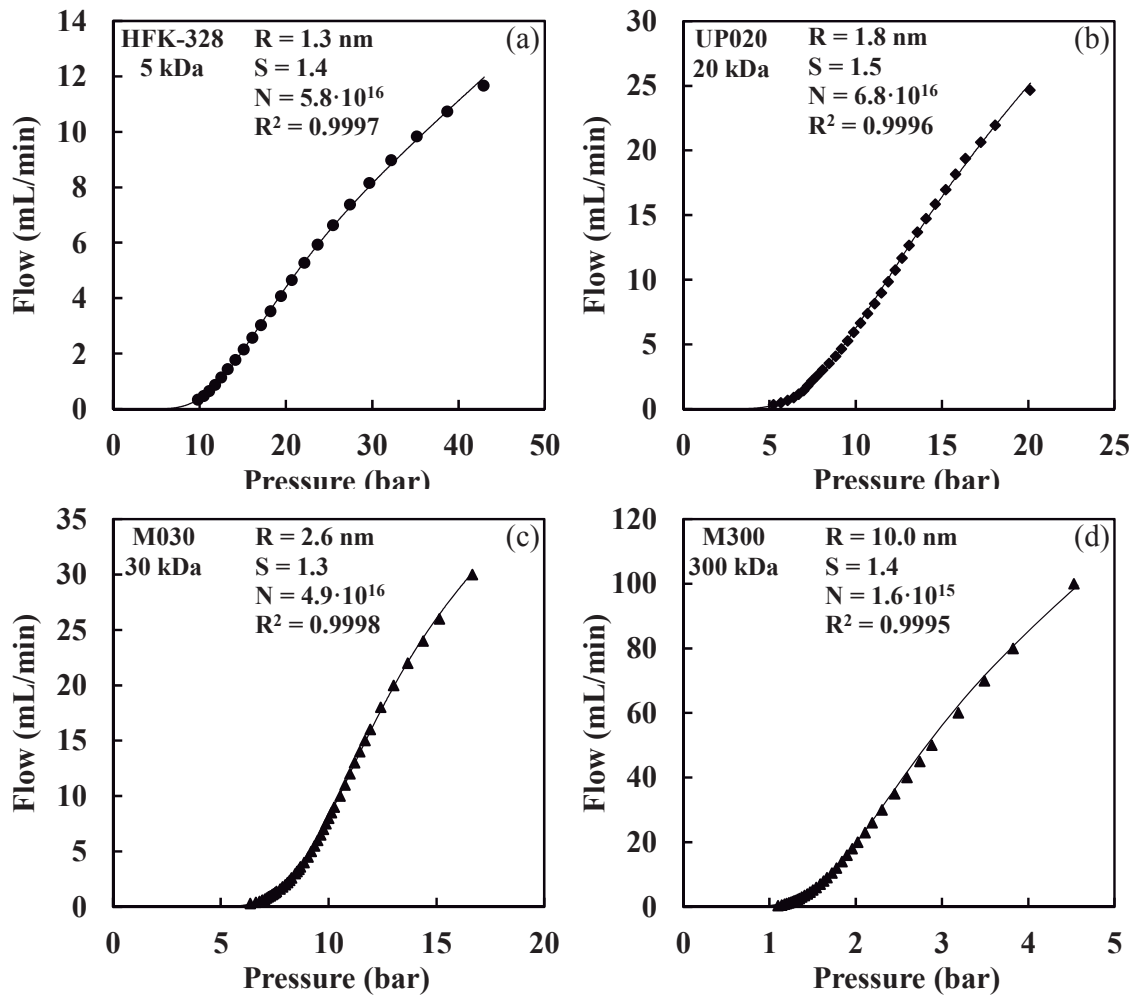


**Fig. 1.** Experimental results obtained through LLDP (symbols) and fitted model (solid line) for HFK-328 (a), UP020 (b), M030 (c) and M300 (d) membranes.

From the fittings shown in Fig. 1, it is possible to determine the permeance distribution. This distribution accounts for the contribution of each pore size class to the total permeance. Fig. 2 shows these distributions for the four studied membranes. In all cases, the agreement between permeance distributions coming from direct application of Grabar-Nikitine algorithm to experimental data (shown as bars) and the fitted ones (solid lines) is remarkable. The influence of model parameters in permeance distributions also appears in Fig. 2. The higher the S value is, the broader the distribution gets especially towards increasing radius values. In addition, the higher the N value is, the lower contribution of each pore to the global permeance is needed and thus, the shorter the distributions are (note that y-axis scale for M300 membrane is different).

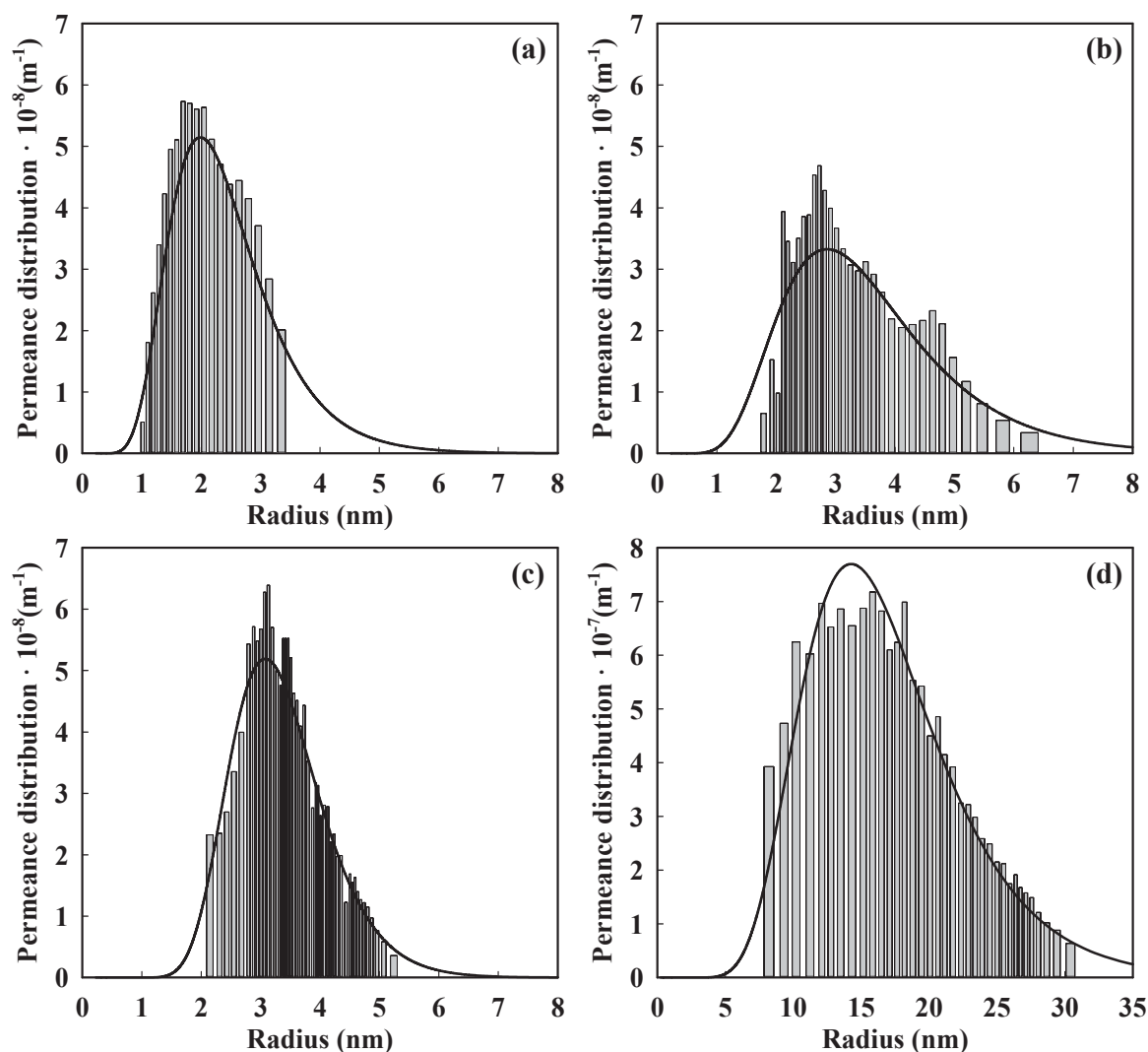


**Fig. 2.** Experimental (bars) and modelled (solid line) permeance distribution of HFK-328 (a), UP020 (b), M030 (c) and M300 (d) membranes.

### 4.3. Pore number distribution. Model validation

The pore number distribution as a function of the pore radius is represented for the experimental and the modeled membranes to compare membrane properties from both methods (Fig. 3).

Fig. 3 shows that the pore number distributions are shifted to the right and curve shapes widen as the R and S values increase, respectively. Since the area of pore number distribution curves gives the total pore number density (N), the maximum value of the distributions increases with N, but for the UP020 membrane which compensates a lower maximum with a higher dispersion (higher S value) giving the highest N value for the tested membranes (note y-axis scale for M300 membrane is different).

It can be observed that the pore distribution of the HFK-328 model membrane (Fig. 3a) fits very well to the Grabar-Nikitine treated data. For the rest of the membranes (Fig. 3), the pore size distribution fitting is not perfect, especially at low radius, but still satisfactory.

In any case, the agreement between traditionally treated and fitted points is not as good as that obtained for permeance distributions (Fig. 2). This was predictable since permeance distributions come directly from experimental data while pore number ones need a transport model inside the pores to be applied (Hagen-Poiseuille). This was one of the conclusions of the Charmme Network and is nowadays generally accepted [17].

The model distribution accurately matches in the area of higher radii whereas for the lower ones, there is a lack of experimental points. In any case, the agreement for the bigger pores would lead to good enough estimations of MWCO.

Finally a couple of physical limitations of the experimental apparatus should be pointed out because they would explain the lack of accurate experimental information for the smallest pores. It is important to consider that small pores are opened at high pressures, which sometimes cannot be reached either because of the physical limitations of the equipment (maximum pressure) or because the experimental run is automatically stopped when software detects non increasing permeance. This last procedure (based on a certain tolerance limit introduced by the operator) will prematurely stop the experiment, under certain circumstances, closing abruptly the distribution. Moreover, membranes having very high permeance (a usual target for membrane manufacturers) could lead to exhausting the pump reservoir (500 mL) before ending the analysis.

#### **4.4. Permeance and cumulative permeance distribution**

The experimental and modelled permeance cumulative distribution, as well as the actual permeance as a function of the pore radius, are depicted in Fig. 4.

The modelled cumulative permeance distributions (solid lines) fits quite well the discretized values (closed symbols) from Grabar-Nikitine method as it was shown for the differential permeance and pore number distributions (Figs. 2 and 3, respectively). Small discrepancies are found on the edges of the distributions, specifically on the areas in which there is a lack of information in the differential permeance distributions (Fig. 2). Besides, Fig. 4 shows that model distributions are smoother than experimental ones since they are based on continuous functions which can predict information in areas where traditional methods are not able to do so.

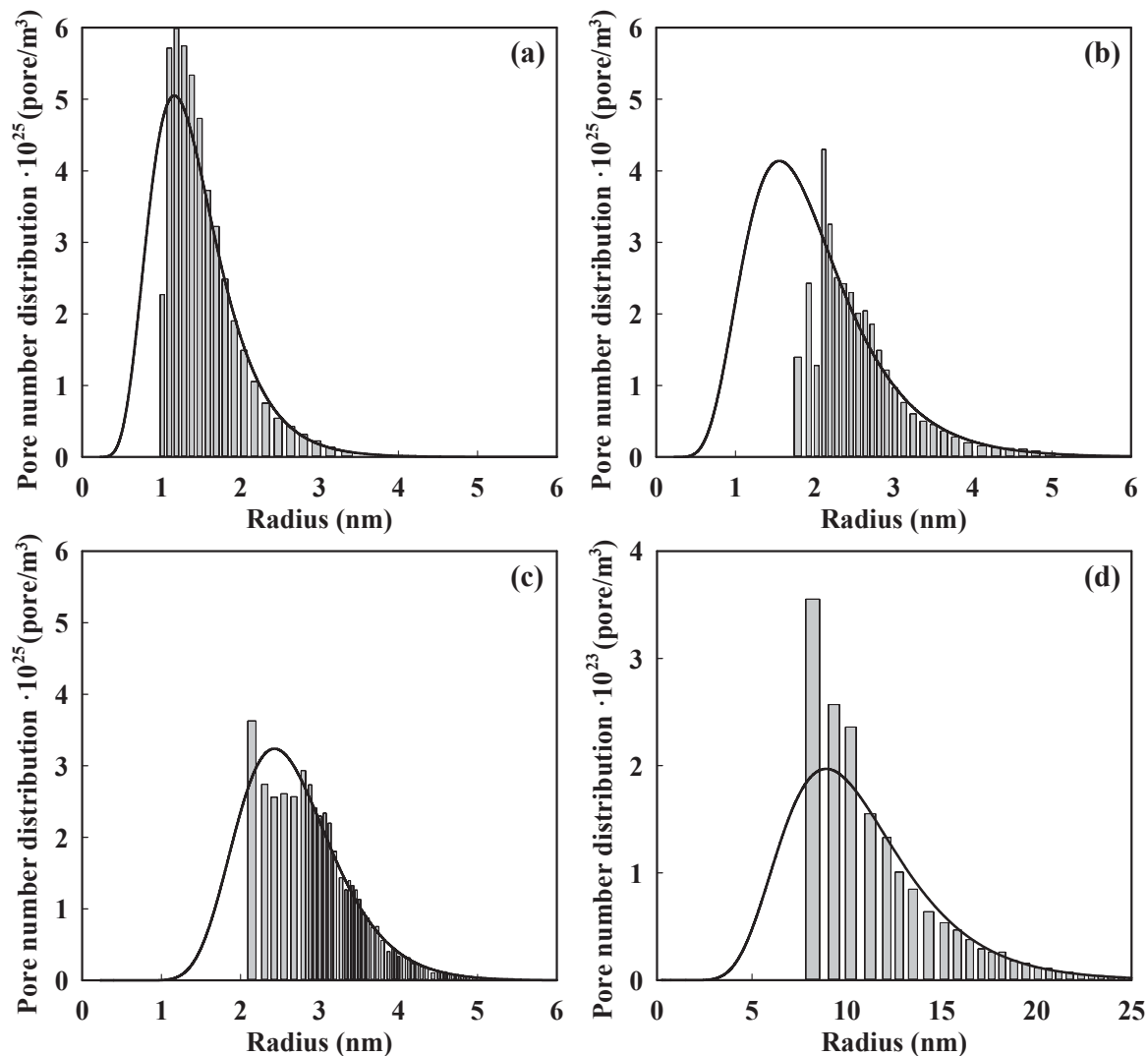


**Fig. 3.** Experimental (bars) and modelled (solid line) pore number distribution of HFK-328 (a), UP020 (b), M030 (c) and M300 (d) membranes.

Fig. 4 also shows the experimental (open symbols) and modelled (broken lines) actual membrane permeance as functions of the radius. Although experimental permeance values are obtained from high to low radii (increasing pressure), through the application of the Grabar-Nikitine method or the proposed model the cumulative contributions of each pore size to the permeance can be determined from low to high radii. Membrane behavior during LLDP analysis is well described by the model in terms of permeance as it happened with the flow (Fig. 1). In addition, Fig. 4 shows that the model predicts the asymptotic permeance more accurately than the Grabar-Nikitine method, since it can extrapolate the information that it is not obtained because of the above mentioned experimental limitations.

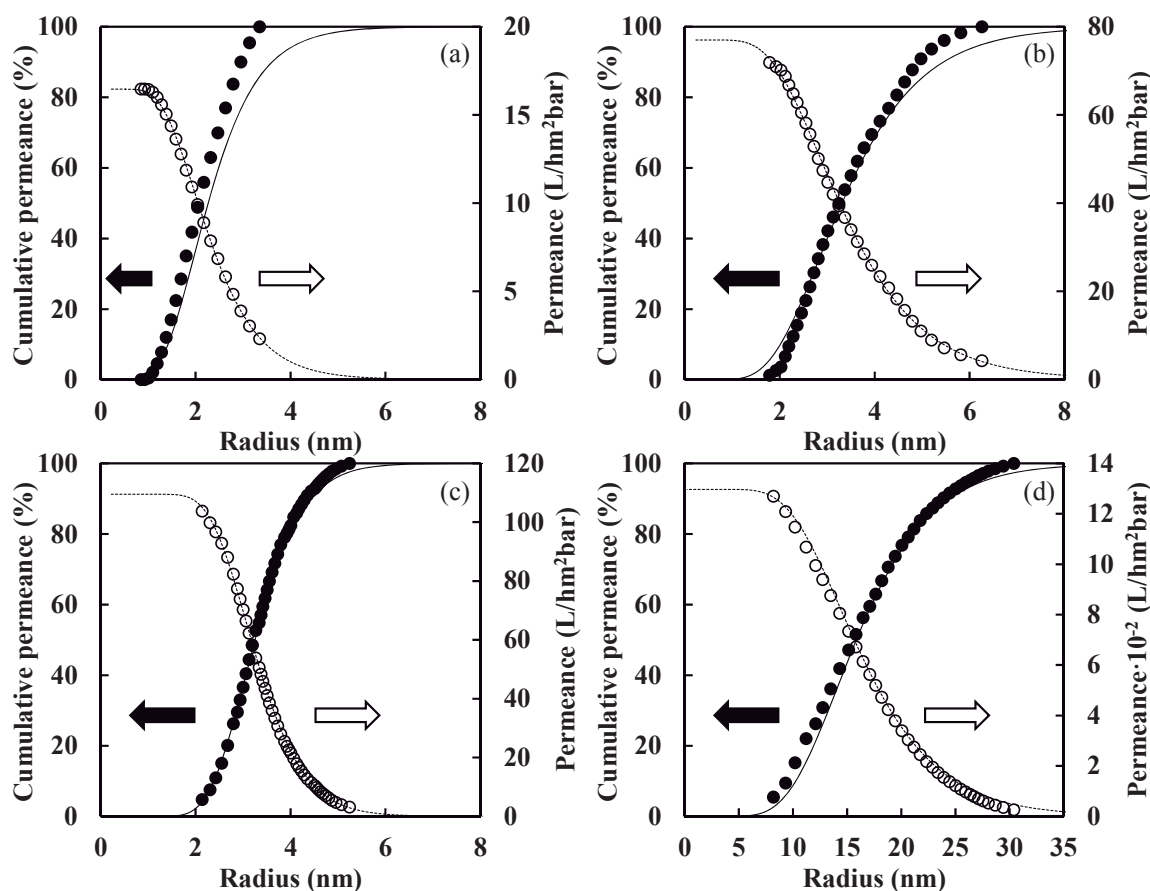


Fig. 4. Experimental (closed symbols) and modelled (solid line) cumulative permeance distribution as well as experimental (open symbols) and modelled (dotted line) permeance as function of pore size for the HFK-328 (a), UP020 (b), M030 (c) and M300 (d) membranes.

#### 4.5. Advantages of the model

Once the model was validated, it can be used to improve results in the characterization of any membrane. The most important feature of this model is that it can be applied with a small amount of experimental data, allowing the extrapolation of the membrane performance throughout the LLDP analysis. This is of great importance, especially in quality control areas where saving time and costs are linked and a comprehensive and deep characterization should have done previously. Moreover, this model can also be useful to characterize many membranes in a short period of time, easing the membrane screening for a given process.

There are several parameters, such as the asymptotic permeance, the mean radius (based on either the pore number or the permeance) and MWCO estimation, which are usually employed to characterize membranes by LLDP. These parameters together with the fitted  $R$ ,  $S$  and  $N$  are gathered in Table 2 for the four tested membranes using different number of experimental data. For each studied membrane, the first two rows compare the resulting LLDP parameters obtained



from direct application of Grabar-Nikitine algorithm with all the experimental data (row GN) with the same parameters obtained by applying the previously explained model/technique (row M). For the studied parameters (asymptotic permeance, mean pore radius based on pore number and on permeance and MWCO) modeled results are accompanied by an error estimation (\*) which considers values from the Grabar-Nikitine algorithm as the exact ones.

It is also interesting to test if the model still works well when only a small set of the experimental data is used in the fitting. In this sense, what has been done is to fit the developed model to a reduced number of data. In all cases it has been considered a minimum number of six experimental points (except for the last one, ItF, in which only three points were used), but the differences rely in which part of the experimental curve are those data pairs obtained from. Therefore, row In presents the results of the model applied using only the six pairs of flux, pressure data corresponding to the initial part of the experiment (corresponding to lower pressures). The next row (It) shows the fitting results using only six data pairs acquired at the intermediate section of the experiment. In the next row (IF), the model was applied using 3 data pairs from the initial part together with the last three pairs. Finally, the last procedure accounts for using one data pair at the beginning of the experiment, another one at intermediate pressure values and last one from the end of the experiment (row ItF).

Finally, for all these partial procedures (In, It, IF, ItF), two different error estimations are presented: the above mentioned (\*) and the (\*\*) error which has been calculated comparing the values of all the selected parameters with those values obtained from the model fitting using all data points (row M). Given the fact that the fitting improves as the number of data pairs increases, the best possible fitting using a part of the points would be that given by the row (M). Therefore, although both errors are included in Table 2, only the (\*\*) error estimation will be considered throughout the discussion.

The asymptotic permeance obtained by the model using all the experimental results (tag M) is similar to that experimentally determined for all the membranes, having relative errors lower than 6 %. Differences appear when the fittings are conducted using the results at low (tag In) and intermediate (tag It) pressures (flows), leading to differences lower than 10 %, except in the case of the M300 membrane, for which the fitting was not really possible in these conditions since errors are above 400 %. Nevertheless, when the fittings are conducted either with the data from the beginning (low pressure) and the end (high pressure) of the tests (tag IF) or with three distributed pairs of points (tag ItF) the modelled asymptotic permeance is again similar to the experimental one (tag GN) and to that modelled with all the experimental information (tag M). In fact, differences are lower than 4 % for all the membranes.

Larger differences are found when the mean pore radius based on the pore number and on the permeance are analyzed. As it was seen in Fig. 3, there is a lack of experimental data of the

pore distribution at low pore radius. Therefore, there are higher discrepancies than for the asymptotic permeance between the mean radii values (based on both the pore number and the permeance) from the Grabar-Nikitine algorithm (tag GN) and those from the proposed model (tag M), which range from 1 to 11 %. However, it is hard to establish which one of both is closer to the actual values for the membrane due to the lack of experimental information for low radii. In general, the mean pore radii (based on either the pore number or the permeance) obtained through the (In) and (It) procedures differ more from the values obtained using the all-data fitting (procedure M) than those using the (IF) and (ItF) procedures. Nonetheless, differences are small in general. The fitting procedures give very good results, especially for the M030 membrane. The ranges of the mean pore radius (based on the pore number) are relatively small for all the membranes: 1.4 - 1.6 nm, 1.7 - 2.3 nm, 2.4 - 2.7 nm and 9.8 - 10.6 nm for the HFK-328, UP020, M030 and M300 membranes, respectively. And a similar observation can be done for the mean pore radius based on permeance. Therefore, the possibility of using fewer experimental data to estimate the mean pore radius of the membranes using the proposed model is feasible.

The estimation of the MWCO gives similar results using the model (tag M) or the Grabar-Nikitine algorithm (tag GN) for all membranes. Concerning the fitting procedures using part of the data (tags In, It, IF and ItF), MWCO estimations show again a good agreement with those values obtained from the model (tag M) and the traditional method (tag GN). However, these MWCOs can only serve as estimation of nominal values (given in Table 1) due to the lack of information from the manufacturers about the conditions in which they were determined.

One of the shortcomings of applying this model to small amounts of experimental data is that the results could be incoherent. For instance, using the procedures (In) and (It) for very open UF membranes, such as the M300 membrane, the results are not successful because there is a lack of information in the high pressure area which is associated to the asymptotic permeance. Therefore, in these cases, a careful analysis of the results should be carried out, leading the LLDP experiment to include more high pressure points to avoid such errors.

In summary, it is possible to obtain reliable information about the membrane while shortening the LLDP characterization time by reducing the number of experimental points. In addition, it is shown that acquiring the data from the areas at the beginning, in the intermediate section (In and It labels, respectively) and especially combining data from the beginning and the end (IF label) or just the first point, one in the middle and one in the end (ItF label) gives accurate values of the asymptotic permeance, mean radius (based on pore number and permeance) and MWCO parameters.

**Table 2.** Main membrane parameters obtained through LLDP.

Membr.	Math. proced.	Asymptotic permeance (L/hm <sup>2</sup> bar)	Relative error (%) (* - **)	Mean radius - Pore number (nm)	Relative error (%) (* - **)	Mean radius - Permeance (nm)	Relative error (%) (* - **)	MWCO (kDa)	Relative error (%) (* - **)	R (mm)	S	N
HFK-328	GN	16.5	-	1.6	-	2.2	-	6.0	-	-	-	-
	M	16.5	1*	1.4	9*	2.4	11*	6.5	8*	1.3	1.44	5.8·10 <sup>16</sup>
	In	15.8	4-1	1.6	2-11	2.5	14-3	7.7	27-18	1.5	1.40	4.1·10 <sup>16</sup>
	It	16.5	1-1	1.4	10-2	2.4	10-1	6.3	5-3	1.3	1.44	6.1·10 <sup>16</sup>
	IF	16.6	1-1	1.5	6-3	2.4	11-1	6.8	13-5	1.4	1.43	5.4·10 <sup>16</sup>
UP020	ItF	16.1	3-2	1.4	8-1	2.4	12-1	6.7	10-2	1.3	1.44	5.4·10 <sup>16</sup>
	GN	72	-	2.6	-	3.5	-	17	-	-	-	-
	M	77	6*	2.0	24*	3.6	2*	13	23*	1.8	1.48	6.8·10 <sup>16</sup>
	In	76	5-2	1.7	34-13	3.5	1-3	10	39-21	1.5	1.53	1.0·10 <sup>17</sup>
	It	72	1-6	2.0	23-1	3.7	5-3	14	21-3	1.8	1.49	6.0·10 <sup>16</sup>
M030	IF	74	2-4	2.3	11-17	3.8	8-5	17	1-30	2.1	1.42	4.1·10 <sup>16</sup>
	ItF	76	6-1	1.9	26-3	3.6	3-1	13	26-4	1.8	1.49	7.1·10 <sup>16</sup>
	GN	106	-	2.8	-	3.3	-	19	-	-	-	-
	M	110	3*	2.7	6*	3.4	1*	19	3*	2.6	1.27	4.9·10 <sup>16</sup>
	In	112	6-2	2.4	16-11	3.2	4-4	16	18-16	2.3	1.32	7.3·10 <sup>16</sup>
M300	It	119	12-9	2.4	14-9	3.2	3-3	16	15-13	2.3	1.31	7.1·10 <sup>16</sup>
	IF	110	4-1	2.6	9-3	3.3	1-1	18	8-5	2.5	1.29	5.5·10 <sup>16</sup>
	ItF	112	5-2	2.5	12-6	3.3	1-2	17	11-9	2.4	1.30	6.1·10 <sup>16</sup>
	GN	1302	-	11.0	-	16.5	-	400	-	-	-	-
	M	1297	1*	10.6	4*	17.0	3*	408	2*	10.0	1.41	1.6·10 <sup>15</sup>
M300	In	10200	700-700	7.5	32-30	12.2	26-28	200	50-51	7.0	1.42	5.0·10 <sup>16</sup>
	It	5300	300-300	6.2	44-41	11.9	28-30	151	62-63	5.7	1.50	4.2·10 <sup>16</sup>
	IF	1334	2-3	9.8	11-7	15.9	3-6	356	11-13	9.3	1.42	2.2·10 <sup>15</sup>
	ItF	1326	2-2	10.1	8-4	17.1	4-1	389	3-5	9.5	1.44	1.8·10 <sup>15</sup>

The meaning of the abbreviations GN, M, In, It, IF, ItF, \* and \*\* is given in the text.

## **5. Conclusions**

In this work a new approach to fit results from LLDP analysis has been proposed. Instead of the usual polynomial fitting equations without physical meaning, a log-normal pore size distribution was assumed for the membrane, requiring only three fitting parameters. Comparing the expected behavior of the model with the actual results, the log-normally shaped distribution is a reasonable choice.

The accuracy of the fitting approach has been tested with several polymeric membranes having a large range of pores, according to the nominal MWCO values. Results of the fitting are reasonably good and in accordance with most of the parameters arising from traditional LLDP analysis.

One of the advantages of the model is that it can be applied using few experimental points which would reduce significantly LLDP procedure times. In addition, it has been shown that acquiring information especially at low and high pressures or just employing the first point, one in the middle and one in the end (indicated by the IF and ItF labels, respectively), the model leads to reliable membrane information.

It must not be forgotten that a good fitting is only possible if good data is collected. Whatever is the procedure for measuring or fitting data, LLDP experiments are not and they will never be so easy to perform as GLDP ones, where only 5 min are enough to get a good pore size distribution.

On the contrary LLDP experiments need longer time (never less than 1 h), so any approach aimed to reduce the number of experimental points, such as that considered in this work, requires a reliable data fitting for a possible extensive or commercial use of the technique.

## **Acknowledgements**

Authors gratefully acknowledge the financial support given by: Junta de Castilla y León (Project VA248U13), Spanish Ministry of Science and Innovation (projects MAT2011-25513 and CTQ2012-31076) and the Spanish Ministry of Education, Culture and Sports via a collaboration scholarship and a FPU grant (AP2010-3549).

## Nomenclature

### Symbols

A: Membrane surface area ( $\text{m}^2$ )

$e_k$ : Difference between the experimental and the modelled membrane flux ( $\text{m}^3/\text{m}^2\text{s}$ )

F: Membrane flow ( $\text{m}^3/\text{s}$ )

$f_l(r)$ : Probability distribution function for the permeance from pores of radius  $r$  ( $\text{m}^{-1}$ )

$f_n(r)$ : Probability distribution function for the number of pores of radius  $r$  ( $\text{m}^{-1}$ )

J: Membrane flux ( $\text{m}^3/\text{m}^2\text{s}$ )

l: Pore length

MWCO: Molecular weight cut-off (Da)

$n(r)$ : Pore number distribution (pore/ $\text{m}^3$ )

N: Total pore number density (pore/ $\text{m}^2$ )

$N_{AB}$ : Pore number density with radii between  $r_A$  and  $r_B$  (pore/ $\text{m}^2$ )

$\Delta P$ : Transmembrane pressure (Pa)

R: Geometric mean radius or location parameter (m)

r: Radius (m)

$R^2$ : Pseudo coefficient of determination

RSS: Residual sum of squares

TSS: Total sum of squares

$\langle r \rangle_{\text{number}}$ : Mean radius based on the pore number distribution (m)

$\langle r \rangle_{\text{perm}}$ : Mean radius based on the permeance distribution (m)

S: Geometric standard deviation or scale parameter (dimensionless)

### Greek symbols

$\eta$ : Viscosity (Pa·s)

$\gamma$ : Interfacial tension (N/m)

**References**

- [1] D. Li, M.W. Frey, Y.L. Joo, Characterization of nanofibrous membranes with capillary flow porometry, *J. Membr. Sci.* 286 (2006) 104-114.
- [2] S. S. Manickam, J.R. McCutcheon, Characterization of polymeric nonwovens using porosimetry, porometry and X-ray computed tomography, *J. Membr. Sci.* 407–408 (2012) 108-115.
- [3] S. Munari, A. Bottino, G.C. Roda, G. Capannelli, Preparation of ultrafiltration membranes. State of the art, *Desalination* 77 (1990) 85-100.
- [4] P. Abaticchio, A. Bottino, G.C. Roda, G. Capannelli, S. Munari, Characterization of ultrafiltration polymeric membranes, *Desalination* 78 (1990) 235-255.
- [5] J.I. Calvo, A. Bottino, P. Prádanos, L. Palacio, A. Hernández, Porosity, in: E.M.V. Hoek, V.V. Tarabara (Eds.), *Encyclopedia of Membrane Science and Technology*, John Wiley and Sons, Hoboken, NJ (USA), 2014.
- [6] A. Hernández, J.I. Calvo, P. Prádanos, F. Tejerina, Pore size distributions in microporous membranes. A critical analysis of the bubble point extended method, *J. Membr. Sci.* 112 (1996) 1-12.
- [7] K.R. Morison, A comparison of liquid–liquid porosimetry equations for evaluation of pore size distribution, *J. Membr. Sci.* 325 (2008) 301-310.
- [8] T.N. Shah, H.C. Foley, A.L. Zydney, Development and characterization of nanoporous carbon membranes for protein ultrafiltration, *J. Membr. Sci.* 295 (2007) 40-49.
- [9] S. Munari, A. Bottino, P. Moretti, G. Capannelli, I. Becchi, Permoporometric study on ultrafiltration membranes, *J. Membr. Sci.* 41 (1989) 69-86.
- [10] P. Aimar, M. Meireles, V. Sanchez, A contribution to the translation of retention curves into pore size distributions for sieving membranes, *J. Membr. Sci.* 54 (1990) 321-338.
- [11] K.D. Knierim, M. Waldman, E.A. Mason, Bounds on solute flux and pore-size distributions for non-sieving membranes, *J. Membr. Sci.* 17 (1984) 173-203.
- [12] K.D. Knierim, E.A. Mason, Heteroporous sieving membranes: Rigorous bounds on pore-size distributions and sieving curves, *J. Membr. Sci.* 42 (1989) 87-107.
- [13] A.L. Zydney, P. Aimar, M. Meireles, J.M. Pimbley, G. Belfort, Use of the log-normal probability density function to analyze membrane pore size distributions: functional forms and discrepancies, *J. Membr. Sci.* 91 (1994) 293-298.
- [14] P. Grabar, S. Nikitine, Sur le diamètre des pores des membranes en collodion utilisées en ultrafiltration, *J. Chem. Phys.* 33 (1936) 721-741.

- [15] F. Erbe, The determination of pore distributions according to sizes in filters and ultrafilters, *Kolloid-Z* 63 (1933) 277-285.
- [16] S. Derjani-Bayeh, V.G.J. Rodgers, Sieving variations due to the choice in pore size distribution model, *J. Membr. Sci.* 209 (2002) 1-17.
- [17] J.I. Calvo, R.I. Peinador, P. Prádanos, L. Palacio, A. Bottino, G. Capannelli, A. Hernández, Liquid–liquid displacement porosimetry to estimate the molecular weight cut-off of ultrafiltration membranes, *Desalination* 268 (2011) 174-181.
- [18] P. Carretero, S. Molina, A. Lozano, J. de Abajo, J.I. Calvo, P. Prádanos, L. Palacio, A. Hernández, Liquid–liquid displacement porosimetry applied to several MF and UF membranes, *Desalination* 327 (2013) 14-23.
- [19] J.M. Sanz, R. Peinador, J.I. Calvo, A. Hernández, A. Bottino, G. Capannelli, Characterization of UF membranes by liquid–liquid displacement porosimetry, *Desalination* 245 (2009) 546-553.
- [20] M.C. Almécija, J.E. Zapata, A. Martínez-Ferez, A. Guadix, A. Hernández, J.I. Calvo, E.M. Guadix, Analysis of cleaning protocols in ceramic membranes by liquid–liquid displacement porosimetry, *Desalination* 245 (2009) 541-545.
- [21] J.I. Calvo, A. Bottino, G. Capannelli, A. Hernández, Pore size distribution of ceramic UF membranes by liquid–liquid displacement porosimetry, *J. Membr. Sci.* 310 (2008) 531-538.
- [22] J.I. Calvo, A. Bottino, G. Capannelli, A. Hernández, Comparison of liquid–liquid displacement porosimetry and scanning electron microscopy image analysis to characterise ultrafiltration track-etched membranes, *J. Membr. Sci.* 239 (2004) 189-197.

#### **5.4. Functionalization of UF membranes with strong polyelectrolyte hydrogels for NF applications with a low fouling prone**

---

Up to now, many techniques have been investigated in order to modify membrane surface properties with the purpose of improving their performance. Some of them have been successfully applied such as the chemical oxidation, the chemical functionalization, the plasma treatment and the radiation-induced grafting. Regardless of the technique, membrane modification usually aims to increase the charge or the hydrophilicity of the membranes which improve the rejection capability and the permeability of the membrane, respectively. Besides, these modifications make membranes more fouling resistant due to the higher electrostatic repulsion and the lower foulant-membrane interaction.

In this section, the modification of a PES UF membrane through the radiation-induced grafting method is presented. The aim of this work was to develop a low fouling prone NF membrane characterized by a high charge density and a low roughness. With this purpose, the effects of different modification conditions on the properties of the polyelectrolyte hydrogel layer created by the copolymerization of the functional monomer VSA and the cross-linker MBAA were investigated.

The main parameters involved in the modification process are the VSA concentration, the MBAA ratio (relative to the functional monomer in mol. %), the irradiation intensity, the modification time and the MWCO of the PES membrane. The influence of these parameters on the performance and the physicochemical properties of the resulting thin-film composite membrane was investigated. Specifically, the surface properties are the degree of grafting (DG) based on both gravimetric and ATR-FTIR measurements, the ion exchange capacity (IEC), the elemental composition, the charge, the roughness and the structure of the polyelectrolyte hydrogel layer.

In addition to the physicochemical characterization, the performance of the modified membranes was also determined through permeability and rejection measurements of charged (single and mixed salt solutions) and uncharged solutes for the different modification conditions. The operational flexibility of the resulting NF membranes was also challenged under extreme pH values and at high salt concentrations. Finally, the modification process was tested at a higher size scale conducting the performance characterization in a cross-flow system.



The results of this work are presented by means of two accepted publications whose reference and status are shown below.

- **Reference:** R. Bernstein, E. Antón, M. Ulbricht, UV-photo graft functionalization of polyethersulfone membrane with strong polyelectrolyte hydrogel and its application for nanofiltration, *ACS Appl. Mater. Interfaces* 4 (2012) 3438-3446.
- **Status:** Published.
  
- **Reference:** R. Bernstein, E. Antón, M. Ulbricht, Tuning the nanofiltration performance of thin film strong polyelectrolyte hydrogel composite membranes by photo-grafting conditions, *J. Membr. Sci.* 427 (2013) 129-138.
- **Status:** Published.

# UV-Photo Graft Functionalization of Polyethersulfone Membrane with Strong Polyelectrolyte Hydrogel and Its Application for Nanofiltration

Roy Bernstein,<sup>†</sup> Enrique Antón,<sup>†,‡</sup> and Mathias Ulbricht<sup>\*,†</sup>

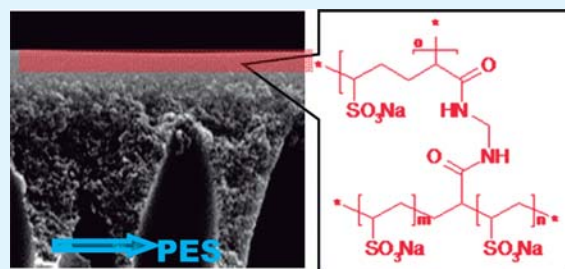
<sup>†</sup>Lehrstuhl für Technische Chemie II, Universität Duisburg-Essen, 45117 Essen, Germany

<sup>‡</sup>Department of Chemical and Environmental Engineering, University of Oviedo, 33006 Oviedo, Spain

**ABSTRACT:** A strong polyelectrolyte hydrogel was graft copolymerized on a polyethersulfone (PES) ultrafiltration (UF) membrane using vinyl sulfonic acid (VSA) as the functional monomer, and N,N'-methylenebisacrylamide (MBAA) as the cross-linker monomer. This was carried out in one simple step using the UV photoirradiation method. The effect of the polymerization conditions on the degree of grafting (DG) was investigated using the gravimetric method which measures the total hydrogel grafted on the membrane, and with ATR-FTIR spectroscopy which indicates the functional monomer fraction in the hydrogel layer.

The VSA could not graft polymerize without the cross-linker as comonomer. An increase in the cross-linker fraction from 0.25 to 2.5 mol % (relative to the functional monomer VSA) resulted in a higher DG. Although the surface morphology changed upon modification, the resulting surface roughness as measured by AFM was very low. From the monitoring of DG with UV time (4.5–30 min) at constant conditions, it was deduced that during the early stages of the polymerization mainly the cross-linker was grafted, thus inducing the graft copolymerization of the functional monomer. Polymerization using a higher monomer concentration (12.5–40% VSA) at constant monomer/cross-linker ratio resulted in a higher VSA fraction in the grafted hydrogel, although the gravimetric DG was similar. Ion exchange capacity and X-ray photoelectron spectroscopy measured after modification under the different conditions supported these findings. The new membranes were tested under nanofiltration (NF) conditions. A NF membrane could be obtained when the MBAA fraction was above 0.25%. The Na<sub>2</sub>SO<sub>4</sub> rejection was 90–99% and the permeability 10–1 L m<sup>-2</sup> h<sup>-1</sup> bar<sup>-1</sup> when the MBAA fraction increased from 0.75 to 2.5%. The order of rejection of single salts solution was Na<sub>2</sub>SO<sub>4</sub> > MgSO<sub>4</sub> ≈ NaCl > CaCl<sub>2</sub>, as expected on the basis of Donnan exclusion for negatively charged NF membranes. An increase in the salts rejection with increasing degree of cross-linking and VSA fraction was attributed to an increase in the membrane charge density and to steric exclusion that also resulted in an increase of rejection for uncharged solutes such as sucrose or glucose. The new membrane presented a high, essentially unchanged Na<sub>2</sub>SO<sub>4</sub> rejection (>97%) in the range of salt concentrations up to 4 g/L, and only slightly reduced rejection (>92%) at a concentration of 8 g/L; this can be related to its high barrier layer charge density measured by ion exchange capacity. In addition, because poly(vinyl sulfonic acid) (PVSA) is a strong polyelectrolyte the membrane separation performance was stable in the range of pH 1.5 to pH 10.

**KEYWORDS:** nanofiltration membrane, polyelectrolyte hydrogel, photografting, membrane modification, surface modification, vinyl sulfonic acid



## INTRODUCTION

The feasibility of charged nanofiltration (NF) membranes fabrication using polyelectrolytes as the active layer is being explored in the past few years.<sup>1</sup> This is primarily done through two methods. The first one is synthesis of a polyelectrolyte, either inside the pores of an ultrafiltration (UF) base membrane, thus obtaining a pore-filling composite membrane,<sup>2</sup> or on the outer surface of an UF membrane, resulting in a thin-film composite membrane.<sup>3–5</sup> The second method is through the deposition of polyelectrolyte, the “layer by layer” (LBL) technique, on or within a porous polymeric support,<sup>6,7</sup> or inorganic support.<sup>8</sup> Both techniques have already demonstrated that a NF membrane for ions separation as well as for other

applications including, for instance, forward osmosis,<sup>9–11</sup> can successfully be produced using various polyelectrolytes. Yet, these membranes still have some drawbacks compared with the commercially available NF membranes that withhold their further expansion.

One of the key factors in the evaluation of the performance in membrane technology is the trade-off between the membrane selectivity and permeability. For polyelectrolyte NF membranes, the rejection of charged solutes is governed

Received: March 9, 2012

Accepted: June 18, 2012

Published: June 18, 2012

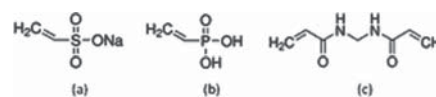
mainly by the Donnan exclusion,<sup>12</sup> which is a consequence of the fixed charge density of the membrane active layer. The steric exclusion, which is directly proportional to the ratio between the size of a solute and the membrane pore size<sup>13</sup> and to the ratio between the active layer thickness and porosity,<sup>14</sup> is responsible for the rejection of uncharged solutes and also contributes to the rejection of charged solutes.<sup>15</sup> To obtain a polyelectrolyte NF membrane with high separation ability, a dense and a “defect free” high charge density polyelectrolyte active layer must be obtained. Therefore, the number of the polyelectrolyte layers deposited on the porous membrane, or the degree of functionalization, should usually be high. However, since membrane permeability is controlled by the active layer pore size distribution, thickness and swelling,<sup>16,17</sup> the consequence is a membrane with reduced permeability. The trade-off between rejection and permeability of polyelectrolyte membranes can be optimized by changing the fabrication conditions and the active layer composition.<sup>2,8</sup> Nevertheless, the performance of the majority of the previously presented NF membranes fabricated by the polymerization method was not better than the commercial ones. On the other hand, the “LBL” method, which can produce a membrane having high performance, is time-consuming, requires several steps, and still presents a challenge to scale-up for commercial application.<sup>9,18</sup>

A different approach to the fabrication of charged NF membrane may be graft copolymerization of a polyelectrolyte hydrogel on a UF support.<sup>19</sup> A hydrogel is a cross-linked polymer network (via chemical or physical interaction), swollen with water, yet insoluble because of the high cross-linking degree. For in situ polymerized hydrogels, swelling, which influences membrane permeability, is mainly controlled by the ratio between the cross-linker monomer and the functional monomer.<sup>19</sup> Therefore, the reduced permeability following surface modification using hydrogel as the active layer might be adjusted. Hydrogels are also well recognized for their relatively small mesh size, which can assist in promoting the membrane selectivity by sieving.<sup>20</sup> In addition, using a charged monomer for the hydrogel synthesis, a highly charged active layer, and thus a high Donnan exclusion may be attained.<sup>21</sup>

The photoirradiation-induced radical graft copolymerization technique was recently successfully applied for surface modification of hydrogels on UF membranes.<sup>22,23</sup> This technique has several advantages: it generates a rapid reaction and is performed under mild conditions with various monomers using simple equipment at a relatively low cost. The polymerization using this technique is mostly surface specific—it is limited to a narrow region close to the outer membrane surface. This technique can also be implemented for commercial production.<sup>24</sup> Moreover, when the modification is performed using a UV-active UF membrane, i.e., the membrane polymer undergoes a homolytic chain cleavage resulting in free radicals on its surface (such as polyethersulfone, PES), the polymerization does not require photoinitiator agents.<sup>24</sup>

In this research, the possibility to graft polymerize a strong polyelectrolyte hydrogel on a commercial PES UF membrane through the photoinitiation technique was investigated. Two charged monomers, vinyl phosphonic acid and vinyl sulfonic acid, with *N,N'*-methylenebisacrylamide as a cross-linker monomer, were evaluated for the polymerization of the polyelectrolyte hydrogel (Scheme 1). These monomers were selected on the assumption that a swollen, high charge density polyelectrolyte hydrogel, which will also be ionizable

**Scheme 1. Chemical Structure of the Functional Monomers and Cross-Linker Monomer Used in This Research: (a) VSA, (b) VPA, and (c) MBAA**



throughout the entire pH range, will be obtained. In addition, the content of cross-linker monomer was varied in order to identify its effects onto charge density and sieving. To the best of our knowledge, these monomers were not used previously for fabrication of a NF membrane using the radical graft copolymerization technique. Therefore, this research investigated the feasibility of using these monomers for fabrication of a polyelectrolyte hydrogel membrane and the effect of the polymerization conditions on the modification efficiency as well as on the membrane characteristics. Then, the new membranes were tested for their performance under NF conditions, also at various pH values and at different salinities.

## EXPERIMENTAL SECTION

**Materials.** The PES membranes were supplied by Sartorius AG (Germany) with nominal molecular weight cut off (MWCO) of 30 kDa as reported by the manufacturer. It should be noted, however, that it was recently found that for these membranes the reported MWCO is different from the MWCO measured with dextran mixtures and that the 30 kDa membrane has a measured MWCO of approximately 90 kDa.<sup>25</sup> Prior to the modification, the membranes were cut with a 56 mm diameter punch hole and washed in methanol for 1 h, then thoroughly washed with Milli-Q water and left in Milli-Q water until used. Vinylsulfonic acid sodium salt (VSA; 25%) from Sigma-Aldrich and vinyl phosphonic acid (VPA) from BASF were used as monomers, and *N,N'*-methylenebisacrylamide (MBAA) from Sigma-Aldrich was used as the cross-linker (Scheme 1). The monomers and cross-linkers were used as received. To obtain monomer solution with 40% VSA, we concentrated the 25% VSA solution under reduced pressure at 37 mbar and 45 °C. The monomer concentration was 40% when the solution density was 1.32 g/L. MgSO<sub>4</sub>, NaCl, Na<sub>2</sub>SO<sub>4</sub>, and CaCl<sub>2</sub> and glucose were purchased from Sigma-Aldrich. Sucrose was purchased from Acros, Geel, Belgium. These test substances were used without purification. All experiments were done with purified water from a Milli-Q system from Millipore.

**Modification Procedure.** A water-wet membrane was placed in a glass holder, leaving only the outer surface of the membrane (diameter 54 mm) in contact with the solution, and remained covered with Milli-Q water until modification. The water was then wiped off with a tissue paper and the membrane surface was covered with 5 mL modification solution (previously degassed with nitrogen for 10 min). Thereafter, the sample was placed inside a UV system (UVA Cube 2000, Hönle AG, Germany, equipped with a 20 cm long mercury lamp, allowing a homogeneous irradiation of 0.1 m<sup>2</sup> area via reflecting walls). The membrane was thereafter irradiated at 55 ± 5 mW/cm<sup>2</sup>, unless stated otherwise, for different times (2–35 min). The UV wavelength was narrowed to λ = 315–400 nm, by using a special filter glass in order to avoid membrane degradation.<sup>26</sup> At the end of the modification, the membrane was washed with Milli-Q water for 24 h at room temperature. To verify chemical grafting, we washed a few membranes at 50 °C for 48 h with Milli-Q water or with ethanol. Negligible differences in performance were found for membranes which were washed at the different conditions. The modification was performed with VSA or VPA as the functional monomers and MBAA as the cross-linker monomer. No modification occurred when VPA was used as a monomer under all conditions tested. Therefore, only results with VSA are presented.

**Degree of Grafting.** The degree of grafting (DG) was calculated using the gravimetry (DG<sub>g</sub>) and spectrometry (DG<sub>s</sub>) methods.

$DG_s$  was determined by attenuated total reflection Fourier transform infrared (FTIR-ATR) spectroscopy (Varian 3100, USA equipped with a one reflection KRS-5 crystal, 45°, 64 scans were taken for each spectrum at a resolution of 4  $\text{cm}^{-1}$ ) and defined as follows:

$$DG_s = \frac{I_{\text{mon}}}{I_{\text{mem}}} \quad (1)$$

where  $I_{\text{mon}}$  is the intensity of the 1040  $\text{cm}^{-1}$  band assigned to the symmetric stretching of the VSA sulfonate group and  $I_{\text{mem}}$  is the intensity of the 1577  $\text{cm}^{-1}$  band, a C–H peak from the aromatic ring in the base PES membrane which does not appear in the monomer or the cross-linker IR spectra. The reported values are the average values of at least 5 distinct samples for every condition and every sample was measured at three different locations and the errors being standard deviations.

For the determination of  $DG_g$ , unmodified and modified membranes were cut with the same punch-hole (either 7 or 25 mm), dried for 24 h at 40 °C in a vacuum, and left in a desiccator for few hours before weighing. The  $DG_g$  was obtained using

$$DG_g = \frac{m_{\text{modified}} - m_{\text{PES}}}{A} \quad (2)$$

where  $m_{\text{modified}}$  is the weight of a modified membrane,  $m_{\text{PES}}$  is the average weight of at least three unmodified PES membranes, and  $A$  is the membrane area.  $DG_g$  was calculated under the assumption that samples from a specific unmodified membrane cut with a punch-hole at the same diameter have the same weight. This was found very accurate; for example, the weight of 7 different samples from pristine PES membranes was  $(7.036 \pm 0.050)$  mg (i.e., less than 7% variation). The reported values are the average of at least 3 distinct membranes when at least two samples were cut from each membrane. Samples from the same membrane with more than 10% difference were excluded.

The gravimetric method was used since it was found that drying the membrane before modification results in a change of its properties. Additionally, the  $DG_s$  is directly correlated with the newly introduced polymer concentration on the surface, whereas, the  $DG_g$  is an indication of the total mass of the modification layer. Hence, the cross-linker content in the modification layer may be estimated from the difference in the DG measured using the two methods.

**Membrane Characterization. Ion Exchange Capacity (IEC).** Modified and pristine membranes that were cut with a punch-hole (25 mm diameter), were submerged in 1 M HCl solution for 24 h. The solution was replaced once during this time in order to ensure complete conversion of the sulfonic group to its acid form. After 24 h, the membranes were washed with Milli-Q water and immersed for 24 h in 10 mL 2 M NaCl solution to convert the sulfonic acid group to its  $\text{Na}^+$  form. The solution was replaced 5 times, so that a total solution of 50 mL was collected. The solution was then titrated with 0.01 N NaOH using a Mettler Toledo (T90) titrator. The membranes were then washed thoroughly with Milli-Q water, dried for 24 h in a vacuum oven at 40 °C and weighed. The IEC [ $\text{mequiv g}^{-1}$ ] was calculated using:

$$\text{IEC} = \frac{(V - V_0)c}{w} \quad (3)$$

where  $V$  is the volume of NaOH [mL] needed for the back-titration,  $V_0$  is the average volume for the titration of three PES control samples,  $c$  is the NaOH concentration [M] and  $w$  is weight of the modification layer [g], measured as the difference between the weight of the modified and the unmodified control PES membrane.

**X-ray Photoelectron Spectroscopy (XPS).** XPS general survey spectra and high-resolution spectra were recorded using ESCALAB 250 (Thermo Fisher Scientific Inc., Waltham, UK) with Al X-ray source and monochromator. Binding energies for probed elements were corrected for the charging effect with reference to the 285 eV C1s peak.

**Atomic Force Microscopy.** (AFM) images of a dry pristine and a dry modified membrane were obtained using a MultiMode AFM with

Nanoscope IIIa controller and equipped with a 10  $\mu\text{m}$  scanner from Digital Instruments, Santa Barbara, CA, USA. The measurements were performed in a tapping mode with a silicon tip having a radius of <10 nm. Average root-mean-square roughness (rms) of 3 distinct samples was obtained at surface areas of 2  $\mu\text{m} \times 2 \mu\text{m}$ .

**Membrane Performance.** The membranes were cut with a punch hole (44 mm) and placed in a dead end cell (Amicon 8050) connected to a reservoir. Salt rejection and permeability were measured at 2–4 bar (pressurized with nitrogen) at 600–700 rpm stirring rate. Salt rejection was calculated by

$$\text{rejection} = 1 - \frac{C_p}{C_f} \quad (4)$$

where  $C_f$  and  $C_p$  are the salt concentration in the feed and permeate, respectively. Salt concentration was measured using conductometry. Membrane permeability ( $L_p$ ) using Milli-Q water was determined by

$$L_p = \frac{V}{AtP} \quad (5)$$

where  $V$  is the water volume collected (L),  $A$  is the membrane area ( $\text{m}^2$ ),  $t$  time (h), and  $P$  is the applied pressure (bar).

Sucrose and glucose rejection, separately, were measured at the same conditions as the salt rejection experiment, and at a concentration of 1 mM. The solute concentrations in the feed and in the permeate were measured by TOC analyzer (Shimadzu, Japan, Model: TOC-VCSH).

The effect of salt concentration on rejection was determined at four  $\text{Na}_2\text{SO}_4$  concentrations (1–8 g/L). The experiments were conducted at the same trans-membrane pressure (TMP) of 3.1 bar, except for the experiment at 8 g/L which was done at TMP of 1.5 bar. This was because the maximum operating pressures allowed using the Amicon 8050 cell is  $\sim 5$  bar, and the osmotic pressure of 8 g/L  $\text{Na}_2\text{SO}_4$  is approximately 3.5 bar.

Membrane stability and performance were tested at three pH values (1.5–2, 7 and 10) by soaking six analogous modified membranes (25% VSA, 1.5% MBAA,  $t = 18$  min,  $I = 55$   $\text{mW}/\text{cm}^2$ ) in solutions of low and higher pH, three in Milli-Q water at pH 2 and three in Milli-Q water at pH 10. Every 24 h, one membrane was removed from the solution and its performance was measured once (the last membrane was measured after 6 days). Every membrane was tested at the three pH values as follows: first the flux and rejection were measured at the pH that it was soaked in (the membrane that was soaked at pH 2 was measured at pH 1.5), then it was washed with Milli-Q water and thereafter it was tested with salt solutions at the other two pH values. The membranes were tested with 1 g/L  $\text{Na}_2\text{SO}_4$  and at a pressure of 4 bar. The pH was adjusted using  $\text{H}_2\text{SO}_4$  or NaOH.

## RESULTS AND DISCUSSION

**Degree of Functionalization As Function of Modification Conditions.** Figure 1 presents the IR spectra, measured using ATR-FTIR, of the pristine and the modified membranes with 25 wt % VSA as monomer and with different cross-linker concentrations (mole%, relative to VSA).

A new band assigned to the stretching vibration of the sulfonic acid group of the monomer is seen at 1040  $\text{cm}^{-1}$ . The intensity of this band increases with cross-linker concentration indicating an increase in the modification degree. The other band marked at 1577  $\text{cm}^{-1}$  is of the base membrane and is used for the DGs calculations (eq 1). Two bands attributed to the cross-linker are observed at 1543  $\text{cm}^{-1}$  and at 1662  $\text{cm}^{-1}$  and are ascribed to the amide I (C=O) and the amide II (N–H) absorption, respectively. The former appears only at high cross-linker concentration. The latter also appears in the pristine PES membrane spectrum, although at a much lower intensity, and it also shifts to 1680  $\text{cm}^{-1}$ . This is probably as a result of poly-N-vinylpyrrolidone (PVP) added to the PES by the manufacturer.<sup>27</sup> Another new band resulting from the modification is

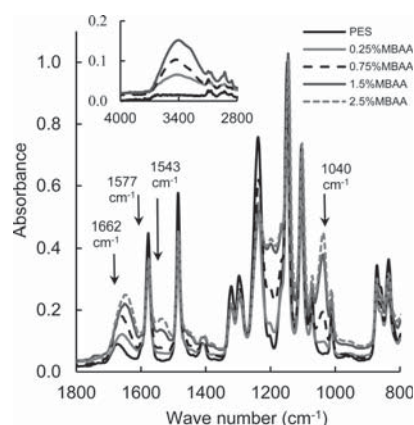


**Figure 1.** ATR-FTIR of the pristine and modified membranes prepared with different cross-linker concentration. Modification conditions: 25% VSA,  $t = 18$  min,  $I = 55$  mW/cm<sup>2</sup>.

seen in Figure 1 in the range 3000–3400 cm<sup>-1</sup> and is attributed to hydrogen bonds.<sup>28</sup>

Figure 2 shows the degree of modification obtained at different cross-linker concentrations under otherwise constant modification conditions.

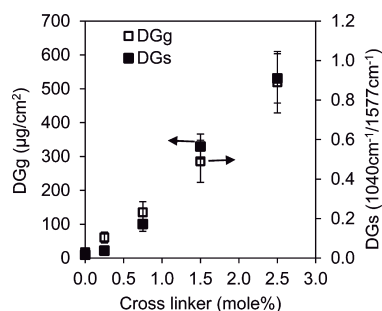


**Figure 2.** Degree of grafting measured using the spectroscopic (DG<sub>s</sub>) and gravimetric (DG<sub>g</sub>) methods after modification at different cross-linker fractions (mole %). Modification conditions: 25% VSA,  $t = 18$  min,  $I = 55$  mW/cm<sup>2</sup>,  $n \geq 5$ .

The degrees of modification measured by the two techniques have a similar trend: a linear increase in the DG with cross-linker concentration. The DG without cross-linker was very low. This is probably a consequence of wetting or diffusion limitation due to incompatibility between the charged monomer and the hydrophobic surface.<sup>29,30</sup> Figure 2 demonstrates that by adding the cross-linker as a comonomer at a low concentration, the VSA can easily be graft copolymerized on a PES membrane. This contrasts a previous report which argued that radical co-polymerization of VSA with MBAA (using ammonium peroxydisulfate as initiator) to form a hydrogel cannot occur.<sup>31</sup> Furthermore, although the copolymerization of VSA and MBAA is similar to copolymerization of VSA with other hydrophilic monomers, due to the low concentration of the MBAA, a hydrogel with high PVSA content can be obtained. In contrast, the VSA fraction when copolymerized with acrylic acid (AA) could only be as high as 25 wt %, and copolymerization of VSA with AA and divinyl benzene resulted only in a 5% PVSA fraction in the gel, regardless of the VSA content used during the polymerization.<sup>31,32</sup>

It was interesting to find out that despite the similar structure of VSA and VPA (Scheme 1) a hydrogel using VPA as a monomer could not be obtained. The reason was not investigated in this research, but it is known that polymerization of VPA by radical polymerization is very difficult and occurs only at high temperature.<sup>33,34</sup> This may be related to the fact that the charge density of VPA is even higher than that of VSA, and that chain propagation is hindered by electrostatic repulsion. Moreover, no report of surface grafting of VPA using radical polymerization was found in the literature.

Figure 3 describes the modification progress with modification time with 1.5 and 2.5% cross-linker fraction under

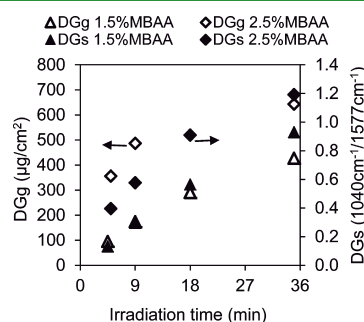


**Figure 3.** Modification progress presented as the DG<sub>s</sub> (solid markers) and DG<sub>g</sub> (empty markers) at two cross-linker fractions (1.5 and 2.5% MBAA). Modification conditions: 25% VSA,  $I = 55$  mW/cm<sup>2</sup>,  $n \geq 3$ .

otherwise constant conditions. The increase of the DG<sub>s</sub> with modification time is monotonic. However, the DG<sub>g</sub> rises fast in the early stages and then the increase moderates. Moreover, the rise and the moderation occur faster with the higher cross-linker concentration. Therefore, it can be assumed that in the early stages it is mainly the cross-linker monomer that is grafted to the surface, and then, either because of the cross-linker's two double bonds or a change in the surface properties, the functional monomer (VSA) grafting is enhanced. This facilitating role of MBAA was also recognized by Wu et al.<sup>35</sup> using the functional monomer N-vinyl-2-pyrrolidone, which can be graft copolymerized without a cross-linker at higher degree than VSA.

The effect of the monomer concentration was also investigated by comparing the ratio of the modification degree measured using the two techniques (Figure 4). The data labels in Figure 4 indicate the cross-linker concentration (mole%). The cross-linker concentration when the modification was carried out without the functional monomer (0% VSA) was the same as for modification with 25% VSA.

The ratio between the DG<sub>s</sub> and the DG<sub>g</sub> using the 12.5% VSA solutions is much lower than with 25 and 40% VSA, although the modification time was higher (18 and 35 min for 12.5 and 25 and 40% VSA, respectively). This can be explained by a higher cross-linker fraction in the modification layer when using 12.5% VSA in comparison with modification at 25% VSA. The ratio between DG<sub>g</sub> and DG<sub>s</sub> for 25% VSA and 40% VSA is similar (Figure 4). However, to achieve a similar modification degree, the required cross-linker concentration using 40% VSA is lower.

The effect of the irradiation intensity on the modification, using similar energy doses, is described in Figure 5. Considering the low modification degree with only VSA, the experiments were conducted mainly at a high intensity (55 mW/cm<sup>2</sup>) and

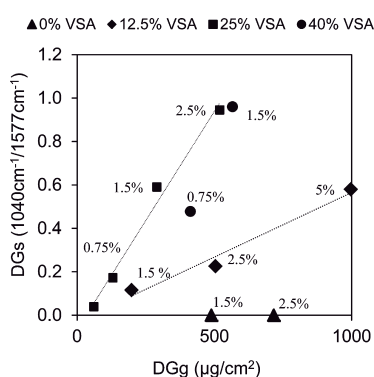


**Figure 4.**  $DG_s$  vs  $DG_g$  following modification obtained with different monomer concentration (0, 12.5, 25, and 40% VSA), different cross-linker fraction (0.25–5% MBAA), and different modification times (18 and 35 min); modification conditions:  $I = 55 \text{ mW/cm}^2$ ,  $n \geq 3$ .

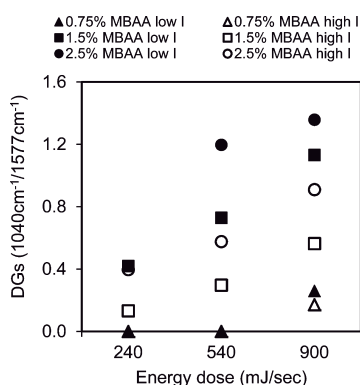


**Figure 5.** Effect of high ( $I = 55 \text{ mW/cm}^2$ , empty marker) and low ( $I = 16 \text{ mW/cm}^2$ , solid marker) irradiation intensities on spectroscopy degree of grafting at different cross-linker concentrations (0.75–2.5% MBAA) and energy doses,  $n \geq 3$ .

with high energy doses. Nevertheless, Figure 5 clearly shows that irradiation at low intensity ( $16 \text{ mW/cm}^2$ ) results in high modification compared with irradiation at high intensity. Generally, it is accepted that the polymerization rate can increase with irradiation intensity.<sup>36,37</sup> However, polymerization at too high intensities can be monomer diffusion limited immediately in the early stages, due to the high initiator radicals concentration, whereas for polymerization at low UV intensities, the diffusion limitation occurs at later stage.<sup>38</sup> This can change the monomer conversion,<sup>39</sup> and hence, the modification degree as well as the modification layer structure and properties.<sup>40</sup> It was also demonstrated, for membrane modification using redox radical polymerization, that when a too high initial radical concentration was used, lower modification degrees were measured, probably because of enhanced efficiency of the termination reaction over the propagation reaction.<sup>41</sup> Additionally, high intensity may result in membrane degradation,<sup>23</sup> which might also influence the modification degree.

**Surface Characterization.** The IEC of membranes modified at different conditions is shown in Table 1. Modification without a cross-linker resulted in an IEC similar to the theoretical value of PVSA ( $9 \text{ mequiv g}^{-1}$ ), but it was difficult to determine exactly because of the low degree of modification.

**Table 1.** Ion Exchange Capacity of Modified Membranes with Similar  $DG_g$  Prepared at Different Cross-Linker Fractions, Different Modification Time, and Different Monomer Concentration<sup>a</sup>

VSA (%)	MBAA (mole %)	modification time (min)	IEC (mequiv $\text{g}^{-1}$ )
25	0.25	18	$3.2 \pm 0.2$
25	0.75	18	$2.8 \pm 0.3$
25	1.5	18	$3.1 \pm 0.4$
25	2.5	18	$3.1 \pm 0.1$
25	1.5	4.5	$1.4 \pm 0.4$
25	1.5	9	$2.2 \pm 0.2$
25	1.5	35	$3.3 \pm 0.2$
12.5	2.5	35	$1.9 \pm 0.4$
40	1.5	18	$4.3 \pm 0.7$

<sup>a</sup>Modification conditions:  $I = 55 \text{ mW/cm}^2$ ,  $n \geq 3$ .

The IEC for membranes prepared with a cross-linker was lower than the theoretical value for PVSA at all conditions, indicating a relatively high cross-linker fraction in the active layer, as was also reported previously for other functional monomers.<sup>40</sup> Still, these IEC values are rather high compared to other charged NF membranes,<sup>40,42</sup> prompting a high Donnan exclusion. Surprisingly, the IEC values at 25% VSA were similar at the different cross-linker concentrations. Thus, it may be speculated that the cross-linker fraction is not very different in the modification layer obtained after varied conditions. On the other hand, increasing the VSA concentration to 40% (at same MBAA concentration, 1.5%, and UV time, 8 min; cf. Table 1) resulted in a higher IEC, i.e., higher VSA fraction in the modified layer. This can be explained by the effect of monomer ratio onto chain propagation and also illustrates that by altering some of the polymerization conditions the VSA fraction in the copolymer hydrogel can be increased.

The IEC at the various modification times and at a constant MBAA concentration (1.5%) is also presented in Table 1. The IEC in the early stages is low and it increases with the modification progress, until it levels off (at 18 min). This reflects the increase in the VSA content during the modification progress, as discussed before (cf. Figure 3).

The increased cross-linker fraction in the modification layer at lower monomer concentration and at the early stages of the modification was also established using elemental analysis of the modified layer at the three monomer concentrations and the different modification times as presented in Table 2.

The pristine PES membrane contains nitrogen, probably because of modification with the additive PVP.<sup>27</sup> The C:O ratio of the modified membranes is much higher than the theoretical value for the VSA. This confirms that the modification layer has relatively high cross-linker fraction because this ratio is much higher for MBAA than for VSA. High resolution XPS revealed the disappearance of the C1s band at 291.1 eV associated with aromatic  $\pi-\pi^*$  carbon and was recorded at 3% only on the unmodified PES membrane, demonstrating complete coverage of the surface of the PES base membrane. The N:S and C:O ratios decrease with modification time and with monomer concentrations for membranes having similar  $DG_g$ . This concurs with the previous assumption that the modification layer has a higher cross-linker fraction at these conditions because the functional monomer VSA does not contain nitrogen.

**Table 2. Elemental Composition (in atomic percent) and Ratios Obtained by XPS for Pristine and Modified PES Membranes<sup>a</sup>**

	%C (285.0 eV)	%O (531.7 eV)	%S (168.0 eV)	%N (399.8 eV)	N/S	C/O	DG <sub>s</sub>	DG <sub>g</sub> (μg/cm <sup>2</sup> )
PES theoretical	75.0	18.8	6.2			3.99		
PES pristine	72.2	18.0	4.7	4.9	1.04	4.30		
VSA theoretical	33.3	50.0	16.7			0.67		
MBAA theoretical	64.0	18.0		18.0		3.56		
25% VSA, 1.5% MBAA, <i>t</i> = 9 min.	71.6	18.7	4.0	5.6	1.40	3.83		
12.5% VSA, 2.5% MBAA, <i>t</i> = 18 min	73.0	18.6	3.1	5.4	1.74	3.92	0.110	438
25% VSA, 1.5% MBAA, <i>t</i> = 18 min.	63.4	23.6	6.1	7.0	1.14	2.69	0.636	337
40% VSA, 1.5% MBAA, <i>t</i> = 18 min.	62.0	26.7	6.9	4.4	0.64	2.32	0.440	490

<sup>a</sup>Modification conditions: *I* = 55 mW/cm<sup>2</sup>.

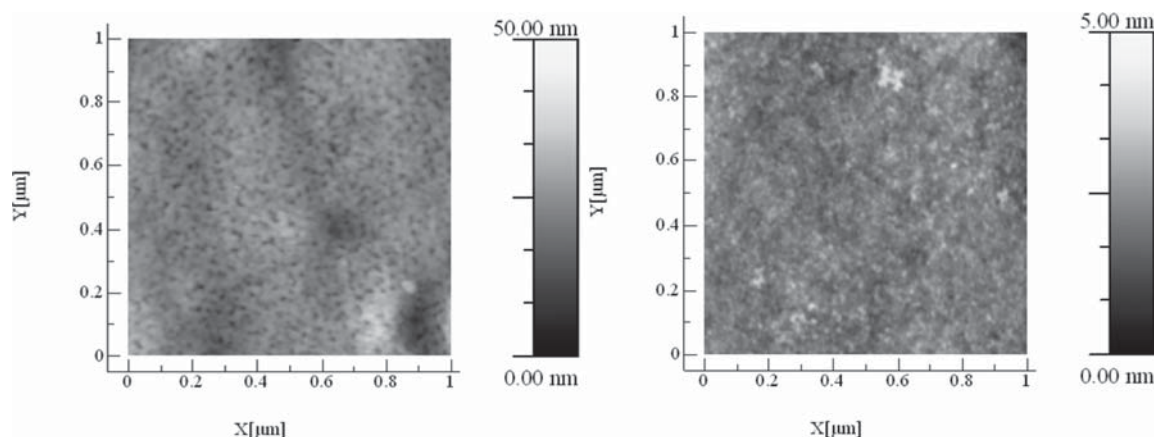


**Figure 6.** AFM images of unmodified PES membrane (left) and modified PES membrane (right, DG<sub>s</sub> = 0.6). Modification conditions: 1.5% MBAA, 25% VSA, *t* = 18 min.

**Surface Morphology.** The change in the membrane surface morphology between the pristine PES membrane and the PES membrane after grafting at high DG<sub>s</sub> (0.6) is evident in the AFM images in Figure 6. Because the UV light can penetrate into the PES membrane, some modification takes also place within the membrane pores.<sup>22</sup> Recently, the modification depth under analogous conditions had been analyzed by scanning electron microscopy and energy dispersive X-ray spectroscopy and found to be up to 5 μm.<sup>27</sup> Therefore, the membrane barrier layer structure can also be described as pore-filling hydrogel composite combined with a thin film hydrogel on the outer surface.

Surprisingly, although the surface morphology changed, the surface roughness which usually increases following graft copolymer modification,<sup>6,11,41,43</sup> decreased from 6 ± 3 nm to 4 ± 2 nm. This is lower than the roughness of most NF membranes.<sup>4,10,11,44</sup> Because the membrane roughness promotes fouling phenomena in NF<sup>45</sup> the very low roughness might reduce the novel membranes' propensity to fouling and biofouling. The low roughness also illustrates the uniform coverage of the membrane surface by the grafted polymeric hydrogel.<sup>41,43</sup>

**Nanofiltration Membrane Performance.** Figure 7 presents the membrane permeability and salt rejection following modification with 25% VSA at different cross-linker concentrations and of a commercial NF membrane (NF 270 Dow Filmtec).<sup>44,46</sup>

A NF membrane was successfully obtained (defined herein when the Na<sub>2</sub>SO<sub>4</sub> rejection was higher than 90%) when the cross-linker fraction was 0.75%. The salt rejection increased, whereas the permeability decreased with increasing cross-linker

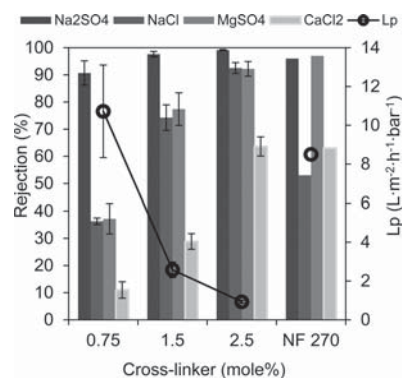


**Figure 7.** Salt rejection and permeability of membranes following modification at different cross-linker fractions. Modification conditions: *I* = 55 mW/cm<sup>2</sup>, *t* = 18 min. Filtration conditions: *P* = 4 bar, salt concentration 1 g/L, *n* ≥ 3. Commercial thin-film polyamide composite membrane for comparison.

concentration, and this was in agreement with increased DG (cf. Figure 2).

The salt rejection was in the order Na<sub>2</sub>SO<sub>4</sub> > MgSO<sub>4</sub> ≈ NaCl > CaCl<sub>2</sub>, as expected for rejection based on Donnan exclusion for negatively charged NF membranes.<sup>47</sup> The higher rejection at a higher cross-linker concentration can be attributed to steric exclusion, because the IEC was similar following modification above 0.75% MBAA (see Figure 3 and Table 1). Because rejection of uncharged solutes with charged NF membranes derives mainly from steric exclusion,<sup>48</sup> the increased rejection of the uncharged sucrose and glucose with increasing cross-linker

concentration (Figure 8), supports the increased steric influence by the more tightly cross-linked polyelectrolyte hydrogel.

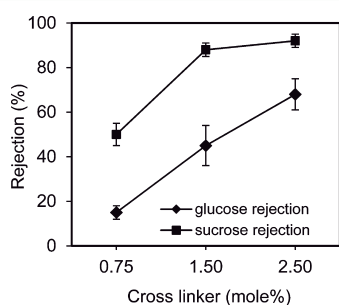


**Figure 8.** Sucrose and glucose rejection of membranes following modification (25% VSA,  $I = 55 \text{ mW/cm}^2$ ,  $t = 18 \text{ min}$ ) with different cross-linker fractions. Nanofiltration conditions:  $P = 4 \text{ bar}$ ,  $1 \text{ mM}$  sucrose or glucose in water,  $n \geq 3$ .

The salt rejection of the new membrane is comparable to that of various other types of NF membranes presented before.<sup>2,4,6,8,46,49–52</sup> However, the permeability is still lower than that of polyelectrolyte membranes fabricated using the “LBL” method and of a commercial polyamide-based membrane (Figure 7). Because the Donnan potential of polyelectrolyte membranes is higher than that of polyamide membranes the better performance of the latter can be attributed to the dielectric phenomena<sup>53</sup> which are probably not significant for polyelectrolyte membranes. Nevertheless, the hydrogel polyelectrolyte membranes have an optimization potential. For example, by increasing the monomer concentration, the IEC (and therefore the Donnan potential) also increased (Table 2). Moreover, such optimization was already demonstrated for polyelectrolyte membranes fabricated using the “LBL” method. These membranes presented a very low permeability when first introduced.<sup>54,55</sup> The performance was then successfully optimized, almost surpassing that of the polyamide membranes.<sup>9</sup> The effect of the various functionalization parameters including the influence of the base membrane pore structure and permeability on the composite membrane performance is the subject of a subsequent report.

**Influence of the Salt Concentration and pH Value on NF Performance.** Figure 9 describes the influence of the concentration of the  $\text{Na}_2\text{SO}_4$  on the membrane rejection.

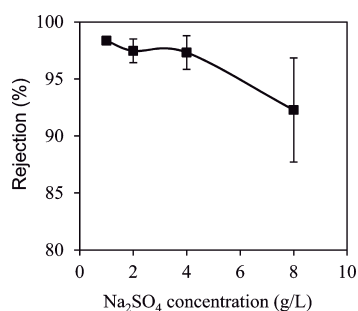


**Figure 9.**  $\text{Na}_2\text{SO}_4$  rejections at various salt concentrations. Modification conditions: 25% VSA and 1.5% MBAA,  $I = 55 \text{ mW/cm}^2$ , and  $t = 18 \text{ min}$ . Filtration conditions: For 1–4 g/L, transmembrane pressure (TMP) 3.1 bar; for 8 g/L, TMP 1.5 bar.

The salt rejection was stable with increased salt concentration up to 4 g/L  $\text{Na}_2\text{SO}_4$  (28 mM) and then decreased at 8 g/L (56 mM). The reduced rejection is probably caused by a decrease in Donnan exclusion. However, the rejection remains high due to the high IEC which suppresses the effect of the salt concentration on the membrane rejection. The lower rejection at 8 g/L is also a result of the lower permeate flux due to the lower TMP (for reasons, see Experimental Section), which can reduce the rejection significantly.<sup>51</sup> Although it is difficult to compare the effect on the salt rejection obtained in this study to other studies because of various operation conditions and the use of different salts, it seems that the influence of salt concentrations on the rejection of new membrane is lower than for many other NF membranes fabricated by various methods.<sup>40,44,51,55–57</sup>

The effects of the feed pH on the rejection of  $\text{Na}_2\text{SO}_4$ , as well as the stability of membrane performance after being soaked in alkaline and acidic solutions are demonstrated in Figure 10.

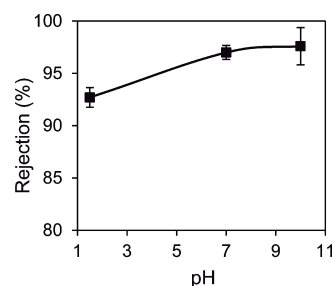


**Figure 10.** Rejection of  $\text{Na}_2\text{SO}_4$  at pH 1.5, pH 7, and pH 10. Modification conditions: 25% VSA, 1.5% MBAA,  $I = 55 \text{ mW/cm}^2$ , and  $t = 18 \text{ min}$ . Filtration conditions:  $P = 4 \text{ bar}$ ,  $1 \text{ g/L}$   $\text{Na}_2\text{SO}_4$ .

The rejection at pH 10 and pH 7 was similar, and it decreased slightly in acidic pH 1.5. However, it is noted that because the pH was adjusted with  $\text{H}_2\text{SO}_4$  the  $\text{SO}_4^{2-}$  concentration at pH 1.5 was similar to the one obtained between 4 – 8 g/L  $\text{Na}_2\text{SO}_4$  (as was also confirmed by conductivity measurement), thus, it can be estimated that the rejection was almost not influenced due to the low pH value. Moreover, salt rejection of membranes that were first tested in pH 1.5 and then at pH 7 was similar to the one measured for membranes that were left only in Milli-Q water (were not soaked in pH 2) before the filtration tests. The high rejection at low pH values and the stability of the membrane in acidic pH is due to the strong polyelectrolyte hydrogel. This is usually not observed for weak or uncharged NF membranes including commercial polyamide-based membranes.<sup>7,46,58</sup>

## CONCLUSIONS

A strong polyelectrolyte hydrogel was graft copolymerized on a PES UF membrane using vinyl sulfonic acid as the monomer and  $N,N'$ -methylenebisacrylamide as the cross-linker monomer. The modification was carried out in one simple step, in aqueous solution and at room temperature using the photoirradiation method. The cross-linker and the functional monomer concentration had a significant influence on the polymerization. As the cross-linker concentration increased both the  $\text{DG}_g$  and  $\text{DG}_s$  increased simultaneously. It was also demonstrated that during the early stages of the modification, mainly the cross-linker was grafted, which then facilitated the graft copoly-



merization of the functional monomer. In contrast, when the monomer concentration was low, the  $DG_g$  was substantially lower compared with the  $DG_g$ . This was explained as a result of a higher cross-linker fraction in the hydrogel. XPS and IEC supported these findings. In addition it was found that when the modification was carried out using low UV intensity the modification degree and the membrane performance were better than for modification at high UV intensity.

A NF membrane was successfully fabricated using the proposed method. The order of rejection of single salts was  $\text{Na}_2\text{SO}_4 > \text{MgSO}_4 \approx \text{NaCl} > \text{CaCl}_2$ , as is expected for the Donnan exclusion of negatively charged NF membranes. A further increase in the salt rejection with modification degree was attributed to an increase in the steric exclusion: The higher degree of modification also induced an increased rejection of uncharged solutes and a corresponding characteristic decrease in the membrane permeability. One advantage of conducting the polymerization using VSA as a functional monomer was evident by the very low surface roughness as measured using AFM which was lower than for most commercial or previously reported NF membranes. The strong acidity of the VSA monomer enabled the membrane to be stable while maintaining a high selectivity at low pH value. The ion exchange capacity was higher than for most charged NF membranes reported in the literature. As a consequence the new membrane had a high salt rejection (especially for sulfate), which was also maintained at relatively high salt concentrations. These features, together with the many possibilities for tailoring the membrane properties and performance, make the here reported material a promising membrane for NF as well as for other applications, for instance forward osmosis. The optimization of the polymerization conditions, the influence of the base membrane pore structure (MWCO) and their effects on membrane performance will be presented in a following paper.

## AUTHOR INFORMATION

### Corresponding Author

\*E-mail: mathias.ulbricht@uni-essen.de.

### Notes

The authors declare no competing financial interest.

## ACKNOWLEDGMENTS

R.B. gratefully acknowledges the 'Young Scientists Exchange Program' of the BMBF-MOST Water Technology Cooperation for the financial support. Further thanks are due to Dr. Steffen Franzka, University Duisburg-Essen, and Yair Kaufman, Ben-Gurion University, Beer-Sheva, Israel, for performing and analyzing the AFM measurements. The XPS analyses were performed by Dr. Natalya Froumin (Ben-Gurion University).

## REFERENCES

- Ulbricht, M. *Polymer* **2006**, *47*, 2217–2262.
- Childs, R. F.; Mika, A. M.; Pandey, A. K.; McCrory, C.; Mouton, S.; Dickson, J. M. *Sep. Purif. Technol.* **2001**, *22*, 507–517.
- Du, R.; Zhao, J. *J. Membr. Sci.* **2004**, *239*, 183–188.
- Deng, H.; Xu, Y.; Chen, Q.; Wei, X.; Zhu, B. *J. Membr. Sci.* **2011**, *366*, 363–372.
- Qiu, C.; Nguyen, Q. T.; Ping, Z. *J. Membr. Sci.* **2007**, *295*, 88–94.
- Deng, H. Y.; Xu, Y. Y.; Zhu, B. K.; Wei, X. Z.; Liu, F.; Cui, Z. Y. *J. Membr. Sci.* **2008**, *323*, 125–133.
- Hollman, A. M.; Bhattacharyya, D. *Langmuir* **2004**, *20*, 5418–5424.
- Miller, M. D.; Bruening, M. L. *Langmuir* **2004**, *20*, 11545–11551.
- Bruening, M. L.; Dotzauer, D. M.; Jain, P.; Ouyang, L.; Baker, G. L. *Langmuir* **2008**, *24*, 7663–7673.
- Saren, Q.; Qiu, C. Q.; Tang, C. Y. *Environ. Sci. Technol.* **2011**, *45*, 5201–5208.
- Li, X.; De Feyter, S.; Chen, D.; Aldea, S.; Vandezande, P.; Du Prez, F.; Vankelecom, I. F. *Chem. Mater.* **2008**, *20*, 3876–3883.
- Dai, J.; Balachandra, A. M.; Lee, J. I.; Bruening, M. L. *Macromolecules* **2002**, *35*, 3164–3170.
- Deen, W. *AIChE J.* **1987**, *33*, 1409–1425.
- Freger, V. *Langmuir* **2003**, *19*, 4791–4797.
- Wang, X. L.; Tsuru, T.; Nakao, S.; Kimura, S. *J. Membr. Sci.* **1997**, *135*, 19–32.
- Bowen, W. R.; Welfoot, J. S. *Chem. Eng. Sci.* **2002**, *57*, 1121–1137.
- Freger, V. *Environ. Sci. Technol.* **2004**, *38*, 3168–3175.
- Hammond, P. T. *AIChE J.* **2011**, *57*, 2928–2940.
- Yang, Q.; Adrus, N.; Tomicki, F.; Ulbricht, M. *J. Mater. Chem.* **2011**, *21*, 2783–2811.
- Eshet, I.; Freger, V.; Kasher, R.; Herzberg, M.; Lei, J.; Ulbricht, M. *Biomacromolecules* **2011**, *12*, 1169–1177.
- Jiang, W.; Childs, R. F.; Mika, A. M.; Dickson, J. M. *Desalination* **2003**, *159*, 253–266.
- Susanto, H.; Ulbricht, M. *Langmuir* **2007**, *23*, 7818–7830.
- Peeva, P. D.; Pieper, T.; Ulbricht, M. *J. Membr. Sci.* **2010**, *362*, 560–568.
- He, D.; Susanto, H.; Ulbricht, M. *Prog. Polym. Sci.* **2009**, *34*, 62–98.
- Peeva, P. D.; Knoche, T.; Pieper, T.; Ulbricht, M. *Sep. Purif. Technol.* **2012**, *92*, 83–92.
- Pieracci, J.; Crivello, J. V.; Belfort, G. *Chem. Mater.* **2002**, *14*, 256–265.
- Peeva, P. D.; Million, N.; Ulbricht, M. *J. Membr. Sci.* **2012**, *390–391*, 99–112.
- Zundel, G. *J. Membr. Sci.* **1982**, *11*, 249–274.
- Behar, D.; Fessenden, R. W.; Hornak, J. P. *Radiat. Phys. Chem.* **1982**, *20*, 267–273.
- Shkolnik, S.; Behar, D. *J. Appl. Polym. Sci.* **1982**, *27*, 2189–2196.
- Kim, S. J.; Park, S. J.; Kim, S. I. *Smart Mater. Struct.* **2004**, *13*, 317–322.
- Yamaguchi, T.; Ibe, M.; Nair, B. N.; Nakao, S. *J. Electrochem. Soc.* **2002**, *149*, A1448–A1453.
- Bingöl, B.; Meyer, W. H.; Wagner, M.; Wegner, G. *Macromol. Rapid Commun.* **2006**, *27*, 1719–1724.
- Ellis, J.; Anstice, M.; Wilson, A. D. *Clin. Mater.* **1991**, *7*, 341–346.
- Wu, Y. H.; Liu, Y. L.; Chang, Y.; Higuchi, A.; Freeman, B. D. *J. Membr. Sci.* **2010**, *348*, 47–55.
- Andrzejewska, E. *Prog. Polym. Sci.* **2001**, *26*, 605–665.
- Kurdikar, D. L.; Peppas, N. A. *Macromolecules* **1994**, *27*, 4084–4092.
- He, H.; Li, L.; Lee, L. J. *React. Funct. Polym.* **2008**, *68*, 103–113.
- Zhang, S.; Xu, T.; Wu, C. *J. Membr. Sci.* **2006**, *269*, 142–151.
- Mika, A.; Childs, R.; Dickson, J.; McCarry, B.; Gagnon, D. *J. Membr. Sci.* **1997**, *135*, 81–92.
- Bernstein, R.; Belfer, S.; Freger, V. *Langmuir* **2010**, *26*, 12358–12365.
- Dalwani, M.; Bargeman, G.; Hosseiny, S.; Boerrigter, M.; Wessling, M.; Benes, N. E. *J. Membr. Sci.* **2011**, *381*, 81–89.
- Kang, G.; Liu, M.; Lin, B.; Cao, Y.; Yuan, Q. *Polymer* **2007**, *48*, 1165–1170.
- Boussu, K.; Zhang, Y.; Cocquyt, J.; Van Der Meeren, P.; Volodin, A.; Van Haesendonck, C.; Martens, J.; Van der Bruggen, B. *J. Membr. Sci.* **2006**, *278*, 418–427.
- Van der Bruggen, B.; Mänttari, M.; Nyström, M. *Sep. Purif. Technol.* **2008**, *63*, 251–263.
- Mänttari, M.; Pihlajamäki, A.; Nyström, M. *J. Membr. Sci.* **2006**, *280*, 311–320.

- (47) Schaep, J.; Van der Bruggen, B.; Vandecasteele, C.; Wilms, D. *Sep. Purif. Technol.* **1998**, *14*, 155–162.
- (48) Liu, X.; Bruening, M. L. *Chem. Mater.* **2004**, *16*, 351–357.
- (49) Nilsson, M.; Trägårdh, G.; Östergren, K. *J. Membr. Sci.* **2008**, *312*, 97–106.
- (50) Malaisamy, R.; Bruening, M. L. *Langmuir* **2005**, *21*, 10587–10592.
- (51) Bason, S.; Kedem, O.; Freger, V. *J. Membr. Sci.* **2009**, *326*, 197–204.
- (52) Stanton, B. W.; Harris, J. J.; Miller, M. D.; Bruening, M. L. *Langmuir* **2003**, *19*, 7038–7042.
- (53) Szymczyk, A.; Fievet, P. *J. Membr. Sci.* **2005**, *252*, 77–88.
- (54) Tieke, B.; Van Ackern, F.; Krasemann, L.; Toutianoush, A. *Eur. Phys. J. E* **2001**, *5*, 29–39.
- (55) Jin, W.; Toutianoush, A.; Tieke, B. *Langmuir* **2003**, *19*, 2550–2553.
- (56) Schaep, J.; Vandecasteele, C.; Wahab Mohammad, A.; Richard Bowen, W. *Sep. Purif. Technol.* **2001**, *22*, 169–179.
- (57) Van Gestel, T.; Vandecasteele, C.; Buekenhoudt, A.; Dotremont, C.; Luyten, J.; Leysen, R.; Van der Bruggen, B.; Maes, G. *J. Membr. Sci.* **2002**, *209*, 379–389.
- (58) Nanda, D.; Tung, K. L.; Li, Y. L.; Lin, N. J.; Chuang, C. J. *J. Membr. Sci.* **2010**, *349*, 411–420.





# Tuning the nanofiltration performance of thin film strong polyelectrolyte hydrogel composite membranes by photo-grafting conditions

Roy Bernstein<sup>a</sup>, Enrique Antón<sup>a,b</sup>, Mathias Ulbricht<sup>a,c,\*</sup>

<sup>a</sup> Lehrstuhl für Technische Chemie II, Universität Duisburg-Essen, 45117 Essen, Germany

<sup>b</sup> Department of Chemical and Environmental Engineering, University of Oviedo, 33006 Oviedo, Spain

<sup>c</sup> Centre for Water and Environmental Research (ZWU), University of Duisburg-Essen, 45141 Essen, Germany

## ARTICLE INFO

### Article history:

Received 31 July 2012

Received in revised form

12 September 2012

Accepted 19 September 2012

Available online 26 September 2012

### Keywords:

Nanofiltration membrane

UV-photo polymerization

Polyelectrolyte hydrogel

Membrane modification

## ABSTRACT

Polyethersulfone ultrafiltration membranes were converted into charged nanofiltration membranes having a strong polyelectrolyte hydrogel as selective barrier layer through the UV-photo initiated graft polymerization technique. This was accomplished by using vinyl sulfonic acid as the functional monomer and N,N'-methylenebisacrylamide as a cross linker monomer (Bernstein et al., ACS Applied Materials & Interfaces, 4 (2012) 3438–3446). In this research the resulting composite membranes were further characterized using different methods (ATR-FTIR spectroscopy, zeta potential, contact angle, scanning electron microscopy). ATR-FTIR data were used to quantify the degree of grafting. The composite membranes' zeta potential was negative throughout the pH range and as high as  $-70$  mV. The hydrogel composite membranes were also very hydrophilic with a contact angle of  $11^\circ$ . The membrane performance—salt rejection and water permeability—obtained at varied functionalization conditions—molecular weight cut-off of the base membrane, monomer concentration, cross linker fraction, UV irradiation intensity and time—was systematically investigated and the results were correlated to the membrane characterization data. Separation performance was also tested using mixed salt solutions. Larger composite membrane samples were prepared and long-term stability of nanofiltration (NF) performance was evaluated in cross-flow experiments. The performance of the best of the newly fabricated composite membranes was comparable to other polyelectrolyte-based NF membranes as well as to some commercial NF membranes presented in the literature.

© 2012 Elsevier B.V. All rights reserved.

## 1. Introduction

The separation properties of nanofiltration (NF) membranes are between those for materials used for reverse osmosis (RO) and ultrafiltration (UF). These membranes are characterized by high rejection of multivalent ions and uncharged solutes (above 300 g/mol), high flux at a relatively low pressure and low operational and maintenance costs [1].

NF membranes are used today in many applications, including water softening [2], and removal of dissolved organic matter from natural [3], municipal [4], and industrial [5] water sources. Because of their advantages, the use of such membranes for other applications is also being explored [6–8]. Yet, the current commercial NF membranes have some shortcomings [1], therefore, new NF membranes are being developed.

NF membranes are usually made from polymeric materials, though ceramic membranes are also available [9]. The most common commercial polymeric NF membrane is a composite structure

with a thin selective barrier layer made of a slightly negatively charged polyamide fabricated by interfacial polymerization. These membranes have a high salt rejection but they have a poor resistance to chlorine and similar oxidative disinfectants [10], and a high fouling and biofouling propensity [11], because of their relatively high hydrophobicity. This type of membrane is also sensitive to temperatures higher than  $40^\circ\text{C}$ , to extreme pH values ( $\text{pH} < 2$  or  $\text{pH} > 12$ ), and to organic solvents. Other commercially available NF membranes are made from positively charged polyamide and negatively charged sulfonated polyethersulfone. The latter membranes have better stability, but usually a lower separation performance.

For the past years many attempts have been made to fabricate NF membranes that will overcome the aforementioned drawbacks. These include the improvement of the current NF membranes [12,13], the synthesis of NF membranes from new materials [14–16] and the use of new fabrication techniques [17–19].

NF membranes having a polyelectrolyte as a selective barrier layer presented promising results, especially thin-film composite membranes which were fabricated using the 'layer by layer' (LBL) deposition technique [17,20–22]. However, this method is still complicated and difficult to up-scale for commercial usage [23,24]. Another appealing and easy method for obtaining a

\* Corresponding author at: Universität Duisburg-Essen Lehrstuhl für Technische Chemie II 45117 Essen, Germany. Tel.: +49 201 1833151; fax: +49 201 1833147.  
E-mail address: [mathias.ulbricht@uni-essen.de](mailto:mathias.ulbricht@uni-essen.de) (M. Ulbricht).

polyelectrolyte-based membrane is by surface graft copolymerization of a thin film of a suited charged polymer on a UF base membrane, most preferably using the UV-photo irradiation method. This method was successfully applied for modification of UF to NF membranes [25–29]. Yet, many of these membranes had either low rejection or low permeability. Another way which might result in an improved polyelectrolyte NF membrane while still using the relatively simple photo-initiated graft copolymerization method is the fabrication of a hydrogel as a selective barrier layer. This can be realized by copolymerization of a functional monomer and a cross linker monomer on a UF support membrane. Functionalization of UF membranes with hydrogel layers by UV-photo initiated graft copolymerization was already performed for other applications such as pervaporation [30], the improvement of protein separation [31] and the reduction of fouling and biofouling propensity for UF and RO membranes [32–34].

In a previous paper, we had explored the possibility of broadening this approach and functionalizing an UF membrane with a polyelectrolyte hydrogel, thus converting it into a NF membrane [35]. It was shown that a negatively charged strong polyelectrolyte hydrogel can be successfully fabricated on a polyethersulfone (PES) UF membrane by means of UV-photo initiated graft polymerization using vinyl sulfonic acid (VSA) as functional monomer and *N,N'*-methylenebisacrylamide (MBAA) as a cross linker monomer. In addition, it was demonstrated that the fabricated membrane had significant advantages over other NF membranes: a very low surface roughness, a stable salt rejection with increased salt concentration which only slightly reduced at high concentration (up to 8 g/L  $\text{Na}_2\text{SO}_4$ ), and a stable performance at low and high pH values (pH 1.5 and pH 10). While the focus of the previous work had been onto the functionalization and its mechanism and the application potential, in the current study, the polyelectrolyte hydrogel composite NF membranes were further characterized and their separation performance as function of different fabrication conditions was investigated in detail. Ultimately, correlations between preparation conditions, surface and barrier structure and separation performance were established, and the membranes were compared with other NF membranes reported in the literature.

## 2. Experimental

### 2.1. Materials

The polyethersulfone (PES) membranes were supplied by Sartorius Stedim Biotech S.A. (Göttingen, Germany) with nominal molecular weight cut off (MWCO) in the range from 10 kDa to 300 kDa. It is noted that in a previous report the MWCO of these membranes measured using dextrans as probes was found higher for all membranes [36]. Prior to the modification the membranes were cut with a 56 mm diameter punch hole and washed in methanol for 1 h, then thoroughly washed with Milli-Q water and left in Milli-Q water until used.

Vinylsulfonic acid sodium salt (VSA; 25% in water), *N,N'*-methylenebisacrylamide (MBAA),  $\text{MgSO}_4$ ,  $\text{NaCl}$ ,  $\text{Na}_2\text{SO}_4$  and  $\text{CaCl}_2$  and glucose were purchased from Aldrich and used without purification. Sucrose was purchased from Acros, Geel, Belgium. As reference substance for the ATR-FTIR spectra polyvinylsulfonic acid (PVSA; 25%, Sigma-Aldrich) was used and air dried before the measurement.

In order to obtain a monomer solution with 40% VSA, the 25% VSA solution was concentrated under reduced pressure at 37 mbar and 45 °C. The monomer concentration was 40% when the solution density was 1.32 g/L.

All experiments were done with purified water from a Milli-Q system from Millipore.

### 2.2. Modification procedure

The modification was carried out as described in our previous report [35]. Briefly, 5 mL monomer/ cross linker solution (which had been deaerated with nitrogen for 10 min) was placed on the surface of a PES membrane (56 mm). The membrane was covered with a special glass filter to narrow the UV wavelength to  $\lambda = 315\text{--}400$  nm, was put inside the UV photo reactor (UVA Cube 2000, Hönle AG, Germany; equipped with a 20 cm long mercury lamp, allowing a homogenous irradiation of 0.1 m<sup>2</sup> area via reflecting walls) and was immediately irradiated for various times (4.5–35 min) and at 16 or at 50 mW/cm<sup>2</sup> irradiation intensity. Thereafter, the membrane was washed with Milli-Q water for 24 h at room temperature and stored in Milli-Q water until further used.

For the long term NF experiment a 30 kDa PES membrane having an effective area of 84 cm<sup>2</sup> was covered with a filter paper to attain a homogenous distribution of the monomer solution over the membrane. The monomer/ cross linker mixture (25% VSA and 1.5% MBAA, in water) was poured over the filter paper soaking it up completely and the membrane was UV-irradiated at 50 mW/cm<sup>2</sup> for 18 min.

### 2.3. Degree of grafting

The degree of grafting ( $DG_s$ ) was determined by attenuated total reflection Fourier transform infrared (ATR-FTIR) spectroscopy (Varian 3100, USA equipped with a one reflection KRS-5 crystal, 45°; sixty-four scans were taken for each spectrum at a resolution of 4 cm<sup>-1</sup>) and defined as follows:

$$DG_s = I_{mon}/I_{mem}, \quad (1)$$

where  $I_{mon}$  is the intensity of the 1040 cm<sup>-1</sup> band assigned to the symmetric stretching of the VSA sulfonate group and  $I_{mem}$  is the intensity of the 1577 cm<sup>-1</sup> band, a C-H peak from the aromatic ring in the base PES membrane which does not appear in the functional monomer or the cross linker IR spectra.

### 2.4. Membrane characterization

**Zeta potential** was measured using a SurPASS streaming current analyzer (Anton Paar GmbH, Graz, Austria) with an adjustable gap cell that was set to 100 μm and at pressure differentials of 0–400 mbar. Prior to measurement the membranes were soaked for few hours in 1 mM KCl solution. Three distinct samples were measured; each sample was measured in two cycles at each direction and was rinsed 10 minutes at each new pH value. The background solution used was 1 mM KCl and the pH was adjusted using HCl (0.1 M) and NaOH (0.1 M). The zeta potential was calculated using the Fairbrother-Mastin equation.

**Contact angle** was determined using the captive bubble method with an optical measurement system (OCA 15 Plus, Dataphysics GmbH, Filderstadt, Germany). An air bubble of 5 μL was released from a stainless steel needle onto the inverted sample with its separation layer surface immersed into Milli-Q water. The reported values are the average of at least 2 distinct membrane samples and 5 measurements on each sample.

**Scanning electron microscopy (SEM)** images of the modified membranes surface and cross section were examined with a ESEM Quanta 400 FEG instrument (FEI) at standard high-vacuum conditions. A K 550 sputter coater (Emitech, U.K.) was used to coat the outer surface of the sample with gold. The cross section images were obtained by cutting the membrane in liquid nitrogen.

## 2.5. Membrane performance

Salt rejection and permeability were measured using a dead-end cell (Amicon 8050, Millipore) connected to a reservoir at 2–4 bar (pressurized with nitrogen) at 600–700 rpm stirring rate. Single salt concentration was typically 1 g/L. Salt rejection ( $R$ ) was calculated by:

$$R = (1 - C_p/C_f) * 100\%, \quad (2)$$

where  $C_f$  and  $C_p$  are the salt concentrations in the feed and permeate, respectively. Actual salt concentrations were obtained from conductivity analyses.

Membrane permeability ( $L_p$ ) using Milli-Q water was determined by:

$$L_p = V/(A*t*P), \quad (3)$$

where  $A$  is the membrane area ( $m^2$ ),  $t$  time (hour),  $P$  applied pressure (bar) and  $V$  the water volume collected ( $L$ ).

Sucrose or glucose rejection, separately, were measured at the same conditions as for the salt rejection and at a concentration of 1 mM. The solute concentrations in the feed and in the permeate were measured by TOC analyzer (Shimadzu, Japan; Model: TOC-VCSH) and the rejection was calculated using Eq. (2).

Mixed-salt experiments were carried out similarly to the experiments with the single salt solutions at 4 bar applied pressure. The solutions composition, the total dissolved salt concentration (TDS), and the ions concentrations are listed in Table 1.

It is noted that due to the different osmotic pressure of the mixed salt solutions the concentration polarization is different and the performance between the solutions can only roughly be compared.

Ion concentrations of the mixed electrolyte solutions were measured with the ion chromatograph 883 Basis IC plus (Metrohm). For the cation analysis a Metrosep C4-100/4.0 column was used and the eluent was 1.7 mM  $HNO_3$  and 0.7 mM pyridine-2,6-dicarboxylic acid. For the anion analysis the column was a MetrosepA Supp4 250/4.0 and the eluent was 1.8 mM  $Na_2CO_3$  and 1.7 mM  $NaHCO_3$  in a 0.8/0.2 V/V Milli-Q water/acetonitrile solution. Eluent flow was fixed at 1 mL/min for both ions analyses.

Long time stability experiment (6 days) was conducted with a cross flow laboratory scale unit (LSta05-2 laboratory CF filtration, Simatec, Germany) in a close loop mode (circulating the permeate and the concentrate back to the feed tank). The filtration test was done with 1 g/L  $Na_2SO_4$  at 4 bar, 25 °C and a cross flow velocity of 40 mL/min corresponding to a linear velocity of 0.314 m/s. The flux and the feed and permeate conductivity were measured every 12 h.

## 3. Results and discussion

### 3.1. Membrane characterization

#### 3.1.1. ATR-FTIR spectroscopy

Fig. 1 presents the ATR-FTIR spectra of the functional polymer (PVSA), the unmodified 30 kDa PES membrane (PES), one modified membrane (PES-g-PVSA-co-PMBAA), and the cross linker monomer (MBAA). The marked peak at  $1577\text{ cm}^{-1}$  is characteristic of the PES

membrane, is assigned to the aromatic ring in PES, and does not appear in the MBAA or the PVSA spectra. The second marked peak at  $1040\text{ cm}^{-1}$  is the characteristic band of the sulfonic acid group of the PVSA which is not present in the MBAA or the PES spectra. Both bands are visible in the spectrum of the newly fabricated membrane (PES-g-PVSA-co-PMBAA); therefore, these bands can indicate a successful modification and were used for the calculation of the  $DG_s$  (see section 2.3).

#### 3.1.2. Zeta potential

Fig. 2 presents the zeta potential of the modified membranes synthesized at different cross linker fractions. It is noted that the zeta potential in Fig. 2 is a representative one for each condition, but the three measurements for each condition were similar in all cases.

The pristine PES membrane has an isoelectric point at pH  $\sim 3.5$ , similar to the one found for other PES or polysulfone membranes [33,37–39]; whereas, the zeta potential of the modified membranes is negative throughout the pH range, even for those prepared without a cross linker (0% MBAA). The relatively high negative surface charge of the pristine PES membrane at pH  $> 4$  can be attributed to the preferred adsorption of the less hydrated anions to the uncharged membrane surface [33,37–39]. The high negative zeta potential of the modified membranes throughout the pH values may be expected because of the strong acidic sulfonic acid group in PVSA and the high charge density of the functional monomer VSA. The zeta potential becomes less negative with a decrease in the pH following modification using a cross linker concentration below 1.5%, due to a relatively low  $DG_s$  [35], leading to a lower charge density of the outer membrane surface. After functionalization with 1.5% (not shown) and 2.5% MBAA the zeta potential is highly negative (approximately  $-70\text{ mV}$ ) and almost constant throughout the pH values. This indicates a high charge density of the newly introduced barrier

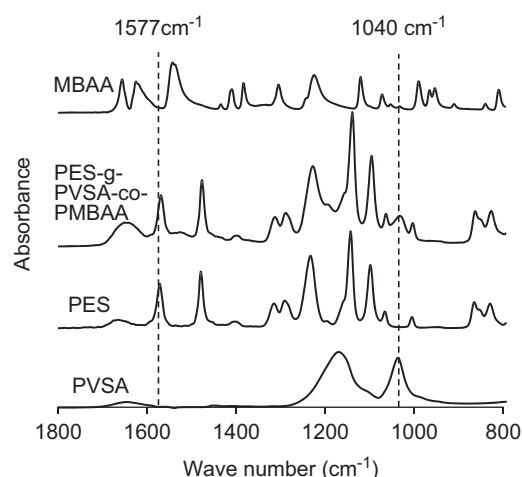


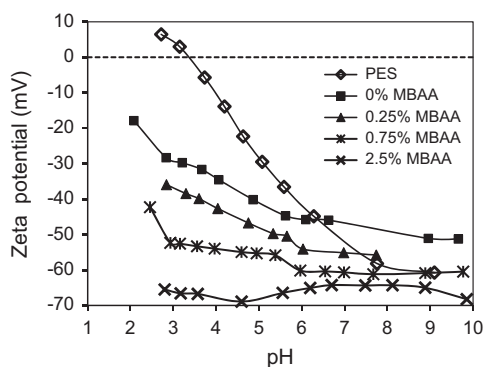
Fig. 1. ATR-FTIR spectra of polyvinylsulfonic acid (PVSA), the pristine 30 kDa PES UF membrane (PES), N,N'-methylenebisacrylamide (MBAA) and one modified membrane (PES-g-PVSA-co-PMBAA). Modification conditions: 25% VSA, 1.5% MBAA,  $I = 50\text{ mW/cm}^2$ ,  $t = 18\text{ min}$ .

Table 1

Mixed salt solution compositions, their total concentrations (TDS) and the specific ions concentrations.

Salt	TDS (ppm)	$Na^+$ (ppm)	$Cl^-$ (ppm)	$SO_4^{2-}$ (ppm)	$Mg^{2+}$ (ppm)
$Na_2SO_4$ and NaCl	1563	563	500	500	–
$Na_2SO_4$ and $MgCl_2$	1750	250	728	522	250
$Na_2SO_4$ and $MgSO_4$	2010	250	–	1510	250
NaCl and $MgCl_2$	1613	250	1113	–	250

layer as was also displayed by the high ion-exchange capacity of the grafted PVSA-based hydrogels reported previously [35]. Zeta potential following modification with 12.5% VSA was also negative at the different pH values (results not shown), but it was less negative than with 25% VSA, consistent with the high cross linker fraction found in the hydrogel using this VSA concentration [35]. Consequently, the evaluation of NF performance was focused onto thin-film hydrogel composite membranes prepared at the higher VSA concentration(s).



**Fig. 2.** Zeta potential vs. pH of pristine and modified 30 kDa PES UF membranes prepared at different cross linker (MBAA) concentrations. Modification conditions: 25% VSA,  $t=18$  min,  $I=50$  mW/cm<sup>2</sup>. The data are a representative set for each condition, but the three measurements for each condition were similar in all cases (max. deviation 10%).

### 3.1.3. Contact angle

The effect of the modification on the membrane characteristics was further investigated by contact angle using the captive bubble method. The contact angle of the control PES 30 kDa membrane was  $(35 \pm 6)^\circ$  which is lower than that observed previously for a pristine PES 30 kDa [40]. This was probably because the control membrane had been irradiated with UV in Milli-Q water prior to the measurement [41], to allow the identification of effects of photo-grafted polymer onto surface wettability. At a low cross linker fraction (0.25% MBAA) the contact angle did not change significantly due to the low degree of modification (DG<sub>s</sub>). However, the contact angle decreased from  $(35 \pm 6)^\circ$  for the irradiated control membrane to  $(11 \pm 6)^\circ$  for the modified membrane (1.5% MBAA and 25% VSA). Moreover, the contact angle of a membrane modified with 12.5% VSA and 5% MBAA was  $(24 \pm 4)^\circ$ , probably due to the relatively high cross linker fraction in the modification layer as discussed before (section 3.1.2 and [35]).

### 3.1.4. Morphology from electron microscopy

The cross section morphology of the pristine PES membrane and the membranes modified with VSA at different cross linker concentrations was analyzed using SEM and the results are presented in Fig. 3a-d.

The barrier layer of the modified membranes appears to be denser than that of the pristine membrane, and its thickness increases with the cross linker concentration used during functionalization.

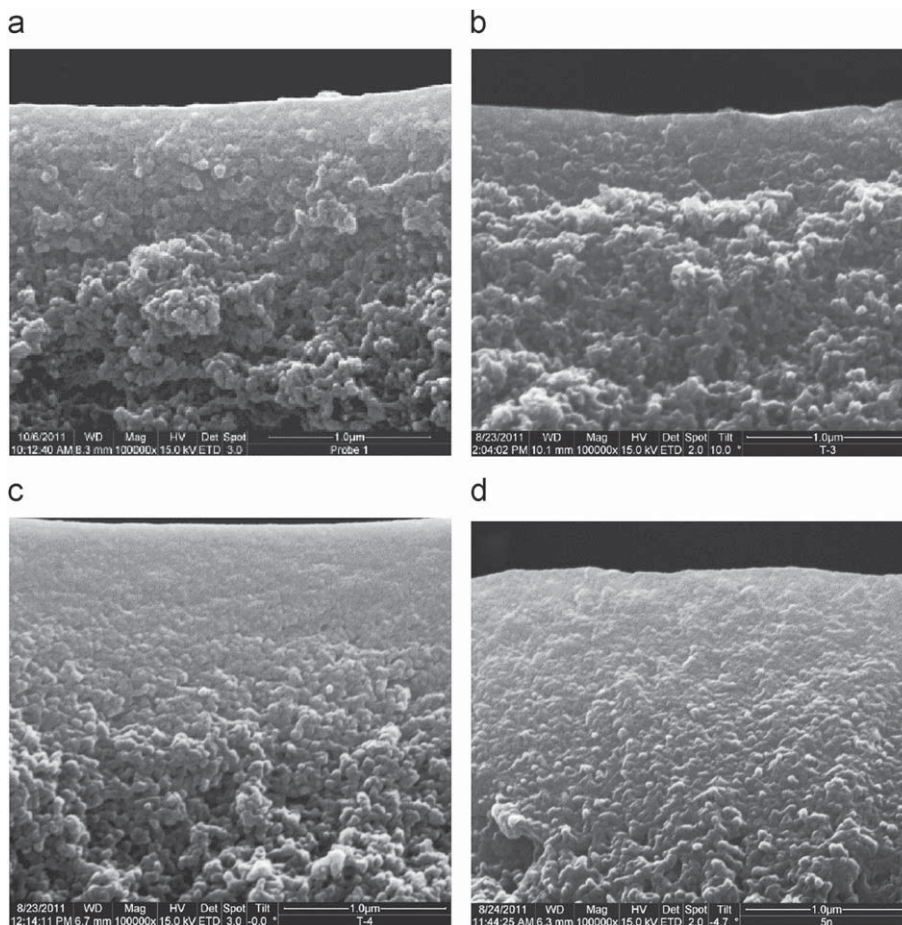


**Fig. 3.** SEM images of cross sections for pristine PES 30 kDa membrane (a) and modified PES 30 kDa membranes obtained with 0.75% (b), 1.5% (c) and 2.5% (d) cross linker (MBAA) concentration. Modification conditions: 25% VSA,  $t=18$  min,  $I=50$  mW/cm<sup>2</sup>.

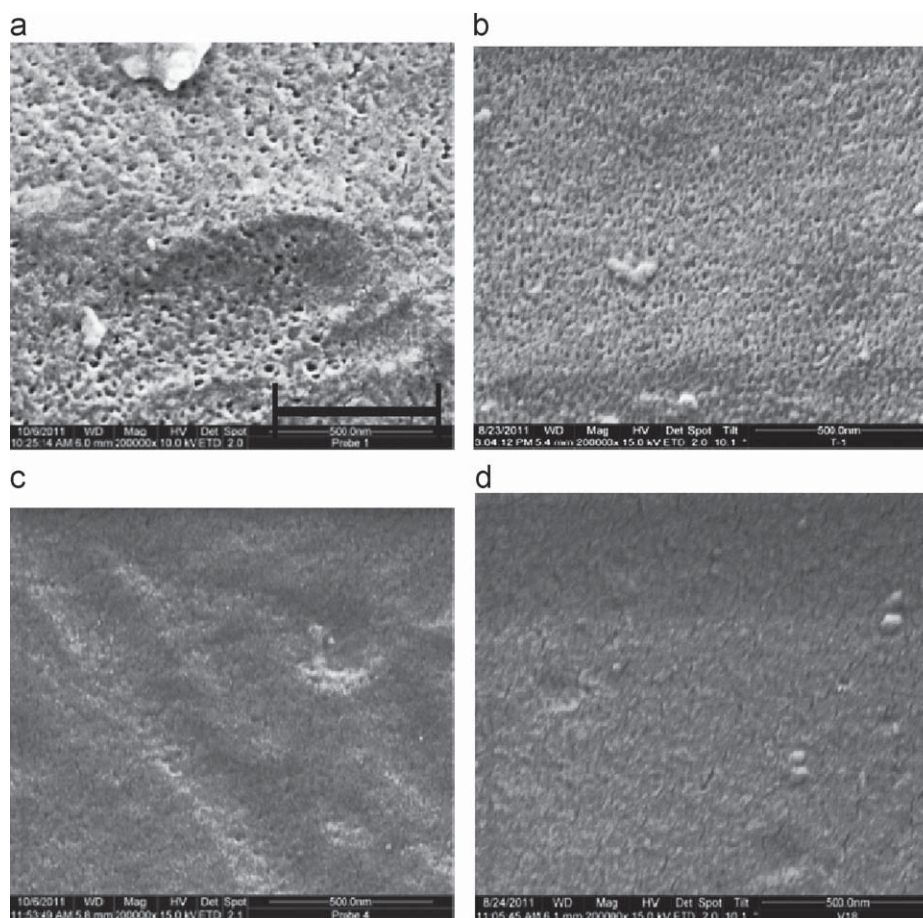


**Fig. 4.** SEM images of unmodified PES 30 kDa membrane (a) and modified PES 30 kDa membranes prepared with 0.25% (b), 0.75% (c), and 1.5% (d) cross linker (MBAA) concentration. Modification conditions: 25% VSA,  $I=50 \text{ mW/cm}^2$ ,  $t=18 \text{ min}$ . The scale bar in (a) represents 500 nm, all images are in the same magnification.

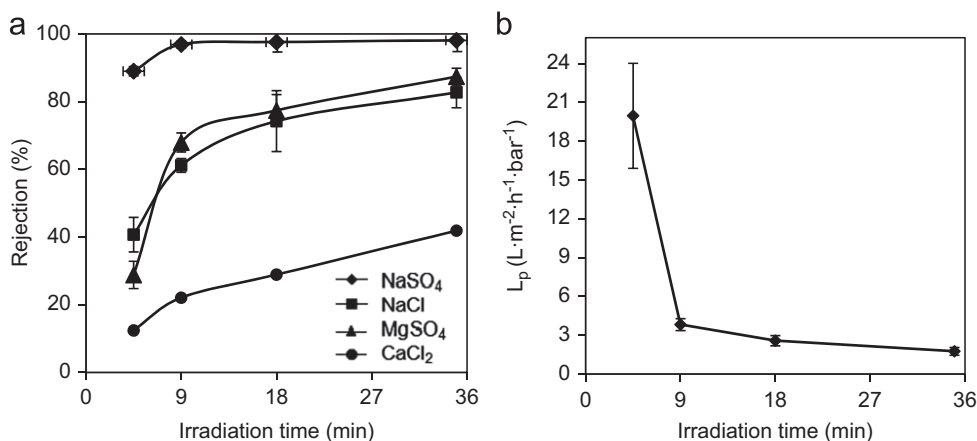


**Fig. 5.** Single salt rejection (a) and water permeability ( $L_p$ ) (b) for polyelectrolyte hydrogel composite membranes (base membrane MWCO 30 kDa) prepared at different UV irradiation time. Modification conditions: 25% VSA, 1.5% MBAA,  $I=50 \text{ mW/cm}^2$ ,  $t=18 \text{ min}$ . NF conditions:  $P=4 \text{ bar}$ , salt concentration 1 g/L.

The outer surface morphology also changed during the modification, as seen in the SEM images in Fig. 4a–d. The pristine membrane is presented in Fig. 4a. After functionalization without addition of cross linker no change in the membrane surface was seen (image is not shown). After functionalization at a low cross linker concentration (0.25% MBAA,  $DG_s=0.06$  and 0.75% MBAA,  $DG_s=0.17$ ) the membrane pores are still visible (Fig. 4b and c) and eventually disappear at higher cross linker concentration (1.5% MBAA,  $DG_s=0.29$ , Fig. 4d). The changes in the barrier layer and on the outer surface of the composite membranes can be very well

correlated with an increasing  $DG_s$  at higher cross-linker fraction at otherwise identical functionalization conditions (cf. [35]).

### 3.2. Membrane performance with single salt solution

The membrane performance was influenced by the different fabrication conditions examined during this study and typically changed in agreement with the  $DG_s$ . It is also important to note that each parameter was examined by itself while the others usually remained constant. Therefore, further investigation by



simultaneous parameter variations would still be possible. Nevertheless, it will be shown that by changing the various parameters the membrane performance can be altered considerably and that there is still room for further optimization.

### 3.2.1. Effect of irradiation time

The salt rejection and the membrane permeability following modification using 25% VSA and 1.5% MBAA at different irradiation times are summarized in Fig. 5a and b, respectively.

From Fig. 5a it is seen that a NF membrane (defined herein when the  $\text{Na}_2\text{SO}_4$  rejection was higher than 90%) was already obtained after 4.5 min of UV irradiation. Although it had been found that under this condition the  $\text{DG}_s$  is relatively low [35], a NF membrane could be obtained due to the high Donnan potential generated by the strong negatively charged polyelectrolyte barrier layer. However, the rejections of sodium chloride, magnesium sulfate and calcium chloride are relatively low at the early stages of the modification because they are less influenced by the Donnan potential. The rejection of these salts improves with the modification progress. This is attributed to the increasing contribution of steric exclusion, that was caused by a higher  $\text{DG}_s$  with a cross-linked hydrogel [35]. Parallel effects with increasing UV irradiation time are lower permeability (Fig. 5b) and increased rejection of uncharged glucose and sucrose (Fig. 6) which are only affected by the size exclusion and the steric hindrance.

### 3.2.2. Effect of the base membrane MWCO

The effect of the MWCO of the base PES membrane on the  $\text{Na}_2\text{SO}_4$  rejection at various cross linker fractions is presented in Table 2. It is seen that only above 0.75% MBAA a NF membrane could be obtained, regardless of the MWCO of the base membrane. Moreover, as the MWCO increased, a higher cross linker fraction was required to obtain a NF membrane. The salt rejection of composite membranes fabricated using base membranes with MWCO 10–50 kDa and 1.5% or 2.5% MBAA was comparable, while the permeability was reduced with decreasing MWCO. On the other hand, the rejection was much lower and the permeability higher when a PES membrane with MWCO of 100 kDa was used. For the latter, a NF membrane could only be obtained when 2.5% MBAA was used. Furthermore, when a base membrane with MWCO of 300 kDa was used the modification did not result in a NF membrane under any conditions.

Modification under identical conditions using a base membrane with MWCO of 100 kDa lead to higher degree of grafting ( $\text{DG}_s$ ) compared to the other membranes but still the salt rejection was significantly lower (Table 2). Therefore, it may be assumed that the

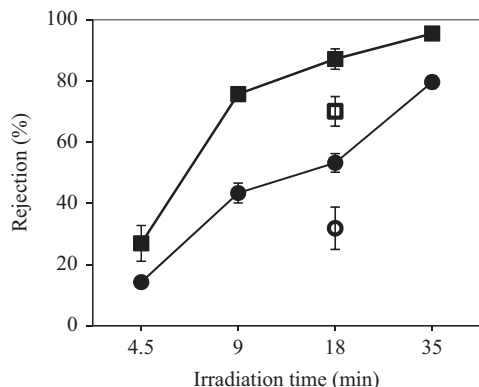


**Fig. 6.** Sucrose (squares) and glucose (circles) rejection of the polyelectrolyte hydrogel composite membranes (base membrane MWCO 30 kDa) prepared at different irradiation times and two monomer concentrations: 25% VSA (filled marks) and 40% VSA (empty marks). Modification conditions: 1.5% MBAA,  $I=50 \text{ mW/cm}^2$ . NF conditions:  $P=4 \text{ bar}$ , 1 mmol/L sucrose or glucose.

**Table 2**

Single salt rejection ( $R$ ) and water permeability ( $L_p$ ) of polyelectrolyte hydrogel composite membranes based on pristine membranes with different MWCO, prepared at different cross linker concentrations. Modification conditions: 25% VSA,  $I=50 \text{ mW/cm}^2$ ,  $t=18 \text{ min}$ . NF conditions:  $P=4 \text{ bar}$ , salt concentration 1 g/L.

MWCO (kDa)	Cross linker fraction (mol %)	$\text{DG}_s$	$R (\text{Na}_2\text{SO}_4)$ (%)	$L_p (\text{L m}^{-2} \text{ h}^{-1} \text{ bar}^{-1})$
10	0.75	0.127	$97.1 \pm 1.9$	$2.4 \pm 0.4$
30		0.172	$90.7 \pm 4.5$	$10.7 \pm 3.4$
50		n.a.*	$84.3 \pm 1.6$	$24.1 \pm 1.5$
10	1.5	0.418	$97.4 \pm 2.1$	$1.5 \pm 0.1$
30		0.564	$97.5 \pm 1.0$	$2.1 \pm 0.4$
50		n.a.*	$96.7 \pm 1.6$	$5.2 \pm 2.3$
100		0.723	$85.6 \pm 4.8$	$16.0 \pm 2.4$
10	2.5	0.799	99.5	0.6
30		0.909	$99.1 \pm 0.2$	$0.9 \pm 0.1$
50		n.a.*	$99.2 \pm 0.2$	$1.3 \pm 0.4$
100		1.520	$95.7 \pm 1.5$	$3.5 \pm 0.5$

\* n.a. not analyzed

different performance with increased MWCO of the base membrane derives from the differences in the base membranes morphology. PES membranes with MWCO 5–50 kDa have a different cross section structure and a lower barrier layer porosity than those with MWCO 100–300 kDa [42]. Since the modification occurs both on the outer membrane surface and inside the pores of the outer surface region [33,35,40], the degree of modification using membranes with a large MWCO can be higher. However, as shown in Table 2 and as was also observed in other work [20], this may not be advantageous for obtaining a NF membrane, since it probably results in a loose and ‘defect’-prone barrier layer. From Table 2 it may also be concluded that based on the tradeoff between rejection and permeability the composite membranes based on the membrane with MWCO 10 kDa have the lowest performance while the membranes fabricated using the one with MWCO 50 kDa have the highest one: At the same rejection, the permeability is at least twofold larger for the composite membranes based on MWCO 50 kDa compared to 10 kDa (@  $R=97\%$ :  $5.2$  vs.  $2.4$  to  $1.5 \text{ L m}^{-2} \text{ h}^{-1} \text{ bar}^{-1}$ ; @  $R>99\%$ :  $1.3$  vs.  $0.6 \text{ L m}^{-2} \text{ h}^{-1} \text{ bar}^{-1}$ ; cf. Table 2).

### 3.2.3. Effect of monomer concentration

The membrane performance following modification with 3 monomer concentrations (12.5%, 25% and 40%) and the varied cross linker concentrations was examined and the results for the 25% and 40% VSA are presented in Fig. 7. The salt rejection ( $\text{Na}_2\text{SO}_4$ ) using 12.5% VSA was lower than 80% ( $L_p \sim 4 \text{ L m}^{-2} \text{ h}^{-1} \text{ bar}^{-1}$ ), therefore, data is not presented. The low performance obtained with this concentration can be expected due to the relatively high cross linker fraction in the barrier layer, leading to relatively low ion-exchange capacity and hence Donnan exclusion [35]. The cross linker fraction in the monomer solutions with 40% VSA could not be higher than 1.5% MBAA, probably due to the ‘salting out’ effect by the strong electrolyte VSA. This limited solubility was seen visually and was also evident from the similar performance of composite membranes fabricated using the two cross linker fractions (Fig. 7).

The salt rejection of composite membranes which were fabricated using 25% VSA was usually higher while the permeability was lower even when the  $\text{DG}_s$  was similar (e.g., 25% VSA and 2.5% MBAA vs. 40% VSA and 1.5% MBAA). This may be due to a higher PVSA fraction in the grafted cross-linked hydrogel layer as was also measured by a higher ion-exchange capacity [35]. The higher PVSA fraction promotes higher swelling and, hence, higher permeability but also leads to lower steric hindrance/exclusion. This is also observed by the lower rejection of uncharged solutes with the composite membrane obtained using 40% VSA in

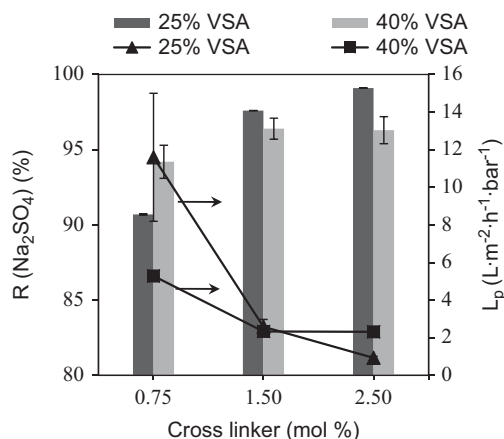


**Fig. 7.** Salt rejection ( $R$ ) and water permeability ( $L_p$ ) of polyelectrolyte hydrogel composite membranes (based on MWCO 30 kDa) prepared with 25% or 40% VSA. Modification conditions:  $I=50$  mW/cm<sup>2</sup>,  $t=18$  min. NF conditions:  $P=4$  bar, salt concentration 1 g/L.

comparison with the one modified using 25% VSA at otherwise the same conditions (cf. Fig. 6).

### 3.2.4. Effect of irradiation intensity

The effect of two irradiation intensities and three energy doses on the membranes rejection and permeability is presented in Table 3.

It was already shown that the  $DG_s$  for membranes irradiated with a similar UV dose was higher when the polymerization was carried out at a low intensity compared with a high one [35]. As a result, the salt rejection was usually higher while the permeability was lower following modification at low intensity (Table 3). Nevertheless, the advantage of irradiation at low intensity was evident only at low cross linker fraction (0.75% MBAA) or using low energy dose (240 mJ/cm<sup>2</sup>). Under the other conditions the salt rejection usually slightly improved but the permeability reduced substantially so that the overall performance deteriorated. This indicates that there is an optimum between the modification degree and the membrane performance as was also found in other work [43].

### 3.3. Membrane performance with mixed salts solutions

The rejection of four mixed salt solutions for composite membranes prepared at different cross linker fractions at otherwise identical fabrication conditions is presented in Fig. 8.

As expected, Fig. 8 shows that the rejection of the individual ions using the mixed salt solution is generally lower than the rejection with a single salt solution [44], even when the salt and the ion concentration are similar. For example, the  $SO_4^{2-}$  rejection (at 1.5% MBAA) is 85% for  $Na_2SO_4$  and  $NaCl$  (500 ppm  $SO_4^{2-}$ ) and 71% for  $Na_2SO_4$  and  $CaCl_2$  (500 ppm  $SO_4^{2-}$ ) compared with 97% for  $Na_2SO_4$  as single salt solution (800 ppm  $SO_4^{2-}$ ). The rejection of mixed salt solutions is governed by the charge and valence of the ions in the solutions. The divalent ions are rejected more than the monovalent ones regardless their electric charge. Moreover, the rejection of all ions decreases when the feed solution does not contain the sulfate ion, the divalent co-ion in respect to the active layer fixed charge (compare rejections for  $Cl^-$  and  $Na^+$  in Fig. 8a–b to Fig. 8c). The rejection of all ions also decreases when the solution contains all four ions (cf. Fig. 8d). The effect of the salt composition and the deviation from rejection based on Donnan exclusion were already explained in details before [45,46]. The decreased rejection for mixed salt solution

reflects the drawback of polyelectrolyte-based NF membranes which are governed by the Donnan exclusion. The rejection of membranes prepared using 2.5% MBAA was relatively high, for example >96% for  $Na_2SO_4$  and  $MgSO_4$  (Fig. 8b) and 67–92% for the various ions in  $CaCl_2$  &  $Na_2SO_4$  (Fig. 8d); however, the permeability was in the range of that for RO membranes, approximately  $1 \text{ L m}^{-2} \text{ h}^{-1} \text{ bar}^{-1}$  (see Table 3 and Fig. 5b). From Fig. 8 it is also seen that ions rejection improves as the cross linker fraction increases. This was also measured for membranes modified with increased UV irradiation time at otherwise constant fabrication conditions (results are not presented). This is similar to the result obtained using single salt solutions and is the consequence of increased steric exclusion with higher cross linker fraction and UV irradiation time as discussed before.

### 3.4. Membrane stability

The modification stability is demonstrated in Fig. 9 which describes the permeability and the  $Na_2SO_4$  rejection of a polyelectrolyte hydrogel composite membrane measured for the duration of 6 days in a cross flow filtration cell.

After a short induction period the permeability and rejection stabilized and remained so throughout the experiment. It is also noted that the membrane performance is similar to the one for membranes prepared using identical modification conditions but as small samples and characterized in the dead-end cells (see Fig. 3). This demonstrates the feasibility of conducting the fabrication using a membrane with larger surface area (here 84 cm<sup>2</sup> compared with 12.56 cm<sup>2</sup> in the dead-end cell experiments) while obtaining analogous results. It can also indicate the scalability of this method to fabricate a charged NF membrane having a polyelectrolyte hydrogel as a barrier layer for commercial applications.

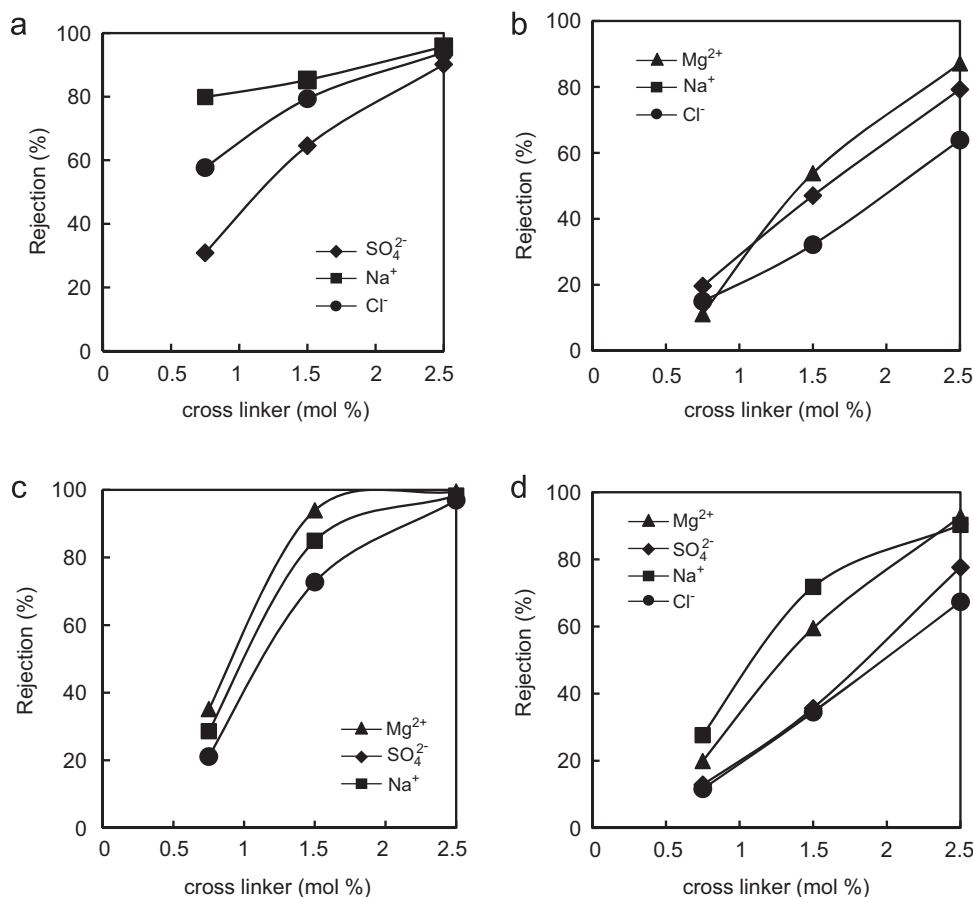
### 3.5. Performance of the newly fabricated composite membranes compared with other polyelectrolyte-based membranes

Fig. 10 presents the single salt passage (1-R) vs. water permeability for a few of the newly fabricated composite membranes (obtained under various conditions), of other polyelectrolyte-based NF membranes fabricated using different methods as reported in the literature (and with salt passage lower than 10% and  $L_p > 2 \text{ L m}^{-2} \text{ h}^{-1} \text{ bar}^{-1}$ ) [17,20–22,25,27,28,47,48] and of three commercial NF membranes [49,50]. The labels in Fig. 10 represent the  $DG_s$  for the newly fabricated membranes, the reference that the data were taken from for the other polyelectrolyte-based membranes and the commercial trade name of the commercial membranes. Because the experiments in the literature are conducted at various conditions, the best result for a single salt passage (if possible for 1 g/L and the lowest from the various salts tested in each reference which depends on the membrane surface charge) and the corresponding water permeability (in case that only salt solution permeability was reported, the osmotic pressure was estimated and the water permeability was calculated) were taken from each reference to represent this membrane in Fig. 10.

Fig. 10 shows that most membranes that were fabricated in this research follow a linear trend between salt passage and water permeability. However, this does not necessarily correlate with the  $DG_s$  (presented in the data labels in Fig. 10). This is probably a result of the different thickness and degree of cross linking of the barrier layer, also indicating that the membranes can be further optimized (not investigated in this research). From Fig. 10 it is also seen that the salt rejection obtained by the new membranes of this study is higher, but the overall performance is similar to the one for other membranes with grafted polyelectrolyte

**Table 3**  
Single salt rejection ( $R$ ) and water permeability ( $L_p$ ) of polyelectrolyte hydrogel composite membranes (base MWCO 30 kDa) obtained at 16 or 50 mW/cm<sup>2</sup> irradiation intensity ( $I$ ) and three different energy doses ( $I \cdot t$ ). NF conditions:  $P=4$  bar, salt concentration 1 g/L.

Cross linker (mol %)	Dose $I \cdot t$ (mJ/cm <sup>2</sup> )	R (Na <sub>2</sub> SO <sub>4</sub> ) (%)		R (NaCl) (%)		R (MgSO <sub>4</sub> ) (%)		R (CaCl <sub>2</sub> ) (%)		$L_p$ (L m <sup>-2</sup> h <sup>-1</sup> bar <sup>-1</sup> )	
		$I=16$	$I=50$	$I=16$	$I=50$	$I=16$	$I=50$	$I=16$	$I=50$	$I=16$	$I=50$
1.5	240	95.7	89.0	62.9	40.7	56.8	28.8	31.3	12.4	4.6	20.0
2.5		97.8	97.2	76.7	71.3	95.9	84.8	62.3	47.0	1.5	2.2
0.75		91.3	<90	48.9	n.a.	29.5	n.a.	n.a.	n.a.	9.6	n.a.
1.5	510	96.8	96.9	76.3	61.2	75.4	68.0	26.5	21.7	2.7	3.8
2.5		98.5	97.2	84.0	83.5	94.2	91.2	47.5	33.4	1.0	1.33
0.75		94.6	90.7	60.2	36.3	46.8	37.2	n.a.	11.0	6.3	10.7
1.5	900	97.5	97.9	81.7	74.3	86.4	61.9	19.5	28.9	1.3	2.6
2.5		97.9	99.1	90.2	92.5	98.9	92.2	39.2	63.6	0.6	0.9



**Fig. 8.** Rejection of individual ions for polyelectrolyte hydrogel composite membranes (base MWCO 30 kDa) prepared at different cross-linker concentration using four mixed-electrolyte solutions as feed: (a) NaCl: Na<sub>2</sub>SO<sub>4</sub>, (b) NaCl: MgCl<sub>2</sub>, (c) Na<sub>2</sub>SO<sub>4</sub>: MgSO<sub>4</sub> and (d) Na<sub>2</sub>SO<sub>4</sub>: MgCl<sub>2</sub>. Modification conditions: 25% VSA,  $I=50$  mW/cm<sup>2</sup>,  $t=18$  min. NF conditions: 4 bar; salt and ions concentration for each solution are listed in Table 1.

fabricated using the UV-photo polymerization technique as well as for the commercial SPES membranes (NF-PES10, NTR 7450; the separation of these membranes is also strongly influenced by Donnan exclusion). For similar, relatively low salt rejection, higher permeability compared to NF-PES10 can be achieved. For relatively high salt rejection, the advantage of using a base membrane with larger MWCO in terms of higher permeability is seen again (see membrane with label “n.a.” relative to dashed trend line in Fig. 10; cf. Section 3.2.2). However, the commercial polyamide thin-film composite NF membrane and thin-film polyelectrolyte composite membranes fabricated using the ‘LBL’ technique generally display a better performance. Nevertheless, the easy fabrication method presented here, its robustness and scalability in comparison with the other techniques, together

with the advantages presented in previous own work [35], make this composite membrane attractive; yet, its overall performance requires further improvement.

#### 4. Conclusions

A NF membrane with a strong polyelectrolyte hydrogel as the separation layer was successfully fabricated using the UV-photo initiated polymerization technique. Due to the strong polyelectrolyte structure of the newly introduced barrier layer, the zeta potential of the fabricated membrane was highly negative and almost constant throughout the entire pH range. SEM images demonstrated that the membrane surface was fully covered at

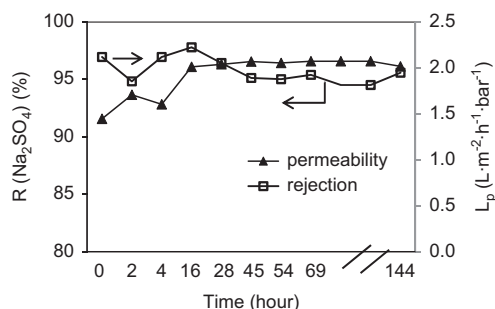


**Fig. 9.** Salt rejection ( $R$ ) and permeability ( $L_p$ ) for a larger composite membrane sample (base MWCO 30 kDa) measured in a cross flow cell vs. filtration time (cf. Experimental). Modification conditions: 25% VSA and 1.5% MBAA,  $I=55$  mW/cm<sup>2</sup>,  $t=18$  min. NF conditions:  $P=4$  bar.

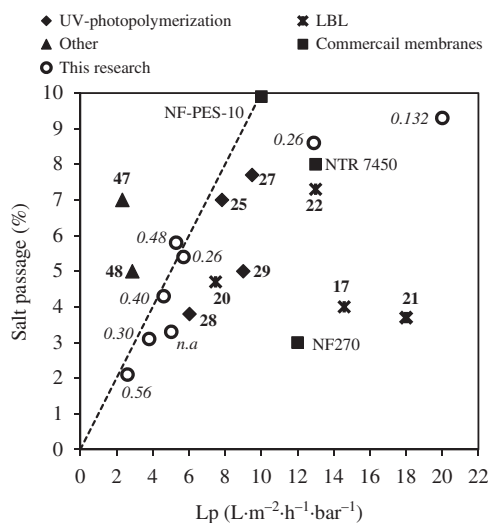


**Fig. 10.** Salt passage and water permeability of various polyelectrolyte-based membranes fabricated using: 'LBL' method (empty square), UV-photo polymerization (full diamond), other methods (full triangle) and from this research (empty circles) as well as three commercial NF membranes (full square). Data labels indicate  $DG_s$  for membrane fabricated in this research (all membranes are based on MWCO 30 kDa, except for "n.a." which is based on MWCO 50 kDa, cf. Table 2; membrane labeled "0.48" is prepared using 40% VSA, all other membranes using 25% VSA and variations of cross linker content, UV time and UV intensity, cf. Figs. 5 and 7 as well as Tables 2 and 3) and literature reference number for the other membranes; trade name is added to the data for commercial membranes (data from [49,50]).

high DGs while the contact angle measurement showed that this membrane is highly hydrophilic. The membrane performance at the various polymerization conditions was investigated. The cross linker and the monomer concentration had a significant influence on the surface functionalization. A NF membrane could be obtained at a cross linker fraction above 0.75 mol% (relative to the functional monomer VSA) and only when the functional monomer (VSA) concentration was equal or above 25%. An increase of VSA concentration to 40% resulted in a higher permeability, but a lower salt rejection for composite membranes with similar DGs, probably due to higher barrier layer swelling. A few minutes of UV irradiation were sufficient for the fabrication of a NF membrane. Further irradiation improved the rejection of all salts, probably because of the increased steric exclusion, but reduced the permeability. In addition, when the modification was carried out using low UV intensity, the membrane performance was better than for modification at high intensity, but only at a relatively low modification degree. It was also shown that when the MWCO of the base membrane was 10–50 kDa the salt rejection was similar while the permeability increased with increasing MWCO. For base membranes

with MWCO 100 kDa a NF membrane could be obtained only at a high cross linker fraction, while when the MWCO of the base membrane was 300 kDa the fabrication did not result in a NF membrane under any conditions. The effect of the MWCO was attributed to the differences in the base membrane cross section morphology. The membrane rejection of mixed salt solutions was lower than with single salt solutions, but was still high for bivalent salts depending on ion composition in the feed solution. This research also demonstrated that the modification can easily be carried out on a UF base membrane having a large area, while the membrane performance remained stable in a long term experiment; thus, it indicated the ability to scale-up the modification technique. The performance of the fabricated NF membranes obtained in this study was comparable to the best performance of polyelectrolyte NF membranes fabricated by various methods as reported in the literature and also to some commercially available membranes (based on sulfonated PES).

## Acknowledgments

R.B. gratefully acknowledges the 'Young Scientists Exchange Program' of the BMBF-MOST Water Technology Cooperation for the financial support. Further thanks are due to Mr. Smail Boukercha, Center for Scanning Electron Microscopy at the University of Duisburg-Essen, for conducting the SEM analyses and Sartorius Stedim A.S. for providing the base membranes.

## References

- [1] B. Van der Bruggen, M. Mänttari, M. Nyström, Drawbacks of applying nanofiltration and how to avoid them: a review, *Sep. Purif. Technol.* 63 (2008) 251–263.
- [2] B. Van der Bruggen, C. Vandecasteele, Removal of pollutants from surface water and groundwater by nanofiltration: overview of possible applications in the drinking water industry, *Environ. Pollut.* 122 (2003) 435–445.
- [3] R. Liikanen, I. Miettinen, R. Laukkanen, Selection of NF membrane to improve quality of chemically treated surface water, *Water Res.* 37 (2003) 864–872.
- [4] S.D. Kim, J. Cho, I.S. Kim, B.J. Vanderford, S.A. Snyder, Occurrence and removal of pharmaceuticals and endocrine disruptors in South Korean surface, drinking, and waste waters, *Water Res.* 41 (2007) 1013–1021.
- [5] S. Mutlu, U. Yetis, T. Gurkan, L. Yilmaz, Decolorization of wastewater of a baker's yeast plant by membrane processes, *Water Res.* 36 (2002) 609–616.
- [6] P. Vandezande, L.E.M. Gevers, I.F.J. Vankelecom, Solvent resistant nanofiltration: separating on a molecular level, *Chem. Soc. Rev.* 37 (2008) 365–405.
- [7] H. Zhang, H. Zhang, X. Li, Z. Mai, J. Zhang., Nanofiltration (NF) membranes: the next generation separators for all vanadium redox flow batteries (VRBs)? *Energy Environ. Sci.* 4 (2011) 1676–1679.
- [8] Y. Kaufman, R. Kasher, R.G.H. Lammertink, V. Freger., Microfluidic NF/RO separation: cell design, performance and application, *J. Membr. Sci.* 396 (2012) 67–73.
- [9] T. Van Gestel, C. Vandecasteele, A. Buekenhoudt, C. Dotremont, J. Luyten, R. Leysen, B. Van der Bruggen, G. Maes, Alumina and titania multilayer membranes for nanofiltration: preparation, characterization and chemical stability, *J. Membr. Sci.* 207 (2002) 73–89.
- [10] Y.N. Kwon, J.O. Leckie, Hypochlorite degradation of crosslinked polyamide membranes II. Changes in hydrogen bonding behavior and performance, *J. Membr. Sci.* 282 (2006) 456–464.
- [11] C.Y. Tang, Y.N. Kwon, J.O. Leckie, Fouling of reverse osmosis and nanofiltration membranes by humic acid—effects of solution composition and hydrodynamic conditions, *J. Membr. Sci.* 290 (2007) 86–94.
- [12] B. Van der Bruggen, Chemical modification of polyethersulfone nanofiltration membranes: a review, *J. Appl. Polym. Sci.* 114 (2009) 630–642.
- [13] A. Ben-David, R. Bernstein, Y. Oren, S. Belfer, C. Dosoretz, V. Freger, Facile surface modification of nanofiltration membranes to target the removal of endocrine-disrupting compounds, *J. Membr. Sci.* 357 (2010) 152–159.
- [14] L. Lianchao, W. Baoguo, T. Huimin, C. Tianlu, X. Jiping, A novel nanofiltration membrane prepared with PAMAM and TMC by in situ interfacial polymerization on PEK-C ultrafiltration membrane, *J. Membr. Sci.* 269 (2006) 84–93.
- [15] S. Cheng, D.L. Oatley, P.M. Williams, C.J. Wright, Positively charged nanofiltration membranes: review of current fabrication methods and introduction of a novel approach, *Adv. Colloid Interface Sci.* 164 (2011) 12–20.
- [16] M. Dalwani, G. Bargeman, S. Hosseiny, M. Boerrigter, M. Wessling, N.E. Benes, Sulfonated poly (ether ether ketone) based composite membranes for nanofiltration of acidic and alkaline media, *J. Membr. Sci.* 381 (2011) 81–89.

- [17] B.W. Stanton, J.J. Harris, M.D. Miller, M.L. Bruening, Ultrathin, multilayered polyelectrolyte films as nanofiltration membranes, *Langmuir* 19 (2003) 7038–7042.
- [18] S. Roy, S.A. Ntim, S. Mitra, K.K. Sirkar, Facile fabrication of superior nanofiltration membranes from interfacially polymerized CNT-polymer composites, *J. Membr. Sci.* 375 (2011) 81–87.
- [19] Z. Tang, C. Qiu, J.R. McCutcheon, K. Yoon, H. Ma, D. Fang, E. Lee, C. Kopp, B.S. Hsiao, B. Chu, Design and fabrication of electrospun polyethersulfone nanofibrous scaffold for highflux nanofiltration membranes, *J. Polym. Sci., Polym. Phys.* 47 (2009) 2288–2300.
- [20] R. Malaisamy, M.L. Bruening, High-flux nanofiltration membranes prepared by adsorption of multilayer polyelectrolyte membranes on polymeric supports, *Langmuir* 21 (2005) 10587–10592.
- [21] L. Ouyang, R. Malaisamy, M.L. Bruening, Multilayer polyelectrolyte films as nanofiltration membranes for separating monovalent and divalent cations, *J. Membr. Sci.* 310 (2008) 76–84.
- [22] H.Y. Deng, Y.Y. Xu, B.K. Zhu, X.Z. Wei, F. Liu, Z.Y. Cui, Polyelectrolyte membranes prepared by dynamic self-assembly of poly (4-styrenesulfonic acid-co-maleic acid) sodium salt (PSSMA) for nanofiltration (I), *J. Membr. Sci.* 323 (2008) 125–133.
- [23] M.L. Bruening, D.M. Dotzauer, P. Jain, L. Ouyang, G.L. Baker, Creation of functional membranes using polyelectrolyte multilayers and polymer brushes, *Langmuir* 24 (2008) 7663–7673.
- [24] P.T. Hammond, Engineering materials layerbylayer: challenges and opportunities in multilayer assembly, *AIChE J.* 57 (2011) 2928–2940.
- [25] C. Qiu, Q. Zhang, Z. Ping, Nanofiltration membrane preparation by photo-modification of cardo polyetherketone ultrafiltration membrane, *Sep. Purif. Technol.* 51 (2006) 325–331.
- [26] A. Akbari, S. Desclaux, J. Rouch, P. Aptel, J. Remigy, New UV-photografted nanofiltration membranes for the treatment of colored textile dye effluents, *J. Membr. Sci.* 286 (2006) 342–350.
- [27] H. Deng, Y. Xu, Q. Chen, X. Wei, B. Zhu, High flux positively charged nanofiltration membranes prepared by UV-initiated graft polymerization of methacrylateoethyl trimethyl ammonium chloride (DMC) onto polysulfone membranes, *J. Membr. Sci.* 366 (2011) 363–372.
- [28] X.L. Li, L.P. Zhu, Y.Y. Xu, Z. Yi, B.K. Zhu, A novel positively charged nanofiltration membrane prepared from N, N-dimethylaminoethyl methacrylate by quaternization cross-linking, *J. Membr. Sci.* 374 (2011) 33–42.
- [29] P. Zhong, N. Widjojo, T.S. Chung, M. Weber, C. Maletzko, Positively charged nanofiltration (NF) membranes via UV grafting on sulfonated polyphenylenesulfone (sPPSU) for effective removal of textile dyes from wastewater, *J. Membr. Sci.* 417–418 (2012) 52–60.
- [30] M. Ulbricht, H.H. Schwarz, Novel high performance photo-graft composite membranes for separation of organic liquids by pervaporation, *J. Membr. Sci.* 136 (1997) 25–33.
- [31] M. Ulbricht, H. Matuschewski, A. Oechel, H.G. Hicke, Photo-induced graft polymerization surface modifications for the preparation of hydrophilic and low-protein-adsorbing ultrafiltration membranes, *J. Membr. Sci.* 115 (1996) 31–47.
- [32] P.D. Peeva, T. Pieper, M. Ulbricht, Tuning the ultrafiltration properties of anti-fouling thin-layer hydrogel polyethersulfone composite membranes by suited crosslinker monomers and photo-grafting conditions, *J. Membr. Sci.* 362 (2010) 560–568.
- [33] H. Susanto, M. Ulbricht, Photografted thin polymer hydrogel layers on PES ultrafiltration membranes: characterization, stability, and influence on separation performance, *Langmuir* 23 (2007) 7818–7830.
- [34] I. Eshet, V. Freger, R. Kasher, M. Herzberg, J. Lei, M. Ulbricht, Chemical and physical factors in design of antibiofouling polymer coatings, *Biomacromolecules* 12 (2011) 1169–1177.
- [35] R. Bernstein, E. Antón, M. Ulbricht, UV-photo graft functionalization of polyethersulfone membrane with strong polyelectrolyte hydrogel and its application for nanofiltration, *ACS Applied Materials & Interfaces* 4 (2012) 3438–3446.
- [36] P.D. Peeva, T. Knoche, T. Pieper, M. Ulbricht, Cross-flow ultrafiltration of protein solutions through unmodified and surface functionalized polyethersulfone membranes-Effect of process conditions on separation performance, *Sep. Purif. Technol.* 92 (2012) 83–92.
- [37] D. Möckel, E. Staude, M. Dal-Cin, K. Darcovich, M. Guiver, Tangential flow streaming potential measurements: hydrodynamic cell characterization and zeta potentials of carboxylated polysulfone membranes, *J. Membr. Sci.* 145 (1998) 211–222.
- [38] C. Werner, U. König, A. Augsburg, C. Arnhold, H. Körber, R. Zimmermann, H.J. Jacobasch, Electrokinetic surface characterization of biomedical polymers—a survey, *Colloids Surf. Physicochem. Eng. Aspects* 159 (1999) 519–529.
- [39] M. Ariza, J. Benavente, Streaming potential along the surface of polysulfone membranes: a comparative study between two different experimental systems and determination of electrokinetic and adsorption parameters, *J. Membr. Sci.* 190 (2001) 119–132.
- [40] P.D. Peeva, N. Million, M. Ulbricht, Factors affecting the sieving behavior of anti-fouling thin-layer cross-linked hydrogel polyethersulfone composite ultrafiltration membranes, *J. Membr. Sci.* 390–391 (2012) 99–112.
- [41] J. Pieracci, J.V. Crivello, G. Belfort, Photochemical modification of 10 kDa polyethersulfone ultrafiltration membranes for reduction of biofouling, *J. Membr. Sci.* 156 (1999) 223–240.
- [42] P.D. Peeva, A.E. Palupi, M. Ulbricht, Ultrafiltration of humic acid solutions through unmodified and surface functionalized low-fouling polyethersulfone membranes-Effects of feed properties, molecular weight cut-off and membrane chemistry on fouling behavior and cleanability, *Sep. Purif. Technol.* 81 (2011) 124–133.
- [43] R. Bernstein, S. Belfer, V. Freger, Toward improved boron removal in RO by membrane modification: feasibility and challenges, *Environ. Sci. Technol.* 45 (2011) 3613–3620.
- [44] J. Schaep, B. Van der Bruggen, C. Vandecasteele, D. Wilms, Influence of ion size and charge in nanofiltration, *Sep. Purif. Technol.* 14 (1998) 155–162.
- [45] J. Garcia-Aleman, J.M. Dickson, Permeation of mixed-salt solutions with commercial and pore-filled nanofiltration membranes: membrane charge inversion phenomena, *J. Membr. Sci.* 239 (2004) 163–172.
- [46] G. Hagemeyer, R. Gimbel, Modelling the salt rejection of nanofiltration membranes for ternary ion mixtures and for single salts at different pH values, *Desalination* 117 (1998) 247–256.
- [47] Y. Ji, Q. An, Q. Zhao, H. Chen, J. Qian, C. Gao, Fabrication and performance of a new type of charged nanofiltration membrane based on polyelectrolyte complex, *J. Membr. Sci.* 357 (2010) 80–89.
- [48] C. Ba, D.A. Ladner, J. Economy, Using polyelectrolyte coatings to improve fouling resistance of a positively charged nanofiltration membrane, *J. Membr. Sci.* 347 (2010) 250–259.
- [49] M. Manttari, A. Pihlajamaki, M. Nystrom, Effect of pH on hydrophilicity and charge and their effect on the filtration efficiency of NF membranes at different pH, *J. Membr. Sci.* 280 (2006) 311–320.
- [50] M. Ernst, A. Bismarck, J. Springer, M. Jekel, Zeta-potential and rejection rates of a polyethersulfone nanofiltration membrane in single salt solutions, *J. Membr. Sci.* 165 (2000) 251–259.

## **6. Conclusions**

---

---



## 6.1. Membrane ageing

---

- Permeability, MWCO determinations (UF) and charged and uncharged solute marker rejection measurements (NF) were successfully employed to follow the membrane functional performance throughout the different ageing conditions.
- The use of surface analysis techniques, specifically ATR-FTIR, SEM-EDS, AFM and contact angle measurements, were positively applied to determine the chemical and morphological changes on membranes as consequence of the exposure to the cleaning chemicals and to explain membrane performance.
- Variations in performance due to both conditioning and ageing usually take place in the very first days of exposure to the ageing solutions for the UF membranes (around 10 days).
- Even though the active layer material of the UF membranes is PES, support layers are made of different materials, specifically PET (Koch and GE Osmonics membranes) and a mixture of PE and PP (Nadir ones), fact which plays an important role in the membrane performance under certain ageing conditions.
- Under the 1.0 M HNO<sub>3</sub> and NaOH ageing solutions, the low MWCO Nadir membranes are affected by the osmotic stress due to the high ionic concentration leading to an apparent effective pore reduction which decreases both permeability and MWCO. This effect is not significant for the rest of the UF membranes. Apart from this phenomenon, performance of all Nadir membranes follows the same pattern as that of the reference ones, meaning a stable behavior. In addition, the lack of significant changes in the functional group composition, the hydrophilicity, the structure and the topography of the active and/or the support layers of the Nadir membranes goes in accordance to their performance.
- Koch and GE Osmonics membranes also shows a high stability in all the tested acidic conditions which is in agreement with the physicochemical characterizations. Under alkaline conditions, permeability and MWCO of PT membrane increases with concentration mainly because of the PET support layer degradation. On the other hand, changes in the HFK-328 membrane performance are only visible for the highest concentration due to its higher active layer thickness.
- The ageing of the NF membranes leads to a continuous increase in permeability and decrease in rejection capability with time, being the membranes more resistant to the acidic than to the alkaline ageing conditions. In addition, NF90 membrane is more stable than the NF270 one under equivalent conditions.



- Changes in performance of both membranes are due to the degradation of the PA active layers through a hydrolysis reaction which is successfully quantified by means of the amide I and II bands from ATR-FTIR measurements. Moreover, SEM micrographs show the degradation of the backing layer of both membranes under high alkaline conditions.
- Degradation of NF membranes takes place faster in soaking mode than in cross-flow, likely because of the more thorough contact with the chemicals. Therefore, extrapolation of membrane lifetimes from data in soaking mode would result in a conservative estimation.

## **6.2. Membrane characterization**

---

---

- Actual membrane performance during LLDP analysis can be successfully described by a model membrane defined through a log-normal pore number distribution and a total pore number density (three fitting parameters). Moreover, the proposed model allows extrapolating the lack of information due to experimental limitations.
- The reliability of the proposed model is confirmed comparing typical LLDP parameters, such as pore number and permeance distributions, asymptotic permeance, mean radius (based on pore number and permeance distributions) and MWCO estimations, obtained from the model with those from the Grabar-Nikitine traditional method.
- One of the advantages of the model is that it can be applied using few experimental points which would reduce significantly LLDP procedure times (one serious drawback from this technique). In addition, the acquisition of the information especially at low and high pressures or just employing the first point, one in the middle and one in the end leads to reliable membrane information.

## **6.3. Membrane modification**

---

---

- NF membranes with a strong polyelectrolyte hydrogel separation layer can be successfully fabricated through the UV-photo initiated co-polymerization of VSA and MBAA on the surface of PES membranes.
- This modification leads to NF membranes with a very low roughness (even lower than commercial ones), with a highly hydrophilicity and with a very high negative charge throughout the entire pH range which makes this membranes less prone to fouling.

- NF membranes can be obtained at MBAA concentrations above 0.75 mol. % (relative to the VSA concentration) and VSA concentration equal or above 25 % using a 30 kDa PES membrane. The higher the MWCO of the base membrane is, the higher permeability and lower rejection of the resulting NF membranes up to 50 kDa. The use of 100 and 300 kDa base membranes do not give so good results.
- Both the gravimetric and the spectroscopic DG increase with the modification time and the cross-linker concentration. This monomer is mainly the only one grafted on the early stages of the modification boosting the following co-polymerization. In addition, at low VSA concentrations, the MBAA fraction of the hydrogel is higher which leads to low ion exchange capacities.
- The rejection performance of the resulting NF membranes using single salt solutions follows the expected Donnan exclusion mechanism. The increase in the rejection with the DG is attributed to the steric exclusion mechanism, which is linked to the decrease in the permeability. In addition, the strong acidity of VSA allows having high salt rejection even at low pHs and at high salt concentrations.



## **6. Conclusiones**

---

---



## 6.1. Envejecimiento de membranas

---

- El comportamiento funcional de las membranas se siguió satisfactoriamente por medio de medidas de permeabilidad, MWCO (UF) y retención de marcadores neutros y cargados (NF) a lo largo de las diferentes condiciones de envejecimiento
- Los cambios químicos y morfológicos de las membranas como consecuencia de los agentes químicos de limpieza se determinaron por medio de técnicas superficiales de caracterización, específicamente ATR-FTIR, SEM-EDS, AFM y medidas de ángulo de contacto, explicando los cambios de comportamiento de las mismas.
- Las variaciones en el comportamiento de las membranas de UF como consecuencia del acondicionamiento y envejecimiento tuvieron lugar en los primeros días de exposición a las disoluciones (aproximadamente 10 días).
- Aunque la capa activa de todas las membranas de UF es de PES, los soportes de las mismas están hechos de materiales diferentes, concretamente de PET (las membranas de Koch y de GE Osmonics) y de una mezcla de PE y PP (las de Nadir), hecho que juega un papel importante su comportamiento bajo ciertas condiciones de envejecimiento.
- Cuando el envejecimiento se lleva a cabo con disoluciones 1.0 M de HNO<sub>3</sub> y NaOH, las membranas de Nadir con bajo MWCO se ven afectadas por un estrés osmótico debido a la elevada concentración iónica, dando lugar a una reducción aparente del poro efectivo que disminuye la permeabilidad y el MWCO de las mismas. Este efecto no es significativo para el resto de las membranas de UF. Quitando este fenómeno, todas las membranas de Nadir presentan un comportamiento estable en todas las condiciones de envejecimiento, siguiendo la misma tendencia que las membranas sometidas a la disolución de referencia. Además, el comportamiento de las membranas de Nadir está de acuerdo con la falta de cambios significativos en la composición de grupos funcionales, la hidrofiliidad, la estructura y la topografía de las capas activas y/o de los soportes.
- Las membranas de Koch y GE Osmonics también presentan una elevada estabilidad en las condiciones ácidas probadas de acuerdo con las caracterizaciones fisicoquímicas. Bajo condiciones alcalinas, la permeabilidad y el MWCO de la membrana PT aumentan con la concentración de NaOH debido principalmente a la degradación del soporte de PET. Por otro lado, este empeoramiento de las propiedades funcionales, solo es visible a 1.0 M para la membrana HFK-328 debido a que presenta una capa activa más gruesa.

- El envejecimiento de las membranas de NF da lugar a un continuo aumento de la permeabilidad y disminución de la retención con el tiempo, siendo las membranas más resistentes a las condiciones ácidas que a las alcalinas. Además, la membrana NF90 es más estable que la NF270 bajo las mismas condiciones.
- Los cambios en el comportamiento de ambas membranas se deben a la degradación de la capa activa de PA por una reacción de hidrólisis que se puede cuantificar satisfactoriamente por medio de las bandas de absorción amida I y II medidas por ATR-FTIR. Además, las imágenes SEM muestran la degradación del soporte de ambas membranas a altas concentraciones alcalinas.
- La degradación de las membranas de NF tiene lugar más rápidamente cuando las membranas se sumergen en la disolución que cuando el contacto se realiza en flujo tangencial, debido probablemente a un mayor contacto con los agentes químicos de limpieza. Por tanto, la extrapolación de tiempos de vida útiles a partir de datos procedentes de ensayos estáticos darían lugar a estimaciones conservadoras.

## **6.2. Caracterización de membranas**

---

- El comportamiento de una membrana real durante el análisis por LLDP se puede describir satisfactoriamente a través de una membrana modelo definida por una distribución de número de poros log-normal y una densidad de número de poros total (tres parámetros de ajuste). Además, el modelo propuesto permite extrapolar la falta de información debida a limitaciones experimentales.
- Las distribuciones de número de poros y de permeabilidad, la permeabilidad asintótica, el radio medio (basado en ambas distribuciones) y la estimación de MWCO son parámetros típicos de LLDP que se han usado en la validación del modelo comparando los resultados obtenidos a través de éste con los obtenidos por el método tradicional de Grabar-Nikitine.
- Una de las principales ventajas del modelo es que se puede aplicar con pocos puntos experimentales reduciendo significativamente la duración del procedimiento experimental (uno de los principales puntos negativos de la LLDP). Además, se ha comprobado que los resultados obtenidos usando datos a baja y alta presión o simplemente usando un punto al principio, otro intermedio y otro al final, dan información fiable de las propiedades de la membrana.

### 6.3. Modificación de membranas

---

---

- La fabricación de membranas de NF, caracterizadas por capa activa constituida por hidrogeles electrolíticos, se ha llevado a cabo por co-polimerización de VSA y MBAA inducida por radiación UV en la superficie de membranas de UF de PES.
- La modificación propuesta da lugar a membranas de NF con una baja tendencia al ensuciamiento debido a la baja rugosidad (menor incluso que la de algunas membranas comerciales), la alta hidrofiliidad y la carga negativa elevada (a todos los valores de pH) que presentan.
- Usando concentraciones de MBAA mayores de 0.75 mol. % (respecto a la concentración de VSA), concentraciones de VSA iguales o mayores del 25 % y utilizando membranas de 30 kDa como soporte, se obtienen membranas en el rango de la NF. Cuanto mayor es el MWCO de la membrana soporte, mayor es la permeabilidad y menor la retención de la membrana modificada hasta valores de 50 kDa. Los resultados no son tan satisfactorios cuando se usan membranas base de 100 y 300 kDa.
- El grado de polimerización gravimétrico y espectroscópico aumentan con el tiempo de modificación y la concentración del reticulador. En las etapas iniciales, este monómero es prácticamente el único que se injerta facilitando la posterior co-polimerización. Además, a bajas concentraciones de VSA, la fracción de MBAA en el hidrogel aumenta disminuyendo la capacidad de intercambio iónico de la membrana resultante.
- Las membranas de NF fabricadas siguen el principio de exclusión de Donnan en la retención de sales individuales. El aumento de la retención y la disminución de la permeabilidad con el grado de polimerización se debe a un aumento de la exclusión por impedimentos estéricos. La elevada acidez del monómero funcional VSA permite mantener una buena retención a pHs bajos y a concentraciones de sal elevadas.





## **7. References**

---

---



---

## 7.1. References

---

- [1] M. Mulder, Basic principles of membrane technology, Kluwer Academic Publishers, Dordrecht, The Netherlands, 1996.
- [2] H. Strathmann, L. Giorno, E. Drioli, An introduction to membrane science and technology, Institute on Membrane Technology, CNR-ITM at University of Calabria, Rende, 2006.
- [3] M. Cheryan, Ultrafiltration handbook, Technomic Publishing Company, Inc., Lancaster, Pennsylvania, USA, 1986.
- [4] R. Field, Fundamentals of fouling, in: K.-V. Peinemann, S. Pereira Nunes (Eds.), Membranes for water treatment, WILEY-VCH Verlag GmbH & Co. KGaA, Weinheim, 2010, pp. 1-24.
- [5] H. Li, V. Chen, Chapter 10. Membrane fouling and cleaning in food and bioprocessing, in: Z.F. Cui, H.S. Muralidhara (Eds.), Membrane Technology, Butterworth-Heinemann, Oxford, 2010, pp. 213-254.
- [6] M. Cheryan, Ultrafiltration and microfiltration handbook, Technomic Publishing Company, Inc., Lancaster, Pennsylvania, USA, 1998.
- [7] E. Gaudichet-Maurin, F. ThomINETTE, Ageing of polysulfone ultrafiltration membranes in contact with bleach solutions, *J. Membr. Sci.* 282 (2006) 198-204.
- [8] S. Rouaix, C. Causserand, P. Aimar, Experimental study of the effects of hypochlorite on polysulfone membrane properties, *J. Membr. Sci.* 277 (2006) 137-147.
- [9] C. Regula, E. Carretier, Y. Wyart, M. Sergent, G. Gésan-Guiziou, D. Ferry, A. Vincent, D. Boudot, P. Moulin, Ageing of ultrafiltration membranes in contact with sodium hypochlorite and commercial oxidant: Experimental designs as a new ageing protocol, *Sep. Purif. Technol.* 103 (2013) 119-138.
- [10] L. Paugam, D. Delaunay, N.W. Diagne, M. Rabiller-Baudry, Cleaning of skim milk PES ultrafiltration membrane: On the real effect of nitric acid step, *J. Membr. Sci.* 428 (2013) 275-280.
- [11] L. Paugam, M. Rabiller-Baudry, D. Delaunay, Physico-chemical effect of simple alkaline and acid solutions in cleaning sequences of spiral ultrafiltration membranes fouled by skim milk, *Desalination* 200 (2006) 192-194.
- [12] N. Wemsy Diagne, M. Rabiller-Baudry, L. Paugam, On the actual cleanability of polyethersulfone membrane fouled by proteins at critical or limiting flux, *J. Membr. Sci.* 425-426 (2013) 40-47.

- [13] L. Bégoin, M. Rabiller-Baudry, B. Chaufer, M.-C. Hautbois, T. Doneva, Ageing of PES industrial spiral-wound membranes in acid whey ultrafiltration, *Desalination* 192 (2006) 25-39.
- [14] H. Zhu, M. Nyström, Cleaning results characterized by flux, streaming potential and FTIR measurements, *Colloids Surf.* 138 (1998) 309-321.
- [15] A. Weis, M.R. Bird, M. Nyström, C. Wright, The influence of morphology, hydrophobicity and charge upon the long-term performance of ultrafiltration membranes fouled with spent sulphite liquor, *Desalination* 175 (2005) 73-85.
- [16] J.Y. Tian, Z.L. Chen, Y.L. Yang, H. Liang, J. Nan, G.B. Li, Consecutive chemical cleaning of fouled PVC membrane using NaOH and ethanol during ultrafiltration of river water, *Water Res.* 44 (2010) 59-68.
- [17] Z.-L. Xu, T.-S. Chung, Y. Huang, Effect of polyvinylpyrrolidone molecular weights on morphology, oil/water separation, mechanical and thermal properties of polyetherimide/polyvinylpyrrolidone hollow fiber membranes, *J. Appl. Polym. Sci.* 77 (1999) 2220-2233.
- [18] J.-J. Qin, Y.-M. Cao, Y. Li, Effect of hypochlorite concentration on properties of posttreated outer-skin ultrafiltration membranes spun from cellulose acetate/poly(vinyl pyrrolidone) blends, *J. Appl. Polym. Sci.* 97 (2005) 227-231.
- [19] S. Platt, M. Nystrom, Cleaning of membranes fouled by proteins to evaluate the importance of fully developed flow, *Desalination* 208 (2007) 19-33.
- [20] B. Jung, J.K. Yoon, B. Kim, H.-W. Rhee, Effect of molecular weight of polymeric additives on formation, permeation properties and hypochlorite treatment of asymmetric polyacrylonitrile membranes, *J. Membr. Sci.* 243 (2004) 45-57.
- [21] E. Arkhangelsky, D. Kuzmenko, V. Gitis, Impact of chemical cleaning on properties and functioning of polyethersulfone membranes, *J. Membr. Sci.* 305 (2007) 176-184.
- [22] S.Z. Abdullah, P.R. Berube, Assessing the effects of sodium hypochlorite exposure on the characteristics of PVDF based membranes, *Water Res.* 47 (2013) 5392-5399.
- [23] P. Väisänen, M.R. Bird, M. Nystrom, Treatment of UF membranes with simple and formulated cleaning agents, *Food and Bioproducts Processing* 80 (2002) 98-108.
- [24] D. Kuzmenko, E. Arkhangelsky, S. Belfer, V. Freger, V. Gitis, Chemical cleaning of UF membranes fouled by BSA, *Desalination* 179 (2005) 323-333.

- [25] M. Rabiller-Baudry, M. Le Maux, B. Chaufer, L. Begoin, Characterisation of cleaned and fouled membrane by ATR-FTIR and EDX analysis coupled with SEM: application to UF of skimmed milk with a PES membrane, *Desalination* 146 (2002) 123-128.
- [26] R. Liikanen, J. Yli-Kuivila, R. Laukkanen, Efficiency of various chemical cleanings for nanofiltration membrane fouled by conventionally-treated surface water, *J. Membr. Sci.* 195 (2002) 265-276.
- [27] B.P. Espinasse, S.-R. Chae, C. Marconnet, C. Coulombel, C. Mizutani, M. Djafer, V. Heim, M.R. Wiesner, Comparison of chemical cleaning reagents and characterization of foulants of nanofiltration membranes used in surface water treatment, *Desalination* 296 (2012) 1-6.
- [28] A.M. Klüpfel, F.H. Frimmel, Nanofiltration of river water — fouling, cleaning and micropollutant rejection, *Desalination* 250 (2010) 1005-1007.
- [29] Y. Mo, J. Chen, W. Xue, X. Huang, Chemical cleaning of nanofiltration membrane filtrating the effluent from a membrane bioreactor, *Sep. Purif. Technol.* 75 (2010) 407-414.
- [30] M. Beyer, B. Lohregel, L.D. Nghiem, Membrane fouling and chemical cleaning in water recycling applications, *Desalination* 250 (2010) 977-981.
- [31] M. Mänttari, A. Pihlajamäki, E. Kaipainen, M. Nyström, Effect of temperature and membrane pre-treatment by pressure on the filtration properties of nanofiltration membranes, *Desalination* 145 (2002) 81-86.
- [32] M. Nilsson, G. Trägårdh, K. Östergren, The influence of different kinds of pre-treatment on the performance of a polyamide nanofiltration membrane, *Desalination* 195 (2006) 160-168.
- [33] M. Nilsson, G. Trägårdh, K. Östergren, Influence of temperature and cleaning on aromatic and semi-aromatic polyamide thin-film composite NF and RO membranes, *Sep. Purif. Technol.* 62 (2008) 717-726.
- [34] A. Al-Amoudi, P. Williams, S. Mandale, R.W. Lovitt, Cleaning results of new and fouled nanofiltration membrane characterized by zeta potential and permeability, *Sep. Purif. Technol.* 54 (2007) 234-240.
- [35] A. Al-Amoudi, Effect of chemical cleaning agents on virgin nanofiltration membrane as characterized by positron annihilation spectroscopy, *Sep. Purif. Technol.* 110 (2013) 51-56.
- [36] A. Simon, J.A. McDonald, S.J. Khan, W.E. Price, L.D. Nghiem, Effects of caustic cleaning on pore size of nanofiltration membranes and their rejection of trace organic chemicals, *J. Membr. Sci.* 447 (2013) 153-162.

- [37] A. Simon, W.E. Price, L.D. Nghiem, Impact of chemical cleaning on the nanofiltration of pharmaceutically active compounds (PhACs): The role of cleaning temperature, *J. Taiwan Inst. Chem. Eng.* 44 (2013) 713-723.
- [38] M. Mänttari, A. Pihlajamäki, M. Nyström, Effect of pH on hydrophilicity and charge and their effect on the filtration efficiency of NF membranes at different pH, *J. Membr. Sci.* 280 (2006) 311-320.
- [39] M. Nilsson, G. Trägårdh, K. Östergren, The influence of pH, salt and temperature on nanofiltration performance, *J. Membr. Sci.* 312 (2008) 97-106.
- [40] N.M. D'Souza, A.J. Mawson, Membrane cleaning in the dairy industry: a review, *Critical reviews in food science and nutrition* 45 (2005) 125-134.
- [41] N. Porcelli, S. Judd, Chemical cleaning of potable water membranes: A review, *Sep. Purif. Technol.* 71 (2010) 137-143.
- [42] C. Liu, S. Caothien, J. Hayes, T. Caothuy, T. Otoyoy, T. Ogawa, Membrane chemical cleaning: from art to science, *Proc. AWWA 2000 Water Quality Technology Conference* (2001) 1-25.
- [43] M. Rabiller-Baudry, L. Paugam, D. Delaunay, S.V. Gorley, Chapter 6. Membrane cleaning: a key for sustainable production in dairy industry, in: S.V. Gorley (Ed.) *Handbook of membrane research: properties, performance and applications*, Nova Science Publishers, Inc., New York, 2010, pp. 219-256.
- [44] M.C. Vincent, S. Alvarez, J. Lora, E. Bergantinos, Methods for cleaning of ultrafiltration membranes, *Ingeniería Química* 37 (2005) 182-186.
- [45] S.S. Kulkarni, E.W. Funk, N.N. Li, Ultrafiltration, in: W.S.W. Ho, K.K. Sirkar (Eds.), *Membrane handbook*, Van Nostrand Reinhold, New York, 1992, pp. 391-454.
- [46] S. te Poele, J. van der Graaf, Enzymatic cleaning in ultrafiltration of wastewater treatment plant effluent, *Desalination* 179 (2005) 73-81.
- [47] J. Xu, G. Ruan, X. Chu, Y. Yao, B. Su, C. Gao, A pilot study of UF pretreatment without any chemicals for SWRO desalination in China, *Desalination* 207 (2007) 216-226.
- [48] Y. Ye, L.N. Sim, B. Herulah, V. Chen, A.G. Fane, Effects of operating conditions on submerged hollow fibre membrane systems used as pre-treatment for seawater reverse osmosis, *J. Membr. Sci.* 365 (2010) 78-88.
- [49] A. Resosudarmo, Y. Ye, P. Le-Clech, V. Chen, Analysis of UF membrane fouling mechanisms caused by organic interactions in seawater, *Water Res.* 47 (2013) 911-921.

- [50] G. Gilabert Oriol, N. Moosa, R. Garcia-Valls, M. Busch, V. Garcia-Molina, Optimizing seawater operating protocols for pressurized ultrafiltration based on advanced cleaning research, *Desalination and Water Treatment* 51 (2012) 384-396.
- [51] G. Tragardh, Membrane cleaning, *Desalination* 71 (1989) 325-335.
- [52] W. Gao, H. Liang, J. Ma, M. Han, Z. Chen, Z. Han, G. Li, Membrane fouling control in ultrafiltration technology for drinking water production: A review, *Desalination* 272 (2011) 1-8.
- [53] C. Regula, E. Carretier, Y. Wyart, G. Gesan-Guiziou, A. Vincent, D. Boudot, P. Moulin, Chemical cleaning/disinfection and ageing of organic UF membranes: a review, *Water Res.* 56 (2014) 325-365.
- [54] G.F. Crozes, J.G. Jacangelo, C. Anselme, J.M. Laine, Impact of ultrafiltration operating conditions on membrane irreversible fouling, *J. Membr. Sci.* 124 (1997) 63-76.
- [55] M. Kennedy, S.-M. Kim, I. Mutenyo, L. Broens, J. Schippers, Intermittent crossflushing of hollow fiber ultrafiltration systems, *Desalination* 118 (1998) 175-188.
- [56] H. Lee, G. Amy, J. Cho, Y. Yoon, S. Moon, I. Kim, Cleaning strategies for flux recovery of an ultrafiltration membrane fouled by natural organic matter, *Water Res.* 35 (2001) 3301-3308.
- [57] K. Kimura, Y. Hane, Y. Watanabe, G. Amy, N. Ohkuma, Irreversible membrane fouling during ultrafiltration of surface water, *Water Res.* 38 (2004) 3431-3441.
- [58] E.P. Jacobs, S.M. Bradshaw, J.P. Botes, V.L. Pillay, Reverse-pressure back-flush in pilot scale, dead-end ultrafiltration of surface water, *J. Membr. Sci.* 252 (2005) 51-63.
- [59] A. Costa, M. Depinho, M. Elimelech, Mechanisms of colloidal natural organic matter fouling in ultrafiltration, *J. Membr. Sci.* 281 (2006) 716-725.
- [60] E. Zondervan, B. Betlem, B. Roffel, Development of a dynamic model for cleaning ultra filtration membranes fouled by surface water, *J. Membr. Sci.* 289 (2007) 26-31.
- [61] E. Zondervan, B. Roffel, Evaluation of different cleaning agents used for cleaning ultra filtration membranes fouled by surface water, *J. Membr. Sci.* 304 (2007) 40-49.
- [62] A. Abrahamse, C. Lipreau, S. Li, S. Heijman, Removal of divalent cations reduces fouling of ultrafiltration membranes, *J. Membr. Sci.* 323 (2008) 153-158.
- [63] W.J.C. van de Ven, I.G.M. Pünt, A. Zwijnenburg, A.J.B. Kemperman, W.G.J. van der Meer, M. Wessling, Hollow fiber ultrafiltration: the concept of partial backwashing, *J. Membr. Sci.* 320 (2008) 319-324.



- [64] Y. Bessiere, C. Guigui, P.J. Remize, C. Cabassud, Coupling air-assisted backwash and rinsing steps: a new way to improve ultrafiltration process operation for inside-out hollow fibre modules, *Desalination* 240 (2009) 71-77.
- [65] X. Guo, Q. Li, W. Hu, W. Gao, D. Liu, Ultrafiltration of dissolved organic matter in surface water by a polyvinylchloride hollow fiber membrane, *J. Membr. Sci.* 327 (2009) 254-263.
- [66] S. Li, S.G.J. Heijman, J.Q.J.C. Verberk, A.R.D. Verliefe, A.J.B. Kemperman, J.C. van Dijk, G. Amy, Impact of backwash water composition on ultrafiltration fouling control, *J. Membr. Sci.* 344 (2009) 17-25.
- [67] S. Li, S.G.J. Heijman, J.Q.J.C. Verberk, J.C. van Dijk, Influence of Ca and Na ions in backwash water on ultrafiltration fouling control, *Desalination* 250 (2010) 861-864.
- [68] C.H. Yu, L.C. Fang, S.K. Lateef, C.H. Wu, C.F. Lin, Enzymatic treatment for controlling irreversible membrane fouling in cross-flow humic acid-fed ultrafiltration, *J. Hazard. Mater.* 177 (2010) 1153-1158.
- [69] P.D. Peeva, A.E. Palupi, M. Ulbricht, Ultrafiltration of humic acid solutions through unmodified and surface functionalized low-fouling polyethersulfone membranes - Effects of feed properties, molecular weight cut-off and membrane chemistry on fouling behavior and cleanability, *Sep. Purif. Technol.* 81 (2011) 124-133.
- [70] A. Maartens, P. Swart, E.P. Jacobs, Removal of natural organic matter by ultrafiltration: Characterisation, fouling and cleaning, *Water Sci. Technol.* 40 (1999) 113-120.
- [71] S. Li, S.G. Heijman, J.Q. Verberk, P. Le Clech, J. Lu, A.J. Kemperman, G.L. Amy, J.C. van Dijk, Fouling control mechanisms of demineralized water backwash: Reduction of charge screening and calcium bridging effects, *Water Res.* 45 (2011) 6289-6300.
- [72] K.-K. Ng, C.-J. Wu, H.-L. Yang, S.C. Panchangam, Y.-C. Lin, P.-K.A. Hong, C.-H. Wu, C.-F. Lin, Effect of ultrasound on membrane filtration and cleaning operations, *Sep. Sci. Technol.* 48 (2012) 215-222.
- [73] R.H. Peiris, H. Budman, C. Moresoli, R.L. Legge, Fluorescence-based fouling prediction and optimization of a membrane filtration process for drinking water treatment, *AIChE J.* 58 (2012) 1475-1486.
- [74] R.H. Peiris, H. Budman, C. Moresoli, R.L. Legge, Fouling control and optimization of a drinking water membrane filtration process with real-time model parameter adaptation using fluorescence and permeate flux measurements, *J. Process Control* 23 (2013) 70-77.
- [75] A. Massé, H.N. Thi, P. Legentilhomme, P. Jaouen, Dead-end and tangential ultrafiltration of natural salted water: Influence of operating parameters on specific energy consumption, *J. Membr. Sci.* 380 (2011) 192-198.

- [76] C. Serra, L. Durand-Bourlier, M. J. Clifton, P. Moulin, J.-C. Rouch, P. Aptel, Use of air sparging to improve backwash efficiency in hollow-fiber modules, *J. Membr. Sci.* 161 (1999) 95-113.
- [77] C. Guigui, M. Mougenot, C. Cabassud, Air sparging backwash in ultrafiltration hollow fibres for drinking water production, *Water Science & Technology: Water Supply* 3 (2003) 415-422.
- [78] S. Heijman, M. Vantieghem, S. Raktoc, J. Verberk, J. Vandijk, Blocking of capillaries as fouling mechanism for dead-end ultrafiltration, *J. Membr. Sci.* 287 (2007) 119-125.
- [79] P.J. Remize, C. Guigui, C. Cabassud, Evaluation of backwash efficiency, definition of remaining fouling and characterisation of its contribution in irreversible fouling: Case of drinking water production by air-assisted ultra-filtration, *J. Membr. Sci.* 355 (2010) 104-111.
- [80] S. Pavlova, Study on the cleaning of new ultrafiltration spiral-wound modules to prevent membrane fouling (including biological fouling), *Desalination* 172 (2005) 267-270.
- [81] K. Katsoufidou, S.G. Yiantsios, A.J. Karabelas, Experimental study of ultrafiltration membrane fouling by sodium alginate and flux recovery by backwashing, *J. Membr. Sci.* 300 (2007) 137-146.
- [82] J.M. Arnal, B. Garcia-Fayos, J. Lora, G. Verdú, M. Sancho, AQUAPOT: study of several cleaning solutions to recover permeate flow in a humanitarian drinking water treatment facility based on spiral wound UF membrane. Preliminary test (I), *Desalination* 221 (2008) 331-337.
- [83] J.M. Arnal, B. Garcia-Fayos, G. Verdu, J. Lora, M. Sancho, AQUAPOT: Study of the causes in reduction of permeate flow in spiral wound UF membrane. Simulation of a non-rigorous cleaning protocol in a drinkable water treatment facility, *Desalination* 222 (2008) 513-518.
- [84] H. Liang, W. Gong, J. Chen, G. Li, Cleaning of fouled ultrafiltration (UF) membrane by algae during reservoir water treatment, *Desalination* 220 (2008) 267-272.
- [85] Y. Zhang, J. Tian, H. Liang, J. Nan, Z. Chen, G. Li, Chemical cleaning of fouled PVC membrane during ultrafiltration of algal-rich water, *Journal of Environmental Sciences* 23 (2011) 529-536.
- [86] Y. Wang, L.-j. Yu, L. Qi, G.-B. Li, Cleaning strategies for flux recovery of ultrafiltration membrane fouled by reservoir water, *Energy Procedia* 11 (2011) 3105-3109.

- [87] J.M. Arnal, B. Garcia-Fayos, M. Sancho, G. Verdu, Ultrafiltration membrane cleaning with different chemical solutions after treating surface water, *Desalination and Water Treatment* 7 (2009) 198-205.
- [88] J.M. Arnal, B. García-Fayos, M. Sancho, G. Verdú, Cleaning ultrafiltration membranes by different chemical solutions with air bubbles, *Desalination and Water Treatment* 10 (2009) 175-180.
- [89] B. García-Fayos, J.M. Arnal, M. Sancho, Cleaning of ultrafiltration membranes after the treatment of surface water: static–dynamic test, *Desalination and Water Treatment* 51 (2013) 609-616.
- [90] X. Sun, C. Wang, Y. Tong, W. Wang, J. Wei, Microalgae filtration by UF membranes: influence of three membrane materials, *Desalination and Water Treatment* (2013) 1-8.
- [91] J.P. Chen, S.L. Kim, Y.P. Ting, Optimization of membrane physical and chemical cleaning by a statistically designed approach, *J. Membr. Sci.* 219 (2003) 27-45.
- [92] J. Kim, F.A. DiGiano, A two-fiber, bench-scale test of ultrafiltration (UF) for investigation of fouling rate and characteristics, *J. Membr. Sci.* 271 (2006) 196-204.
- [93] E. Arkhangelsky, U. Goren, V. Gitis, Retention of organic matter by cellulose acetate membranes cleaned with hypochlorite, *Desalination* 223 (2008) 97-105.
- [94] X. Zheng, M. Ernst, M. Jekel, Stabilizing the performance of ultrafiltration in filtering tertiary effluent - Technical choices and economic comparisons, *J. Membr. Sci.* 366 (2011) 82-91.
- [95] C.G. Kumar, M.P. Tiwari, Use of alkaline proteases for ultrafiltration membrane cleaning, *Biotechnol. Tech.* 13 (1999) 235-238.
- [96] A. Makardij, X. Chen, M. Farid, Microfiltration and ultrafiltration of milk: some aspects of fouling and cleaning, *Food and Bioproducts Processing* 77 (1999) 107-113.
- [97] T. Mohammadi, S. Madaeni, M. Moghadam, Investigation of membrane fouling, *Desalination* 153 (2002) 155-160.
- [98] D. Delaunay, M. Rabiller-Baudry, L. Paugam, A. Pihlajamaki, M. Nystrom, Physico-chemical characterisations of a UF membrane used in dairy application to estimate chemical efficiency of cleaning, *Desalination* 200 (2006) 189-191.
- [99] M. Rabiller-Baudry, D. Delaunay, L. Paugam, L. Begoin, B. Chaufer, Role of physico-chemical and hydrodynamic aspects in cleaning of spiral PES ultrafiltration membranes of dairy industry, *Desalination* 199 (2006) 390-392.

- [100] M. Rabiller-Baudry, L. Paugam, L. Begoin, D. Delaunay, M. Fernandezcruz, C. Phinaziebin, C. Laviadesgarciadeguadiana, B. Chaufer, Alkaline cleaning of PES membranes used in skimmed milk ultrafiltration: from reactor to spiral-wound module via a plate-and-frame module, *Desalination* 191 (2006) 334-343.
- [101] M. Rabiller-Baudry, L. Begoin, D. Delaunay, L. Paugam, B. Chaufer, A dual approach of membrane cleaning based on physico-chemistry and hydrodynamics Application to PES membrane of dairy industry, *Chemical Engineering and Processing: Process Intensification* 47 (2007) 267-275.
- [102] M. Kazemimoghadam, T. Mohammadi, Chemical cleaning of ultrafiltration membranes in the milk industry, *Desalination* 204 (2007) 213-218.
- [103] A. Maskooki, S. Mortazavi, A. Maskooki, Cleaning of spiralwound ultrafiltration membranes using ultrasound and alkaline solution of EDTA, *Desalination* 264 (2010) 63-69.
- [104] L. Paugam, D. Delaunay, M. Rabiller-Baudry, Cleaning efficiency and impact on production fluxes of oxidising disinfectants on a pes ultrafiltration membrane fouled with proteins, *Food and Bioproducts Processing* 88 (2010) 425-429.
- [105] K.E. Smith, R.L. Bradley, Evaluation of efficacy of four commercial enzyme-based cleaners of ultrafiltration systems, *J. Dairy Sci.* 70 (1987) 1168-1177.
- [106] H.F. Bohner, R.L. Bradley, Effective cleaning and sanitizing of polysulfone ultrafiltration membrane systems, *J. Dairy Sci.* 75 (1992) 718-724.
- [107] T. Coolbear, C. Monk, K. Peek, H.W. Morgan, R.M. Damel, Laboratory-scale investigations into the use of extremely thermophilic proteinases for cleaning ultrafiltration membranes fouled during whey processing, *J. Membr. Sci.* 67 (1992) 93-101.
- [108] S.S. Madaeni, S. Sharifnia, Chemical cleaning of ultrafiltration membranes fouled by whey, *Iranian Polymer Journal* 9 (2000) 143-151.
- [109] S. Muthukumar, K. Yang, A. Seuren, S. Kentish, M. Ashokkumar, G. Stevens, F. Grieser, The use of ultrasonic cleaning for ultrafiltration membranes in the dairy industry, *Sep. Purif. Technol.* 39 (2004) 99-107.
- [110] S. Muthukumar, S. Kentish, S. Lalchandani, M. Ashokkumar, R. Mawson, G.W. Stevens, F. Grieser, The optimisation of ultrasonic cleaning procedures for dairy fouled ultrafiltration membranes, *Ultrason. Sonochem.* 12 (2005) 29-35.
- [111] V. Chen, H. Li, D. Li, S. Tan, H. Petrus, Cleaning strategies for membrane fouled with protein mixtures, *Desalination* 200 (2006) 198-200.

- [112] X. Tang, S.H. Flint, R.J. Bennett, J.D. Brooks, The efficacy of different cleaners and sanitisers in cleaning biofilms on UF membranes used in the dairy industry, *J. Membr. Sci.* 352 (2010) 71-75.
- [113] S. Muthukumar, S.E. Kentish, G.W. Stevens, M. Ashokkumar, R. Mawson, The application of ultrasound to dairy ultrafiltration: The influence of operating conditions, *J. Food Eng.* 81 (2007) 364-373.
- [114] K.E. Smith, R.L. Bradley Jr, Ineffective cleaning of polysulfone ultrafiltration membrane systems and corrosion by bisulfite used as a sanitizer, *J. Dairy Sci.* 69 (1986) 1232-1240.
- [115] S.S. Madaeni, E. Rostami, A. Rahimpour, Surfactant cleaning of ultrafiltration membranes fouled by whey, *International Journal of Dairy Technology* 63 (2010) 273-283.
- [116] M. Muñoz-Aguado, D. Wiley, A. Fane, Enzymatic and detergent cleaning of a polysulfone ultrafiltration membrane fouled with BSA and whey, *J. Membr. Sci.* 117 (1996) 175-187.
- [117] M.H. Tran-Ha, D.E. Wiley, The relationship between membrane cleaning efficiency and water quality, *J. Membr. Sci.* 145 (1998) 99-110.
- [118] M.H. Tran-Ha, V. Santos, D.E. Wiley, The effect of multivalent cations on membrane protein interactions during cleaning with CTAB, *J. Membr. Sci.* 251 (2005) 179-188.
- [119] M. Nigam, B. Bansal, X. Chen, Fouling and cleaning of whey protein concentrate fouled ultrafiltration membranes, *Desalination* 218 (2008) 313-322.
- [120] N. Norazman, W. Wu, H. Li, V. Wasinger, H. Zhang, V. Chen, Evaluation of chemical cleaning of UF membranes fouled with whey protein isolates via analysis of residual protein components on membranes surface, *Sep. Purif. Technol.* 103 (2013) 241-250.
- [121] K.-J. Kim, P. Sun, V. Chen, D.E. Wiley, A.G. Fane, The cleaning of ultrafiltration membranes fouled by protein, *J. Membr. Sci.* 80 (1993) 241-249.
- [122] K.-J. Kim, A.G. Fane, Performance evaluation of surface hydrophilized novel ultrafiltration membranes using aqueous proteins, *J. Membr. Sci.* 99 (1995) 149-162.
- [123] M. Nystrom, H. Zhu, Characterization of cleaning results using combined flux and streaming potential methods, *J. Membr. Sci.* 131 (1997) 195-205.
- [124] H. Zhu, M. Nystrom, Cleaning results characterized by flux, streaming potential and FTIR measurements, *Colloids Surf.* 138 (1998) 309-321.
- [125] S. Platt, M. Nystrom, Amido black staining of ultrafiltration membranes fouled with BSA, *Desalination* 214 (2007) 177-192.
- [126] H. Petrus, H. Li, V. Chen, N. Norazman, Enzymatic cleaning of ultrafiltration membranes fouled by protein mixture solutions, *J. Membr. Sci.* 325 (2008) 783-792.

- [127] I. Levitsky, A. Duek, R. Naim, E. Arkhangelsky, V. Gitis, Cleaning UF membranes with simple and formulated solutions, *Chem. Eng. Sci.* 69 (2012) 679-683.
- [128] I. Levitsky, R. Naim, A. Duek, V. Gitis, Effect of time in chemical cleaning of ultrafiltration membranes, *Chem. Eng. Technol.* 35 (2012) 941-946.
- [129] Y. Hao, C. Liang, A. Moriya, H. Matsuyama, T. Maruyama, Visualization of protein fouling inside a hollow fiber ultrafiltration membrane by fluorescent microscopy, *Ind. Eng. Chem. Res.* 51 (2012) 14850-14858.
- [130] M.H.M. Isa, R.A. Frazier, P. Jauregi, Cleaning potential of surfactin on fouled ultrafiltration (UF) membranes, *Sains Malaysiana* 41 (2012) 1117-1124.
- [131] M.J. Luján-Facundo, J.A. Mendoza-Roca, B. Cuartas-Urbe, S. Álvarez-Blanco, Ultrasonic cleaning of ultrafiltration membranes fouled with BSA solution, *Sep. Purif. Technol.* 120 (2013) 275-281.
- [132] S. Razavi, J. Harris, F. Sherkat, Fouling and cleaning of membranes in the ultrafiltration of the aqueous extract of soy flour, *J. Membr. Sci.* 114 (1996) 93-104.
- [133] J. Lipnizki, S. Casani, G. Jonsson, Optimisation of ultrafiltration of a highly viscous protein solution using spiral-wound modules, *Desalination* 180 (2005) 15-24.
- [134] A. Maartens, P. Swart, E. Jacobs, An enzymatic approach to the cleaning of ultrafiltration membranes fouled in abattoir effluent, *J. Membr. Sci.* 119 (1996) 9-16.
- [135] X. Melamane, B.I. Pletschke, W.D. Leukes, C.G. Whiteley, Cleaning fouled membranes using sludge enzymes, *Water SA Special Edition: WISA Proceedings* (2002) 100-104.
- [136] Z. Allie, E.P. Jacobs, A. Maartens, P. Swart, Enzymatic cleaning of ultrafiltration membranes fouled by abattoir effluent, *J. Membr. Sci.* 218 (2003) 107-116.
- [137] X. Chai, T. Kobayashi, N. Fujii, Ultrasound-associated cleaning of polymeric membranes for water treatment, *Sep. Purif. Technol.* 15 (1999) 139-146.
- [138] T. Kobayashi, T. Kobayashi, Y. Hosaka, N. Fujii, Ultrasound-enhanced membrane-cleaning processes applied water treatments: influence of sonic frequency on filtration treatments, *Ultrasonics* 41 (2003) 185-190.
- [139] A. Weis, M.R. Bird, The influence of multiple fouling and cleaning cycles upon the membrane processing of lignosulphonates, *Food and Bioproducts Processing* 79 (2001) 184-187.
- [140] A. Maartens, E.P. Jacobs, P. Swart, UF of pulp and paper effluent: membrane fouling-prevention and cleaning, *J. Membr. Sci.* 209 (2002) 81-92.

- [141] J. Li, D. Hallbauer, R. Sanderson, Direct monitoring of membrane fouling and cleaning during ultrafiltration using a non-invasive ultrasonic technique, *J. Membr. Sci.* 215 (2003) 33-52.
- [142] A. Weis, M.R. Bird, M. Nystrom, The chemical cleaning of polymeric UF membranes fouled with spent sulphite liquor over multiple operational cycles, *J. Membr. Sci.* 216 (2003) 67-79.
- [143] L. Wang, X. Wang, K. Fukushi, Effects of operational conditions on ultrafiltration membrane fouling, *Desalination* 229 (2008) 181-191.
- [144] O. Wallberg, A.-S. Jönsson, P. Wickström, Membrane cleaning - a case study in a sulphite pulp mill bleach plant, *Desalination* 141 (2001) 259-268.
- [145] S.A. Jones, A. Pihlajamäki, M.R. Bird, The role of synthetic membrane pre-treatment in influencing filtration performance over multiple operational cycles, *Sep. Sci. Technol.* 47 (2012) 1119-1128.
- [146] P.J. Evans, M.R. Bird, Solute-membrane fouling interactions during the ultrafiltration of black tea liquor, *Food and Bioproducts Processing* 84 (2006) 292-301.
- [147] P.J. Evans, M.R. Bird, A. Pihlajamäki, M. Nyström, The influence of hydrophobicity, roughness and charge upon ultrafiltration membranes for black tea liquor clarification, *J. Membr. Sci.* 313 (2008) 250-262.
- [148] D. Wu, M.R. Bird, The fouling and cleaning of ultrafiltration membranes during the filtration of model tea component solutions, *Journal of Food Process Engineering* 30 (2007) 293-323.
- [149] G. Zhang, Z. Liu, Membrane fouling and cleaning in ultrafiltration of wastewater from banknote printing works, *J. Membr. Sci.* 211 (2003) 235-249.
- [150] G.J. Zhang, Z.Z. Liu, L.F. Song, J.Y. Hu, S.L. Ong, W.J. Ng, One-step cleaning method for flux recovery of an ultrafiltration membrane fouled by banknote printing works wastewater, *Desalination* 170 (2004) 271-280.
- [151] J. Lindau, A.-S. Johnson, Cleaning of ultrafiltration membranes after treatment of oily waste water, *J. Membr. Sci.* 87 (1994) 71-78.
- [152] G. Busca, N. Hilal, B.P. Atkin, Optimisation of washing cycle on ultrafiltration membranes used in treatment of metalworking fluids, *Desalination* 156 (2003) 199-207.
- [153] W. Jin, W. Guo, X. Lü, P. Han, Y. Wang, Effect of the ultrasound generated by flat plate transducer cleaning on polluted polyvinylidene fluoride hollow fiber ultrafiltration membrane, *Chin. J. Chem. Eng.* 16 (2008) 801-804.

- [154] A. Salahi, M. Mohammadi, M. Abbasi, F. Rekabdar, Chemical cleaning of ultrafiltration membrane after treatment of oily wastewater, *Iranian Journal of Chemical Engineering* 7 (2010) 17-28.
- [155] S. Lee, Y. Aurelle, H. Roques, Concentration polarization, membrane fouling and cleaning in ultrafiltration of soluble oil, *J. Membr. Sci.* 19 (1984) 23-38.
- [156] X. Li, J. Li, X. Fu, R. Wickramasinghe, J. Chen, Chemical cleaning of PS ultrafilters fouled by the fermentation broth of glutamic acid, *Sep. Purif. Technol.* 42 (2005) 181-187.
- [157] H. Chen, Y. Chen, R. Juang, Flux decline and membrane cleaning in cross-flow ultrafiltration of treated fermentation broths for surfactin recovery, *Sep. Purif. Technol.* 62 (2008) 47-55.
- [158] L. Wang, Q. Wang, Y. Li, H. Lin, Ultrasound-assisted chemical cleaning of polyvinylidene fluoride membrane fouled by lactic acid fermentation broth, *Desalination* 326 (2013) 103-108.
- [159] A.M. Mimi Sakinah, A.F. Ismail, R.M. Illias, O. Hassan, Fouling characteristics and autopsy of a PES ultrafiltration membrane in cyclodextrins separation, *Desalination* 207 (2007) 227-242.
- [160] M. Cai, S. Wang, Y. Zheng, H. Liang, Effects of ultrasound on ultrafiltration of Radix astragalus extract and cleaning of fouled membrane, *Sep. Purif. Technol.* 68 (2009) 351-356.
- [161] M. Cai, S. Zhao, H. Liang, Mechanisms for the enhancement of ultrafiltration and membrane cleaning by different ultrasonic frequencies, *Desalination* 263 (2010) 133-138.
- [162] J.A. Mendoza-Roca, M.V. Galiana-Aleixandre, J. Lora-García, A. Bes-Piá, Purification of tannery effluents by ultrafiltration in view of permeate reuse, *Sep. Purif. Technol.* 70 (2010) 296-301.
- [163] D. Veerasamy, A.F. Ismail, Rehabilitation of fouled membrane from natural rubber skim latex concentration through membrane autopsy and ultrasonication enhanced membrane cleaning procedure, *Desalination* 286 (2012) 235-241.
- [164] N.K. Saha, M. Balakrishnan, Short chemical cleaning of polymeric ultrafiltration membranes fouled by sugarcane juice polysaccharides, *Desalination and Water Treatment* 2 (2009) 266-277.
- [165] V. Singh, P.K. Jain, C. Das, Performance of spiral wound ultrafiltration membrane module for with and without permeate recycle: Experimental and theoretical consideration, *Desalination* 322 (2013) 94-103.



- [166] V.G.J. Rodgers, R.E. Sparks, Reduction of membrane fouling in the ultrafiltration of binary protein mixtures, *AIChE J.* 37 (1991) 1517-1528.
- [167] E.M. Shugman, C. Aldrich, R.D. Sanderson, D.S. McLachlan, Infrasonic backpulsed membrane cleaning of micro- and ultrafiltration membranes fouled with alumina and yeast, *Water SA* 39 (2013).
- [168] R. Naim, I. Levitsky, V. Gitis, Surfactant cleaning of UF membranes fouled by proteins, *Sep. Purif. Technol.* 94 (2012) 39-43.
- [169] C. Astudillo, J. Parra, S. González, B. Cancino, A new parameter for membrane cleaning evaluation, *Sep. Purif. Technol.* 73 (2010) 286-293.
- [170] N. Lawrence, J. Perera, M. Iyer, M. Hickey, G. Stevens, The use of streaming potential measurements to study the fouling and cleaning of ultrafiltration membranes, *Sep. Purif. Technol.* 48 (2006) 106-112.
- [171] M.C. Kaplan, A. Jégou, B. Chaufer, M. Rabiller-Baudry, M.C. Michalsky, Adsorption of lysozyme on membrane material and cleaning with non-ionic surfactant characterized through contact angle measurements, *Desalination* 146 (2002) 149-154.
- [172] A. Maartens, P. Swart, E.P. Jacobs, Characterisation techniques for organic foulants adsorbed onto flat-sheet UF membranes used in abattoir effluent, *J. Membr. Sci.* 119 (1996) 1-8.
- [173] R.H. Peiris, H. Budman, C. Moresoli, R.L. Legge, Understanding fouling behaviour of ultrafiltration membrane processes and natural water using principal component analysis of fluorescence excitation-emission matrices, *J. Membr. Sci.* 357 (2010) 62-72.
- [174] N.P. De Souza, O.D. Basu, Comparative analysis of physical cleaning operations for fouling control of hollow fiber membranes in drinking water treatment, *J. Membr. Sci.* 436 (2013) 28-35.
- [175] M. Pontié, L. Durand-Bourlier, D. Lemordant, J.M. Lainé, Control fouling and cleaning procedures of UF membranes by a streaming potential method, *Sep. Purif. Technol.* 14 (1998) 1-11.
- [176] I. Levitsky, A. Duek, E. Arkhangelsky, D. Pinchev, T. Kadoshian, H. Shetrit, R. Naim, V. Gitis, Understanding the oxidative cleaning of UF membranes, *J. Membr. Sci.* 377 (2011) 206-213.
- [177] L. Bégoïn, M. Rabiller-Baudry, B. Chaufer, M. Hautbois, T. Doneva, Ageing of PES industrial spiral-wound membranes in acid whey ultrafiltration, *Desalination* 192 (2006) 25-39.

- [178] K. Yadav, K. Morison, M.P. Staiger, Effects of hypochlorite treatment on the surface morphology and mechanical properties of polyethersulfone ultrafiltration membranes, *Polym. Degrad. Stab.* 94 (2009) 1955-1961.
- [179] H.A. Barnes, *A handbook of elementary rheology*, The University of Wales Institute of Non-Newtonian Fluid Mechanics, Wales, 2000.
- [180] C. Causserand, G. Pierre, S. Rapenne, J.-C. Schrotter, P. Sauvade, O. Lorain, Characterization of ultrafiltration membranes by tracer's retention: Comparison of methods sensitivity and reproducibility, *Desalination* 250 (2010) 767-772.
- [181] C. Causserand, S. Rouaix, A. Akbari, P. Aimar, Improvement of a method for the characterization of ultrafiltration membranes by measurements of tracers retention, *J. Membr. Sci.* 238 (2004) 177-190.
- [182] C.M. Tam, A.Y. Tremblay, Membrane pore characterization - comparison between single and multicomponent solute probe techniques, *J. Membr. Sci.* 57 (1991) 271-287.
- [183] N. Hilal, M. Al-Abri, H. Al-Hinai, Characterization and retention of UF membranes using PEG, HS and polyelectrolytes, *Desalination* 206 (2007) 568-578.
- [184] C. Bhattacharjee, S. Datta, A mass transfer model for the prediction of rejection and flux during ultrafiltration of PEG-6000, *J. Membr. Sci.* 125 (1997) 303-310.
- [185] Q.T. Nguyen, P. Aptel, J. Neel, Characterization of ultrafiltration membranes. Part II — Mass transport measurements for low and high molecular weight synthetic polymers in water solutions, *J. Membr. Sci.* 7 (1980) 141-155.
- [186] T.K. Sherwood, R.L. Pigford, C.R. Wilke, *Mass Transfer*, McGraw-Hill, New York, 1975.
- [187] I. Horcas, R. Fernández, J.M. Gómez-Rodríguez, J. Colchero, J. Gómez-Herrero, A.M. Baro, WSXM: A software for scanning probe microscopy and a tool for nanotechnology, *Rev. Sci. Instrum.* 78 (2007).
- [188] C.J. Walsh, A.J. Leistner, B.F. Oreb, Power spectral density analysis of optical substrates for gravitational-wave interferometry, *Appl. Opt.* 38 (1999) 4790-4801.
- [189] E.L. Church, Fractal surface finish, *Appl. Opt.* 27 (1988) 1518-1526.
- [190] C. Deumié, R. Richier, P. Dumas, C. Amra, Multiscale roughness in optical multilayers: atomic force microscopy and light scattering, *Appl. Opt.* 35 (1996) 5583-5594.
- [191] Y. Wyart, G. Georges, C. Deumié, C. Amra, P. Moulin, Membrane characterization by microscopic methods: Multiscale structure, *J. Membr. Sci.* 315 (2008) 82-92.
- [192] C. Ruppe, A. Duparré, Roughness analysis of optical films and substrates by atomic force microscopy, *Thin Solid Films* 288 (1996) 8-13.

- [193] R.N. Wenzel, Surface roughness and contact angle, *The Journal of Physical and Colloid Chemistry* 53 (1949) 1466-1467.
- [194] A. Marmur, Wetting on hydrophobic rough surfaces: to be heterogeneous or not to be?, *Langmuir* 19 (2003) 8343-8348.
- [195] A. Marmur, Penetration and displacement in capillary systems, in: M. Schrader, G. Loeb (Eds.), *Modern Approaches to Wettability*, Springer US, 1992, pp. 327-358.
- [196] C.J. Van Oss, M.K. Chaudhury, R.J. Good, Interfacial Lifshitz-van der Waals and polar interactions in macroscopic systems, *Chem. Rev. (Washington, DC, U. S.)* 88 (1988) 927-941.
- [197] S. Bargir, S. Dunn, B. Jefferson, J. Macadam, S. Parsons, The use of contact angle measurements to estimate the adhesion propensity of calcium carbonate to solid substrates in water, *Appl. Surf. Sci.* 255 (2009) 4873-4879.
- [198] H. Brack, M. Wyler, G. Peter, G.G. Scherer, A contact angle investigation of the surface properties of selected proton-conducting radiation-grafted membranes, *J. Membr. Sci.* 214 (2003) 1-19.
- [199] S. Belfer, R. Fainchtain, Y. Purinson, O. Kedem, Surface characterization by FTIR-ATR spectroscopy of polyethersulfone membranes-unmodified, modified and protein fouled, *J. Membr. Sci.* 172 (2000) 113-124.
- [200] A. Pihlajamäki, P. Väisänen, M. Nyström, Characterization of clean and fouled polymeric ultrafiltration membranes by Fourier transform IR spectroscopy-attenuated total reflection, *Colloids Surf.* 138 (1998) 323-333.
- [201] H. Rajandas, S. Parimannan, K. Sathasivam, M. Ravichandran, L. Su Yin, A novel FTIR-ATR spectroscopy based technique for the estimation of low-density polyethylene biodegradation, *Polym. Test.* 31 (2012) 1094-1099.
- [202] L.-S. Shi, L.-Y. Wang, Y.-N. Wang, The investigation of argon plasma surface modification to polyethylene: Quantitative ATR-FTIR spectroscopic analysis, *Eur. Polym. J.* 42 (2006) 1625-1633.
- [203] Z. Chen, J.N. Hay, M.J. Jenkins, FTIR spectroscopic analysis of poly(ethylene terephthalate) on crystallization, *Eur. Polym. J.* 48 (2012) 1586-1610.
- [204] B.J. Holland, J.N. Hay, Analysis of comonomer content and cyclic oligomers of poly(ethylene terephthalate), *Polymer* 43 (2002) 1797-1804.

- [205] M. Kallioinen, M. Mänttari, M. Nyström, J. Nuortila-Jokinen, P. Nurminen, T. Sutela, Membrane evaluation for the treatment of acidic clear filtrate, *Desalination* 250 (2010) 1002-1004.
- [206] D. Jermann, W. Pronk, R. Kagi, M. Halbeisen, M. Boller, Influence of interactions between NOM and particles on UF fouling mechanisms, *Water Res.* 42 (2008) 3870-3878.
- [207] R. Ng, X. Zhang, N. Liu, S.-T. Yang, Modifications of nonwoven polyethylene terephthalate fibrous matrices via NaOH hydrolysis: Effects on pore size, fiber diameter, cell seeding and proliferation, *Process Biochem. (Amsterdam, Neth.)* 44 (2009) 992-998.
- [208] M. Peyravi, A. Rahimpour, M. Jahanshahi, A. Javadi, A. Shockravi, Tailoring the surface properties of PES ultrafiltration membranes to reduce the fouling resistance using synthesized hydrophilic copolymer, *Microporous Mesoporous Mater.* 160 (2012) 114-125.
- [209] L. Puro, M. Kallioinen, M. Mänttari, G. Natarajan, D. C. Cameron, M. Nyström, Performance of RC and PES ultrafiltration membranes in filtration of pulp mill process waters, *Desalination* 264 (2010) 249-255.
- [210] B.J. Ryan, K.M. Poduska, Roughness effects on contact angle measurements, *American Journal of Physics* 76 (2008) 1074-1077.
- [211] M. Mänttari, T. Pekuri, M. Nyström, NF270, a new membrane having promising characteristics and being suitable for treatment of dilute effluents from the paper industry, *J. Membr. Sci.* 242 (2004) 107-116.
- [212] C.Y. Tang, Y.-N. Kwon, J.O. Leckie, Effect of membrane chemistry and coating layer on physiochemical properties of thin film composite polyamide RO and NF membranes: I. FTIR and XPS characterization of polyamide and coating layer chemistry, *Desalination* 242 (2009) 149-167.
- [213] Y.-N. Kwon, J.O. Leckie, Hypochlorite degradation of crosslinked polyamide membranes: II. Changes in hydrogen bonding behavior and performance, *J. Membr. Sci.* 282 (2006) 456-464.
- [214] P. Duan, L. Dai, P.E. Savage, Kinetics and mechanism of N-substituted amide hydrolysis in high-temperature water, *The Journal of Supercritical Fluids* 51 (2010) 362-368.
- [215] M. Liu, Z. Chen, S. Yu, D. Wu, C. Gao, Thin-film composite polyamide reverse osmosis membranes with improved acid stability and chlorine resistance by coating N-isopropylacrylamide-co-acrylamide copolymers, *Desalination* 270 (2011) 248-257.



## **8. Appendix**

---

---



### 8.1. Program for the data acquisition and permeability determination in the dead-end filtration system (LabVIEW code)

The functional characterization of the UF and NF membranes at small scale was carried out using two stirred dead-end cells in parallel which were pressurized with nitrogen. The experimental setup consisted of two cells, two magnetic stirrers, two weight scales, one pressure transducer, one temperature sensor and two indicators (Fig. 8.1).

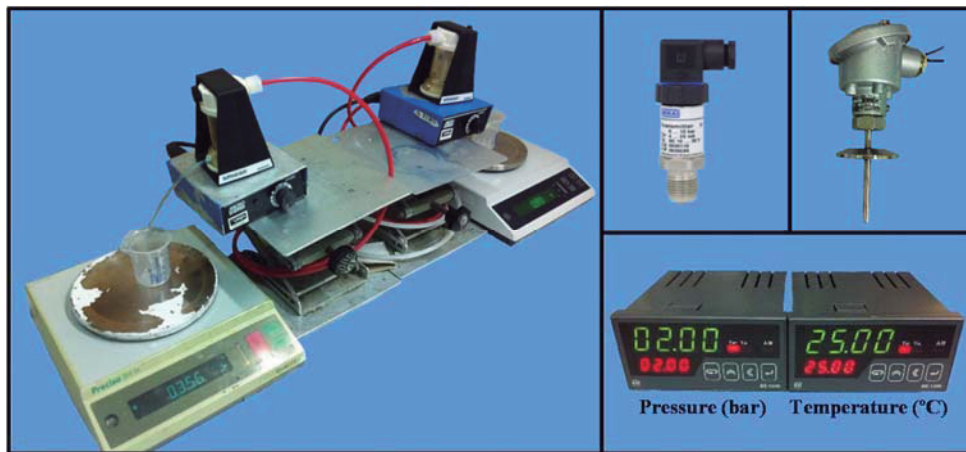


**Fig. 8.1.** Experimental setup for the functional characterization of UF and NF membranes at small scale.

A self-made program, developed in LabVIEW code (National Instruments), was used for the acquisition on real-time of the permeate weight, the temperature and the pressure of both filtration systems during the membrane performance characterization. Additionally, permeability was automatically determined from the recorded data and corrected following the mathematical procedure described in “section 4.4.1”, to take into account viscosity variations with respect an arbitrary reference temperature.

The main features of this program are described below.

- Permeability determinations can be conducted at the same time in both filtration systems. Moreover, they can work independently.
- All the experimental parameters, which are also independently fixed for both systems by the user, includes folder and file names, effective membrane surface area (in case other type of cells were used), reference temperature, experiment time and measurement frequency.
- Different experiment times and intervals between measurements can be set and modified throughout the characterization. Furthermore, experiments can be stopped as you go.



- The first recorded permeate weight is automatically taken as the zero. Therefore, no manual weight tare is needed at the beginning of the characterization.
- Permeability results are shown on live numerically and through graphical representations (weight, permeate flux or permeate flux at the reference temperature *vs.* time).
- At the end of the characterization one window pops up to introduce the experiment information which gathers the user, the membrane, its manufacturer, the stirring rate, the filtered solution (solvent, solutes and concentrations), the membrane pre-treatments and remarks about the experiment.
- A report is generated at the end of the permeability characterization in TXT format which includes the experimental parameters, the experiment information and the permeate flux and membrane permeability results. This file is properly formatted to be easily opened with Microsoft Excel.
- The date, with the format “YEAR\_MONTH\_DAY\_TIME\_”, is automatically included in the filename of this report in order to not overwrite consecutive files.
- At the end of the characterization, the software is ready for the next permeability measurement. Furthermore, the experiment information is auto saved, being available for the next time.
- An instruction guide is included in the main software window and several prompts and warnings are set to remind the mandatory information to conduct the experiments.
- Even though it is not required for this experimental setup, the program is easily scalable. Thus, the addition of a new physical filtration system could be easily programmed in order to characterize the permeability of three membranes at the same time.
- The program can be installed in personal computers as long as the following recommended system requirements are met: Pentium 4/M processor or equivalent, 1 GB of RAM, Windows XP/7/8 (32-bit or 64-bit), 1024 x 768 screen resolution and 150 MB of disk space.

The main software window of the developed program is shown in **Fig. 8.2**. This window is divided into two areas for the two filtration systems. Each of them has a container to define the experimental parameters, a container with for the graphical permeate flux results and two double indicators for the individual (gauge dial) and averaged (digital indicator) pressure and temperature values.

The first container (**Fig. 8.3**) consists of one tab to configure the port communication between the computer and the scale, two tabs to turn on the scale and send manual commands, one tab for the experimental information and another one to display the permeability results on live.

The second container shows the graphical results (Fig. 8.4). Note that two different permeate fluxes are calculated. A differential one which gives the flux between two consecutive weight measurements and the global one which gives the averaged permeate flux from the beginning of the characterization.

At the end of the characterization a pop-up window (Fig. 8.5) comes up to introduce all the experiment information and then, a report in TXT format is generated in the specified folder (Fig. 8.6).

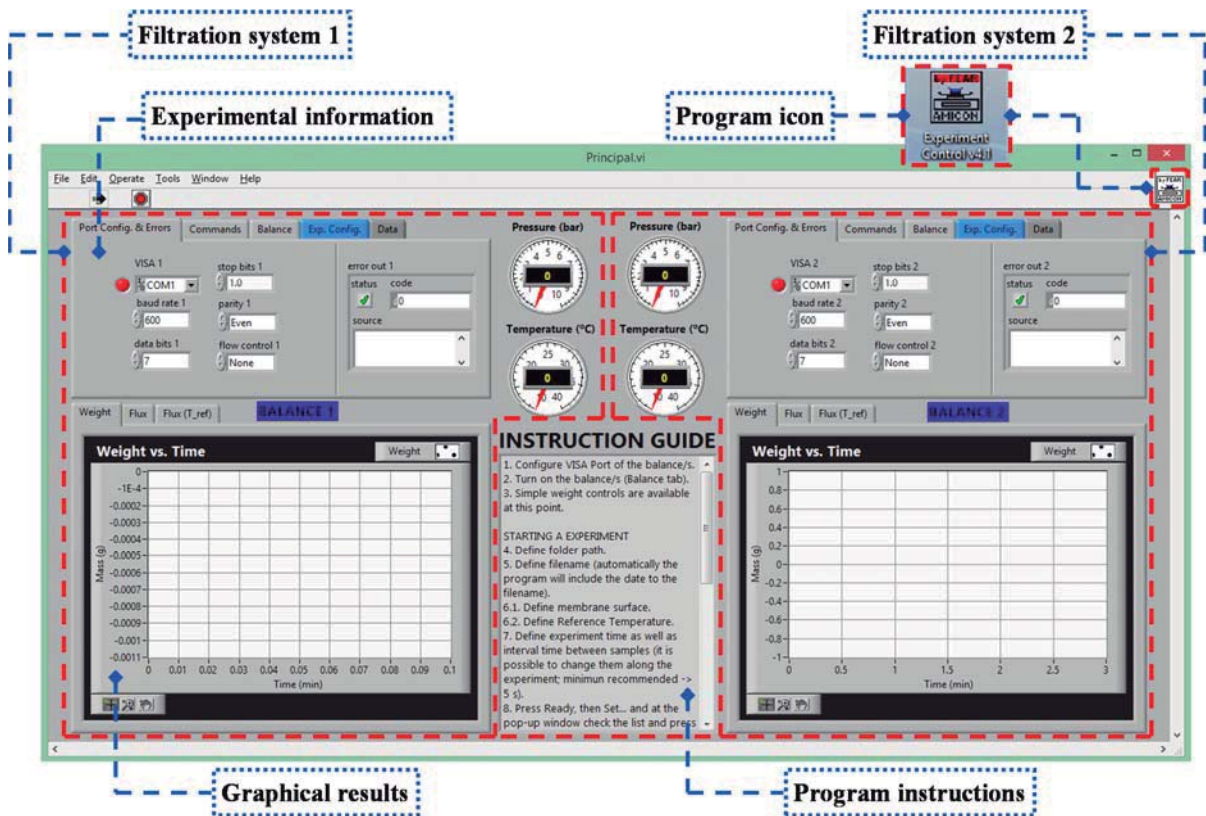
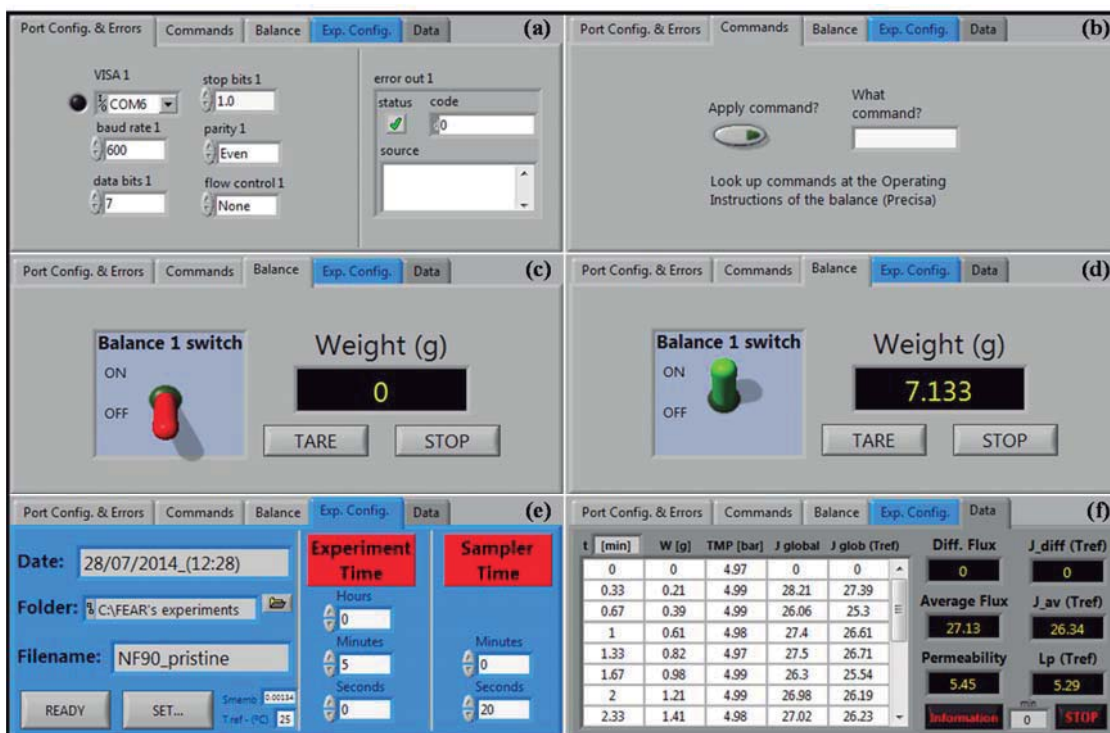
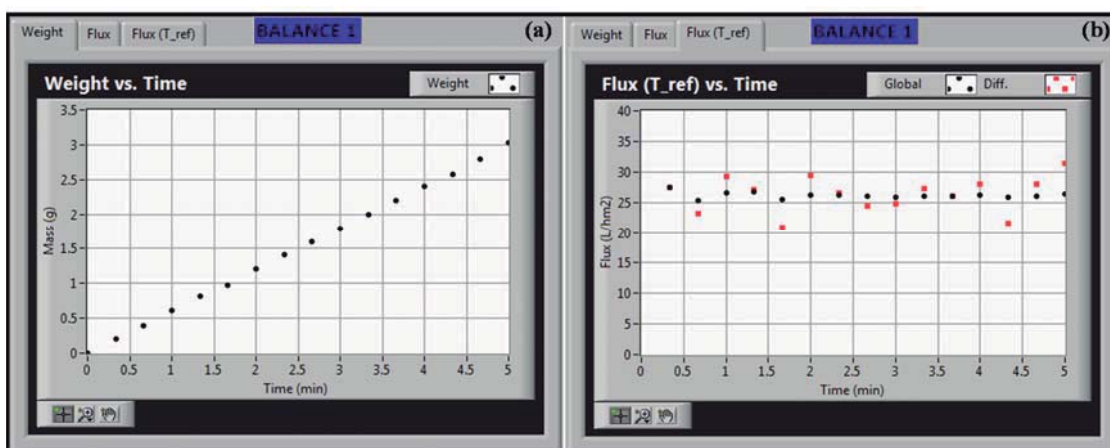


Fig. 8.2. Main window of the program for the permeate weight, pressure and temperature data acquisition to determine membrane permeability from two filtration systems.



**Fig. 8.3.** Container for the configuration of the weight scale communication (a), scale commands (b), turning on and off the scale (c and d), the experimental parameters (e) and the display of the permeability results (f).



**Fig. 8.4.** Example of graphical permeate flux results as function of time, throughout the permeability determination of one membrane.

Experiment information.vi

User: FEAR

Membrane: NF90 Company: Dow Filmtec

EXPERIMENT:

Stiring: 400 rpm

Solution:

Solvent: DI water

Solute: - Concentration: -

Membrane pre-treatments: Rinsed with DI water

Remarks: Permeability determination.

BALANCE 1 OK

Fig. 8.5. Window to introduce all the experiment information details.

2012\_04\_30\_(12.28)\_NF90\_pristine - Notepad

Date: 28/07/2014 12:28

User: FEAR

Membrane: NF90 Company: Dow Filmtec

EXPERIMENT:

Stiring: 400 rpm

Solution:

Solvent: DI water

Solute: - Concentration: -

Membrane pre-treatments: Rinsed with DI water

Membrane surface: 0.00134 m<sup>2</sup>

Remarks: Permeability determination.

TMP: 4.98 bar

Temperature: 26.29 °C

Total time: 0:5:0 hh:mm:ss

Interval time: 0.333 [min]

Flux average: 27.125 L/hm<sup>2</sup>

Permeability: 5.452 L/hm<sup>2</sup>bar

Reference Temperature: 25 °C

Flux average (Tref): 26.338 L/hm<sup>2</sup>

Permeability (Tref): 5.294 L/hm<sup>2</sup>bar

Time [min]	Weight (g)	TMP (bar)	J global (L/hm <sup>2</sup> )	J global (Tref) (L/hm <sup>2</sup> )	J diff. (L/hm <sup>2</sup> )	J diff. (Tref) (L/hm <sup>2</sup> )
0.000000	0.000000	4.969468	0.000000	0.000000	0.000000	0.000000
0.333333	0.210000	4.991722	28.208955	27.389979	28.208955	27.389979
0.666667	0.388000	4.987800	26.059701	25.303124	23.910448	23.216268
1.000000	0.612000	4.976033	27.402985	26.607409	30.009552	29.215978
1.333333	0.819000	4.970917	27.503731	26.705230	27.805970	26.998694
1.666667	0.979000	4.991296	26.301493	25.537895	21.492537	20.868556
2.000000	1.205000	4.987885	26.977612	26.194385	30.358209	29.476835
2.333333	1.408000	4.978591	27.019190	26.234756	27.268657	26.476980
2.666667	1.595000	4.974584	26.781716	26.004177	25.119403	24.390125
3.000000	1.785000	4.969553	26.641791	25.868314	25.522388	24.781410
3.333333	1.994000	4.971514	26.785075	26.007438	28.074627	27.259551
3.666667	2.194000	4.969638	26.792402	26.014552	26.865672	26.085695
4.000000	2.409000	4.968530	26.966418	26.183516	28.880597	28.042122
4.333333	2.574000	4.967422	26.597015	25.824838	22.164179	21.520698
4.666667	2.789000	4.963329	26.760128	25.983215	28.880597	28.042122
5.000000	3.029000	4.965375	27.125373	26.337856	32.238806	31.302834

by FEAR

Fig. 8.6. Example of one report with the functional characterization of one membrane.



## 8.2. List of publications

---

The Doctoral Thesis gathers the information published in three following peer reviewed articles.

- R. Bernstein, E. Antón, M. Ulbricht, UV-photo graft functionalization of polyethersulfone membrane with strong polyelectrolyte hydrogel and its application for nanofiltration, *ACS Applied Materials and Interfaces* 4 (2012) 3438-3446. **Impact factor: 5.008**
- R. Bernstein, E. Antón, M. Ulbricht, Tuning the nanofiltration performance of thin film strong polyelectrolyte hydrogel composite membranes by photo-grafting conditions, *Journal of Membrane Science* 427 (2013) 129-138. **Impact factor: 4.093**
- E. Antón, J.I. Ignacio, J.R. Álvarez, A. Hernández, S. Luque, Fitting approach to liquid-liquid displacement porosimetry based on the log-normal pore size distribution, *Journal of Membrane Science* (2014). <http://dx.doi.org/10.1016/j.memsci.2014.07.035>. **Impact factor: 4.093**

Additional information from articles that have been submitted to be considered for publication are also included in this Doctoral Thesis.

- E. Antón, D. Vázquez, J.R. Álvarez, S. Luque, Ageing of nanofiltration polymeric membranes under the exposure to acidic and alkaline cleaning solutions, *Separation and Purification Technology*. Submitted (2014).
- E. Antón, J.R. Álvarez, L. Palacio, P. Prádanos, A. Hernández, A. Pihlajamäki, S. Luque, Ageing of polyethersulfone ultrafiltration membranes under long-term exposures to alkaline and acidic cleaning solutions. Part I: physicochemical changes, *Journal of Membrane Science*. Submitted (2014).
- E. Antón, J.R. Álvarez, S. Luque, Ageing of polyethersulfone ultrafiltration membranes under long-term exposures to alkaline and acidic cleaning solutions. Part II: membrane performance, *Journal of Membrane Science*. Submitted (2014).



### 8.3. List of figures

<b>Fig. 1.1.</b>	Number of publications in the past three decades related to membrane fouling and cleaning in pressure driven processes according to Scopus (July 2014). Search criteria contained the words fouling or cleaning in the title, keywords or abstract.	5
<b>Fig. 3.1.</b>	Typical UF fouling/chemical cleaning cycle at constant TMP.	27
<b>Fig. 3.2.</b>	Typical UF fouling/physical and chemical cleaning cycles at constant $J_F$ .	29
<b>Fig. 3.3.</b>	<i>Water flux recovery</i> and residual quantity of protein, measured by ATR-FTIR, on a flat PES membrane fouled with skim milk after the rinsing and treatment with various oxidants. Taken from Paugam <i>et al.</i> [104].	44
<b>Fig. 3.4.</b>	<i>Cleaning efficiency</i> of proteinase M as a function of cleaning time for membranes fouled after filtrating a protein mixture for 2 h (◆,◇) and 5 h (■,□). Closed symbols are those evaluated with Eq. (3.15) and open symbols correspond to the results from the Lowry analysis. Lines are only guides for the eye. Adapted from Petrus <i>et al.</i> [126].	44
<b>Fig. 5.1.</b>	ATR-FTIR spectra of the active (a) and the support (b, c) layers of UP020 (black solid line), UP010 (black broken line), UP005 (black dotted line), UH004 (gray solid line), HFK-328 (gray broken line) and PT (gray dotted line). Spectra of the HFK-238 and PT support layers were represented separately from those of the Nadir ones for the sake of clarity.	79
<b>Fig. 5.2.</b>	Relative permeability of UH004 (a), UP005 (b), UP010 (c) and UP020 (d) membranes aged at 50°C with NaOH solutions of 0.01 M (▲; short-dash line), 0.1 M (◆; long-dash line) and 1.0 M (■; solid line) and soaked in DI water (○; dotted line).	81
<b>Fig. 5.3.</b>	Relative permeability of UH004 (a), UP005 (b), UP010 (c) and UP020 (d) membranes aged at 50°C with HNO <sub>3</sub> solutions of 0.01 M (▲; short-dash line), 0.1 M (◆; long-dash line) and 1.0 M (■; solid line) and soaked in DI water (○; dotted line).	82
<b>Fig. 5.4.</b>	Intrinsic rejection curves as function of the PEG fraction MW for the UP005 (a, b) and UP020 (c, d) aged at 50°C with NaOH (a, c) and HNO <sub>3</sub> (b, d) solutions of 0.01 M (broken line) and 1.0 M (solid line) and soaked in DI water (dotted line).	85



- Fig. 5.5.** ATR-FTIR spectra of the active (1) and support (2) layers of UP020 (a), UP010 (b), UP005 (c) and UH004 (d) membranes after the soaking in DI water (solid line, S) and after the ageing with 0.01, 0.1 and 1.0 M HNO<sub>3</sub> solutions (broken line, B) and with 0.01, 0.1 and 1.0 M NaOH solutions (dotted line, D) at 50°C. 86
- Fig. 5.6.** SEM micrographs of the support layers of UP005, UP010 and UP020 Nadir membranes in their original conditions and after the ageing with 0.01, 0.1 and 1.0 M HNO<sub>3</sub> and NaOH solutions. 87
- Fig. 5.7.** AFM images of the UP005 membrane active layer in its original condition (a) and after the ageing with 0.01 and 1.0 M HNO<sub>3</sub> and NaOH solutions (b, c, d and d). All the AFM images has the same z-axis scale and the Z values are the maximum height of each image. 88
- Fig. 5.8.** Two dimensional power spectral density (a) and PSD fractal dimension (bars) and R<sub>q</sub> roughness (b) for the 0.8 x .0.8 μm scanned areas of the UP005 membrane after the ageing in HNO<sub>3</sub> and NaOH solutions at different concentrations. 89
- Fig. 5.9.** Relative permeability of HFK-328 (a) and PT (b) membranes aged at 50°C with NaOH solutions of 0.01 M (▲; short-dash line), 0.1 M (◆; long-dash line) and 1.0 M (■; solid line) and soaked in DI water (○; dotted line). 93
- Fig. 5.10.** Relative permeability of HFK-328 (a) and PT (b) membranes aged at 50°C with HNO<sub>3</sub> solutions of 0.01 M (▲; short-dash line), 0.1 M (◆; long-dash line) and 1.0 M (■; solid line) and soaked in DI water (○; dotted line). 93
- Fig. 5.11.** Intrinsic rejection curves as function of the PEG fraction MW for the HFK-328 (a, b) and PT (c, d) aged at 50°C with NaOH (a, c) and HNO<sub>3</sub> (b, d) solutions of 0.01 M (broken line) and 1.0 M (solid line) and soaked in DI water (dotted line). 95
- Fig. 5.12.** ATR-FTIR spectra of the active (1) and support (2) layers of HFK-328 (a) and PT (b) membranes at their original conditions (solid line, S) and after aged with 0.01, 0.1 and 1.0 M HNO<sub>3</sub> solutions (broken line, B) and with 0.01, 0.1 and 1.0 M NaOH solutions (dotted line, D) at 50°C. 96

- Fig. 5.13.** ATR-FTIR spectra of HFK-328 (a) and PT (b) support layers at their original conditions (black solid lines) and after the ageing with 0.01 (black broken lines), 0.1 (black dotted lines) and 1.0 M (black dotted lines) at 50°C. The grey solid line that appears at the top of each graph is the spectrum of the active layer, taken from **Fig. 5.1** and displayed here for the sake of comparison. 97
- Fig. 5.14.** SEM micrographs of support layer and membrane cross-section of HFK-328 and PT membranes in their original conditions and after the ageing with 0.01, 0.1 and 1.0 M HNO<sub>3</sub> and NaOH solutions at 50°C. 99
- Fig. 5.15.** AFM images of the active (A) and the support (B) layers of the HFK-328 and PT membranes in their original conditions and after the ageing with 1.0 M NaOH or HNO<sub>3</sub> solutions. All the AFM images has the same z-axis scale and the Z values are the maximum height of each image. 101
- Fig. 5.16.** PSD fractal dimension (bars) and RMS roughness for the 0.8 x 0.8 μm scanned areas of the HFK-328 (a) and PT (b) membranes after the ageing in HNO<sub>3</sub> and NaOH solutions at different concentrations. 102
- Fig. 5.17.** Relative permeability (a) and MWCO (b) changes of UP005 membrane soaked in DI water (open symbols and dotted lines) and aged with 1.0 M NaOH solution (closed symbols and solid lines) at 25°C (△, ▲), 35°C (◇, ◆) and 50°C (□, ■). 104
- Fig. 5.18.** Relative permeability of HFK-328 (a) and PT (b) membranes soaked in DI water (open symbols and dotted lines) and aged with 1.0 M NaOH solution (closed symbols and solid lines) at 25°C (△, ▲), 35°C (◇, ◆) and 50°C (□, ■). 105
- Fig. 5.19.** Permeability and Na<sub>2</sub>SO<sub>4</sub>, glucose and sucrose rejection behavior of the NF90 membrane aged at 50°C in HNO<sub>3</sub> (left column) and NaOH (right column) solutions of 0.01 M (▲; short-dash line), 0.1 M (◆; long-dash line) and 1.0 M (■; solid line) and soaked in DI water (○; dotted line). 109
- Fig. 5.20.** Example of one amide bond hydrolysis reaction of the NF90 PA active layer under alkaline conditions. 110
- Fig. 5.21.** ATR-FTIR spectra of the active layer of the NF90 membrane in its pristine state, soaked in DI water and aged in HNO<sub>3</sub> (a) and NaOH (b) ageing solutions at different concentrations. 111

- Fig. 5.22.** SEM micrographs of the backing layer and the cross-section of the NF90 membrane in its pristine state, soaked in DI water and aged in HNO<sub>3</sub> and NaOH ageing solutions at different concentrations. 113
- Fig. 5.23.** Permeability and Na<sub>2</sub>SO<sub>4</sub>, glucose and sucrose rejection behavior of the NF270 membrane aged at 50°C in HNO<sub>3</sub> (left column) and NaOH (right column) solutions of 0.01 M (▲; short-dash line), 0.1 M (◆; long-dash line) and 1.0 M (■; solid line) and soaked in DI water (○; dotted line). 115
- Fig. 5.24.** Example of one amide bond hydrolysis reaction of the NF270 poly(piperazinamide) active layer under acidic conditions. 116
- Fig. 5.25.** ATR-FTIR spectra of the active layer of the NF270 membrane in its pristine state, soaked in DI water and aged in HNO<sub>3</sub> (a) and NaOH (b) ageing solutions at different concentrations. 117
- Fig. 5.26.** SEM micrographs of the backing layer and the cross-section of the NF270 membrane in its pristine state, soaked in DI water and aged in HNO<sub>3</sub> and NaOH ageing solutions at different concentrations. 118
- Fig. 5.27.** Permeate flux (a) and Na<sub>2</sub>SO<sub>4</sub> rejection (b) of the NF270 membrane throughout the aging in 0.1 M NaOH at 50°C in soaking mode (●) and in cross-flow mode with the permeate valve open (■) and close (▲). 119
- Fig. 8.1.** Experimental setup for the functional characterization of UF and NF membranes at small scale. 203
- Fig. 8.2.** Main window of the program for the permeate weight, pressure and temperature data acquisition to determine membrane permeability from two filtration systems. 205
- Fig. 8.3.** Container for the configuration of the weight scale communication (a), scale commands (b), turning on and off the scale (c and d), the experimental parameters (e) and the display of the permeability results (f). 206
- Fig. 8.4.** Example of graphical permeate flux results as function of time, throughout the permeability determination of one membrane. 206
- Fig. 8.5.** Window to introduce all the experiment information details. 207
- Fig. 8.6.** Example of one report with the functional characterization of one membrane 207

---

**8.4. List of tables**

---

<b>Table 1.1.</b>	Typical operation conditions and targets of pressure driven membrane processes.	3
<b>Table 3.1.</b>	Summary of all the publications focused on the cleaning of polymeric UF membranes as function of the feed stream.	21
<b>Table 3.2.</b>	Removal of suspended matter for different BW procedures [79].	46
<b>Table 4.1.</b>	Details of the membranes used in the ageing studies and the development of the LLDP model. Data reported by manufacturers.	62
<b>Table 4.2.</b>	Lifshitz-Van der Waals, electron acceptor and electron donor contributions as well as the total liquid surface energies of the probe liquids [198].	72
<b>Table 5.1.</b>	SEM-EDX analysis of active and support layers of GE Osmonics, Koch and Nadir membranes.	78
<b>Table 5.2.</b>	Determined MWCO of the membranes at the end of the different ageing procedures.	84
<b>Table 5.3.</b>	Contact angle measurements (using ultrapure water) of the active layers of the UP005, UP010, UP020, HFK-328 and PT membranes after the ageing in different conditions at 50°C. Intervals expressed as standard deviations.	90
<b>Table 5.4.</b>	Contact angle measurements (using ultrapure water) of the support layers of the HFK-328 and PT membranes after the ageing in 0.01, 0.1 and 1.0 M NaOH solutions at 50°C. Intervals expressed as standard deviations.	102
<b>Table 5.5.</b>	Total solid surface energies ( $\text{mJ/m}^2$ ) and their dispersive and polar components of HFK-328 and PT active layers after the ageing in 0.01, 0.1, 1.0 M NaOH solutions at 50°C.	103
<b>Table 5.6.</b>	Infrared peak ratios for the NF90 and NF270 membranes after being subjected to different ageing conditions.	111



## 8.5. Nomenclature

### 8.5.1. Symbols

$c_B$ :	Solute concentration in the feed bulk	M
$c_m$ :	Solute concentration at the membrane wall	M
$c_P$ :	Solute concentration in the permeate	M
$D$ :	Diffusivity	$m^2 s^{-1}$
$d_{fr}$ :	Fractal dimension	Dimensionless
$j$ :	PEG molecular weight fraction $j$	-
$J$ :	Permeate flux	$m s^{-1}$
$J_c$ :	Permeate flux during the cleaning step	$m s^{-1}$
$J_F$ :	Permeate flux during the feed filtration	$m s^{-1}$
$J_{w0}$ :	Permeate flux (filtering pure water) of the pristine membrane	$m s^{-1}$
$J_{wc}$ :	Permeate flux (filtering pure water) after the cleaning step	$m s^{-1}$
$J_{wF}$ :	Permeate flux (filtering pure water) after the feed filtration	$m s^{-1}$
$k$ :	Mass transfer coefficient	$m s^{-1}$
$L_p/L_{p0}$ :	Relative membrane permeability	Dimensionless
$L_p$ :	Membrane permeability	$m s^{-1} Pa^{-1}$
$L_p^{25^\circ C}$ :	Membrane permeability at $25^\circ C$	$m s^{-1} Pa^{-1}$
$L_p^T$ :	Membrane permeability at temperature $T$	$m s^{-1} Pa^{-1}$
$L_{pc}$ :	Permeability during the cleaning step	$m s^{-1} Pa^{-1}$
$L_{pF}$ :	Permeability during the feed filtration	$m s^{-1} Pa^{-1}$
$L_{p_{i,0}}^{25^\circ C}$ :	Measured permeability of a coupon $i$ in its pristine state	$m s^{-1} Pa^{-1}$
$L_{p_{i,t}}^{25^\circ C}$ :	Measured permeability of a coupon $i$ after an ageing period $t$	$m s^{-1} Pa^{-1}$
$L_{pw0}$ :	Permeability (filtering pure water) of the pristine membrane	$m s^{-1} Pa^{-1}$
$L_{pwc}$ :	Permeability (filtering pure water) after the cleaning step	$m s^{-1} Pa^{-1}$
$L_{p_{wF}}$ :	Permeability (filtering pure water) after the feed filtration	$m s^{-1} Pa^{-1}$

MW:	Molecular weight	g/mol
n:	Number of samples	-
P:	Total number of points (AFM images)	-
r:	Stirred cell radius	m
RI <sub>B,j</sub> :	RI signal from the PEG fraction <i>i</i> in the feed	Dimensionless
r <sub>if</sub> :	Resistance due to irremovable fouling	m <sup>-1</sup>
RI <sub>P,j</sub> :	RI signal from the PEG fraction <i>i</i> in the permeate	Dimensionless
R <sub>m</sub> :	Intrinsic membrane rejection	Dimensionless
r <sub>m</sub> :	Membrane resistance	m <sup>-1</sup>
R <sub>obs</sub> :	Observed membrane rejection	Dimensionless
R <sub>q</sub> :	Root mean square roughness	m
r <sub>res</sub> :	Residual resistance of r <sub>if</sub> after the cleaning step	m <sup>-1</sup>
r <sub>rf</sub> :	Resistance due to removable fouling	m <sup>-1</sup>
r <sub>tot</sub> :	Total resistance	m <sup>-1</sup>
r <sub>w</sub> :	Wenzel's coefficient	Dimensionless
r <sub>wc</sub> :	Total resistance (filtering pure water) after the cleaning step	m <sup>-1</sup>
S:	Standard deviation	-
T:	Temperature	K
TMP:	Transmembrane pressure	Pa
TMP <sub>0</sub> :	TMP at the beginning of the feed filtration (equivalent to TMP <sub>w0</sub> )	Pa
TMP <sub>w0</sub> :	TMP of the pristine membrane filtering pure water	Pa
t <sub>n-1, 1-<math>\alpha</math>/2</sub> :	Student's t-distribution with <i>n-1</i> degrees of freedom and <i>1-<math>\alpha</math>/2</i> confidence level	Dimensionless
W <sub>a</sub> :	Work of adhesion	J m <sup>-2</sup>
z <sub>i</sub> :	Height at the point <i>i</i> (AFM images)	m
Z <sub>m</sub> :	Mean height of the <i>P</i> points (AFM images)	m

**8.5.2. Greek symbols**

$1-\alpha$ :	Confidence level	Dimensionless
$\gamma^-$ :	Electron donor contribution to the total surface energy	$\text{J m}^{-2}$
$\gamma^+$ :	Electron acceptor contribution to the total surface energy	$\text{J m}^{-2}$
$\gamma^{\text{AB}}$ :	Polar acid-base contribution to the total surface energy	$\text{J m}^{-2}$
$\gamma^{\text{LW}}$ :	Lifshitz-Van der Waals contribution to the total surface energy	$\text{J m}^{-2}$
$\gamma^{\text{TOT}}$ :	Total surface energy	$\text{J m}^{-2}$
$\Delta\text{TMP}$ :	TMP difference between the start and the end of the feed filtration	Pa
$\theta_{\text{app}}$ :	Apparent contact angle	rad
$\theta_{\text{Y}}$ :	Actual or Young contact angle	rad
$\mu$	Viscosity	Pa s
$\mu^{25^\circ\text{C}}$ :	Viscosity at temperature $25^\circ\text{C}$	Pa s
$\mu^{\text{T}}$ :	Viscosity at temperature T	Pa s
$\rho$ :	Density	$\text{kg m}^{-3}$
$\omega$ :	Stirring rate	$\text{rad s}^{-1}$

**8.5.3. Abbreviations**

$\alpha$ -CT:	$\alpha$ -chymotrypsin enzyme
AFM:	Atomic force microscopy
ATR-FTIR:	Attenuated total reflection Fourier transform infrared
b-LG:	beta-lactoglobulin
BSA:	Bovine serum albumin
BW:	Backwashing
CA:	Cellulose acetate
CE:	Cellulose ester
CF:	Cross-flow
CFV:	Cross-flow velocity



ClO <sub>2</sub> :	Chlorine dioxide
CTAB:	Cetyltrimethylammonium bromide
DCP:	Dichlorodiphenyl sulfone-phenolphthalein
DE:	Dead-end
DG:	Degree of grafting
DI:	Deionized
DMSO:	Dimethyl sulfoxide
DTAB:	Dodecyltrimethylammonium bromide
EDS:	Energy-dispersive X-ray spectroscopy
EDTA:	Ethylenediaminetetraacetic acid
EPS:	Extracellular polymeric substances
FF:	Forward flushing
FP:	Fluoropolymer
GC-MS:	Gas chromatography - mass spectrometer
H <sub>2</sub> O <sub>2</sub> :	Hydrogen peroxide
H <sub>2</sub> SO <sub>4</sub> :	Sulfuric acid
H <sub>3</sub> PO <sub>4</sub> :	Phosphoric acid
HCl:	Hydrochloric acid
HNO <sub>3</sub> :	Nitric acid
HPLC:	High performance liquid chromatography
HPSEC:	High pressure size exclusion chromatography
ICP-OES:	Inductively coupled plasma optical emission spectroscopy
IEC:	Ion exchange capacity
KCl:	Potassium chloride
KOH:	Potassium hydroxide
LC-OCD:	Liquid chromatography organic carbon detector
LLDP:	Liquid-liquid displacement porosimetry
MALDI-MS:	Matrix assisted laser desorption ionization - mass spectrometry

---

MBAA:	N,N'-methylenebisacrylamide
MF:	Microfiltration
MW:	Molecular weight
MWCO:	Molecular weight cut-off
Na <sub>2</sub> SO <sub>4</sub> :	Sodium sulfate
NaCl:	Sodium chloride
NaClO:	Sodium hypochlorite
NaN <sub>3</sub> :	Sodium azide
NaOH:	Sodium hydroxide
NF:	Nanofiltration
NOM:	Natural organic matter
NPS:	Nominal pore size
PA:	Polyamide
PAN:	Polyacrylonitrile
PE:	Polyethylene
PEG:	Polyethylene glycol
PES:	Polyethersulfone
PET:	Polyethylene terephthalate (PET)
PP:	Polypropylene
PSD:	Power spectral density
PS <sub>u</sub> :	Polysulfone
PVC:	Polyvinyl chloride
PVDF:	Polyvinylidene fluoride
PVP:	Polyvinylpyrrolidone
RC:	Regenerated cellulose
RI:	Refractive index
RMS:	Root mean square
RO:	Reverse osmosis

SDD:	Silicon drift detector
SDS:	Sodium dodecyl sulfate (SLS)
SEM:	Scanning electron microscopy
SLS:	Sodium lauryl sulphate (SDS)
SP:	Streaming potential
TAZ:	Terg-A-zyme
TMP:	Transmembrane pressure
TTAB:	Tetradecyltrimethylammonium bromide
UF:	Ultrafiltration
VSA:	Vinyl sulfonic acid
XPS:	X-ray photoelectron spectroscopy
ZnSe:	Zinc selenide
ZP:	Zeta potential



